

**THE UNIVERSITY OF HULL**

**A TRIBOLOGICAL & MECHANICAL STUDY OF ION ASSISTED  
DIAMOND-LIKE CARBON THIN FILMS**

being a Thesis submitted for the Degree of

**Doctor Of Philosophy**

at the University of Hull

by

Peter Stuart Holiday, BEng (Hons)(Hull)

November 1992

# CONTENTS

<b>ACKNOWLEDGEMENTS</b>	<b>6</b>
<b>LIST OF ABBREVIATIONS</b>	<b>7</b>
<b>I. SUMMARY</b>	<b>8</b>
<b>II. INTRODUCTION</b>	<b>10</b>
A. Objectives	10
B. Property Overview	12
1. Rationale Of Carbon-based Coatings	12
a) Philosophy Of Surface Engineering	12
b) Chemical Bonding And Structure	14
c) Market	20
d) The Properties of Diamond	20
e) Diamond & Diamond-like Thin Films: Properties & Applications	22
f) Property & Process Limitations	25
2. Characterisation of Diamond & Diamond-like films	27
C. Process Overview	33
1. Background To Technology	33
a) Historical Perspective	33
b) More Recent Events	34
c) CVD Diamond Development	38
d) PVD Diamond & Diamond-like Development	40
e) Nucleation	41
2. Latest Developments	45
a) Peter Bachmann's C-H-O CVD Diagram	45
b) Diamonds From Alcohol	49
c) Deposition From Fluorines	50
d) Epitaxial Growth From Combustion Flames	50
e) Cheria Recrystallisation Process	51
f) Prins's & Narayan's Copper Implantation Process	51
g) Isotopically Enriched <sup>12</sup> C 'White' Diamond	53
h) Fullerenes	54
3. The Tribology of Coatings	58
a) General	58
b) Surface Characteristics	59
c) Sliding Friction	60
d) Wear	63

Adhesive	64
Abrasive	65
Chemical Wear	66
4. Development of DLC Tribology	67
<b>III. EXPERIMENTAL</b>	<b>70</b>
A. Coating Equipment	70
a) Experimental Hybrid DC PVD	70
b) Experimental Hybrid DC/RF EBPVD	70
c) Fast Atom Beam	73
d) Edwards S150B Sputter Coater	75
B. Substrate Choice & Preparation	76
C. Laboratory Characterisation Methods	77
1. Intrinsic Material Property Evaluation	77
a) Resistivity/Conductivity	77
b) Stress Measurement - Cantilever Beam	81
c) Thickness Measurement - Profilometry	82
2. Extrinsic Material Property Evaluation	83
a) Microhardness	83
b) Nanohardness	85
c) Adhesion Strength	88
3. Assessment of Coating Durability	91
a) Pin on Disc	91
b) Fundamental Properties: Load & Distance	93
c) Sliding Speed & Radius	95
d) Pin Material	96
e) Tribological Methodology	99
4. Surface Analytical Studies	103
a) Optical Microscopy	103
b) SEM/EDX	103
c) Raman	107
d) LIMA	107
e) Optical Spectroscopy/FTIR	109

<b>IV. RESULTS</b>	<b>110</b>
<b>A. Initial Studies</b>	<b>110</b>
1. Preliminary Studies Into DC Evaporated PVD Films	111
a) Film Preparation & Experimental Details	111
b) Film Properties	112
c) Discussion	118
2. A Mechanical & Tribological Study of Doped Carbon Films	119
a) Film Preparation & Experimental Details	120
b) Film Properties	120
c) Tribological Performance	121
d) Summary	121
<b>B. Further Studies</b>	<b>125</b>
1. Investigations into DC & 380kHz Radio Frequency EBPVD Films	126
a) Film Preparation & Experimental Details	126
b) Results - Adhesion & Deposition Rate	126
c) Internal Stress	128
d) Micro & Nanoindentation Measurements	131
e) Analytical Characterisation: Electron Microscopy & Raman	131
f) Resistivity & Optical Measurements	137
g) Annealing	139
h) Tribological Properties	139
i) Summary	142
2. Investigations Into Fast Atom Beam Films	147
a) Film Preparation & Experimental Details	147
b) Results - Mechanical & Optical Properties	149
c) Annealing	151
d) Raman	151
e) Tribological Properties - A Comparison	151
f) The Effect of Surface Roughness	153
g) Humidity and Atmospheric Conditions	160
h) Chemical Effects at the Wear Interface.	160
i) Summary	166
<b>C. The Presence of a Titanium Nitride Interlayer</b>	<b>168</b>
a) Raman	168
b) Nanoindentation	168
c) Results	173
d) Conclusions	180

<b>V. DISCUSSION &amp; CONCLUSIONS</b>	<b>181</b>
a) Recent Research	181
b) Review of Tribology	186
c) Pin on disc	189
d) Process Control	192
e) The Role of Hydrogen	194
f) Test Methodologies	198
<b>VI. RECOMMENDATIONS FOR FUTURE WORK</b>	<b>200</b>
A. Fundamental Studies	200
B. Analytical Characterisation and Test Development	201
<b>REFERENCES</b>	<b>203</b>
<b>APPENDICES</b>	<b>214</b>

## **ACKNOWLEDGEMENTS**

I am particularly grateful to my supervisor, Prof.Allan Matthews, for his commitment, guidance and enthusiasm towards this piece of work and his constructive criticism of the text.

The author is grateful for the support of Dr.Trevor Farrell, of the Electricity Development & Research Centre for acting as industrial supervisor, the Department of Engineering Design & Manufacture for the use of its facilities and the Science and Engineering Research Council for financial support.

Additionally, the author would like to thank various people & institutions around the country, in particular Dr.Sandy Fitzgerald & Dr.Trevor Dines (University of Dundee) for XRD, Raman & XPS analysis; Gerry Smith (Heriot Watt) for LIMA work, Tony Sinclair (University of Hull) for early EDX work, Dr.Clark Cooper (United Technologies Research Center) for nanoindentation analysis, Dr.Christina Doyle (Howmedica) for obtaining substrates, Dr.Chris Hogg (University of Hull) for his advice on RBS and Jim Smith (Micro Materials, Wrexham) for the use of their NanoTest.

My sincere thanks also go to all my colleagues at the Research Centre in Surface Engineering, particularly Dr.Azzedine Dehbi-Alaoui, Dr.Peter Robinson, Dr.Adrian Leyland & Dr.Adrian James for their assistance and constructive suggestions. Thanks go also to John Hebden, David Wright and the EDM workshop for their vital contribution and especially Garry Robinson for help in the preparation of the photographic material.

P.S.Holiday

## LIST OF ABBREVIATIONS

$\alpha_f$	coefficient of thermal expansion (film)
$\alpha_s$	coefficient of thermal expansion (substrate)
$\delta$	deflection
$\varnothing, d$	diagonal length (mm)
$d'$	interplanar distance of atoms in crystal
$E_b$	binding Energy
$E_f$	Young's modulus of film
$E_{si}$	Young's modulus for silicon (133 GPa)
$L$	load (kg)
$\lambda$	wavelength of X-ray
$P$	pressure
$p_o$	yield pressure
$\theta$	angle of incidence
$r$	radius of curvature
$R_a$	roughness average ( $\mu\text{m}$ )
$\sigma_f$	stress in film
$\sigma_i$	intrinsic stress
$\sigma_{th}$	thermal stress
$t_f$	thickness of film
$t_s$	thickness of substrate
$T_r$	room temperature
$T_s$	substrate temperature
$T_c$	critical temperature
$\nu_f$	Poisson's ratio of film
$\nu_{si}$	Poisson's ratio for silicon (~0.28)
$V$	voltage

## I. SUMMARY

Amorphous hydrogenated carbon (a-C:H), diamond & diamond-like (DLC) thin films are some of the many terms used when referring to the generic group of coatings based on hard carbon. They are an emerging technological area within the surface coating discipline and are being increasingly used to improve the efficiency of a wide range of engineering components. In addition, the unique and extreme characteristics of these films result in unequalled material properties, such that in many cases a wide range of new and superior performance devices have only recently begun to be realised.

This study focuses on hydrogenated & non-hydrogenated diamond-like thin films deposited by various plasma based, hybrid and beam deposition techniques. The wear resistant and low friction properties of these films are of great importance in many of the potential application areas and has attracted particular interest in recent years. Therefore the major thrust of this research has been on the tribological aspect, particularly in relation to other advanced ceramic coatings, and to highlight the applicability of endurance wear tests used to evaluate diamond-like films. The main findings have been:-

a) That carbon can be deposited by several techniques in a hard amorphous phase, the properties of which depend heavily upon the conditions, substrate choice and method of deposition. For a particular technique, material properties can be made to be repeatable by a good understanding of deposition process control.

b) The use of plasma based hybrid PVD and beam methods have resulted in a considerably improved structural performance of the films over those produced by the direct evaporation of graphite. The introduction of a hydrocarbon gas into the plasma at the synthesis stage has also been shown to provide further improvements in the physical properties which has correspondingly led to an enhancement in the tribological behaviour. The levels of hydrogen, whether in an unbonded or bonded form, included in the film after deposition has been demonstrated to affect the mechanical and optical properties of the considerably.

c) The wear resistant and frictional performance of these coatings has been shown to be variable, depending upon the method and conditions of deposition as well as test parameters such as humidity, surface roughness, film structure, adhesive strength and oxide/impurity formation. In some cases the tribological performance was found to be excellent. The presence of the diamond-like carbon coating has been shown to be beneficial in reducing wear between contacting bodies experiencing relative movement by encouraging the formation of a carbon transfer layer on the surface of the counterface material which acts as a zone of low shear and provides a physical barrier to tribo-chemical interactions. Under certain conditions, such tribo-chemical interactions can occur readily at the interface, facilitating the formation of strong interfacial bonding and increased wear.

d) The inclusion of metallic elements into the carbon matrix has been shown to enhance the wear resistant properties of the film to only a small extent, although at the expense of a deterioration in the friction coefficient. The most beneficial effect of doping carbon films with metal species has been the improved resistance to thermal degradation.

e) Thin intermediate layers of titanium nitride have also been shown to produce a remarkable improvement in both wear resistance and frictional performance of the diamond-like carbon films to an extent which appears to be related to the level of stoichiometry of the titanium nitride. The main mechanism behind this increased performance appears to be due largely to an enhancement in adhesive strength at the diamond-like carbon/titanium nitride junction, with an increase in load support being provided as a secondary benefit.

f) A critical assessment of the available techniques and methodology available for testing hard carbon films has been made and in some cases methods have been found to be either entirely inappropriate or appropriate only when suitable precautionary measures have been taken. These difficulties largely stem from the exacting demands of thin, hard layers of diamond-like carbon due to its unique and extreme mechanical, electrical and optical properties.

## **II. INTRODUCTION**

### **A. Objectives**

Hard carbon coatings have emerged as a potentially new and exciting technological area with numerous advantages over existing advanced ceramic films. However, if exploitation of these properties is to be achieved many very important deposition issues such as coverage, poor deposition rates, adhesion and thermal constraints have to be addressed. The number and diversity of techniques available is partially an indication of the many attempts to solve these sticking points and partly a result of a field of study still largely at the research stage. To complicate this issue further, the structural forms of synthetic diamond films are generally process dependent and vary from epitaxially grown polycrystalline diamond, hard amorphous carbon, hydrogenated amorphous carbon to composite metal/carbon films; each with its associated material qualities.

The main objective of this study has been to evaluate and assess the most suitable techniques, in terms of coating performance, for the deposition of diamond-like coatings and to identify possible drawbacks, in terms of deposition constraints. To overcome a traditional constraint of poor deposition rate; combustion flame techniques (typically achieving 100-150 $\mu\text{m/hr}$ ) have been developed and have proved an effective process for producing high quality polycrystalline diamond heat sinks. Constraints, however, on physical coverage and the unfavourably high deposition temperatures make this method unsuitable for most other applications. Similarly, microwave plasma CVD processes can be used to produce high purity crystalline diamond, with sufficient coverage to make it a popular technique in the electronics field for coating of silicon discs but this method suffers from insufficient rates of deposition ( $\sim 1\mu\text{m/hr}$ ).

Generally, plasma assisted PVD enables greater control over the quality of diamond-like carbon coatings for a wide range of parameters and suffers from fewer deposition constraints such as deposition temperature, uniformity and coverage. Hence the first objective of the study has been to understand and create a knowledge base of the various deposition parameters involved in the PAPVD process vis a vis repeatable coating deposition.

Prominent parameters include most notably the plasma properties of cathode voltage, current density and pressure but also substrate temperature, precursor species and concentration. The effect and range of these parameters were evaluated in relation to the tribological performance of the thin films produced. In view of this tribological criteria, good mechanical and physical properties, in particular adhesion strength, hardness and a dense structure, were important research objectives.

Another aim of this work was to evaluate the fundamental factors affecting the tribological performance and durability of films both from variations in deposition conditions and test variables such as operating temperature, humidity, contact speed and tribo-chemical behaviour. This was achieved using a pin on disc geometry tribotester to simulate high Hertzian pressure, dry sliding conditions.

Lastly, tribological and analytical methods for analysing DLC films were continually evaluated for their suitability and effectiveness particularly, since in many instances the applicability of many of these tests was pushed to the limit due to the coatings' extreme properties of hardness, friction and wear. With this understanding of the range of limitations, it was intended that areas of possible improvement should be highlighted in the methodology of testing, and the interpretation, presentation and comparison of the results.

## **B. Property Overview**

### **1. Rationale Of Carbon-based Coatings**

#### ***a) Philosophy Of Surface Engineering***

The introduction and growth of surface engineering in recent years has been prompted by the realisation that the surface of a component is often more important than the bulk. Indeed, failure mechanisms such as fatigue, corrosion and all forms of wear are initiated and dependent on the properties of the surface. This has led gradually to an awareness that certain surface restrictions constrain technological progress in areas of industrial development and the modification of these surfaces by thin film technology can increase a component's performance. Simply, surface engineering enables the reduction of constraints imposed by surface initiated phenomenon.

This philosophy has led to a quest for superior and sometimes unique material properties by coupling into one composite the important bulk characteristics, such as strength, with the versatile properties of advanced engineering coatings. Recent research has highlighted the merit of multiple interlayers where the structure of the films may be a distinct or graded composite of anti corrosion, thermal barrier, wear resistant or friction reducing layers. By way of an example, hard magnetic media storage discs typically consist of ion sputtered Ni-Co (100nm) as the recording media deposited onto a 250nm thick layer of chromium for improved adhesion. The disc substrate consists of several micrometers of electroless Ni-P deposited onto a disc blank of AA5086 aluminium alloy. The contacting surface to the read/write head is then finished with a thin film of hard, wear resistant and friction reducing diamond-like carbon<sup>1</sup> (Fig.1). The design criteria used in the selection of aluminium as the disc substrate is then one of low density (hence reduced rotational inertia) and low cost, with its protective and electro-magnetic properties being satisfied by surface coating technology. Other benefits of surface engineering, other than those relating to increased performance, can include a greatly reduced production and operating cost, flexibility in design, improved utilisation of materials and a reduction in energy requirements.

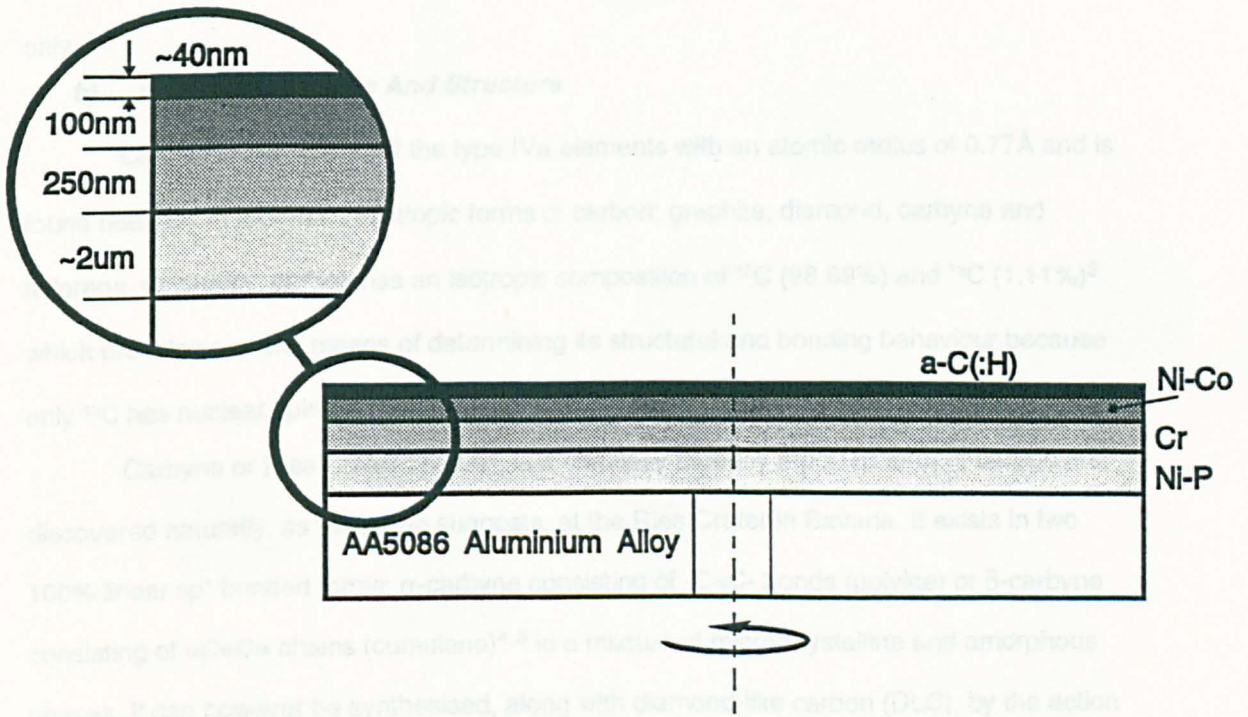


**Fig 1 A Schematic Diagram of a Read/Write Magnetic Media Disc**



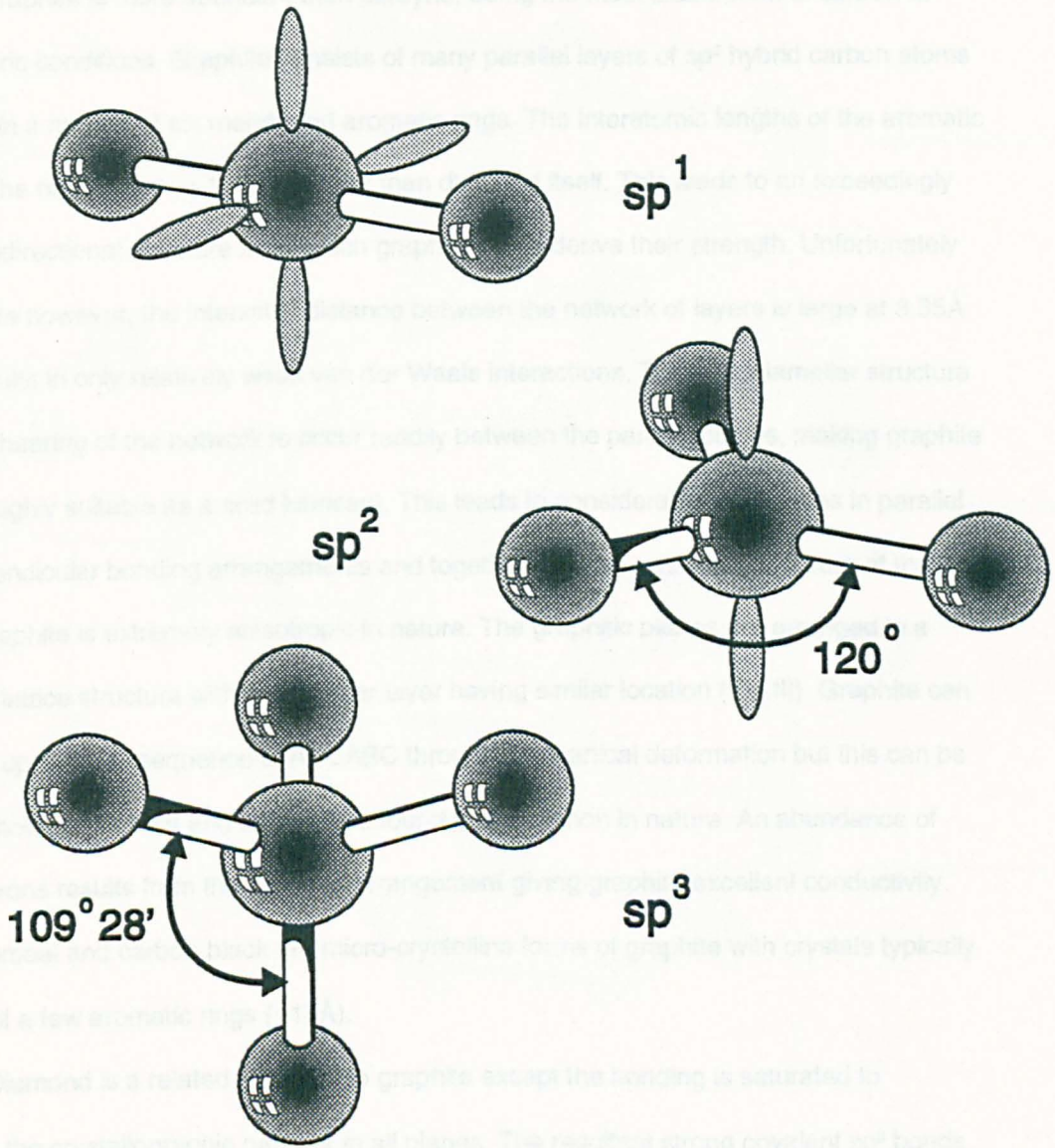


**Fig II The Bonding Configurations Of Carbon**

structure, thus 100%  $sp^3$  hybridised bonds are most desirable for strong structural properties.

Graphite is more abundant than carbyne, being the most stable form of carbon at atmospheric conditions. Graphite consists of many parallel layers of  $sp^2$  hybrid carbon atoms arranged in a mosaic of six membered aromatic rings. The interatomic lengths of the aromatic bonds in the ring system is  $1.42\text{\AA}$ , shorter than diamond itself. This leads to an exceedingly strong unidirectional structure from which graphite fibres derive their strength. Unfortunately for graphite however, the interstitial distance between the network of layers is large at  $3.35\text{\AA}$  which results in only relatively weak van der Waals interactions. This weak lamellar structure enables shearing of the network to occur readily between the parallel planes, making graphite soft and highly suitable as a solid lubricant. This leads to considerable differences in parallel and perpendicular bonding arrangements and together with the unsaturated nature of the bonds, graphite is extremely anisotropic in nature. The graphitic planes are arranged in a ABABAB lattice structure with every other layer having similar location (Fig.III). Graphite can also take up a lattice sequence of ABCABC through mechanical deformation but this can be easily removed with heat and is therefore found less common in nature. An abundance of free electrons results from this bonding arrangement giving graphite excellent conductivity. Soot, charcoal and carbon black are micro-crystalline forms of graphite with crystals typically the size of a few aromatic rings ( $\sim 15\text{\AA}$ ).

Diamond is a related structure to graphite except the bonding is saturated to complete the crystallographic network in all planes. The resultant strong covalent  $sp^3$  bonds gives rise to many of diamond's desirable properties such as hardness, resistivity and a bandgap which is higher than that of silicon or germanium (Table I). The  $sp^3$  hybridised bonds, with an interatomic distance of  $1.55\text{\AA}$ , predominate to form an interconnected array of tetrahedrons in a cubic crystal lattice (Fig.IV). This takes the form of an ABCABC stacking sequence so that every third plane is of similar arrangement. As with graphite, diamond can adopt a modified hexagonal crystallographic network of ABABAB, known as lonsdaleite, which has similar physical and electrical properties to diamond since it too is predominantly  $sp^3$  bonded. Nevertheless a greater repulsion between nearest neighbours exists due to this

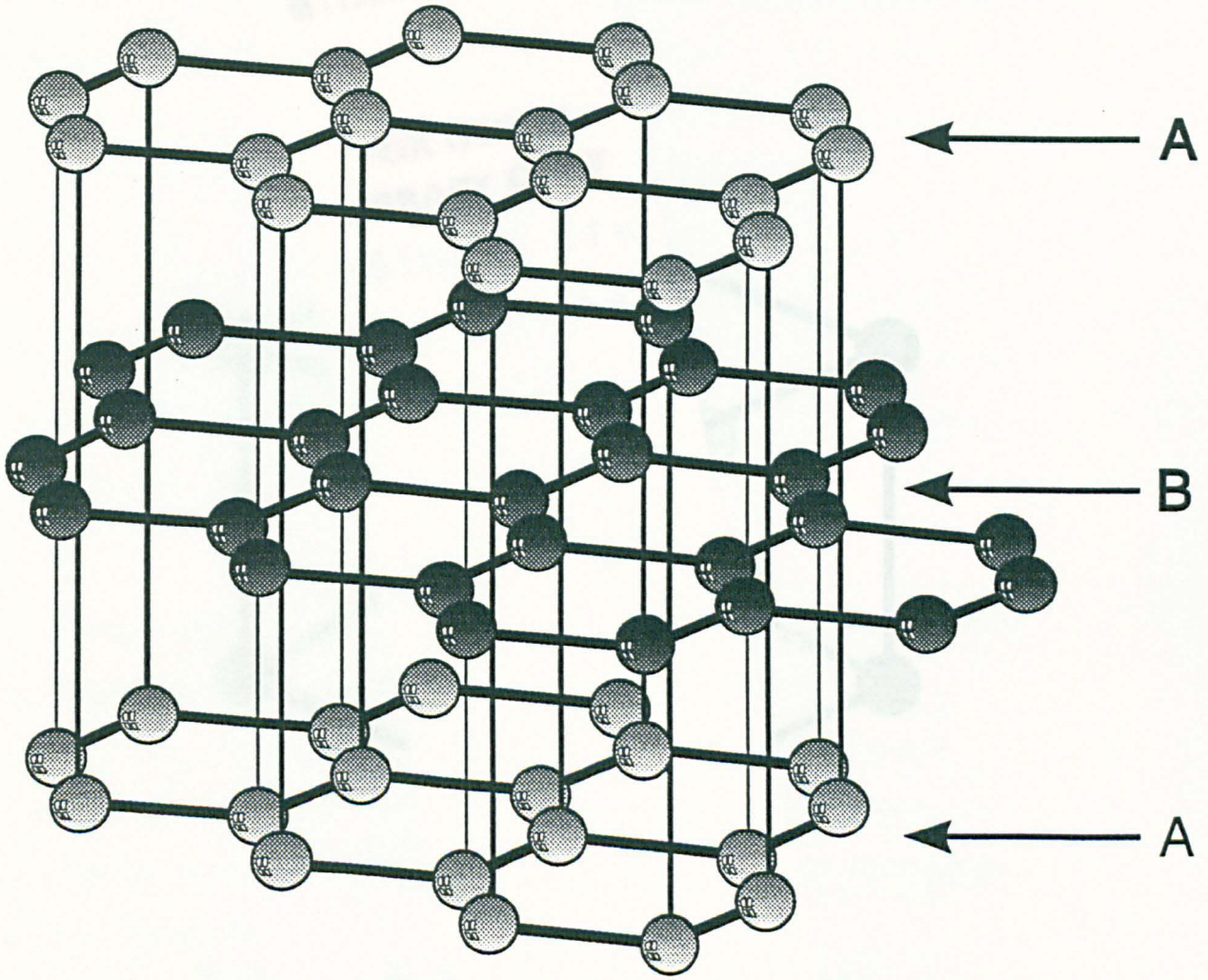


Fig III The Lattice Network Of Graphite



tighter stacking order. Although this distance is small and therefore the energy difference minimal, it is for this reason that lonsdaleite is rarely found naturally and only in uncommon phenomena like meteorites.

<b>Material</b>	<b>Bandgap (eV)</b>
c-BN	6.2
Diamond	5.5
GaN	3.6
SiC	2.9
$\beta$ -SiC	2.2
GaAs	1.4-2.2
Si	1.1
Diamond-like	1-3

*Table 1 Optical Bandgap*

Diamond is thermodynamically unstable with respect to graphite. Although the Gibb's energy needed to alter the bonding formation from one to the other is small ( $\Delta G=0.04\text{eV/atom}$ )<sup>6</sup>, a large potential well with an associated large activation energy is required to initiate such a change. Hence diamond remains diamond, with no evidence of a transformation to graphite, unless subjected to high radiation doses or a high oxidising, high temperature atmosphere.

The vapour deposition of diamond can result in two distinct types of film; firstly vapour deposited diamond films, which have comparable atomic structure and chemical properties to that of natural diamond, and secondly, diamond-like carbon (DLC) which is a hard form of carbon with some properties resembling that of diamond. The favoured bonds in DLC films are  $sp^2$  (triagonal) and  $sp^3$  (tetrahedral) ( $sp^1$  bonding being rarely detected in these materials) forming an amorphous or micro-crystalline structure radically different to that of diamond. The bonding ratio of  $sp^3/sp^2$  is often used to characterise DLC films where 100%  $sp^3/sp^2$  bonding (assuming no hydrogen bonds) is indicative of a structural similarity to diamond whereas 0%  $sp^3/sp^2$  ratio is indicative of a graphitic structure.

Furthermore, diamond-like carbon films contain varying amounts of impurities such as argon (~1%), oxygen (<10%)<sup>7</sup> and up to 55% hydrogen<sup>8</sup>. Thus the film properties vary enormously depending upon the conditions and methods of deposition and the level of impurities. Hydrogenated or non-hydrogenated diamond-like carbon a-C(:H) are suitable for many applications where high temperature, high pressure (HT HP) synthesised polycrystalline diamond (PCD) or CVD diamond are unnecessary or too costly. The performance in tribological and optical situations, due to a superior surface finish, is usually better than that of synthetic diamond together with the possibility of optimising one or several properties depending upon the deposition conditions. In addition DLC production on large area and complex geometrical shapes is more easily achievable.

### ***c) Market***

The market for diamond and diamond-like films is potentially huge. Although accurate market information is difficult to uncover for such an embryonic technology, some preliminary data is available. Currently the world-wide market for diamond thin films stands at \$200 million and is believed to be expanding rapidly, with an average annual growth rate for the next five years of 30%, to reach around \$1 billion before the end of the 1990's<sup>9</sup>. Other sources predict demand to continue and reach \$2 billion by 1995 with the possibility of exceeding \$4 billion by the end of the century<sup>10</sup>. Commercial semiconductor applications are expected to provide the greatest demand for diamond research growth, with a share of 60% of the diamond thin film market by 1996 followed by coated tools with ~20% share<sup>11</sup>.

### ***d) The Properties of Diamond***

Diamond is probably one of the most technologically and scientifically valuable crystalline material found in nature. It has unrivalled properties and because of these characteristics, synthetic production has been a long held goal. Among these unequalled characteristics are the highest hardness of any known material (typically  $H_v=7,000-10,000$  (10g), Table II) and a low coefficient of friction of  $\mu=0.01-0.05$  against itself, making it a suitable material for wear applications such as a protective films on hard discs, lenses, bearings and cutting tools. Tribological situations also benefit from diamond's high thermal conductivity (9-26W/cm<sup>2</sup>·K, Table III) which is five times that of copper at 20°C and twenty

five times at  $-190^{\circ}\text{C}$ <sup>12</sup>. It is this thermal conductivity, together with an inherently large resistivity ( $\sim 10^{16}\Omega\text{cm}$ ), that has made diamond an ideal choice for heat sinks, particularly in the micro-electronics field.

Diamond is a material with a high density ( $\rho=3.5\text{g/cm}^3$ , Table IV), extreme environmental and chemical stability due to the strong saturated covalent bonding. It is optically transparent from the near ultra-violet into the infra-red ( $\sim 250\text{-}2500\eta\text{m}$ ) spectrum and from the mid infrared spectrum to beyond ( $>6000\eta\text{m}$ )<sup>13</sup>.

Material	$H_v$ (10g)	Material	$\mu$
Diamond	7,000-10,000	Diamond	<0.05
cubic Boron Nitride	4,500	Teflon	0.05
Titanium Carbide	3,200	Diamond-like	0.1-0.05
Diamond-like	3,000-8,000	Graphite	0.1
Silicon Carbide	2,150	Lubricated Metals	0.1
Sapphire $\text{Al}_2\text{O}_3$	1,350	Sapphire $\text{Al}_2\text{O}_3$	0.2
Iron Carbide	1,000-1,400	Tungsten Carbide	0.2
Tool Steel (ASP23)	800-900	Iron	1.0
Aluminium	15-160	Aluminium	1.3

Table II Microhardness and Coefficient of Friction

Material	$K$ ( $\text{W/cm}^{\circ}\text{K}$ ) at $20^{\circ}\text{C}$
Diamond	9-26
Graphite	K(II) 30-40, (I) 1-2
Diamond-like	10
Copper	4
BeO	2.6
AlN	1.4
$\text{Al}_2\text{O}_3$	0.2

Table III Thermal Conductivity

Material	Density ( $\text{g/cm}^3$ )
Diamond	3.50
c-BN	3.50
Graphite	2.28-3.51
h-BN	2.27
Diamond-like	1.80-2.80
Vitreous Carbon	1.60
Glassy Carbon	1.50-1.55
Hydrocarbon Polymers	$\sim 1.00$
Organic Polymers	1.00

Table IV Density

### **e) *Diamond & Diamond-like Thin Films: Properties & Applications***

The scope of coating technology has now made it possible for the creation of synthetic diamond in the forms of polycrystalline diamond or hydrogenated/non-hydrogenated diamond-like carbon (DLC) thin films. The versatility of plasma deposition techniques, the greater range of properties compared to those of natural diamond and the reduced production costs have led to some interesting possibilities. For instance it has enabled both n- and p-type doping of diamond films by the controlled introduction of impurities at the deposition stage. Diphosphorous pentoxide is a common pentavalent substance used to introduce the phosphorus impurity into n-type CVD diamond. Likewise boron trioxide is commonly used to produce trivalent p-type diamond acceptor material (Fig.V). However PACVD methods are by no means the only methods for achieving doping of diamond; ion implantation<sup>14</sup> and even the hot filament method<sup>15</sup> have also been used.

The high thermal conductivity (allowing for higher operating temperatures), the high charge carrier mobility,  $1600\text{cm}^2\text{V}^{-1}\text{s}^{-1}$  (enabling a higher electron velocity) together with a high breakdown voltage makes diamond an excellent material for high power micro- and millimetre wave devices. The dielectric constant for diamond films is around 5.6<sup>16</sup>, compared to 12 and 13 for silicon and germanium respectively. The speed or frequency of transistors is inversely proportional to the dielectric constant and diamond clearly provides advantages in applications involving solid state power amplification, impact avalanche transit time transistors (IMPATT), metal semiconductor field effect transistors (MESFET) and high voltage Schottky diodes. The potential therefore of diamond thin films in semiconducting microelectronics and optoelectronics industries means that it could supersede all previously used materials including GaAs and  $\beta$ -SiC.

With an optical bandgap of 5.5eV and a refractive index of 2.42<sup>17</sup>, uses include scratch resistant anti-reflection infrared windows, low noise UV detectors, UV absorbing coatings, free standing X-ray windows, X-ray lithographic masks, laser windows and accelerator detectors (Fig.VI). Shatter proof lenses, watch crystals and scratch free mirrors may also follow these developments if the price per carat of synthetic crystalline diamond

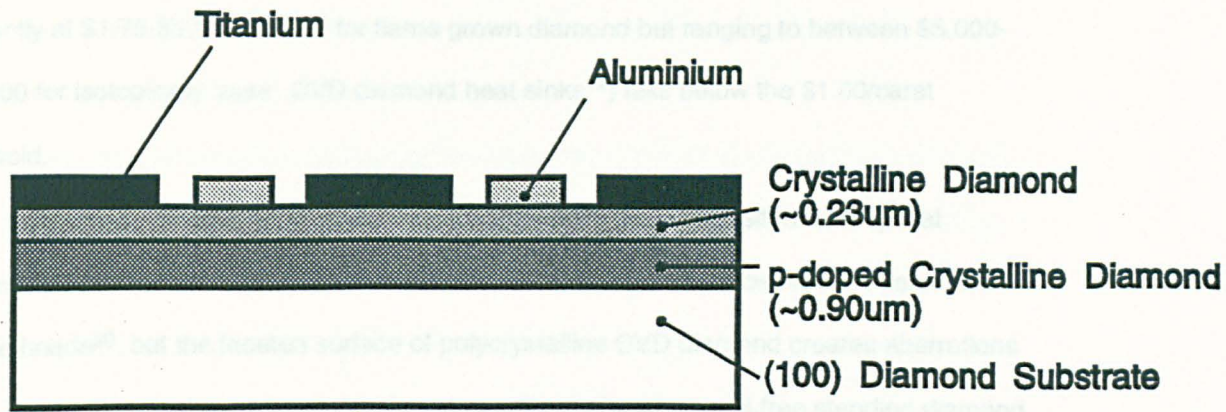


Fig V A Schematic Diagram of a Schottky Diode

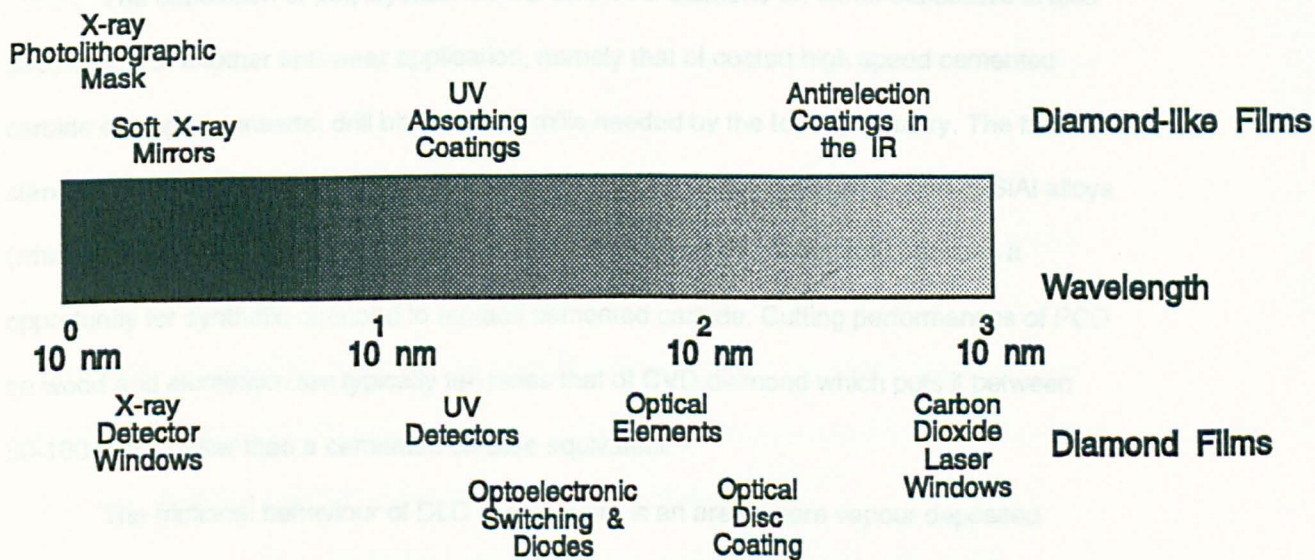


Fig VI Potential Applications For Diamond and Diamond-like Synthetic Films

(currently at \$1.75-\$17.50/carats<sup>18</sup> for flame grown diamond but ranging to between \$5,000-\$20,000 for isotopically 'pure' CVD diamond heat sinks<sup>19</sup>) falls below the \$1.00/carats threshold.

Synthetic diamond wear protective coatings have been deposited onto optical windows for some time in an effort to reduce dust and rain particle erosion of IR detectors on missile heads<sup>20</sup>, but the faceted surface of polycrystalline CVD diamond creates aberrations in the image. Westinghouse have developed a method whereby small free standing diamond windows 1½ inches in diameter are pre-deposited onto a donor material and then the uneven faceted surface embedded into a chalcogenide glass lens. The outer surface of the donor material is then removed by etching to expose the highly optically transmitting diamond nucleation surface which significantly reduces light scattering, lens wear and IR image distortion<sup>21</sup>.

The deposition of polycrystalline PCD and CVD diamond on donor substrates is also used widely in another anti-wear application, namely that of coated high speed cemented carbide cutting tool inserts, drill bits and end mills needed by the tooling industry. The free-standing film is simply brazed onto the surface of the tool body. The introduction of SiAl alloys (which are abrasive) requires low cost, improved wear resistant tooling and provides a opportunity for synthetic diamond to replace cemented carbide. Cutting performances of PCD on wood and aluminium are typically ten times that of CVD diamond which puts it between 50-100 times better than a cemented carbide equivalent<sup>22</sup>.

The frictional behaviour of DLC in a vacuum is an area where vapour deposited diamond-like carbon can display considerably better performances than even that of conventional synthesised diamond or even natural diamond. Usually, tribological conditions in vacuum lead rapidly to conditions of seizure due to the absence of weakly chemisorbed lubricating surface layers which help prevent the freshly sheared metal surfaces from coming into heavy adhesive contact with each other. It is widely known that atomically clean surfaces of bulk material, exposed by the action of wear, exhibit dramatically increased friction leading to seizure if the operating atmosphere prevents the formation of adsorbed layers. Diamond-like carbon films under similar conditions have demonstrated the characteristic property of

being able to maintain a low coefficient of friction under vacuum, making it an interesting material for many demanding applications in space.

The biomedical field is yet another area benefiting from DLC diamond development. Combined with its good tribological performance, corrosion resistance and biocompatibility, diamond-like carbon is becoming a candidate for implants, prostheses and surgical blades. Additionally, the low atomic number of diamond ( $Z=6$ ) results in excellent resistance to radiation damage. It is reported that the cross-sectional impact parameter of carbon to neutron damage is almost a magnitude lower than silicon.

The combination of high specific rigidity and strength has led to one of the first commercial available products. Hitachi, JVC and Sumitomo of Japan are all now marketing CVD diamond hi-fi tweeter speakers which they claim achieve a higher resolution of sound at high frequency by being able to propagate sound faster. The Sumitomo product is now marketed in the United States as a tweeter in Sony's \$1,000/pair APM-66ES speakers and consist of a laminate of aluminium, diamond and other damping material enclosed in a rigid honeycombed structure.

#### ***f) Property & Process Limitations***

Diamond, although inert and resistant to chemical attack in ordinary environmental conditions, reacts readily with ferrous and carbide forming metals and oxygen at temperatures greater than 1000°C. This limits its use in the cutting tool applications area to essentially non-ferrous materials. In addition, an insufficient fracture toughness confines its use to near continuous cutting rather than intermittent operations.

Small inclusions of impurities within the lattice provide diamonds with spectacular lustres, such as a bluish colour resulting from minute amounts of boron in type IIb diamonds. However their presence can affect considerably the transmission optical properties so that 0.24-1% of nitrogen<sup>23,13</sup> in type Ia diamonds raises the limit of UV absorption from 250 to >320nm and reduces the thermal conductivity to 9 W/cm<sup>2</sup>·K (25°C). In contrast type IIa diamonds are practically free of nitrogen and are subsequently transparent in the UV above 225nm. The need to adopt a gaseous hydrocarbon precursor in most CVD and PVD technologies, typically a mixture of ~99% H<sub>2</sub> and 1% hydrocarbon, has resulted in large



impurity levels of hydrogen in the films. The hydrogen content is a parameter which greatly influences the mechanical and material performance<sup>24</sup>.

Vapour synthesis of diamond (and to a lesser extent Diamond-like carbon) suffers from some inherent problems, not least of these being poor adhesion against steel and other ferrous substrates and generally a high intrinsic stress. This stress increases with thickness to a critical point where the coating debonds completely from the substrates and in certain processes limits the maximum thickness to less than 1-2 $\mu$ m. Thermal annealing during/after deposition together with ion bombardment has improved the control of the stress and adhesion in the film. Traditionally synthetic diamond has been limited to substrate materials with similar lattice parameters, however progress in this direction is increasing with epitaxial growth of diamond reported on nickel, c-BN<sup>25</sup> and iron for the first time<sup>26</sup>.

Diamond-like carbon films, both hydrogenated and non-hydrogenated, have an effective operating temperature of between 400-500°C since at the lower end of this temperature range, both physical, optical and chemical property changes are witnessed due to the atomic structural rearrangement in the form of graphitic bonding.

## 2. Characterisation of Diamond & Diamond-like films

Determining whether a film can be termed diamond, diamond-like or polymeric can be a difficult task. The problem being one of assessing the quantity of tetrahedral  $sp^3$  covalent bonding present in the film and measuring the extent to which the material is crystalline. The analysis is made more difficult when one considers the extent of the possible structures for diamond-like carbon (amorphous, micro crystalline, macro crystalline, single crystal or mixture), together with the affect of impurities (hydrogen, oxygen, argon) and structural defects resulting from the deposition processes. Whilst the presence of bonded impurities in amorphous structures adversely affects the long range bonding order, unbonded impurities can be incorporated interstitially or substitutionally in the diamond lattice, so that some doping can be performed with insignificant structural defects.

Two methods most commonly utilised to differentiate between the structure of diamond and diamond-like thin films are Raman and X-ray diffraction (XRD). Only those films which display the simultaneous characteristic XRD and Raman spectra can be said to be diamond. Thus amorphous films with  $sp^3$  bonding approaching 100% cannot, for the purposes of this terminology, be referred to as diamond since this label would imply a significant degree of crystallinity which they do not possess. Such films are termed hydrogenated or non-hydrogenated diamond-like films depending on the proportion of bonded hydrogen present.

A diamond film for the practical purposes of this study must contain a minimum degree of crystallinity equivalent to an average grain size of  $\sim 100\text{\AA}$ <sup>27</sup>, below which X-ray diffraction patterns characteristic of diamond, are not reliably observed. XRD requires a high degree of interpretation and consideration of many factors. For instance, the relative intensity of the diffraction patterns can vary greatly depending upon the crystallographic planes being observed and their orientation. The patterns produced may be distorted, shifted or weak due to stress distortion, defects or crystal size, but their presence is essential for diamond verification. The problems of interpreting XRD data was highlighted recently by an apparent 'discovery' of diamond through a novel recrystallisation technique (Chap.II Sec.C2(f)). However, further XRD/TEM results showed highly oriented pyrolytic graphite to be the source of the misleading results.

Raman, unlike XRD, is sensitive to non-diamond and graphite phases as well as crystalline material within the sample, making it a more useful technique for analysing the structure of hydrogenated and non-hydrogenated diamond-like carbon films. The resulting spectra can be resolved into two components; first and second order scattering. Generally the second order scattering occurs at twice the frequency to the first order phonon scattering event. The characteristic first order scattering frequency (single phonon interaction) of diamond and graphite is  $1332.5\text{cm}^{-1}$  and  $1580\text{cm}^{-1}$  respectively<sup>28</sup>; the higher frequency of diamond over graphite being indicative of the stronger bond strength (Fig.VII). An increase in disorder, defects and a reduction in crystal size decreases the intensity and broadens the full width half maximum (FWHM) of the characteristic peaks. In addition shifts of up to  $\pm 4\text{-}8\text{ cm}^{-1}$  can be present depending upon the residual stresses in the film<sup>29</sup>.

The presence of increasing disorder and decreasing crystal size begins to give rise to secondary phonon interactions resulting in a second and higher Raman frequency. The two peaks in micro-crystalline graphite represent the defect induced disorder at  $1330\text{-}1350\text{cm}^{-1}$  (D peak) and an associated broader peak at  $1500\text{-}1600\text{cm}^{-1}$  known as the G peak. This large, poorly defined feature in the spectrum has been a topic of debate between those who attribute it to the presence of graphitic  $\text{sp}^3$  hybridised bonds and those which suggest that it represents the presence of a disordered diamond-like phase with percentages of  $\text{sp}^2$  and  $\text{sp}^3$ . The relative intensities of the D and G peaks is said to relate to the proportion of diamond and disordered carbon in the film or more simply its nearness to diamond. However until such time as the interpretation of the G peak is clarified, this idea can not be fully accepted. Furthermore, Raman sensitivity to graphite is 55 times greater than for diamond which sometimes makes it difficult to resolve the diamond contribution from the broad  $1355\text{cm}^{-1}$   $\text{sp}^2$  disordered feature.

Diamond-like carbon is characterised by a Raman spectrum with a first order broad band around  $1520\text{cm}^{-1}$  and a weaker signal at  $\sim 3000\text{cm}^{-1}$  due to second order, carbon-carbon vibrational modes<sup>30</sup>. Similarly highly oriented pyrolytic graphite (HOPG) is characterised by a sharp peak at  $1576\text{cm}^{-1}$ <sup>31</sup> (Fig.VIII).

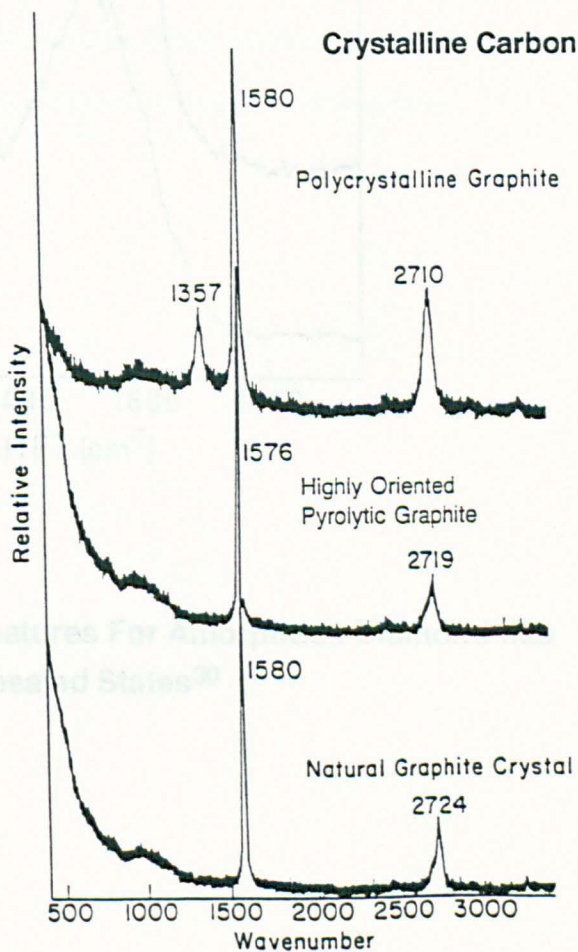
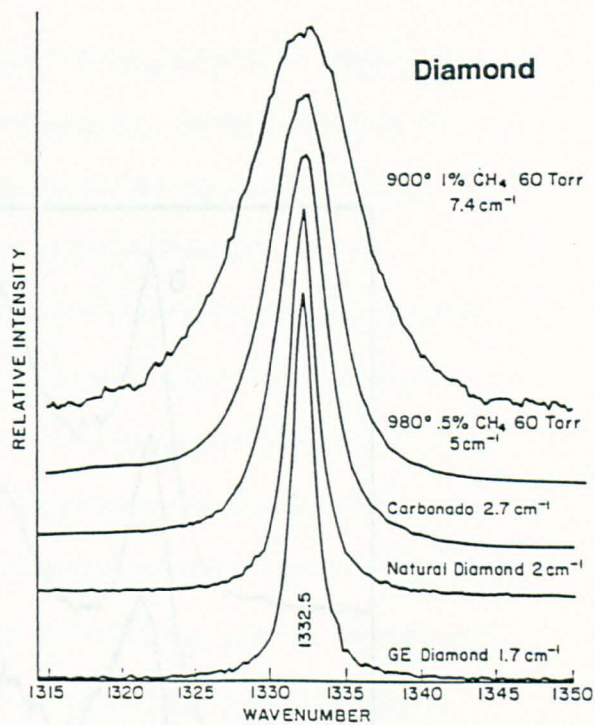
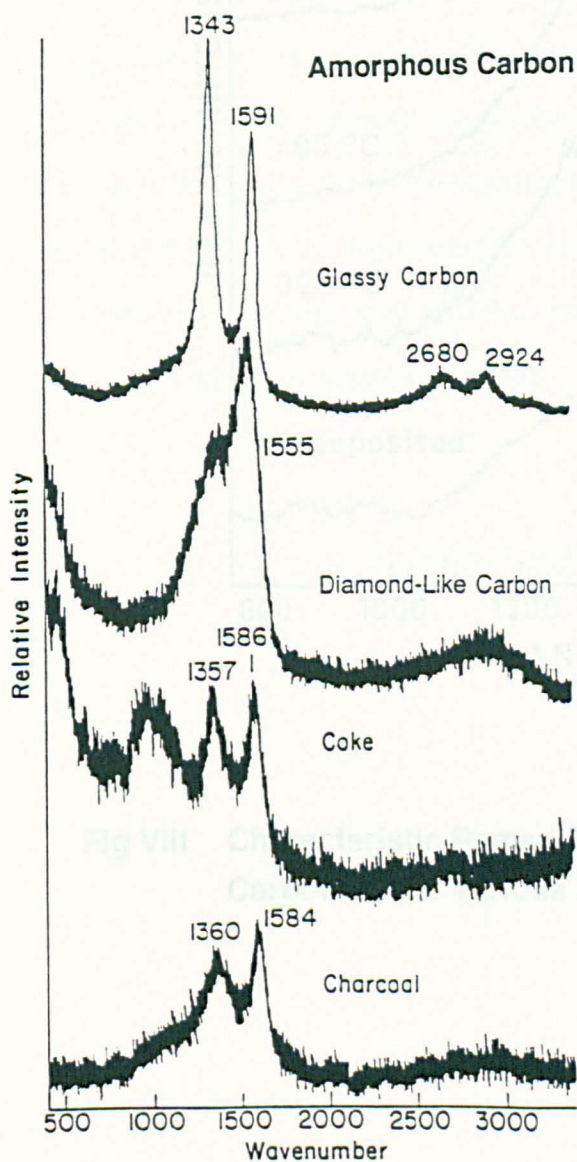


**Fig VII Characteristic Raman Signatures For Diamond and Amorphous/Crystalline Forms of Carbons<sup>31</sup>**

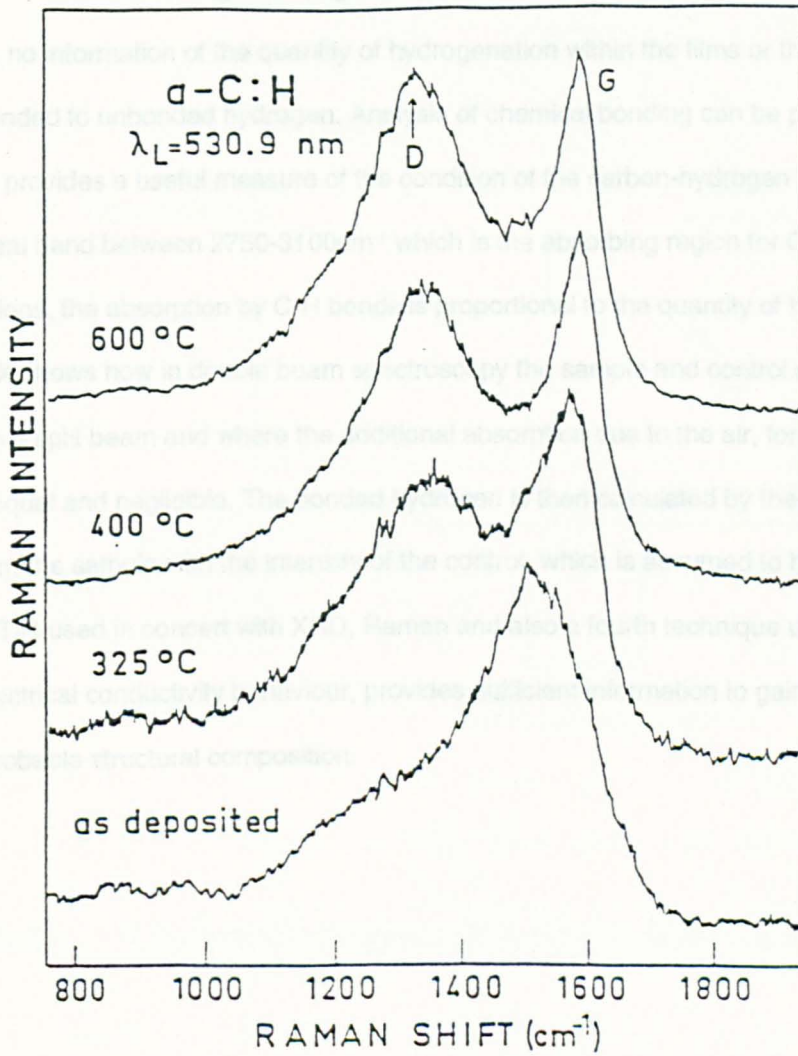


**Fig VIII Characteristic Raman Signatures For Amorphous Diamond-like Carbon Under Various Annealed States<sup>30</sup>**

Despite some small uncertainties in interpretation, Raman remains the single most important method for analysing the 'quality' of carbon films and assessing the proximity of amorphous films to diamond through bonding considerations. However XRD and Raman techniques give no information of the quantity of hydrogenation within the films or the proportion of bonded to unbonded hydrogen. Analysis of chemical bonding can be performed using FTIR and provides a useful measure of the condition of the carbon-hydrogen bonds. Using the spectral band between  $2750\text{-}3100\text{cm}^{-1}$  which is the absorbing region for C-H stretched vibrations, the absorption by C-H bonds is proportional to the quantity of hydrogen in the film. Fig.IX shows how in double beam spectroscopy the sample and control substrate are subjected to a split beam and where the additional absorption due to the air, for both, can be considered equal and negligible. The bonded hydrogen is then calculated by the ratio of the intensity from the sample with the intensity of the control, which is assumed to have little C-H bonding. FTIR used in concert with XRD, Raman and also a fourth technique used to measure the electrical conductivity behaviour, provides sufficient information to gain a good picture of the probable structural composition.

## C. Process Overview

### 1. Background Technology

#### a. Historical Perspective

The first synthetic diamond was made by

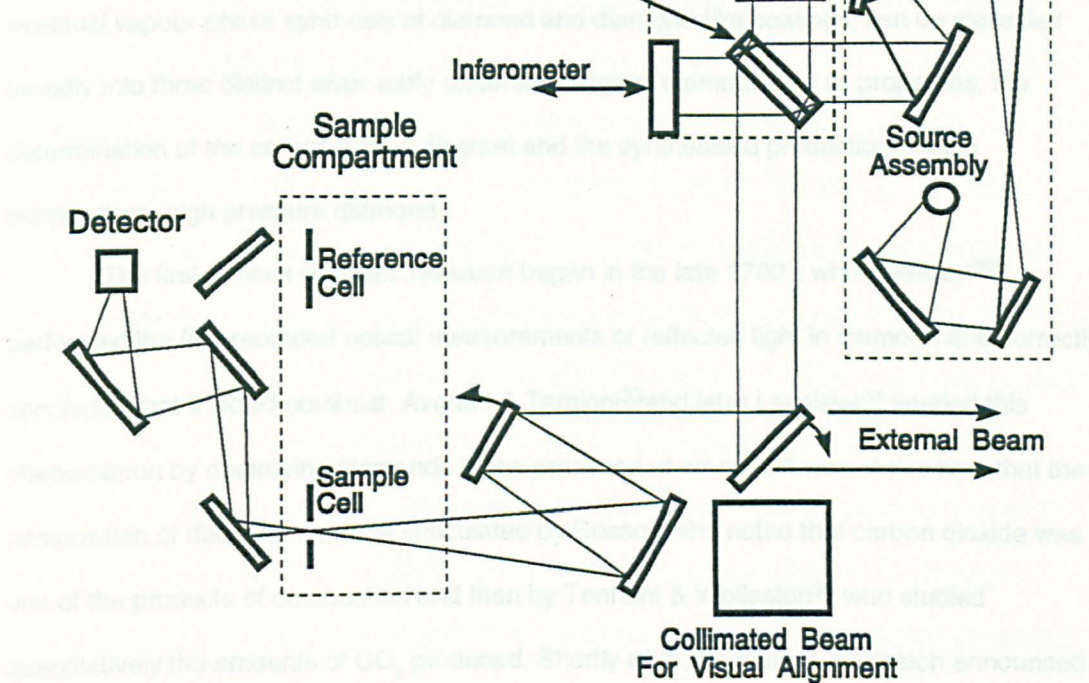


Fig IX A Schematic Diagram Of A Double Beam Spectrometer

by these early discoveries & subsequent successes, motivated by the

prospect of synthesizing diamonds, took up the challenge and attempted experiments. This

early and colorful part of the history abounded with fraudulent claims of synthesis and is well

documented in the literature<sup>20-21, 23-25</sup>. However, there remains the distinct possibility that in

several cases, the first successful synthesis may have actually occurred<sup>26-28</sup>.

A second resurgence of interest occurred when it was finally realized that a simple

transition from carbon to diamond did not exist, at least not at the near atmospheric

conditions most of these early experiments were being performed under. Knowledge of the

synthetical properties of natural diamonds, indicated that during the history of materials or

such moments, high-temperature and high-pressure must have been present. This led to

the pursuit for the dependence between pressure and temperature at which diamonds and

## **C. Process Overview**

### **1. Background To Technology**

#### ***a) Historical Perspective***

The major historical events concerning the synthesis of diamond, leading up to the eventual vapour phase synthesis of diamond and diamond-like coatings, can be classified broadly into three distinct eras: early understandings of diamond and its properties, the determination of the carbon phase diagram and the synthesised production of high temperature, high pressure diamond.

The first serious scientific research began in the late 1700's when Newton<sup>32</sup> performed the first recorded optical measurements of reflected light in diamond and correctly concluded that it would combust. Averani & Targioni<sup>33</sup> and later Lavoisier<sup>34</sup> verified this phenomenon by destroying diamonds in the presence of air only. It was at this time that the composition of diamond was first speculated by Brisson who noted that carbon dioxide was one of the products of combustion and then by Tennant & Wollaston<sup>35</sup> who studied quantitatively the amounts of CO<sub>2</sub> produced. Shortly after, Tennant & Wollaston announced that on the basis of the simple chemistry taking place, diamond was composed entirely of carbon. Hence initiating an era of the greater understanding of the chemistry and properties of carbon and the realisation that carbon was the basis for both diamond and graphite.

Inspired by these early discoveries a succession of scientists, motivated by the prospect of synthesising diamond, took up the challenge and attempted experiments. This early and colourful part of the history abounded with fraudulent claims of synthesis and is well documented in the literature<sup>10,11,36,37</sup>. However, there remains the distinct possibility that in several cases, the first successful synthesis may have actually occurred<sup>38,39</sup>.

A second resurgence of interest occurred when it was finally realised that a simple transition from carbon to diamond did not exist, at least not at the near atmospheric conditions most of these early experiments were being performed under. Knowledge of the geographical presence of natural diamond, indicated that during the impact of meteorites or earth movements, high temperatures and high pressures must have been present. This led to the pursuit for the dependence between pressure and temperature at which diamond and

graphite were in equilibrium. Berman & Simon<sup>40</sup>, Rossini & Jessop<sup>41</sup> paved the way forward, but it was Leipunsky<sup>42</sup> in 1939 who finally completed what remains today a largely unaltered carbon phase diagram (Fig.X). He also drew the important conclusion that crystalline diamond could be more advantageously synthesised by recrystallisation from a molten metal because of the higher molecular mobility. Years later Cheria's atmospheric recrystallisation involving the precipitation of diamond from a carbon rich sodium hydroxide solution in a nickel crucible utilises Leipunsky's view on molecular mobility (Chap.II Sec.C2(e)). The phase diagram also led Bridgeman<sup>43</sup>, Bundy & Hall<sup>44</sup> in America to realise that equilibrium could only be achieved if the conditions of temperature and pressure exceeded 20kAtm and 500°K respectively. Conditions of growth at these conditions were found to be slow however, since there was an additional requirement for sufficient thermal energy to activate the bonding rearrangements. Such temperatures (>2000°K) necessitated a corresponding increase in applied pressure (~60kAtm). Finally production of diamond was achieved by Swedish scientists at ASEA in 1953 just ahead of the American group directed by Bundy and Hall at General Electric, who achieved the same feat two years later in 1955. Today, high pressure synthesis has developed into three distinct techniques: static conversion with the aid of catalysts, static conversion without the aid of catalysts and a shock synthesis method. It could be argued that the formulation of the first accurate and reliable phase diagram was the single most important historical feature in the development of HT HP diamond synthesis. It also undoubtedly opened the way for the more recent chapter of vapour phase synthesis.

### ***b) More Recent Events***

Scientific curiosity in vapour phase deposition of films took a serious turn in the late 1950's and early 1960's although evidently Bolton had limited success with the decomposition of acetylene in mercury vapours in 1911<sup>45</sup>. Attention was unfortunately firmly fixed on the now widely accepted thermodynamic equilibrium diamond synthesis via the high temperature, high pressure route. The possibility of utilising kinetic factors in the metastable region of the carbon phase diagram was overshadowed for a long period.

Manipulation of the kinetic factors, such as the energy of the bombarding species, began to be tried in an effort to allow the thermodynamic equilibrium conditions to be

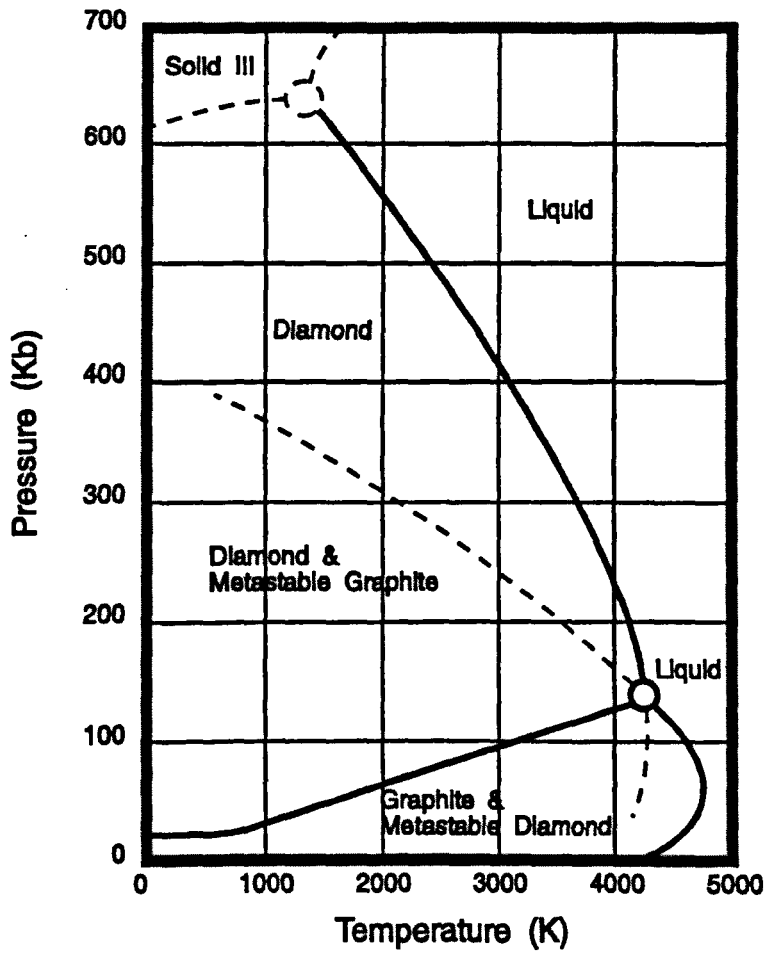


Fig X The Leipunsky Carbon Phase Diagram <sup>225</sup>

circumvented in the region of diamond's metastability. Control of the energised ions was sufficient to induce irreversible physical and chemical changes through a series of processes involving collision cascades, recombination, interstitial penetration and sputtering. The latter phenomenon is a distinctive element of high energy ion bombardment, the upper limit of energy being governed by the point where the sputtering/etching action exceeds deposition. For ions of energy  $\sim 1$  keV, microscopically localised temperature rises or spikes ( $1000^\circ\text{C}$ ) can develop in atomic cascades which are translated into a localised pressure rise of  $\sim 10^9$  Pa through a thermal shock wave. Diamond and diamond-like materials generally have excellent thermal conductivity properties thus keeping any thermal rearrangements to a minimum. A highly disordered and amorphous network results from this behaviour although ordering of the structure can be encouraged by raising the substrate temperature.

After the initial early efforts by Bolton, the subject declined until the late 1950's when excellent work by Derjaguin and Fedoseev was first reported in the West<sup>4</sup>. Their theories of metastable deposition were treated with some acrimony by fellow scientists who were sceptical of the kinetic route and who argued that preferential growth of graphite would arise. This latter phenomenon did in fact occur, but the two Soviet scientists overcame this problem by adopting a cyclic process of deposition and chemical etch. They managed to deposit epitaxially grown diamond from hydrocarbon precursors onto diamond seed crystals. This was achieved by alternating the deposition from thermal decomposition to a hydrogen etch whenever they observed the preferential growth of graphite, thereby removing the graphite before continuing again with the period of growth. Deposition of crystalline diamond was later achieved homoepitaxially and on metallic surfaces by Derjaguin & Spitsyn<sup>46</sup>. In 1962, Eversole filed the first patent applications<sup>47,48</sup> utilising a very similar process to Derjaguin and Fedoseev. The results were impressive: electron diffraction showed them to be crystalline and further analysis showed them to have a high purity.

At a similar time Schmellenmeier<sup>49</sup> was also having success with what turned out to be the earliest diamond-like coatings, found fortuitously as the by-product of electrical discharges in the presence of a hydrocarbon gas. He utilised a DC plasma and introduced acetylene into the discharge. He postulated the presence of diamond formations within the

films but they were more probably graphitic films with significant hydrogen and  $sp^3$  content. Thus two clearly different and parallel research efforts continued to emerge; one with the ultimate goal of achieving heteroepitaxially grown crystalline diamond and another effort concerned with the hard, dense and amorphous forms of carbon being produced by glow discharge disassociation of hydrocarbon precursor materials.

A problem however remained concerning both approaches and this amounted to the poorly understood role of hydrogen in the reactive process. Its importance was first noted by Derjaguin et al when they related the rate of diamond formation with the partial pressure of atomic hydrogen liberated by the hydrocarbon precursor. Eventually it was realised that a dominant presence of hydrogen in the deposition chamber was advantageous, resulting in typical  $H_2/C_nH_m$  mixtures used today of 98-99.9%  $H_2$  and 0.1-2%  $C_nH_m$  with temperatures of greater than 800°C. Even at the present time, two views on the role of hydrogen exist. The initial theory suggested by the Soviet scientists that the suppression of graphite relative to diamond was being achieved because of the widely different gasification rates of the two materials and the knowledge that graphite reacts readily with atomic hydrogen. Thus the growth of diamond was possible by virtue of the fact that it was more kinetically stable, in such conditions, relative to graphite. This theory however fails to account for some deposition conditions used today which use high pressures and temperatures lower than 400°C, where a dramatic reduction in the kinetic mobility of the depositing species occurs and yet deposition continues to take place.

The opposing opinion holds that the kinetic argument is misleading and may even be erroneous. The large quantity of atomic hydrogen produced by the thermal or plasma dissociation of  $H_2/C_nH_m$  in a typical CVD process is thought to stabilise the surface of the diamond rather than preferentially etch the graphite. C-H bonding at the diamond surface stabilises the otherwise unbonded or 'dangling' bonds preventing weaker  $sp^2$  C-C bonds from forming<sup>50,51</sup>. The suppression of graphite would then result from the thermodynamic stability of the surface rather than any kinetic competition with diamond. Hence, while the kinetic argument can explain in simple terms the growth of diamond over graphite, it cannot explain why cubic diamond is always synthesised and not the ABAB lattice network found in

lonsdaleite. Unfortunately this theory is also flawed. The stabilisation process assumes that inherently hydrogen must exist in quantities of many hundreds of times greater than carbon so that all the potential growth sites can be stabilised. Combustion flame processes however operate with a H/C ratio of unity and still diamond can be formed (Chap.II sec.C2(a)). It can be argued that the presence of some other agent, in this case the likely candidate would be oxygen, is having an equally influential affect. Indeed it seems almost inconceivable that elements other than hydrogen were not involved in the natural production of diamond. Small quantities of iron<sup>36</sup>, oxygen<sup>52</sup> and nitrogen were often reported to be beneficial in stimulating diamond growth in some early synthesis attempts.

Further research has been carried out to understand the function of hydrogen in the reaction gas process more fully. Gas mass analysis experiments<sup>53</sup> have been performed and seem to indicate that the presence of hydrogen aids the formation of one or several secondary species responsible for growth. CH<sub>3</sub> is the most likely candidate although extensive testing including isotope tracing of <sup>13</sup>C have drawn no firm conclusions<sup>54</sup>.

### ***c) CVD Diamond Development***

After the early work of Derjaguin, Fedoseev and Spitsyn, a lull in activity of crystalline diamond synthesis occurred until in 1982 when Setaka & Matsumoto announced several major breakthroughs. First they utilised hot tungsten filaments<sup>55,56</sup> and RF glow discharges<sup>57</sup> then microwave plasmas<sup>58</sup> to produce polycrystalline diamond films at a rate far exceeding that of previous thermal techniques. Substrates were silicon and molybdenum and the temperatures were kept relatively high (>400°C) so that the removal of hydrogen in the films could be encouraged. It was quickly realised that the variety of hydrocarbon sources used (Appendix II) did not significantly affect the eventual properties of the film, only the deposition rate. Ideally a 100% reduction of the precursor into its constituent parts is required and in order to achieve this, greater levels of ionisation was achieved by progressively higher frequency agitation of the plasma. Indeed low frequency plasmas have been shown to produce more of the undesirable sp<sup>2</sup> bonded carbon than higher frequency RF plasmas<sup>59</sup>. Electron cyclotron resonance microwave CVD<sup>64</sup> deposition operates at typically 10<sup>-4</sup>-10<sup>-2</sup>Torr to achieve plasma densities of 10<sup>11</sup>cm<sup>-3</sup> compared to corresponding values for typical RF

plasmas of  $10^{19}\text{cm}^{-3}$ . Certain techniques support sufficiently intense energy environments for chemical reaction and rearrangement to occur readily at atmospheric pressure conditions. A chronological view of the CVD techniques illustrates graphically how, with newer methods, the ionisation and plasma density levels have increased, simultaneously improving properties of the films:

#### **Thermal Assisted CVD**

Thermally assisted CVD<sup>60,61</sup>

Hot Filament CVD<sup>62,63,64</sup>

Electron Assisted Hot Filament CVD<sup>65</sup>

#### **Plasma Assisted CVD**

DC Plasma CVD<sup>66</sup>

RF (Low Freq. 50kHz) CVD<sup>67</sup>

RF (Low Freq. 380kHz) CVD<sup>68</sup>

RF (Low Freq. 2.3MHz) CVD<sup>69</sup>

RF (High Freq. 14MHz) CVD<sup>70</sup>

RF (High Freq. 13.56MHz) CVD<sup>71,72</sup>

RF (High Freq. 27MHz) CVD<sup>73</sup>

Microwave (2.45GHz) Assisted CVD<sup>74</sup>

UV & Laser Assisted Deposition<sup>75</sup>

Hot, Hollow Cathode<sup>76</sup>

Electron Cyclotron Resonance<sup>77</sup>

#### **Flame & Jet Methods**

Combustion Flame<sup>78,79</sup>

DC plasma jet<sup>80</sup>

By the mid 1980's the Japanese and Soviet research was extensive and well established, whereas American and European research involvement in this area had been patchy. In these countries the situation soon changed after it became obvious that the Japanese had solved many of the major difficulties concerning nucleation and growth. Research started hurriedly again in America with duplication and extension of the Japanese radio frequency and microwave plasma work being undertaken at Pennsylvania State University. Larger initiatives were then instigated primarily as a result of the SDI military programme.

#### **d) PVD Diamond & Diamond-like Development**

Following the findings of Derjaguin, PVD techniques were proving themselves beneficial in the synthesis of diamond-like films. Agarwell & Haubold<sup>81</sup> were able to electron beam evaporate carbon into an argon plasma at negative bias voltages of 1.5-5.0kV. Such high voltage conditions were not conducive to non defective growth of sp<sup>3</sup> bonded carbon layers, at a good rate. It was left to the work by Aisenberg and Chabot<sup>82</sup> in 1971 to demonstrate that at lower deposition energies than had previously been contemplated (>100eV), the production of amorphous films up to 3µm thick could be successful. The method they used was described as an ion beam because ions of carbon and argon were generated by an arc within the source and accelerated as a fully directional beam to the substrate. The announcement of this caused a resurgence of interest not least because the films appeared to be more intuitively promising and more immediately capable of use commercially, especially because of their relatively high deposition rates. The films were analysed in terms of hardness, optical and crystalline properties. They were found to be insoluble in organic acids and to have DC resistivities of greater than 10<sup>12</sup>Ωcm. Further work identified the presence of sp<sup>2</sup> and sp<sup>3</sup> bonding configurations and X-ray and electron diffraction<sup>83</sup> studies indicated an amorphous character with crystalline regions 5µm across.

The enormous interest in diamond-like coatings was continued by Weissmantel et al<sup>84</sup> using single and double ion beam sputtering techniques, Martin & McKenzie<sup>85</sup> using DC arc evaporation of graphite and Koskinen who experimented with the direct implantation of <sup>12</sup>C<sup>+</sup> ions<sup>86</sup>. The range of PVD techniques in use today is considerable and include the following:

##### **Ion Sources**

FAB source<sup>87</sup>

Kauffman Ion source<sup>88,89</sup>,

Ion Beam sputter<sup>90</sup>

Dual Ion beam sputter<sup>91</sup>,

Mass selected C<sup>+</sup> ion beams<sup>92</sup>

Ion Implantation (C<sup>+</sup>)<sup>93</sup>

Evaporation & Implantation(N<sub>2</sub><sup>+</sup>) of Pentaphenyl Silioxane  
& Polyphenyl Ether<sup>94</sup>

DC magnetron sputtering<sup>95</sup>

## Evaporation

Pulsed Arc-Discharge<sup>96,97</sup>

Electron Beam Evaporation<sup>88</sup>

Laser Evaporation<sup>98,99</sup>

Pulsed Electromagnetic Inductive Plasma CVD<sup>100</sup>

Several excellent review papers exist on the subject of the interdependence of plasma properties such as bias voltage and hydrogen content on the mechanical, electrical and optical properties of diamond-like films<sup>101,102</sup>.

### **e) Nucleation**

During the homoepitaxial nucleation of diamond, the most stable planar growth is found in the octahedral (111) surface followed by the (100) and (110) planes respectively. Thus under deposition conditions close to equilibrium, the growth of polycrystalline diamond occurs in a predominantly triangular or octahedral habit (111) whilst conditions progressively more distant from equilibrium result in, first the cubo-octahedral arrangement before a cubic (100) form establishes itself as the dominant crystalline habit. This rudimentary and simple concept reflects the presently scant understanding of the exact conditions and mechanisms leading to the production of crystalline surface structures. What is realised however is that the preferred morphology is profoundly dependent on the deposition conditions. Of these conditions, the hydrogen or oxygen to hydrocarbon ratio is known to be one of the significant factors demonstrated by recently performed combustion flame experiments (Fig.XI). Temperature also is widely acknowledged to be highly influential, such that above typically 1200°C non-diamond or micro-crystalline graphite is readily formed and below 800°C amorphous carbon is witnessed. Between these extremes diamond is formed with well faceted structures occurring in a small temperature band. Transition through this temperature band produces a transformation of the diamond morphology from one crystal habit to another, similar to that of increasing mixture ratio. It appears that the relative growth rates of the most energetically favourable crystal planes is not great, such that small changes in growth conditions have a considerable effect on the relative crystal growth rates and final morphology, which makes reproduction of previous attained deposition conditions exceedingly difficult.

The mechanism of diamond growth on non-diamond is another area which has yet to be fully clarified. Results of deposition periods of several minutes to many hours have been examined to date. It has been found that indications of diamond are observed. Scratching of the substrate surface is a commonly used as a pre-treatment to minimize the induction period, and nucleation and enhance the density of nuclei. This is achieved successfully to date by

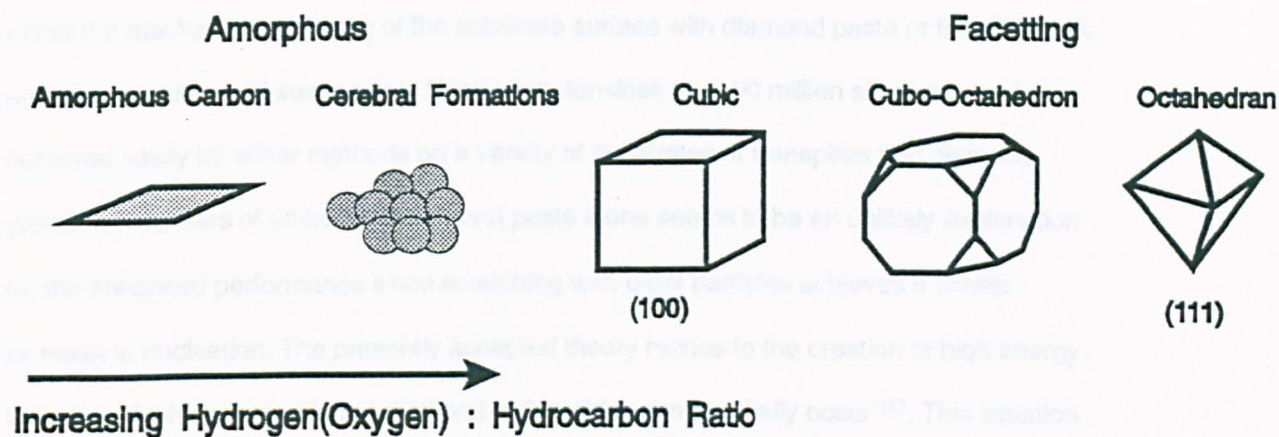


**Fig XI A Simple Model Of The Dependence Of Crystal Morphology On Deposition Conditions**

Modern methods of ultrasonic, selective techniques which involve the complete oxidation of the substrate at elevated temperature for 12 hours to 1.0-1.5 μm surface depth of oxide. This is then photo-lithographically patterned using a oxide mask (Fig 1-6). By carefully controlling the ultrasonic energy of the 50um diameter methanol dispersion, selective and movement of the substrate surface can be achieved where the photo-lithographic mask has been etched away<sup>124</sup>. Another selective dry nucleation technique known as electrophoretic seeding has recently been reported. Again an oxide or polymer mask is created on the surface which is then subjected to electrolysis where the selected microscopic diamond particles and water. Embedding of the diamond is sufficiently selective to resist removal by ultrasonic agitation. High surface densities can then be achieved using standard microwave CVD deposition techniques already mentioned.<sup>125</sup>

The mechanism of diamond growth on non-diamond is another area which has yet to be satisfactorily resolved. Induction periods of several minutes to many hours have been observed to take place before the first indications of diamond are observed. Scratching of the substrate's surface is extensively utilised as a pre-treatment to minimise the induction period, aid nucleation and enhance the density of nuclei. This is achieved successfully to date by either the mechanical polishing of the substrate surface with diamond paste or the ultrasonic agitation in a diamond suspension. Nucleation densities of ~100 million sites/cm<sup>2</sup> can be achieved easily by either methods on a variety of substrates. It transpires that diamond growth on residues of embedded diamond paste alone seems to be an unlikely explanation for the enhanced performance since scratching with c-BN particles achieves a similar increase in nucleation. The presently accepted theory relates to the creation of high energy locations at which nucleation of diamond is thought to preferentially occur<sup>103</sup>. This situation however is made more complicated by the apparent differences in nucleation between abrading material of the same grade and pastes of different particle size.

Somewhat contradicting the present beliefs, Badzian proposed that in the case of silicon substrates the formation of a SiC diffusion zone was being created, producing chemically favourable conditions for diamond nucleation. The previously mentioned induction period then being the time taken for the formation of this zone.

Modern methods of pre-treatment include ultrasonically selective techniques which involve the complete oxidation of the substrate at elevated temperatures for 12 hours to 1.0-1.5µm case depth of oxide. This is then photo-lithographically patterned using a oxide (HF:NH<sub>4</sub>F 1:6). By carefully controlling the ultrasonic energy of the 90µm diamond/methanol suspension, selective pre treatment of the substrate surface can be achieved where the photo-lithographic mask has been etched away<sup>104</sup>. Another selective area nucleation technique known as electrophoretic seeding has recently been reported. Again an oxide or photoresist is created on the surface which is then subjected to electrolysis where the solution comprises diamond particles and water. Embedding of the diamond is sufficiently effective to resist removal by ultrasonic agitation. High nucleation densities can then be achieved using standard microwave CVD deposition techniques already mentioned<sup>105</sup>.

Latest reports indicate that the extensively used wet polishing treatment might be superseded by a technique using short exposures of high energy ion bombardment in a 60:40 hydrogen:methane atmosphere to a substrate held at negative voltage. Densities of 10 billion crystals/cm<sup>2</sup> have been quoted compared to densities of approaching 1 billion crystals/cm<sup>2</sup> for scratching techniques<sup>106</sup>.

## 2. Latest Developments

In finishing this section, the author has taken the opportunity to review several interesting, and undoubtedly important, current areas in carbon research:

### a) *Peter Bachmann's C-H-O CVD Diagram*

The range of CVD processes together with the variety of hydrocarbon and organic precursors has been shown in previous sections to be extensive, leaving the rationalisation of the diamond growth region for many deposition methods an almost impossible task. However such a discerning approach has been put forward by Peter Bachmann in the form of a C-H-O ternary diagram (Fig.XII). The outcome of diamond synthesis is plotted on the diagram by knowing the atomic percentages of C, H & O taking part in the reaction. A clearer picture is then formed of the regions in which low pressure diamond synthesis is possible and the associated non-diamond and no growth regions.

The diagram has the advantage of encompassing all the deposition information to date from early CO plasma experiments to typical CVD gas mixtures ( $H_2/CH_4 < 1$ ) used extensively today, as well as ethane, ethylene and combustion flame processes. The single most important feature of the diagram is a thin wedged shaped growth domain, extending for all percentages of hydrogen, along the carbon monoxide line. For gas compositions close to or on this line, diamond has been known to form experimentally.

Established approaches using acetylene or methane with the addition of large amounts of hydrogen bisect this region at progressively narrow bands where quite clearly the small presence of oxygen becomes critical (enlarged section). The traditional approaches using CO have unknowingly provided the most susceptible conditions for growth since as long as the carbon/oxygen ratio continues to be equimolar, the quantity of hydrogen is unimportant. Another important fact which the data suggests is that under no circumstances will diamond be formed for any hydrogen/carbon dioxide mixtures. The implication being that on this side of the oxygen rich growth domain, conditions are such that chemical etching of the diamond is preferentially occurring.

Quite clearly the diagram demonstrates that while the presence of hydrogen is essential, its quantity is not. Alternatively the presence of oxygen/carbon ratio is singularly the

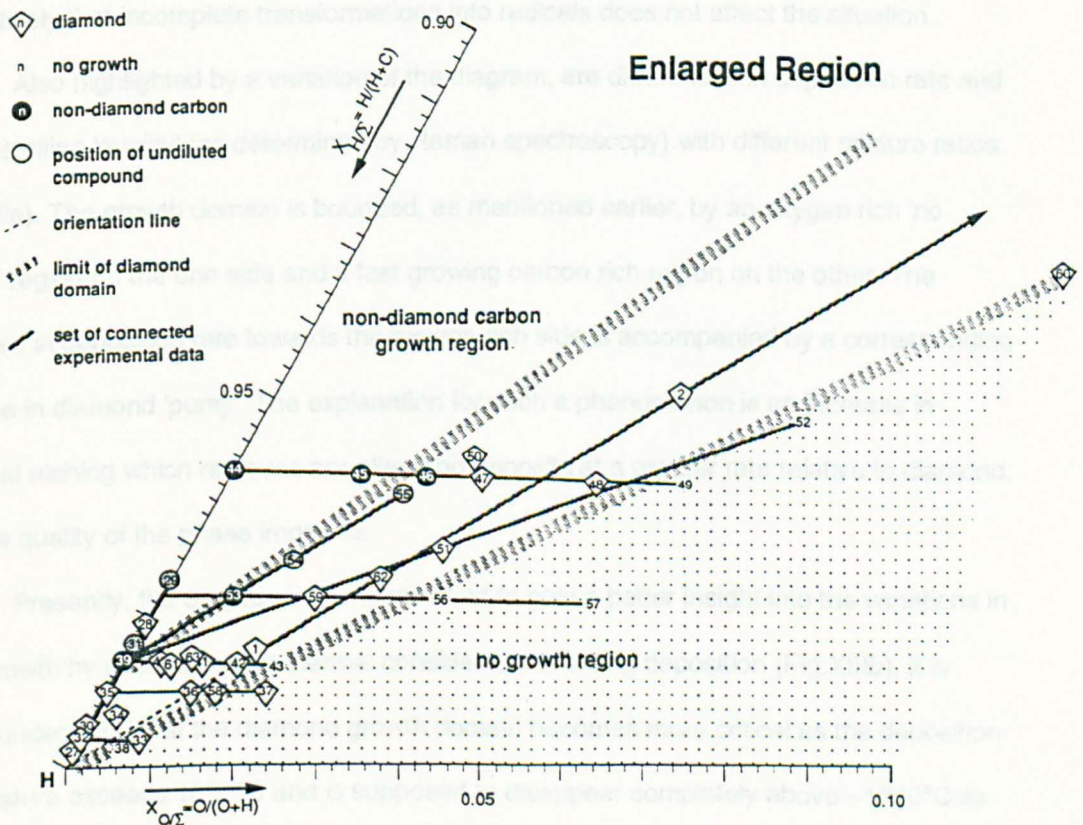
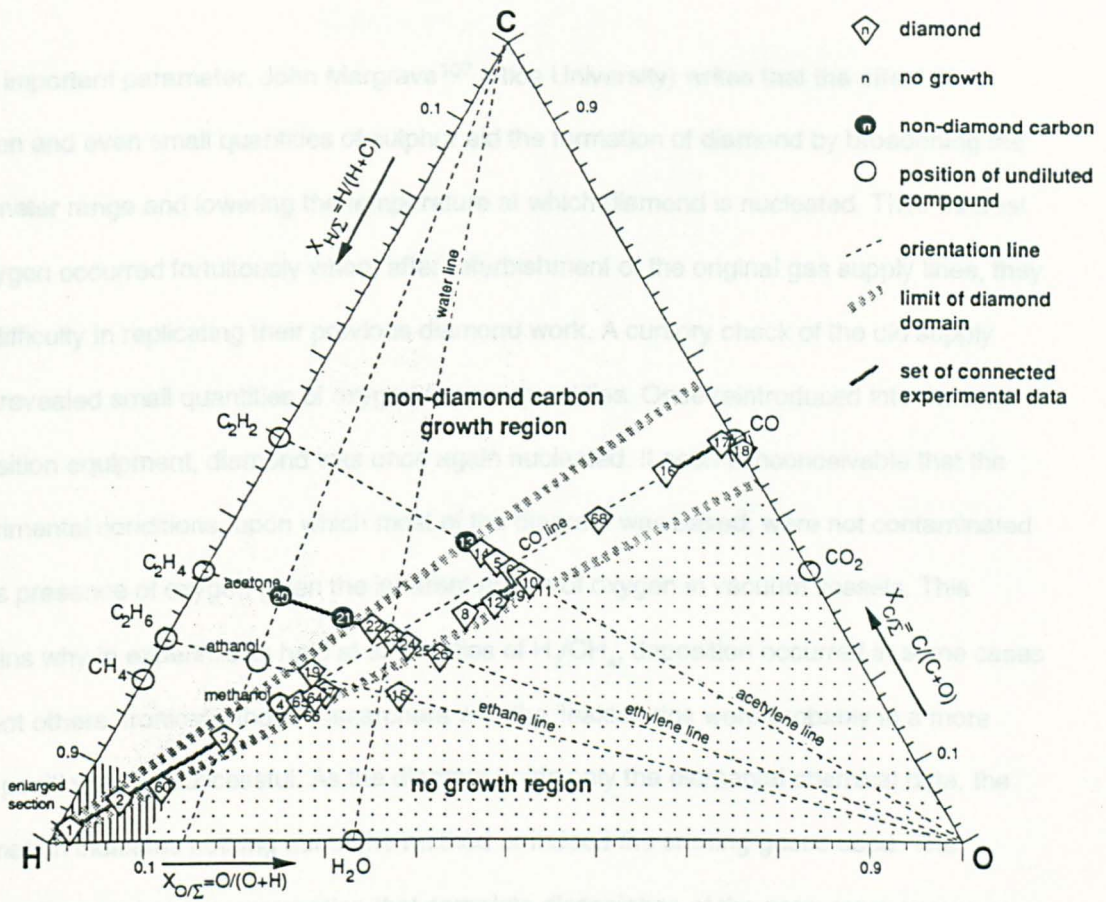


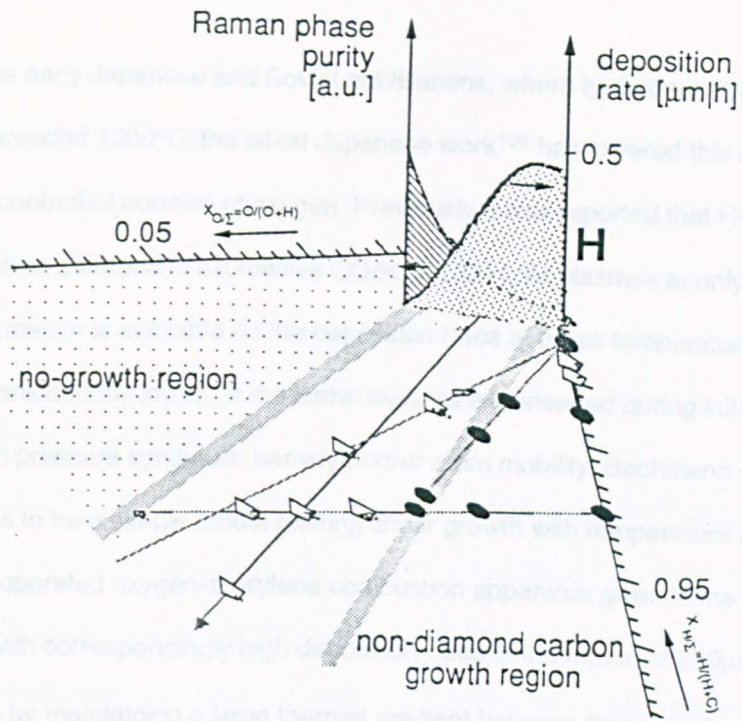
Fig XII

The C-H-O Ternary Diagram

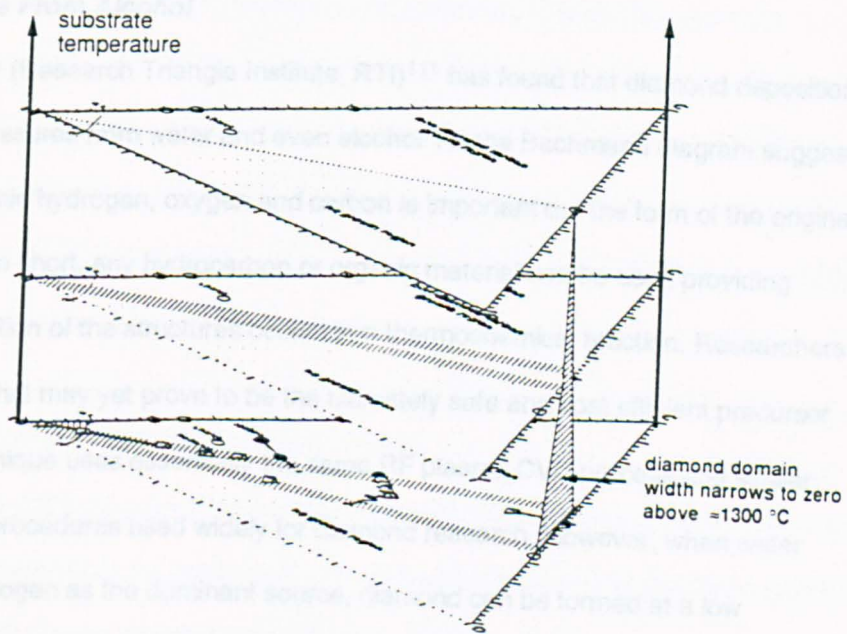
most important parameter. John Margrave<sup>107</sup> (Rice University) writes that the effect of oxygen and even small quantities of sulphur aid the formation of diamond by broadening the parameter range and lowering the temperature at which diamond is nucleated. Their interest in oxygen occurred fortuitously when, after refurbishment of the original gas supply lines, they had difficulty in replicating their previous diamond work. A cursory check of the old supply lines revealed small quantities of oxygen in ppm quantities. Once reintroduced into the new deposition equipment, diamond was once again nucleated. It seems inconceivable that the experimental conditions, upon which most of the diagram was based, were not contaminated by the presence of oxygen given the inherent nature of oxygen in vacuum vessels. This explains why in experiments held at strict ratios of  $H_2/CH_4$ , deposition occurred in some cases and not others. Ironically those researchers with the 'leakier' rigs were probably in a more likely position to be successful. As the diagram holds only the elemental chemical data, the information indicates nothing about the method or indeed the starting gases used. The diagram thus makes the assumption that complete dissociation of the precursors occurs or alternatively that incomplete transformations into radicals does not affect the situation.

Also highlighted by a variation of the diagram, are differences in deposition rate and polycrystalline 'quality' (as determined by Raman spectroscopy) with different mixture ratios (Fig.XIIIa). The growth domain is bounded, as mentioned earlier, by an oxygen rich 'no growth' region on the one side and a fast growing carbon rich region on the other. The decrease in deposition rate towards the oxygen rich side is accompanied by a corresponding increase in diamond 'purity'. The explanation for such a phenomenon is an increase in chemical etching which removes non-diamond deposits at a greater rate relative to diamond, thus the quality of the phase improves.

Presently, the diagram is being modified to gain a better insight into the variations in CVD growth by encompassing thermal considerations during deposition (Fig.XIIIb). It is widely understood that the diamond growth domain becomes more critical as the deposition temperature exceeds 1000°C and is supposed to disappear completely above ~1300°C as graphite begins to be deposited. The work is still being researched and its result and implications will be of immense interest in all areas of diamond synthesis.



**a) Deposition Rate & Purity**



**b) Deposition Temperature**

**Fig XIII The C-H-O Ternary Diagram**

Since the early Japanese and Soviet publications, where typical substrate temperatures exceeded 1000°C, the latest Japanese work<sup>108</sup> has lowered this minimum limit to 130°C by the controlled addition of oxygen. Previously it was reported that Hitachi had grown polycrystalline diamond in microwave CO/H<sub>2</sub> & CO/H<sub>2</sub>/Ar plasmas at only 410°C<sup>109</sup>. Although no information is available on the deposition rates at these temperatures, it is expected to be considerably lower for the same reasons experienced during initial high temperature, high pressure synthesis: namely poorer atom mobility. Bachmann demonstrates that there appears to be a simple model relating linear growth with temperature of the gas phase. Optimum operated oxygen-acetylene combustion apparatus gives flame temperatures of 2900-3000°C with correspondingly high deposition rates in the region of 200µm/hr<sup>110</sup>. The method succeeds by maintaining a large thermal gradient between flame or plasma and the substrate surface, by means of rapid cooling of the specimen. Thus thermodynamically stable conditions are achieved at lower surface temperatures of ~1000°C whilst benefiting from the highly efficient thermodynamic reactions occurring in the flame/plasma.

***b) Diamonds From Alcohol***

Ron Rudder (Research Triangle Institute, RTI)<sup>111</sup> has found that diamond deposition can occur at low pressures from water and even alcohol. As the Bachmann diagram suggests the presence of atomic hydrogen, oxygen and carbon is important but the form of the original precursor(s) is not. In short, any hydrocarbon or organic material can be used providing sufficient decomposition of the structures occurs in a thermochemical reaction. Researchers at RTI have found what may yet prove to be the ultimately safe and cost efficient precursor available. Their technique uses essentially the same RF plasma CVD process and similar sample preparation procedures used widely for diamond research. However, when water vapour replaces hydrogen as the dominant source, diamond can be formed at a low temperature (600°C), together with an unexpected reduction in RF power consumption. Thus the researchers headed towards the use of alcohol by introducing sake, Tennessee Bourbon whiskey and Budweisser beer in addition to hydrogen. Nevertheless it was not until a paper on diamond deposition from methanol only, was presented at the 1989 Fall Meeting of the Materials Research Society, that diamond could be truly said to have been synthesised from

alcohol. Their realisation that deposition was possible without additional hydrogen came principally from the findings of Hirose<sup>78</sup>, who used combustion flames to form diamond.

One interesting observation noted in the paper was the increased purity of the diamond produced and that small additions of argon into the feed gas was beneficial to the deposition performance. It is suggested this behaviour is probably due to a contamination of oxygen in argon which is itself derived industrially from the fractionation of air.

### **c) Deposition From Fluorines**

An interesting follow up to their previous work on methanol, Ron Rudder et al successfully attempted direct formation of diamond using halogens<sup>112</sup>. This pioneering work was taken up at Rice University under Donald Patterson who confirmed such a process was feasible for the homoepitaxial growth on type IIa {100} substrates at atmospheric pressure. The method utilises  $CF_4/F_2$  gas mixtures analogous to the pyrolysis of  $CH_4/H_2$  in common plasma and filament assisted CVD techniques. Similarly etching of non diamond deposits takes place after thermal dissociation of  $F_2$ , except that with  $F_2$  this occurs more readily at lower temperatures. The most notable difference in the two methods was the resultant smoother morphology, although heavily faceted polycrystalline diamond has been reproduced on Si{100}. Reports of deposition temperature vary from between 850-875°C at 0.5-5Torr. Current RTI interest has centred on quadrupole mass spectroscopy to detect the behaviour of the  $CF_4/F_2$  mixture during excitation in the plasma. This is the latest in a series of experiments in many laboratories, to determine the affect of hydrogen or halogen in the nucleation of diamond.

### **d) Epitaxial Growth From Combustion Flames**

Since the first publication by Hirose in 1988 several research groups world-wide have concentrated on combustion flame synthesis<sup>84</sup>. The apparatus is based on the commercially available oxy-acetylene torch apparatus and with some additions in the way of mass flow gas control, depositions in the region of 20-200 $\mu$ m/hr can be easily achieved. There are many groups currently studying in this area: including Ravi & Joshi (Lockheed Missile & Space Comp.), Hanssen, Snail & Carrington (Naval Research Labs.), Pfender and Herberlein<sup>113</sup> (University of Minnesota) and Janssen, Enkevort & Gilling (University of Nijmegen). It was

however this latter group who first announced at the Diamond Films 1990 conference that single crystal homoepitaxial growth had been achieved<sup>114</sup>. Shortly afterwards Ravi & Joshi announced similar findings<sup>115</sup>. Both groups claimed epitaxial grow rates up to 100-200 $\mu\text{m/hr}$ .

#### **e) Cherian Recrystallisation Process**

The theoretical considerations of the high pressure, high temperature thermodynamic equilibrium process are largely understood and (despite the often unclear growth mechanisms behind metastable vapour synthesis) the production of diamond by both means has been a great technological achievement. However, Cherian (Sadar Patel University, India) has recently proposed the existence of a third nucleation route which threatens to challenge all the existing theories on nucleation<sup>116</sup>, by revealing an easier route to diamond at atmospheric pressure. In his recent paper on the subject, Cherian discusses the oxidation of diamond by  $\text{O}_2$  and  $\text{CO}_2$  and the resultant formation of  $\text{CO}$  and surface oxides. Further oxidation yields carbon dioxide and graphite. Cherian argues that this process is reversible if dissolution of carbon and surface recrystallisation can take place. Such an idea was put forward by Leipunsky during his work on the carbon phase diagram (Chap.II Sec.C1(a)) when he believed that an increase in atom mobility from the dissolution of carbon in molten metal, would be advantageous. Cherian increased the mobility of dissolved carbon in a sodium hydroxide solution by increasing the temperature to  $\sim 1000^\circ\text{C}$ . On rapid cooling to room temperature ( $>1000^\circ\text{C/min}$ ), the contents of the nickel crucible revealed solidified crystalline carbonaceous remains.

Analysis of the crystals showed the residue to be diamond formed initially, it is suggested, by a complex Ni-C intermediary which subsequently decomposes to facilitate the crystallisation of  $\text{sp}^3$  bonded carbon as diamond. Cherian's postulates that the technique could be used to perform the recrystallisation process more efficiently at lower pressures.

#### **f) Prins's & Narayan's Copper Implantation Process**

Prins (University of Witwatersrand) has attracted considerable attention to another new technique for the growth of epitaxial diamond layers on copper substrates. The attention has largely been a result of his claim in 1989<sup>117</sup> that crystallisation of diamond was subsequently formed from carbon implantation in copper. However, there appear to be

widespread doubts about his claim.

The controversy surrounds a technique which seems to combine the low pressure diamond forming discipline with the reasoning developed from HT HP synthesis. The principle is simple; another substance with a similar lattice spacing parameter to diamond is implanted with carbon ions to a point where levels of implantation reach saturation point in the copper crystal. A carbon structure can then be encouraged to crystallise at the surface, the thickness of which is determined by the implantation dose. Typical candidates for implantation along with copper, are nickel, cobalt and germanium which all share lattice parameters within ~5% of diamond and can accommodate implanted carbon without reaction. However, single crystal {111} or {110} phases of these materials are essential if autoepitaxial diamond is to be formed.

<b>Semiconductor</b>	<b>Lattice Constant (Å)</b>
Diamond	3.567
Silicon	5.43
Silicon Carbide	4.36
Boron Nitride	3.60
<b>Metal (FCC)</b>	<b>Lattice Constant (Å)</b>
Nickel	3.52
Copper	3.61

*Table V Lattice Parameters*

Narayan (North Carolina State University) used ultraviolet (0.308µm) laser heating of the copper to encourage crystallisation at the surface<sup>118,119</sup>. At the implantation doses used, the actual continuous layer thickness of 500Å was achieved against a theoretical layer equivalent of 560Å. This represents almost the maximum layer thickness achievable. However for a laser duration of only 0.45 ηsec at an effective energy density of ~4.5J/cm<sup>2</sup>, it must be a contender for one of the highest deposition rates. The thickness limitation is not considered a problem since it is suggested that this a process can provide a means to precoat an epitaxial layer which can be used as a base for conventional CVD growth techniques.

A sharp Raman signature at  $1332\text{cm}^{-1}$  (FWHM  $5\text{cm}^{-1}$ ) indicates good phase purity but the controversy surrounds the inconclusive X-ray and electron transmission data, which initially were interpreted as diamond by Prins, but turn out to be characteristic of highly oriented graphite<sup>120</sup>. It is not the first time that preferentially oriented structures have caused confusion (Chap.II Sec.B2) and this shows a deficiency in diffraction techniques which is worth highlighting.

**g) *Isotopically Enriched  $^{12}\text{C}$  'White' Diamond***

White diamond refers to the existence of 'clear' polycrystalline CVD growths with thermal conductivity surpassing even that of the best natural type IIa diamonds ( $\sim 21\text{W/cm}\cdot^\circ\text{K}$ ). The thermal conductivity of natural diamond is restricted under normal conditions by three processes; isotope concentration, nitrogen concentration and the presence of grain boundaries. The existence of nitrogen in natural diamond ranges from 4-2800ppm with a typical value for type IIa of  $\sim 50\text{ppm}$ . Interestingly enough, at this contamination level the colour is not clear but a watery whiskey colour owing to the absorption of light in the  $2.5\text{-}6.0\mu\text{m}$  spectral region. Laboratories have managed to fabricate 'clear' diamond at high pressures by minimising the nitrogen content using getters. The rarification process clearly suffers from diminishing returns with the best results reported for Man-Made™ diamond manufactured by General Electric Corporation (thermal conductivity of  $22\text{W/cm}\cdot^\circ\text{K}$  at a nitrogen concentration of  $0.1\text{ppm}$ ).

Another limiting factor for thermal diffusivity is the incorporation of  $\sim 1\%$  of the natural isotope  $^{13}\text{C}$  and in a recently published paper by Anthony et al the feasibility of synthesis of diamond using isotopically enriched methane ( $99.9\% \text{ }^{13}\text{C}$ ) in a CVD reaction chamber was demonstrated<sup>121</sup>. The theoretical arguments predict isotopically pure diamond to increase the diffusivity by  $\sim 5\%$ . However after the pioneering work at General Electric, they showed that for films containing  $0.1\% \text{ }^{13}\text{C}$ , the thermal diffusivity could be increased by up to  $50\%$ , thus achieving the highest values measured by natural or previously synthesised material. It is now predicted that  $^{12}\text{C}99.93\%$  pure diamond could achieve a thermal conductivity as high as  $35\text{W/cm}\cdot^\circ\text{K}$ .

## ***h) Fullerenes***

For the past six years, chemists and scientists have been gathering overwhelming evidence to suggest a further allotrope of carbon, known generically as fullerenes. The most widely known of these is Buckminsterfullerene ( $C_{60}$ ), named because the molecule resembles the geodesic domes designed by the architect Richard Buckminster Fuller. The extraordinary stability of the  $C_{60}$  'buckyball' is a result of the closed array of carbon atoms shaped into a 32 faceted pseudo-sphere by means of 20 hexagons and 12 pentagons (Fig.XIV). Reports that  $C_{60}$  can be deformed to a small fraction of its original volume and recover when the pressure is released are coming from researchers at the Naval Research Laboratories<sup>122</sup>. Theoretical calculations show that even when compressed to  $\frac{1}{3}$  of its original diameter (7Å), it maintains its integrity and is still capable of rolling. Hence the possible application as bearings in micro motors needed to power miniature robots which doctors hope one day will be used in micro-surgery.  $C_{60}$  is not however the ultimately stable compound since it is vulnerable to chemical attack and on burning converts to graphite.

The pseudo-spherical molecules are held together with strong  $sp^2$  carbon bonds which are in turn mutually attracted by weaker van der Waals interactions (Fig.XV). The molecular spacing is  $10.4\text{Å}$ <sup>123</sup> ( $\rho=1.697\text{g/cm}$ ,  $300\text{K}$ <sup>124</sup>) compared to the interstitial spacing of graphite at  $\sim 3\text{Å}$ . Since the initial discovery by Kroto & Walton (University of Sussex) during laser ablation of graphite, reports of further unique properties of  $C_{60}$  and the possibility of other caged forms of fullerene have begun to rapidly emerge. Indeed oval shaped 28, 32, 50, 70 and 80 atom versions are known to exist, however it remains to be seen whether the  $C_{84}$  component of fullerite is cylindrical or tetrahedral in shape.

The establishment of an efficient extraction method for fullerenes has been central to the progress of buckyball development. The first extraction methods used by Kroto and Huffman consisted of heating graphite rods electrically at low pressures in the presence of helium and argon. Separation of  $C_{60}$  from its  $C_{70}$  'impurity' is achieved easily due to the solubility of fullerenes in benzene<sup>125</sup>. Since then the method has been slightly modified to produce gram quantities of fullerite by incorporating arc evaporation of the graphite rods. Currently a easier and more efficient method using a combustion process is being

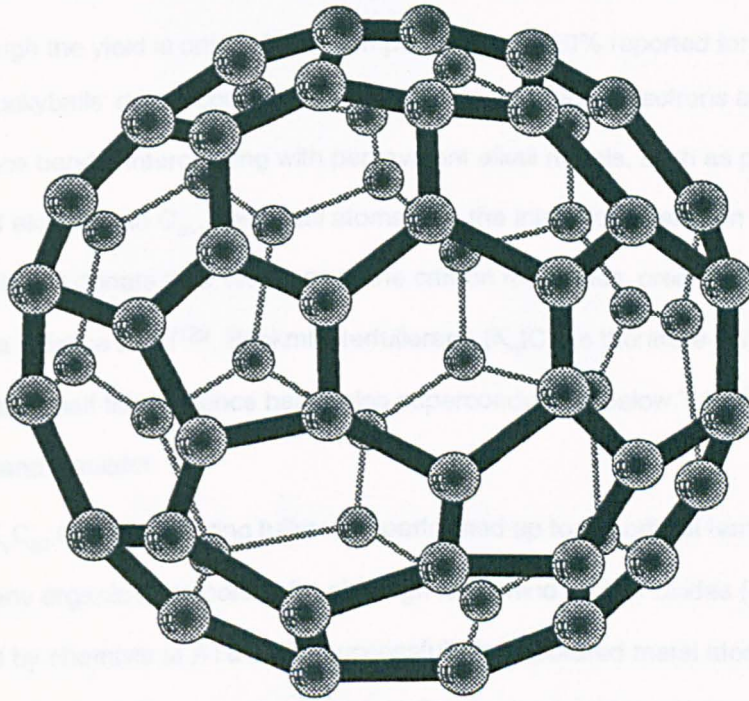


**Fig XIV Buckminsterfullerene C<sub>60</sub>**

developed<sup>126, 127</sup>. Although only recently discovered, it is ironic that fullerenes appear to be produced whenever a combustion process gives soot! There are even reports of fullerenes in coal<sup>128</sup>. Whilst the temperature window where fullerenes are the favoured species is only between 2000-2600°C, indications are that combustion methods will be the preferred methods even though the yield is only 1-2% in comparison to 10-20% reported for arcs.

Usually 'buckyballs' do not conduct electricity because all their electrons are tightly bound in the valence bands. Intercalating with pentavalent alkali metals, such as potassium, result in transfer of electrons to  $C_{60}$ . The alkali atoms fit in the interstices between the  $C_{60}$  molecules (Fig.XVI) and donate their electrons to the carbon molecules, creating an ionically bonded solid with a valence band<sup>129</sup>. Buckminsterfullerene ( $K_0$ ) $C_{60}$  is therefore insulating,  $K_3C_{60}$  is a metal with a half filled valence band (also superconducting below  $T_c$ ) and  $K_8C_{60}$  is once again a full band insulator.

The first  $K_xC_{60}$  superconducting fullerenes performed up to the critical temperature of 18K, a record for any organic superconductor although far behind copper oxides ( $T_c < 125K$ ). This was achieved by chemists at AT&T who successfully incorporated metal atoms inside the fullerite cage in March of this year, shortly before Stephens et al (State University of New York) described how  $K_3C_{60}$  doped could behave as a superconductor to 19.3K<sup>130</sup>. Pure  $C_{60}$  is stable and unreactive in air, but when doped the potassium reacts so violently with the air that the carbon structure is destroyed. This phenomenon and the fact that other intercalated material reverses the doping process in atmospheric conditions has resulted in all the doping experiments being carried out in vacuo. However, in future it is hoped that the dopant will be able to be trapped inside the carbon cage as a way of improving the stability. More recently, Japanese scientists (NEC) have found better results using caesium  $Cs_5C_{60}$  and rubidium  $Rb_xC_{60}$  which conduct electricity without resistance up to 33K<sup>131</sup>. Unconfirmed reports from America (Allied Signal Inc.) suggest even further improvements in superconductivity to temperatures of 44K by adding the metal thallium, more than 10K higher than any previous attempt. What is certain is that the critical temperature will inevitably rise in the near future as more research effort is focused in this area. As 'buckyball' compounds move closer to the relatively high temperature threshold achieved by ceramic superconductors (77K), fullerenes will become the favoured material.

### 3. The Tribology of Coatings

#### a) General

Tribology is the science of surfaces in relative motion and thus involves many widely different mechanisms in different environments. For example, metal cutting and extrusion dies are exposed to high pressure and are often in a high temperature, low moving plastic state. In contrast, ball bearings and mixing applications the counterface is both heterogeneous, hard and clean. Additional problems of unconfined impact damage. Components are required to perform precise movement in operating environments as diverse as space instrumentation, high vacuum environments and biological situations; inkjet printers, surgical instruments, optical storage systems (where a read/write head is expected to operate at several micrometers above the surface of a hard disc travelling at a relative speed of between 2-4m/sec).

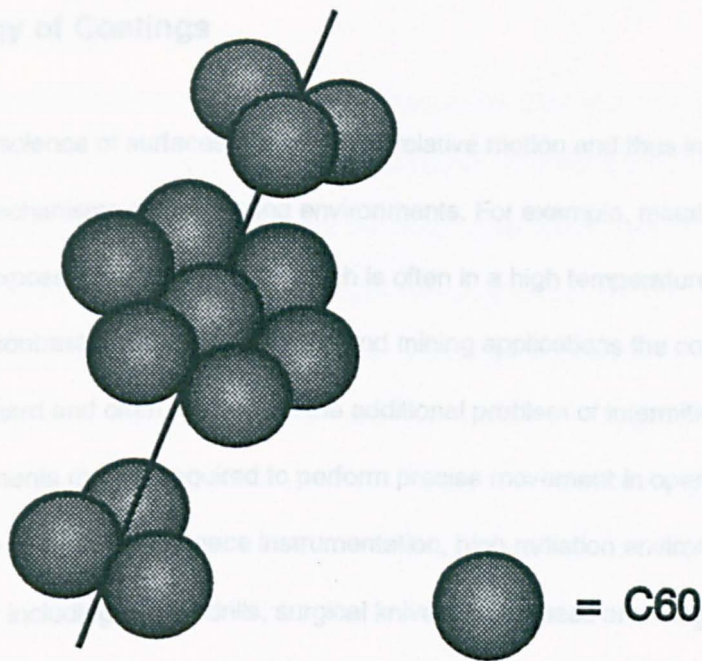


Fig XV Molecular C60

The nature of the interaction between two bodies is related to many influences based on the geometry of the contact (microscopic roughness, macroscopic geometry, nature and quantity of debris formation) and the properties of the surfaces (chemical composition, mechanical properties, shear properties, elastic behavior, etc.). The level of these interactions is essentially related to the relative velocity in the contact zone through the application of heat, velocity and temperature. Energy is retained in the contact region due to resistance to movement (friction) and the formation of debris (wear).

Often hard coatings are designed for tribological applications on the basis of their enhanced structural and mechanical properties. In some cases however, the use of such coatings may not be appropriate since the wear mechanism is not understood. The wear mechanism may be shifted or altered. A clear understanding therefore of the performance advantages (through an understanding of the applications, wear mechanisms involved and the properties of the coating) are essential if improvements are to be achieved.

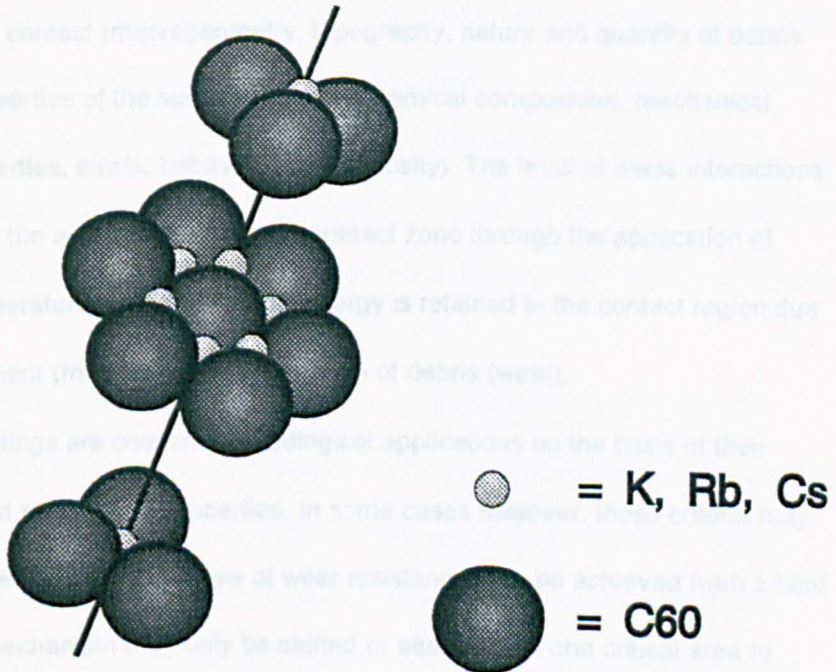


Fig XVI Doped C60

### **3. The Tribology of Coatings**

#### **a) General**

Tribology is the science of surfaces interacting in relative motion and thus involves many widely different mechanisms and operating environments. For example, metal cutting and extrusion dies are exposed to a counterface which is often in a high temperature, fast moving plastic state. In contrast, during earth moving and mining applications the counterface is both heterogeneous, hard and often sharp, with the additional problem of intermittent impact damage. Components may be required to perform precise movement in operating environments as diverse as bearings in space instrumentation, high radiation environments and biological situations; including dentist drills, surgical knives, prostheses and magnetic media storage systems (where a read/write head is expected to operate at several micrometers above the surface of a hard disc travelling at a relative speed of between 1-4m/sec).

The nature of the interaction between two bodies is related to many influences based on the geometry of the contact (macrogeometry, topography, nature and quantity of debris formation) and the properties of the surface (such as chemical composition, mechanical interaction, shear properties, elastic behaviour and viscosity). The level of these interactions is essentially related to the energy applied to the contact zone through the application of load, velocity and temperature and much of this energy is retained in the contact region due to resistance to movement (friction) and the formation of debris (wear).

Often hard coatings are chosen for tribological applications on the basis of their enhanced structural and mechanical properties. In some cases however, these criteria may not be appropriate since, although a degree of wear resistance may be achieved from a hard film, the critical wear mechanism may only be shifted or altered from one critical area to another. A clear understanding therefore of the performance advantages (through an understanding of the applications, wear mechanisms involved and the properties of the coating) are essential if improvements are to be achieved.

## ***b) Surface Characteristics***

All surfaces, even when mirror polished, have a discernible roughness when viewed at high magnification. The most common criterion by which this is quantified is the centre line average (CLA) or the  $R_a$  parameter. In addition there are many other parameters including amplitude criteria - peak to peak  $R_t$ , skewness, kurtosis as well as spacing and hybrid parameters (i.e. bearing area curves). Their usefulness in tribology has been demonstrated by Whitehouse<sup>132</sup>, Moore<sup>133</sup> & Czichos<sup>134</sup>, although there has yet to be a parameter which suitably links the quality of the contacting surface with performance in wear and friction. This situation is made more problematical when one takes into account any topographical patterning such as that resulting from the directionality of machined surfaces<sup>135</sup>.

When metallic surfaces (and other ductile materials) are brought together, contact is made initially at the highest asperities. After the elastic limit is exceeded, plastic deformation proceeds until the real area of contact is sufficient to support the applied load, such that the applied pressure is approximate to the indentation hardness value of the metal. The onset of plastic flow has been estimated by Bowden & Tabor<sup>136</sup> to be 0.4 of the indentation hardness value and may often occur at low loads. Despite such deformation, the real area of contact remains very much lower than that of the apparent area. For ceramic solids the elastic contribution is likely to be minimal whereas in polymeric materials the deformation may be a combination of visco-elastic/plastic or purely elastic behaviour depending upon the load and the strain rate.

The nature of the asperity interaction is further complicated by the near surface chemical and physical characteristics of a surface which in turn is largely dependent upon the composition of the materials and the surrounding environment. The near-surface region of machined components may be changed as the result of strain hardening, recrystallisation and texturing. Furthermore, formation of an oxide layer on the metallic surface will often occur to an extent determined by the concentration of alloying elements exposed to the environment and their affinity for the available oxygen. Once an oxide layer has formed, the outer surface becomes contaminated by absorbed gases which, it is argued by Buckley<sup>137</sup> and Suh<sup>138</sup> prevent strong adhesion between materials of similar composition.

### **c) *Sliding Friction***

The coefficient of friction is taken to be simply the tangent of the resistance to motion and is calculated by dividing the friction force by the applied normal load. Traditionally, the mechanism for friction was explained by adhesion resulting between sliding asperities and this concept was first put forward by Bowden & Tabor<sup>136</sup>. They postulated that asperities forced into contact would form cold-welded micro-junctions, due to the adhesion, and these junctions would shear on continuing sliding either at the micro-weld or in the bulk of one of the materials. In such a way, the shear strength or shear stress required to breach these junctions, gives rise to the frictional resistance to motion due to adhesion. They also recognised that the total friction was the result of many components including a component due to the deformation of the two solids. For metals of similar hardnesses, they assumed that the friction due to this deformation was negligible and in such a case, the total friction would be dominated by a large adhesive contribution.

This early adhesion model has been criticised widely, not only because intuitively such a simple concept could not be expected to adequately model many of the more complicated contact conditions found in many common wear systems, but because a poor agreement exists between the theoretically calculated values and the empirical data. In addition, objections were raised to the fact that the force required to produce such welds was insufficient and on unloading the surfaces could be separated easily without experiencing any breaking of residual junctions. This latter point was explained by Bowden & Tabor<sup>139</sup> to be the result of compressive strain, formed during initial loading, being relieved by tensile recovery such that the welds would separate upon removal of the load. Nevertheless, it is fair to say that adhesion theory devised by Bowden & Tabor<sup>136</sup> was not all embracing and, in particular, was not sufficiently thorough to account for such variables as asperity retention, work-hardening and surface roughness.

In addressing some of these problems Rabinowicz<sup>140</sup> presented a model based on the energy, roughness angle and radius of the surface asperities. At a similar time, a molecular-mechanical theory was developed by Kragelsky<sup>141</sup>, which included an adhesional component called the piezo coefficient, in an attempt to correlate the shear strength with the

compressive force. This idea was developed by Kragelsky and his co-workers because they felt that the adhesion model presupposed clean contact conditions free from contaminating films of moisture, adsorbed gases, liquids and oxides. They noted that when a penetrating asperity traverses a surface, a bulge was formed in front of the contact zone whose dimensions increased with the strength of the adhesive bond. Thus the surface material ahead of the asperities was raised by deformation resulting in work hardening and the ultimate embrittlement of this surface layer. Further work on the plastic deformation of the asperities to the resistance to motion was carried out by Rigney & Hirth<sup>142</sup>, Green<sup>143</sup> and Edwards and Halling<sup>144</sup> while Landheer & Zaat<sup>145</sup> studied the influence of metal transfer in the sliding friction and Heilmann & Rigney<sup>146</sup> the metallurgical effects. A review of these classic friction theories can be found in Tabor<sup>147</sup>.

A new and interesting concept of friction, known as the Genesis of Friction, was published by Suh & Sin<sup>148</sup> in which they attempted to combine the previously studied effects of friction in metals into one model. They stated that friction would comprise of various elements including one for asperity deformation, one due to adhesional contact and an element due to the effect of ploughing. The asperity deformation was thought to be responsible for the high initial static coefficient of friction and once the original asperities were deformed asperity interlocking became less significant. The adhesion contribution to friction was observed to vary over a range of values depending upon whether the surfaces were well lubricated (giving a low value) or made of similar materials free from surface oxides or contaminants (high value). Friction due to ploughing was stated to have a low contribution when wear particles were absent from the interface or a soft surface was slid against a hard, optically smooth surface. A high level of friction due to ploughing being associated with identical materials slid against each other with an abundance of deep penetrating wear particles. It was further stated that these three effects would only dominate the friction behaviour over chemical effects if the temperature rise at the interface was moderate.

Under normal conditions of sliding contact, the wear and friction performance can be differentiated into a short period of running-in wear followed by a steady state situation. This

latter period may last for a considerable period of time depending upon the stability of the contacts. After this period, an event such as film failure may occur whereupon the wear rate and friction accelerate in an uncontrolled manner and the component can be said to have failed. Suh & Sin<sup>148</sup> recognised the importance of the chronological development of these changes during the life of tribocontact and offered six stages thought to be typical of an unlubricated steel contact.

- Stage One describes the initial moments during sliding contact, where the increase in friction force is due largely to asperity ploughing which increases with asperity deformation. The surfaces become more conformed and polished as a result of the flattening of the asperity heights. It is believed that adhesion would not play a large role since intimate contact between bulk materials would be prevented by surface contaminants and oxides. The coefficient of friction therefore would be largely independent of material composition and environment conditions.
- In Stage Two, the polishing action of the asperity deformation removes significant portions of the surface contaminants and oxides so that the bulk surfaces are exposed resulting in a slow increase in friction due to the strong adhesional contact between 'clean' freshly sheared surfaces.
- Stage Three is dominated by a large increase in friction due to the wear debris formed in Stage Two. This work-hardened debris becomes entrapped between the two surfaces leading to a rise in the ploughing friction, the severity of which depends upon the relative hardnesses of the surfaces. If a softer counterface is used the particulates can become completely entrapped in the bulk and thereby significantly reducing their effect in ploughing. Conversely if the materials are of similar hardness, debris may become partially embedded, preventing removal of the particulates and provided conditions of maximum ploughing friction. Deformation of asperities and adhesional effects continue to increase creating larger areas of exposed, contaminant free bulk material.

- Stage Four is noted for an equilibrium in friction due to the stabilisation in the amount of debris being formed at the interface equalling that leaving the system. Thus, the shearing of the interface reaches a maximum so that further increases in adhesional friction are prevented. In most cases (other than in Stage Five & Six), this situation signifies the steady state tribological condition.
- Stage Five describes a further modification which may occur if a soft material is slid against a very hard counterface. Removal of the asperities on the hard material results in time with a consequent decrease in surface roughness. The coefficient of friction decreases as the contribution to friction from the asperity deformation reduces and the ploughing friction is reduced by decreasing debris entrapment.
- Stage Six; further reduction in friction to a steady state value as the softer as well as the harder, material become mirror smooth.

These six stages represent a model performance for steel samples under experimental conditions and clearly these will be different for other material combinations and operating parameters. For instance, Blau<sup>149</sup> reported a similar chronological series of wear events where a transfer layer was formed and reaffirmed the idea that the interfacial friction was the result of the combined effect of asperity deformation, adhesion and ploughing.

#### ***d) Wear***

Wear is the removal of material during tribological events and is consequently linked to the condition of friction in an inter-relationship which is still not well understood. It is generally experienced that high friction encourages high wear and vice versa, although examples of contradictory behaviour have also been reported<sup>150</sup>. The manner in which the removal of material is achieved during the wear process is used to categorise the wear mechanism where such mechanisms include abrasive, fatigue, chemical, adhesive, erosive and fretting wear<sup>151</sup>. It is most unlikely that during the wear of two surfaces, only one mechanism acts in isolation and, more typically, several or more mechanisms may be involved. Since the classification of the wear mode is based on the appearance of the surface after the tribological event, several different classification systems have been suggested<sup>152</sup>.

## **Adhesive**

Adhesive wear is characterised by the formation of micro-welds at contact points between two mutually moving bodies which results in the failure of the junction occurring in the bulk of the weaker of the two materials. Since failure occurs near the interface in the weaker of the materials, a net transfer of matter occurs from one body to the other. During this process, work-hardened particles can become detached from either of the bodies to form third bodies which greatly accelerate the process of wear by abrasive action.

As shearing of the worn material takes place, fresh and unoxidised material is exposed and in many cases it is the rate of reaction of this shear surface with the environment which determines the tribological behaviour. Buckley<sup>137</sup> demonstrated that the formation of surface oxides acts in a manner similar to a solid lubricant by limiting adhesive removal. Conversely, where oxide formation was impeded by vacuum, an increase in adhesive shearing could be witnessed until total seizure for most metals was observed to occur. Chemically inert materials such as diamond and diamond-like compounds ought then to display less change in friction behaviour when in vacuum - which is indeed the case. Surface chemistry therefore plays a dominant role in the progression of adhesive wear by determining the degree of chemical bonding taking place which, in turn, is controlled by the environmental conditions.

Since Bowden & Tabor<sup>136</sup> first described the adhesive wear mechanism in 1950, many modifications have been made to this theory by Rabinowicz<sup>153</sup>, Eyre<sup>154</sup>, Tabor<sup>155</sup>, Buckley<sup>137</sup> and Kragelsky<sup>141</sup>. The theory however is not without its critics, Jahanmir<sup>156</sup> argued that the strength of the junction, because of the numerous impurities and vacancies present at the interface, could not be as strong as that of the bulk material. Furthermore, the theory failed to account for the surface roughness and the fact that harder surfaces can frequently be worn by a much softer counterfaces. In addition, the theory fails to relate the relationship between friction and wear and does not take into account the microstructural and metallurgical parameters.

Despite high adhesive conditions such as sliding in vacuum/inert atmospheres or when the asperity flash temperature is high, according to analysis by Suh & Sin<sup>148</sup>,

Jahanmir<sup>156</sup> & Suh<sup>138</sup> the most dominant wear mechanism may not be adhesive. Certain failure modes such as scuffing and seizure are greatly affected by adhesive contact but many of the more common tribological contact conditions are thought to contain only a small adhesive contribution.

Following the early development of a simplified law of adhesive wear from Bowden & Tabor<sup>136</sup>, Archard<sup>157</sup> derived a mathematical approach for the determination of adhesive wear loss based on the theoretical model. It assumed similarly sized asperity contacts and included a coefficient  $k$  which accounted for the fact that not all contacts produce a wear particle.

$$W = k \frac{F_n}{3p_o}$$

where:  $p_o$  is the yield pressure,  
 $F_n$  is the normal load  
 $W$  is the total wear volume

All the quantities in the above equation are measurable except  $k$  and this value can be found for different combinations of sliding materials and for different loading conditions. For practical purposes the volumetric wear loss can be expressed as:

$$W = k \frac{F_n}{H_v} \quad (\text{per unit sliding length})$$

where:  $H_v$  is the hardness  
 $W$  is the wear volume

From this equation three 'laws' of adhesive wear have been developed:

- the volume of wear material is proportional to the distance of sliding
- the volume of material is proportional to the load
- the volume of material is inversely proportional to the yield stress or hardness of the softer material

### **Abrasive**

During the process of abrasive wear, particles or asperities of one hard material, plough through and remove particles of a relatively soft counterface. It is during the initial

stages of contact that abrasive wear is usually the most severe since a high level of non-conformity exists at the contact due to many work hardened asperities. After an initial stage of contact, during which the load bearing capacity is improved by wear of these asperities, the abrasive situation is usually improved except when third bodies become involved.

Depending upon the geometry of the harder surface and the extent to which the harder asperities penetrate the counterface governs the type of abrasive action which can be ploughing, wedge formation or cutting. This mechanism has been studied and reported extensively by Kruschov<sup>158</sup>, Zum Gahr<sup>159</sup> & Suh<sup>138</sup>.

In an attempt to express quantitatively the level of abrasive wear, Archard<sup>157</sup> derived a formula which assumed that the surface consists of a uniform array of hard conical asperities, all with the same included angle of  $\theta$ . These asperities would then create many wear tracks on the surface of a flat, soft counterface. Assuming also that the softer material would yield under the load of the relatively hard asperity, the wear volume was derived to be:

$$k' = \frac{2 \cot \theta}{\pi}$$

$$\therefore W = \frac{k' F_n}{H_v} \quad (\text{per unit sliding distance \& for a given } \theta)$$

It is interesting to note that this formula is in a similar form to that for adhesive wear discussed in the previous section so that the three 'laws' of adhesive wear will equally apply to abrasive wear. This derivation however is somewhat limited as it is based on an extremely simple model which fails to take into account asperity heights and shapes as well as disregarding mathematically complex processes as asperity deformation and material pick-up.

### **Chemical Wear**

Chemical wear is heavily inter-related to the two main modes of wear discussed above. The environmental conditions clearly determine the levels of surface reaction together with the amounts of heat being dissipated at the contact junction by the sliding process. This can lead to the creation of surface cracks which provide a greater surface area for more chemical reactions to take place. The mechanism of chemical wear has been discussed by Czichos<sup>160</sup> and Buckley<sup>137</sup>.

Oxidation wear is the most common of the chemical wear processes since a thin layer of oxide will always be present on the surface of metals. This layer serves to prevent heavy adhesional contact between the two bulk materials and is continuously removed and re-created during sliding contacts. The rate at which it is formed can be accelerated by humid environments and can thus encourage oxidational wear. Oxidational wear has been reviewed by Quinn<sup>161</sup> and Sullivan<sup>162</sup> and the thermal aspects covered by Quinn & Winer<sup>163</sup>.

It could be argued that chemical wear should not really be classified as a separate wear mechanism since it is always combined and inter-related to the other wear mechanisms. Conversely, if none of the other wear mechanisms were present such as adhesion, abrasion or fatigue, the tribological contact would be purely corrosion. It must therefore be considered as an influencing parameter which changes the material properties of the surface layer with time rather than a basic wear mode.

#### **4. Development of DLC Tribology**

It has been recognised that wear processes can be separated into the basic wear processes outlined above, which in turn are influenced by many material and environmental factors. Wear resistance therefore must be treated more like a system variable rather than an inherent material property. Properties such as normal load, sliding speed and material hardness have been dealt with frequently in previous studies and for numerous combinations<sup>159,164</sup>. The study of the tribological performance of DLC, however, is a relatively new area of investigation but, as the awareness of the wear resistant potential of this material has increased, the pursuit of such work has accelerated.

It was Enke<sup>165</sup> in 1981, who really began the first serious investigation into the wear behaviour of a-C:H films and quickly discovered that the unique combination of hardness coupled with low coefficient of friction (typically  $\mu \approx 0.03$ , but as low as  $\mu = 0.01$  for like on like) provided many interesting opportunities.

Dimigen<sup>166</sup> demonstrated that the otherwise low coefficient of friction could be made to increase after annealing the carbon films at a temperature above 550°C - a significant temperature where optical, electrical and structural changes take place as hydrogen is desorbed from the coating and reordering of the remaining carbon takes place.

Several authors detected a strong dependence on humidity and environmental conditions on the tribological performance with an increasing friction with elevated humidity<sup>167</sup>. This observation ran contrary to previous experiments on graphite and crystalline diamond by Savage & Schaefer<sup>168</sup>, Savage<sup>169</sup> and Bowden & Young<sup>170</sup>. An excellent paper by Memming et al<sup>73</sup>, demonstrates the adverse affect on friction with increased humidity and the dependence on the type of gaseous environment. Evidence of higher friction with oxygen atmospheres and a correspondingly lower friction with an inert nitrogen atmosphere lend weight to the argument that some form of chemical process was taking part in the tribological interaction. Timsit<sup>1</sup> found that changes in humidity conditions led to an observable change in the kinetic friction only after the sample had undergone an incubation period of several hours. This implies that the surfaces are generally inert except when subjected to prolonged exposure to moisture or oxidising atmospheres.

Papers by Judge & Speliotis<sup>171</sup> and Marchon et al<sup>172</sup> focused on the physical interaction during sliding conditions, particularly the parameter of surface roughness and its effect on the tribology of DLC films. If the friction force is taken to be the energy needed to shear the asperities at the contact points, then clearly as the surface finish is improved below 20Å the conformity between the surfaces is increased, requiring a greater force to shear the contact.

As the surface roughness deteriorates the coefficient of friction would initially improve as the surfaces are prevented from large area capillary and atomic attraction. However, with further increases in surface roughness, asperity formation becomes increasingly important as greater ploughing and work-hardening of the asperity contacts begins to dominate the friction behaviour. This is demonstrated practically by magnetic media hard discs where it has been known for some time that texturing after polishing reduces considerably the contact of the reader head and reduces the so called static friction (stiction) force. Marchon<sup>172</sup> calculated that a surface roughness average  $R_a$  of greater than 18Å was necessary to obtain this friction behaviour, below this strong contact occurs. Studies have shown a strong correlation between the surface roughness of the hard disc and initial friction and more importantly the rate at which friction develops<sup>173</sup>. At the other extreme, polycrystalline diamond films which

display poor surface roughness, due to the facetting of its surface, cause heavy abrasive ploughing with little asperity deformation. Therefore the counterface is subjected to a larger area of contact and high friction and wear<sup>174</sup>.

### **III. EXPERIMENTAL**

#### **A. Coating Equipment**

##### ***a) Experimental Hybrid DC PVD***

This unit comprises of a small (~0.06m<sup>3</sup> total internal volume) water cooled experimental chamber, constructed internally with removable stainless steel shields. Vacuum was achieved by means of a 6" oil diffusion pump backed by a two stage rotary pump. The deposition system was designed to deposit carbon and carbon based films at a range of pressures between 10<sup>-2</sup>-10<sup>-5</sup>Torr and at substrate temperatures of between ambient and 500°C. Gas supply and control was primarily performed by needle valves and glass flow indicators and pressure monitoring was achieved by a standard Penning-Pirani arrangement.

Deposition from solid or gaseous precursors was facilitated by means of an elementary electron beam gun. Electrons, emitted from a tungsten filament, were then accelerated through a 'focusing' ring towards a graphite crucible held at DC bias voltages of up to 1kV. Substrates were suspended vertically from the roof of the chamber, directly above the focusing ring and held electrically neutral via an insulated water-cooled feedthrough (Fig.XVII).

##### ***b) Experimental Hybrid DC/RF EBPVD***

This experimental unit comprises of a ~0.1m<sup>3</sup> stainless steel vacuum chamber, in which a 3kW, 225° water cooled electron beam gun was mounted on a horizontal diaphragm located in the plenum chamber. The unit was exhausted to high vacuum by means of both a 9" oil diffusion pump connected directly to the chamber via a throttling port and a 6" oil diffusion pump situated in the plenum chamber, to provide differential pumping of the electron gun. Both oil diffusion pumps were simultaneously backed by a single two stage rotary vane pump.

Substrates were suspended vertically from the centre of the chamber roof and insulated electrically from the chamber via a separate feedthrough. The substrate assembly could then be operated as a cathode via a 3kV DC sputter supply or alternatively a low frequency 380kHz RF power supply. This 3kW Electrotech RF supply, incorporating inductively coupled voltage sensing electronics, was used primarily as a means of

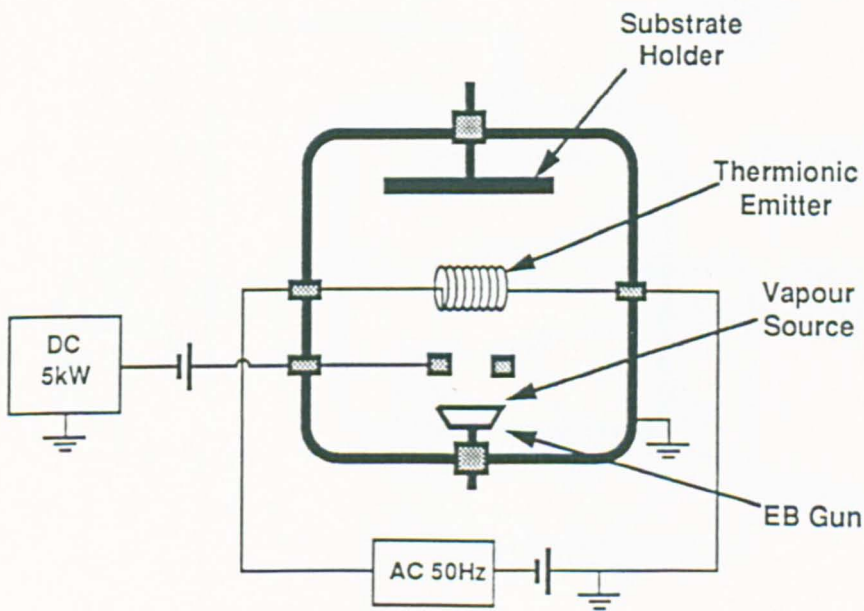
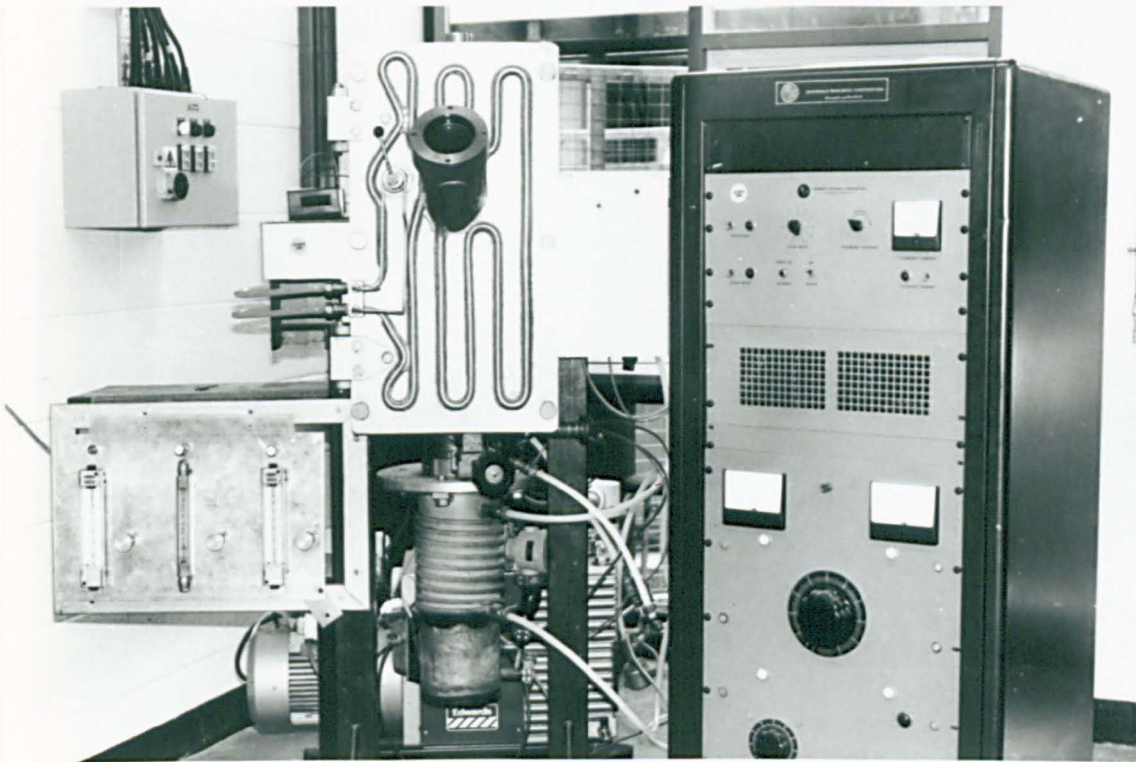
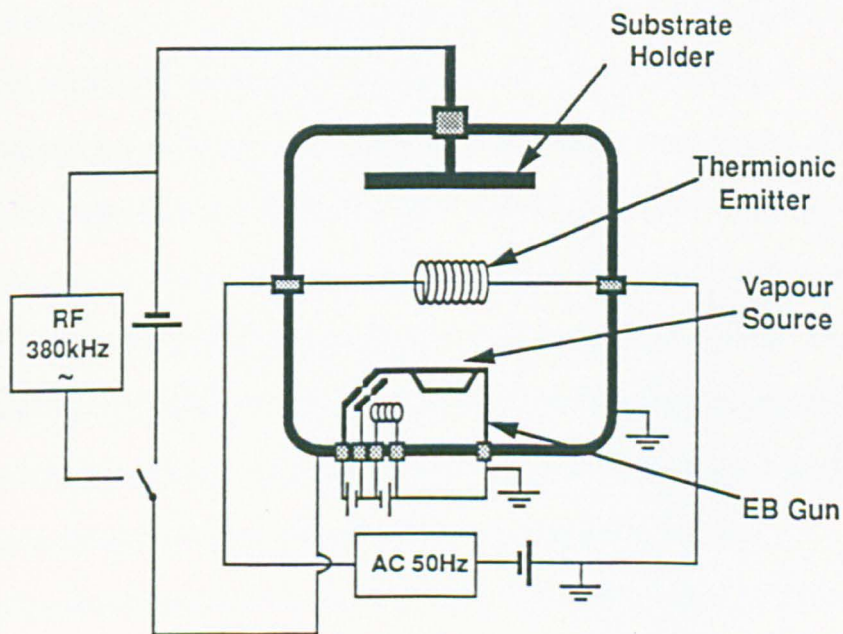
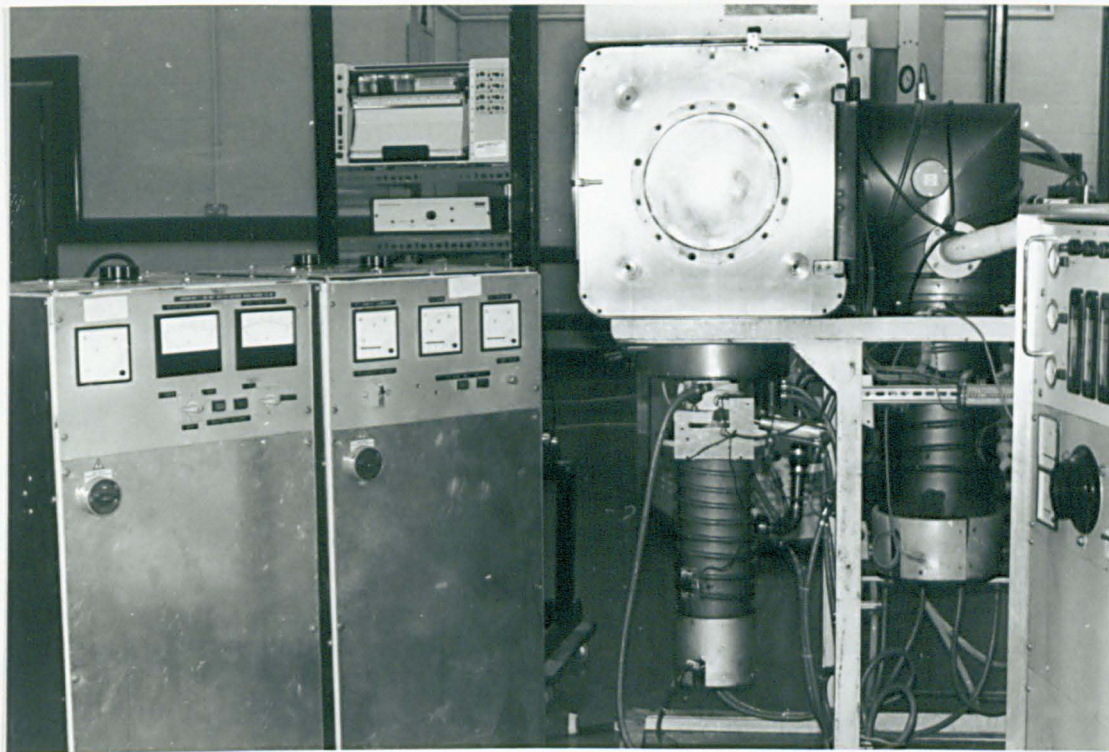


Fig XVII A Pictorial and Schematic Layout of the Experimental Hybrid DC PVD Deposition Equipment



**Fig XVIII** A Pictorial and Schematic Layout of the Experimental Hybrid DC/RF Electron Beam PVD Deposition Equipment

overcoming the deposition of highly insulating coatings such as thermal barriers and diamond films. No matching network was necessary for this arrangement due to the capacitive nature of the plasma sheath created between the cathode and the chamber walls (Fig.XVIII).

Solid precursor material could be evaporated from a water cooled copper crucible by means of the electron beam gun whilst simultaneous ion plating of the substrate surface could be achieved in either argon or hydrocarbon plasmas. Gas monitoring was accomplished using a mixture of glass flow tubes and mass flow controllers. A filament made from  $\varnothing 0.5\text{mm}$  tungsten wire, 380mm long was positioned 150mm below the substrate as a combined heating stage and electron source for plasma enhancement. The filament temperature was maintained between 1750-1875°C during deposition (as recorded by an optical pyrometer). Through the combined action of plasma and filament heating it was possible to achieve substrate temperatures in excess of 600°C, as measured by a NiCr/NiAl type K thermocouple.

### **c) *Fast Atom Beam***

The FAB source used, is a saddle field device<sup>175</sup>, operated in the chamber of an Edwards E19A commercial evaporator. Electrons emitted from the graphite source walls are attracted to the twin anodes at its centre. There they are made to oscillate in the anodic region under the influence of the saddle field. The probability of ionisation between electrons and introduced gas molecules is therefore greatly increased. This enhanced ionisation allows the source to be operated at lower pressures than achieved for similar devices. The resulting beam of ionised particles emerges from a  $\varnothing 25\text{mm}$  aperture in the top of the source via a graphite grid. This grid serves to facilitate charge exchange so that the beam, external to the source, contains wholly (98%) neutral carbon or hydrogen species (Fig.XIX).

Source gases of butane and acetylene, with or without the addition of hydrogen were metered through separate mass flow controllers to maintain a chamber pressure of typically 10mTorr. A power supply operated at between 1.0-2.5kV, 0.5-2A was used to bias the anode element and the resulting beam produced substrate temperatures in the order of 35-50°C at a distance of 300mm.

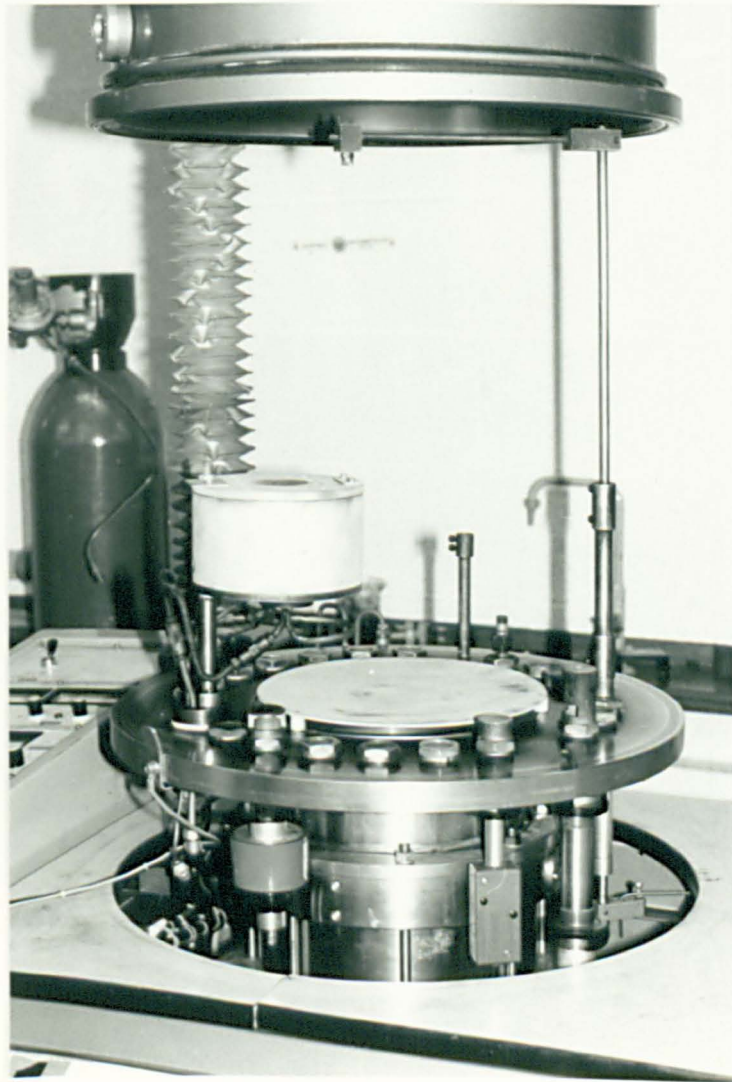
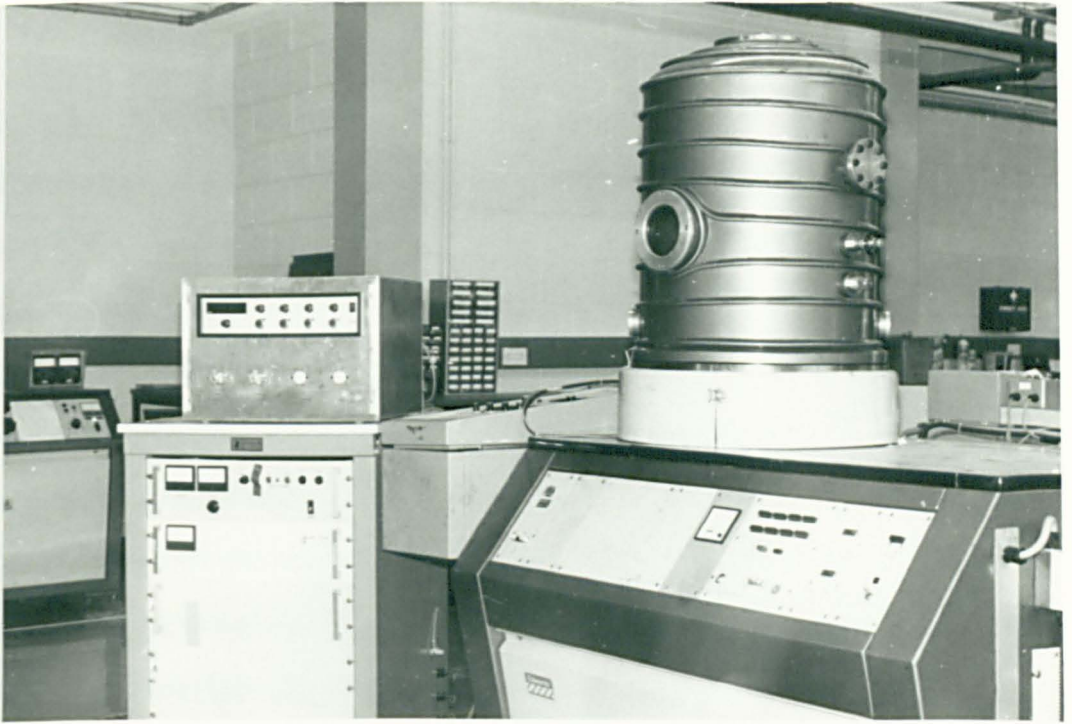


Fig XIX The Edwards E19A Chamber And The Fast Atom Beam Source

**d) *Edwards S150B Sputter Coater***

A common problem associated with the study of insulating or semi-insulating materials during SEM/EDX analysis, is charge build-up on the surface of the specimen. As the electron beam impinges on the surface, electrons accumulate at the point of incidence and without the presence of an available conducting path, excessive fluorescence occurs.

In order to study these films in detail, without encountering this phenomenon, thin layers of gold were sputtered onto the surface of the specimens. For this purpose an Edwards S150B sputter coater was used. A deposition rate of  $2\text{ }\mu\text{m}$  per minute could be repeatably obtained for conditions of pressure, voltage and current of  $3 \times 10^{-2}$  mbar of argon, 700V and 20mA respectively. Typically, films of gold between 6-12 $\mu\text{m}$  were found to provide the sufficient electrical conductivity needed and retain the level of surface detail.

## **B. Substrate Choice & Preparation**

A combination of substrate materials was coated during this study, either because suitable applications utilising such materials were envisaged or because analytical test conditions required such materials, as in the case of glass for optical measurements. The grade and composition of the main substrate materials are outlined in Appendix I.

The metallic substrates were manufactured in discs of dimensions  $\varnothing 40 \times 6\text{mm}$  for ASP23 tool steel ( $64R_c$ ) and  $\varnothing 20 \times 1.5\text{mm}$  for cobalt-chrome, for use in the pin on disc wear tests. These were then subjected to a polishing sequence ranging, from finishing to  $1\mu\text{m}$  diamond slurry polishing, to give a surface finish of  $R_a = 8-17\text{nm}$ . Optical microscope slides ( $60 \times 20 \times 1.5\text{mm}$ ,  $R_a = 4\text{nm}$ ) were utilised as glass substrates.

Prior to deposition, particular attention was made to ensure the substrates underwent a thorough precleaning procedure. This procedure involved ultrasonic degreasing in freon for thirty minutes, followed by an acetone wipe and a fifteen minute argon or hydrogen plasma etch under vacuum. The choice between an argon or hydrogen plasma etch was primarily determined on the basis of whether a relatively severe physical removal of impurities was required or the less damaging chemical removal, respectively. Argon sputtering of the steel substrates was considered necessary to thoroughly remove any well bonded surface contaminants and oxides, whereas such an etch was not attempted on the cobalt-chrome samples since preferential removal of the cobalt in the matrix was known to occur. In this case and in the case of glass specimens, where strong oxide formations presented less of a problem, a hydrogen etch was adopted. This form of etch involves the chemical removal of loosely bonded species, particularly carbonaceous deposits. Any foreign deposits, particularly those of a carbonaceous nature, are known to promote growth of graphitic deposits which are undesirable for hard diamond-like structures because this results in an increase in  $\text{sp}^2$  formation.

## **C. Laboratory Characterisation Methods**

The numerous coating variants and substrate combinations derived during the course of this study were selectively tested by many mechanical, optical, electrical and micro analytical techniques for the purpose of assessing their characteristic properties and practical performance. Hardness tests, thickness measurements and adhesion tests were performed as a matter of course for all films produced. In general the more interesting coatings, based on the criteria of wear resistance and/or optical transparency were subjected to closer chemical and structural examination in an effort to characterise further the favourable conditions under which they were formed.

### **1. Intrinsic Material Property Evaluation**

#### **a) *Resistivity/Conductivity***

Hydrogenated carbon films can display a range of resistivity values between  $10^3$  to  $10^{13}\Omega\text{cm}$ , compared to CVD and crystalline diamond of  $10^{14}$ - $10^{16}\Omega\text{cm}$ . This range covers values of typical semiconductors ( $10^3$ - $10^6\Omega\text{cm}$ ) through to good insulators and serves to highlight the extensive property variation associated with these materials. The conductivity is dependent, as indeed is the optical bandgap, on the amount of  $sp^2$  and  $sp^3$  bonds, which in turn is heavily influenced by the electron scattering effects of any bonded impurity.

Due to the high values of electrical resistance commonly encountered for wide bandgap semiconductors conventional methods for resistivity testing are not possible. Current leakage, cable capacitance and interference all compound to render measurement inaccurate. A useful technique is the van der Pauw<sup>176</sup> method used in conjunction with the high impedance, guarded circuitry proposed by Hemenger<sup>177</sup>. It requires only four intimate contacts to be made on the periphery of a uniformly thick, pin hole free sample of arbitrary size. The test procedure corrects for geometrical asymmetry but assumes uniform coating thickness between the point contacts. The method maintains a current between two adjacent contacts whilst measuring the resultant voltage drop across the two remaining contacts. The measurement configuration must then be interchanged for the other three configurations to comply with ASTM standards (Fig.XX a-d). Although the two remaining arrangements possible can be measured for accuracy (Fig.XX e,f) only the four basic configurations are

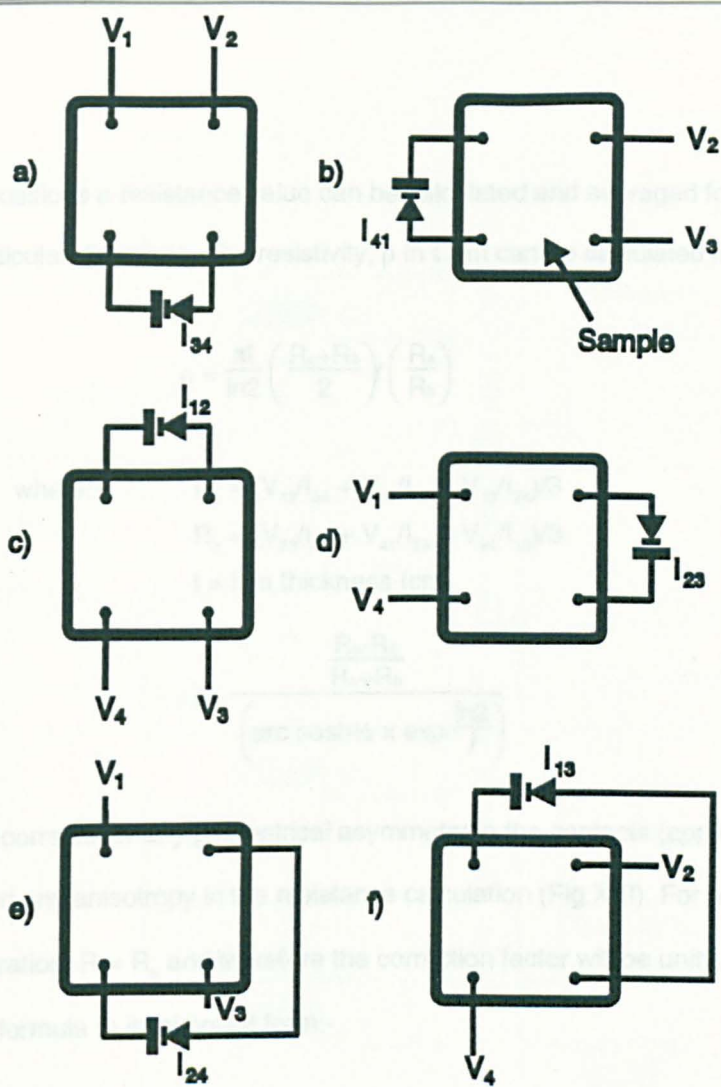


Fig XX Van der Pauw Resistivity Measurement - Test Configurations

Equipment used for the van der Pauw measurements throughout this study, unless

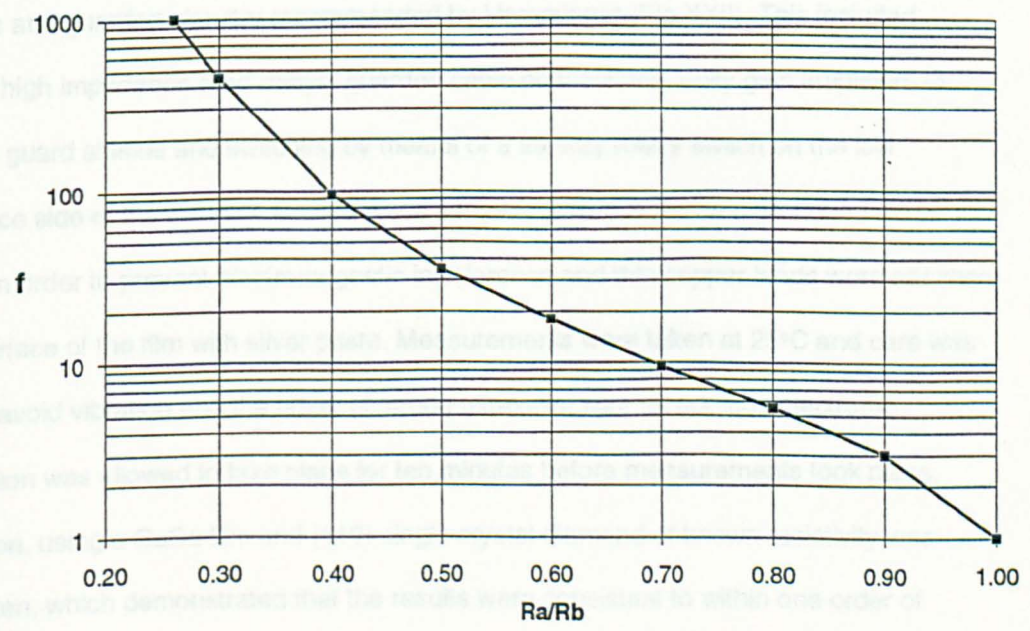


Fig XXI Van der Pauw Resistivity Measurement - Correction Factor Chart

essential. In these positions a resistance value can be calculated and averaged for both the parallel and perpendicular directions. The resistivity,  $\rho$  in  $\Omega\text{cm}$  can be calculated from:-

$$\rho = \frac{\pi t}{\ln 2} \left( \frac{R_a + R_b}{2} \right) f \left( \frac{R_a}{R_b} \right)$$

where:-

$$R_a = (V_{12}/I_{34} + V_{43}/I_{12} + V_{13}/I_{24})/3$$

$$R_b = (V_{23}/I_{41} + V_{41}/I_{23} + V_{24}/I_{13})/3$$

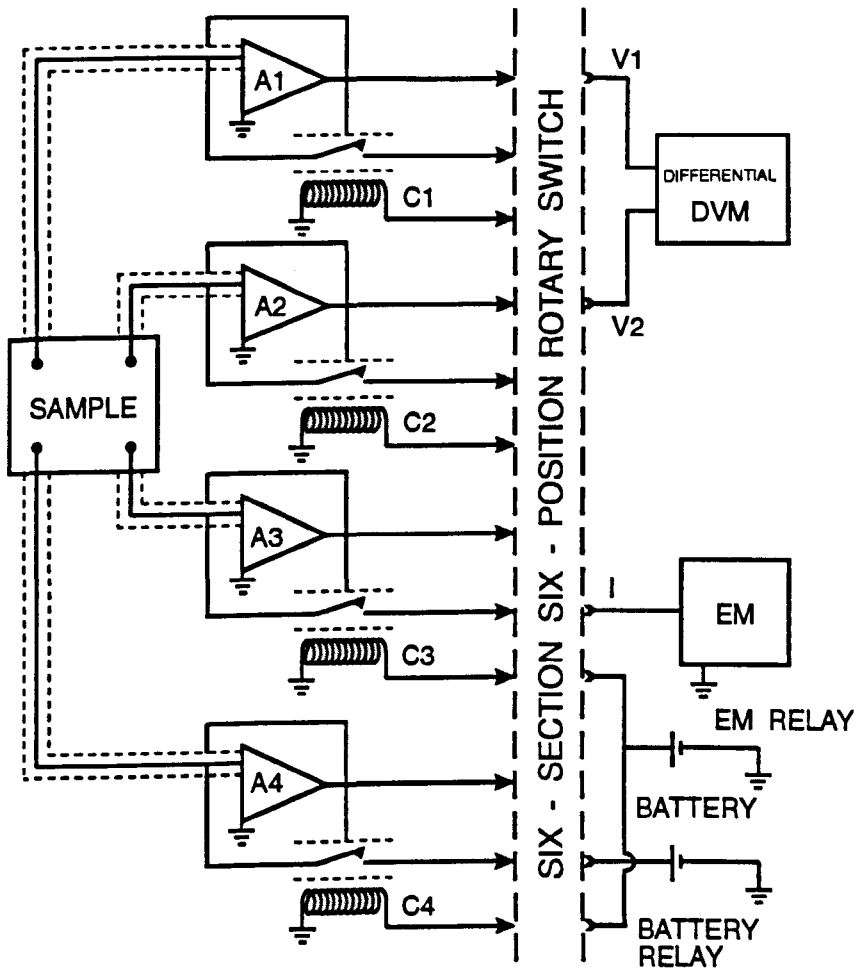
$t$  = film thickness (cm)

$$f = \frac{\frac{R_a - R_b}{R_a + R_b}}{\left( \text{arc cosh} \frac{1}{2} \times \exp \frac{\ln 2}{f} \right)}$$

The factor  $f$  corrects for any geometrical asymmetry in the contacts (applicable for  $R_a/R_b=0.20-1.00$ ) and any anisotropy in the resistance calculation (Fig.XXI). For a completely symmetrical configuration,  $R_a = R_b$  and therefore the correction factor will be unity, resulting in the reduction of the formula to its simplest form:-

$$\rho = \left( \frac{\pi t}{\ln 2} \right) R$$

Equipment used for the van der Pauw measurements throughout this study, utilised the ideas and guarded circuitry recommended by Hemminger (Fig.XXII). This included guarded high impedance reed relays, guarded cable connections, unity gain amplifiers to drive the guard shields and switching by means of a six way rotary switch on the low impedance side of the circuitry. Coated glass samples were placed on a grounded metal surface in order to prevent electromagnetic interference and thin copper leads were attached to the surface of the film with silver paste. Measurements were taken at 25°C and care was taken to avoid vibration and the affect of strong ultraviolet light. In addition electronic stabilisation was allowed to take place for ten minutes before measurements took place. Calibration, using a GaSe film and (110) single crystal diamond of known resistivity was undertaken, which demonstrated that the results were consistent to within one order of magnitude.



A1-A4      unity gain amplifiers to drive the guarded shield  
 C1-C4      coils to activate the relays  
 EM          high impedance electrometer

**Fig XXII                      The van der Pauw Resistivity Equipment**

## **b) Stress Measurement - Cantilever Beam**

The internal stress can be most basically expressed in terms of the sum of the thermal component and an intrinsic contribution.

$$\sigma_f = \sigma_{th} + \sigma_i$$

If it can be assumed that there are no intrinsic stresses, ideally a film with the smallest difference in coefficient of thermal expansion to that of the substrate will result in the least internal stress when cooled from deposition to ambient temperature. Practically however, even for this idealised condition, variation in the thermal expansion coefficient will occur between the two materials, resulting in stress. The thermal contribution to the stress can be expressed as:-

$$\sigma_{th} = \frac{E_f}{(1 - \nu_f)} ( (\alpha_f - \alpha_s) (T_s - T_r) )$$

Total values for film stress were obtained by measuring the curvature of a 4" single crystal silicon (100) wafer using a Form Talysurf 50 profilometer. A 4" optically flat microscope slide was used to calibrate the system and initially an uncoated silicon wafer was evaluated to establish the inherent curvature before deposition. This initial deflection together with the deflection after deposition, establishes the net deflection resulting from the internal stresses in the film. The value of the stress could then be calculated by employing a simple formula developed by Maissel & Glang<sup>178</sup>:-

$$\sigma = \frac{\delta}{r^2} \times \frac{E_{si}}{3(1-\nu_{si})} \times \frac{t_s^2}{t_f}$$

where:-  $\delta, r, t_f = (\text{cm})$                        $t_s = (0.055\text{cm})$                        $\sigma, E_{si} = (\text{GPa})$

A stress resolution of 0.01GPa and compressive and tensile stresses as low as 1.5MPa for extremely flat substrates are claimed for this method<sup>179</sup>.

### **c) Thickness Measurement - Profilometry**

For the measurement of film thickness and surface topography, a Rank Taylor Hobson Talysurf 50 and Talystep were utilised. The Talysurf 50 uses a standard conispherical diamond stylus (tip radius 1.5-2.5 $\mu\text{m}$ ) on the end of a pivoted arm, the deflection of which was detected by means of a sensitive inferometric helium/neon laser transducer. This gave a vertical resolution of between 10.0-37.5 $\mu\text{m}$ . Traversing of the stylus is achieved by a precision stage which rides on an optically flat reference surface to give a scan length of 120mm.

The Talystep is a profilometer developed specially for the requirements of thin film technology. It is used for the determination of very small step heights and thus can record profiles at extremely high magnifications (up to x 2,000,000). Since it is not necessary for this machine to resolve fine detail, the stylus has a comparatively large tip radius (12.5 $\mu\text{m}$ ), a short traverse length (<1mm) but the ability to measure microsteps as small as 0.005 $\mu\text{m}$  (1000 the wavelength of light) up to 10 $\mu\text{m}$ .

The measurement of the film thicknesses by either machine requires the sample to be masked during deposition so that an uncoated area could be exposed for use as a reference surface. In addition, the sample surface should have an optical quality finish, since the accuracy of this method decreases rapidly with surface roughness. Resolution of the thickness is a sufficiently accurate measurement in most instances, however films of sub-micron levels (<500 $\text{\AA}$ ) pose problems as their thicknesses approach that of the surface roughness. It was therefore necessary on occasion to abandon profilometry and derive the thickness more accurately by fracturing and observing the cross-section of the film using an SEM.

In a recent study<sup>180</sup>, coating thickness were measured using four techniques, gravimetric, profilometry, coulometry and X-ray florescence and their results compared. The findings showed unexpectedly large differences between methods. Profilometry was shown to be an excellent instrument for film characterisation by being a relatively quick method which possessed good resolution and accuracy. However for this method to produce reasonable results the coated samples have to be as optically flat as possible. The main conclusion is that thickness measurement is not always as straightforward as it may appear and in the light of this work the author has paid particular attention in achieving optimum surface finish for substrates in all cases.

## 2. Extrinsic Material Property Evaluation

### a) *Microhardness*

Microindentation hardness measurement is a simple and relatively non-destructive technique which is now used routinely for property measurement and quality control. Hardness, in the simplest terms, is a measure of the resistance to penetration of a second solid and although this principle appears easy to understand, it quickly becomes apparent that microhardness measurement involves a complex train of events involving many more parameters than first envisaged. Factors which could adversely affect the hardness measurement are loading variations, substrate support effect, penetration rates, dwell time of the indenter in the material, surface roughness, temperature and vibration. These factors are either fixed, as in the case of the penetration rate or fall inside the envelop of operator error at loads greater than 100grams. However it has to be remembered that at the low loads, such as those used during this study, their influence becomes particularly prevalent<sup>181</sup>. Dynamic indentation methods have thus been developed in an attempt to overcome these problems.

The indentation material is usually diamond since, other than at high temperatures, it will indent all materials and even itself<sup>182</sup>. Square based pyramidal indentors with angles of 136° and 148° between opposing facets and diagonals respectively are known as the Vickers type (Fig.XXIII) and are used widely for indentation of bulk materials. Vickers hardness can be expressed in terms of load and the length of the resultant diagonal length by:-

$$H_v = \frac{1.854L}{d^2} \quad (\text{Kg/mm}^2)$$

It is typical that indentations will experience some elastic recovery depending upon the material being indented and strictly speaking the elastic recovery should be distinguished from the plastic deformation, since it is only the plastic deformation which is actually measured by way of the indentation diagonal. At high loads the elastic recovery can be largely ignored but when the thickness of the material to be indented becomes small and the corresponding applied load is reduced, the elastic contribution can predominate. The need for an indenter with a shallower penetration, for a given load, is required when looking at thin



films and to this end, the Knoop indenter was developed<sup>183</sup>. It has an indenter in the form of a rhombohedral based pyramid with a longitudinal angle of 172°30' and an included angle of 130° (Fig.XXIV). Indentation with a Knoop indenter results in a penetration depth of less than one quarter the depth of a similarly loaded Vickers indent. Equally, the geometry results in the long diagonal being x 7.11 larger than that of the short diagonal. If elastic recovery does occur, relaxation occurs mostly uniaxially along the short diagonal leaving the long diagonal as the basis of the hardness measurement. Knoop hardness is given as:-

$$H_k = \frac{14.23W}{d^2} \quad (\text{Kg/mm}^2)$$

The measurement of Knoop microhardness were performed on a Leitz Miniload microindentation instrument. A range of loads between 10-2000g were available, although due to the thin nature of the films loads of typically 10-15g were more usually employed. To ensure greater accuracy, optical measurement of the resulting indents were carried out on a Nikon Optiphot x 400 magnification microscope and an average of ten readings taken at every load used.

#### **b) Nanohardness**

It has been reported that for thin films ( $t_f < 1\mu\text{m}$ ), the penetration depth during hardness testing should not exceed 10% of the film thickness<sup>184</sup>. This is necessary in order to obtain hardness values which relate to the film properties and are not influenced by the rigidity/plasticity of the underlying substrate. This is not always possible for the microindentation measurement of sub-micron thin films and in order to achieve this, analysis of the films was performed using either a NanoIndenter II or a NanoTest ultra-low load hardness tester. These machines, unlike conventional hardness testers, produce continuous curves of load versus indentation depth. When the depth is plotted for increasing and decreasing load, a hysteresis curve is produced the area of which represents the plastic work performed (Fig.XXV). The principle of the NanoTest instrument has been discussed by Pollock et al<sup>185</sup>.

The NanoTest utilises a sensitive capacitive transducer for indentation depth measurement, giving a depth resolution of typically 0.1nm. Depth calibration is performed

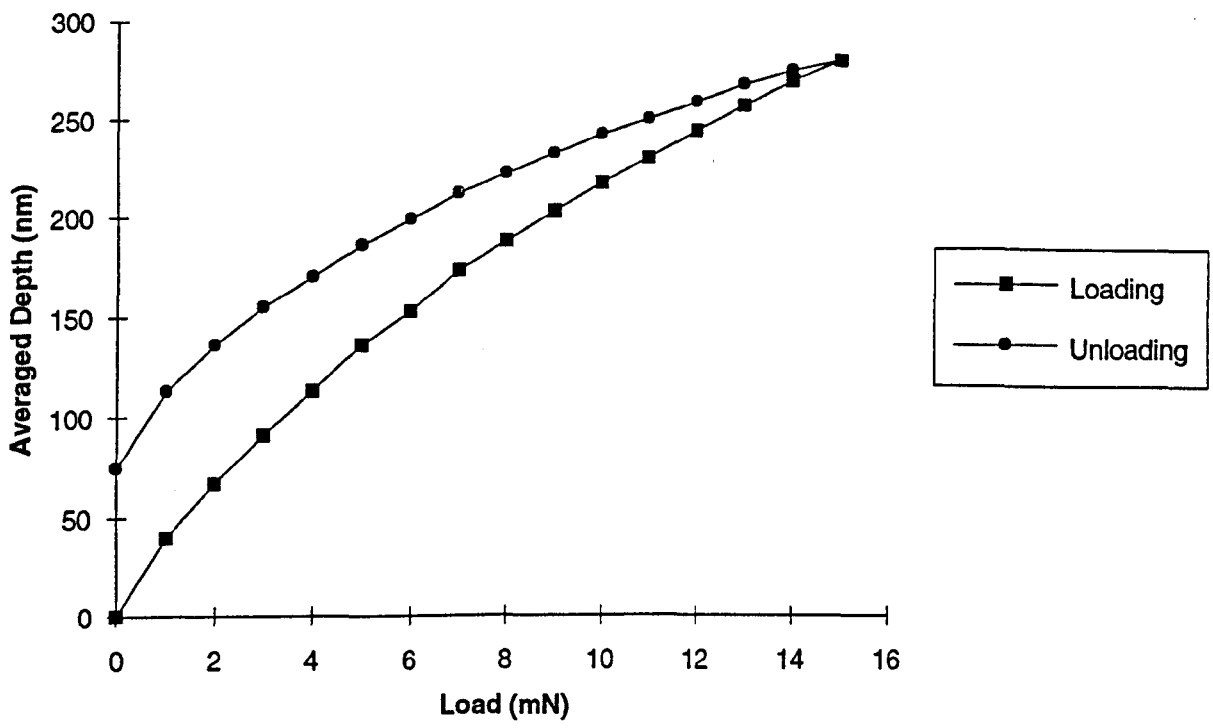


**Fig XXV A Typical Nano Indentation Hysteresis Curve**

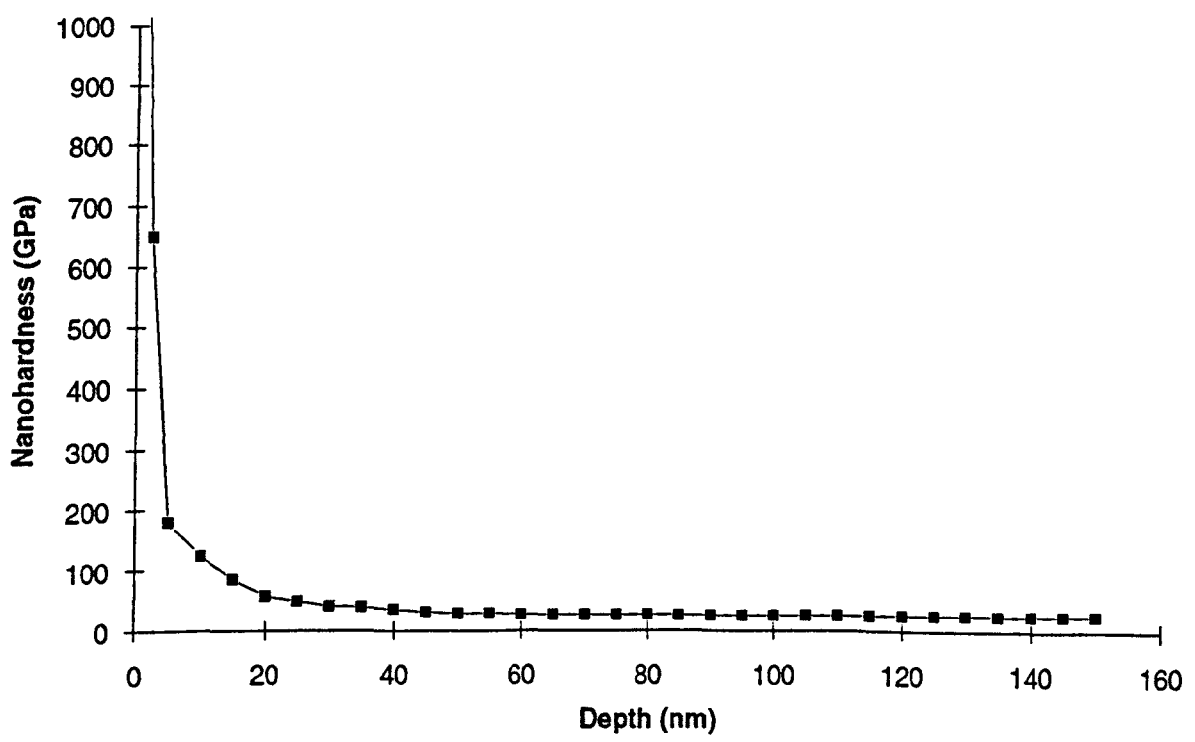


**Fig XXVI A Typical Nano Indentation Hardness/Depth Curve**

with an LVDT and remains within 1% provided that the environment is suitably controlled. Load calibration was carried out by relating the force produced by the loading coil to weights applied directly to the loading assembly and is capable of a load resolution of  $100\text{ nN}$ . The loading rate for all measurements was  $36 \times 10^{-3}\text{ N/min}$  to a maximum load set at a pre-determined level. The load would then be automatically reversed. The indenter was a triangular Berkovich pyramid with the same area to depth ratio as a Vickers diamond. This was chosen over other sharper diamond configurations in view of a number of reports indicating that diamond tips are particularly prone to damage when making contact with diamond-like films. In addition, the difficulty in producing a well defined point at the tip of Vickers and Knoop indentors arises from the fact that it is difficult to grind the four faces so that they meet at one point; the so called 'chisel affect'. The Berkovich<sup>186</sup> indenter, comprising of a three sided pyramidal shaped point which when ground closes to the sharpest tip available.

During operation of the NanoTest, specimen/indenter contact is detected when a change in capacitance occurs. The specimen is then moved towards the diamond in sub-micron increments at low velocity. The specimens were mounted on a 2.5cm diameter aluminium stub using a cyanoacrylate adhesive. As a test of consistency, measurements were performed periodically on a polished silicon standard. The unloading curves were also averaged and the resulting mean hysteresis curve produced. The depth values therefore contain both plastic and elastic contributions. In order to eliminate the elastic contributions, it was necessary to determine the elastic recovery parameter ERP<sup>187,56</sup>. This is found from the unloading branch of the hysteresis curve where the intercept at zero load represents the plastic depth. To determine variations in the ERP with depth, hysteresis curves were produced over a range of maximum depth values. Curve fitting procedures were then used to express the relationship in the form of a second-order polynomial. The determination of absolute hardness numbers depends on a detailed knowledge of the diamond geometry. No diamond will be perfectly sharp, and therefore a higher load than the theoretical will be required to initiate an indentation. Hardness versus depth curves often exhibit high apparent hardness values very close to the surface for this reasons (Fig.XXVI).

### **c) Adhesion Strength**

The adhesive strength of a coating is considered to be the amount of energy which is required to separate it from the substrate at the interface, but accurate and practical measurement of this energy proves more difficult. Therefore, the force required to separate these two junctions is more often employed as a measure of adherence. Many methods have been developed to evaluate coatings with relatively low adhesive strengths, such as Scotch tape, ASTM bond cap and bend tests<sup>188</sup>. However, there are no direct methods for measuring coatings of high adhesive strength, only indirect methods. Amongst these techniques, the scratch test appears to be the one that has led to the most meaningful and consistent results<sup>189</sup>.

The scratch test consists of introducing stresses at the interface by traversing a diamond indenter under an increasing load. The minimum load to damage the coating is called the critical load. This failure can be either cohesive (lower critical load) or adhesive (upper critical load) and is determined by examination of the tangential force and acoustic emission traces in conjunction with optical and/or electron microscopy of the scratch surfaces. Cohesive failure (fracture) is typified by an increase in acoustic emission and variations in tangential force; using microscopic observation, a good correlation between the acoustic emission and the first occurrence of delamination can be seen. Adhesive failure which results in the complete removal of the coating by ploughing into the softer substrate is characterised by large increases in tangential force (often accompanied by heavy acoustic emission). The scatter in these load measurements on the same specimen was reported generally to be within 10%<sup>190</sup>. However, there remains the difficulty in expressing adherence quantitatively since the critical load depends upon many aspects of the test procedure and of the film under test. In an excellent paper by Steinmann et al<sup>191</sup>, the inter-dependence of extrinsic parameters such as scratching speed, loading rate, diamond tip radius and diamond wear, and the intrinsic parameters, such as substrate hardness, coating thickness, substrate/coating roughness and friction coefficient are discussed in great detail.

A scratch tester produced commercially by the VTT Technology Ltd. Technical Research Centre of Finland was used during this study for films greater than 500nm in

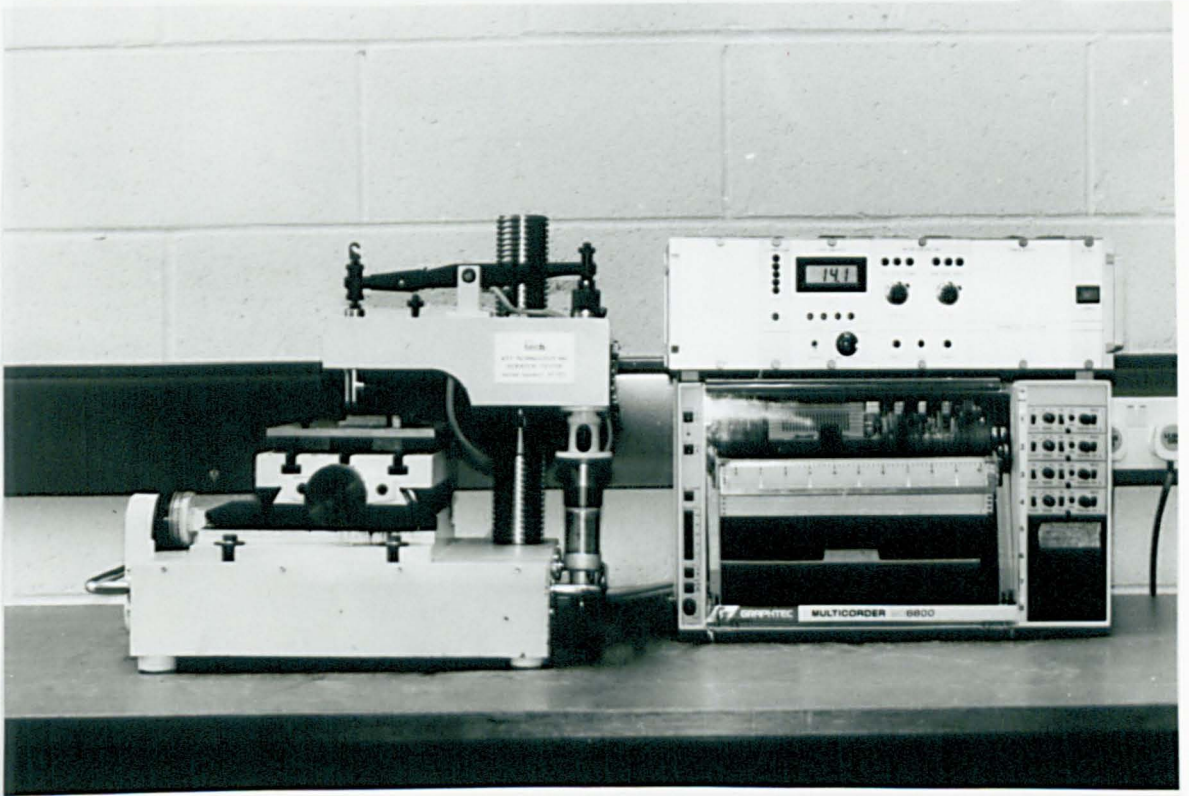


**Fig XXVII**

**A Photograph Of A Scratch Tester**

thickness (Fig.XXVII). Normal and tangential force measurements of the stylus and acoustic were monitoring with vibration-sensitive piezoelectric load cells. Operational details are given below:-

Stylus	-	Ø200µm Rockwell C diamond
Normal Force	-	0-10N (Max.)
Loading Rate	-	10N/min
Table Traversing Speed	-	0.1mm/sec

However, for films less than this arbitrary thickness it was found that a Leitz Miniload hardness tester with the diamond Knoop indenter locked in place provided a method with greater resolution for assessing the adhesive strength of these ultra thin films.

### **3. Assessment of Coating Durability**

#### **a) Pin on Disc**

The pin on disc test is a *de facto* standard test since it is used extensively for the evaluation of sliding wear and friction measurement in both industry and academia<sup>188</sup>. There are a great many characteristics of this test which strongly influence the tribological behaviour and degree of wear observed. Of these parameters; some are intrinsic such as contact pressure<sup>167</sup>, relative speed<sup>167</sup>, distance or number of wear passes<sup>192,193</sup> and system vibration<sup>194</sup> which are discussed in more detail at the end of this section. The remaining factors depend upon the environmental and physical condition of the sliding pairs. These extrinsic factors are dominated by humidity<sup>1,167</sup>, pin/disc/film chemistry<sup>193,195</sup>, lubrication or chemi-sorbed contaminants<sup>167</sup>, surface topography<sup>196,171,197</sup> and contact temperature<sup>198,195</sup>. In view of the many test variables, the complexity involved in achieving reproducible and comparable results between institutions is apparent. By fixing intrinsic factors (particularly those associated with operating procedure) more meaningful results can be obtained and this was the aim of the VAMAS (Versailles Project on Advanced Materials & Standards) interlaboratory test programme. Operating guidelines published by VAMAS and the UK Forum on Wear and Friction Testing were adopted throughout the study including the use of an environmentally stabilised and controllable test condition.

Films produced in this study were studied for their unlubricated tribological characteristics using fixed SAE 52100 tool steel balls as the pin material and coated ASP23 tool steel or cobalt chrome substrates as the disc. A schematic diagram of the pin on disc tribo-tester is given in Fig.XXVIII. Loads were applied at the pin through the action of weights positioned at the end of a lever arm. Specimens were clamped to a holder and precisely mounted on a horizontally rotating table so as to provide movement in the rotational plane only. At the beginning of a test, the pin material was brought into contact with the coated disc. By means of the normal load and the friction force measured by a load cell mounted perpendicular to the lever arm, the coefficient of friction could be calculated. Temperature and humidity stabilisation was achieved by a system of water evaporators, cooling elements and heating lights to provide the injection and extraction of water vapour and a source of heat respectively. The experimental details are given in the table overleaf:

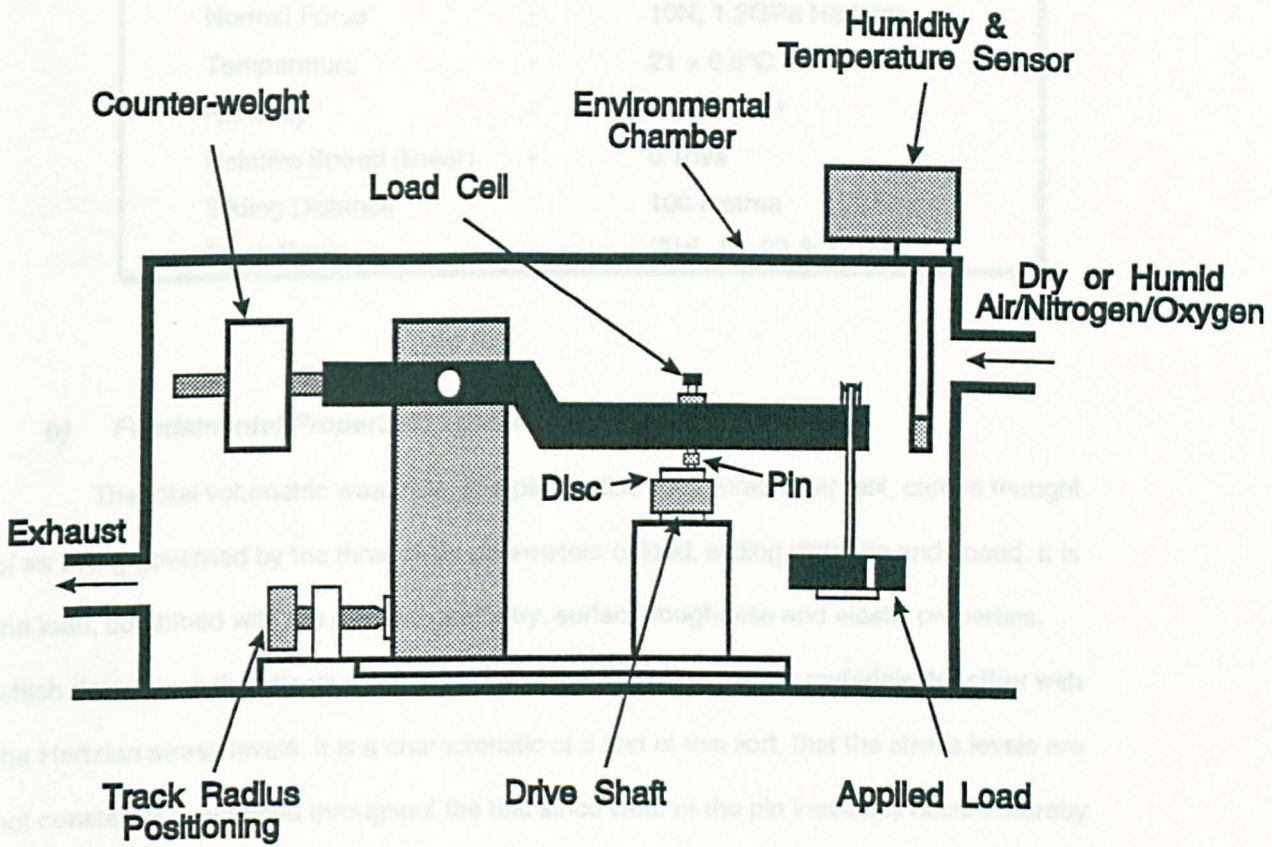


**Fig XXVIII A Schematic Diagram of a Pin On Disc Tribotester**

Pin Material	-	Ø10mm SAE 52100 (H <sub>v</sub> 700)
Normal Force	-	10N, 1.2GPa Hertzian
Temperature	-	21 ± 0.5°C
Humidity	-	50 ± 3%RH
Relative Speed (linear)	-	0.1m/s
Sliding Distance	-	100 metres
Track Radii	-	Ø16, 18, 20 & 22 mm

**b) Fundamental Properties: Load & Distance**

The total volumetric wear rate, in a pin on disc configured wear test, can be thought of as being governed by the three main parameters of load, sliding distance and speed. It is the load, combined with the pin/disc geometry, surface roughness and elastic properties, which determines the effective contact area between the two sliding materials, together with the Hertzian stress levels. It is a characteristic of a test of this sort, that the stress levels are not constantly maintained throughout the test since wear of the pin inevitably occurs thereby reducing the contact pressure. In fact, Fig.XXIX shows that as the size of the pin scar area for a typical SAE 52100/DLC pairing increases at an ever decreasing rate with sliding distance, the corresponding volumetric wear rate remains nearly constant. However due to this increase in the pin scar area a marked reduction in Hertzian contact pressure, particularly during the initial few metres of sliding, was observed. This situation is reasonably acceptable when testing DLC films as the levels of counterface wear can be relatively low. Thus high Hertzian stresses are maintained at roughly the same levels throughout the test providing the wear rates and contact areas do not rapidly increase due to premature failure of the film.

If the microscopic contact conditions can be imagined between the pin and the film, the actual contact can be thought of as being made up of many asperity contacts. An incremental increase in the applied load will provide a greater tribo-contact due to elastic and plastic deformation of these peaks. An increase in contact with load will generally increase the rate of material removal, for a given material combination and sliding speed (Fig.XXX).

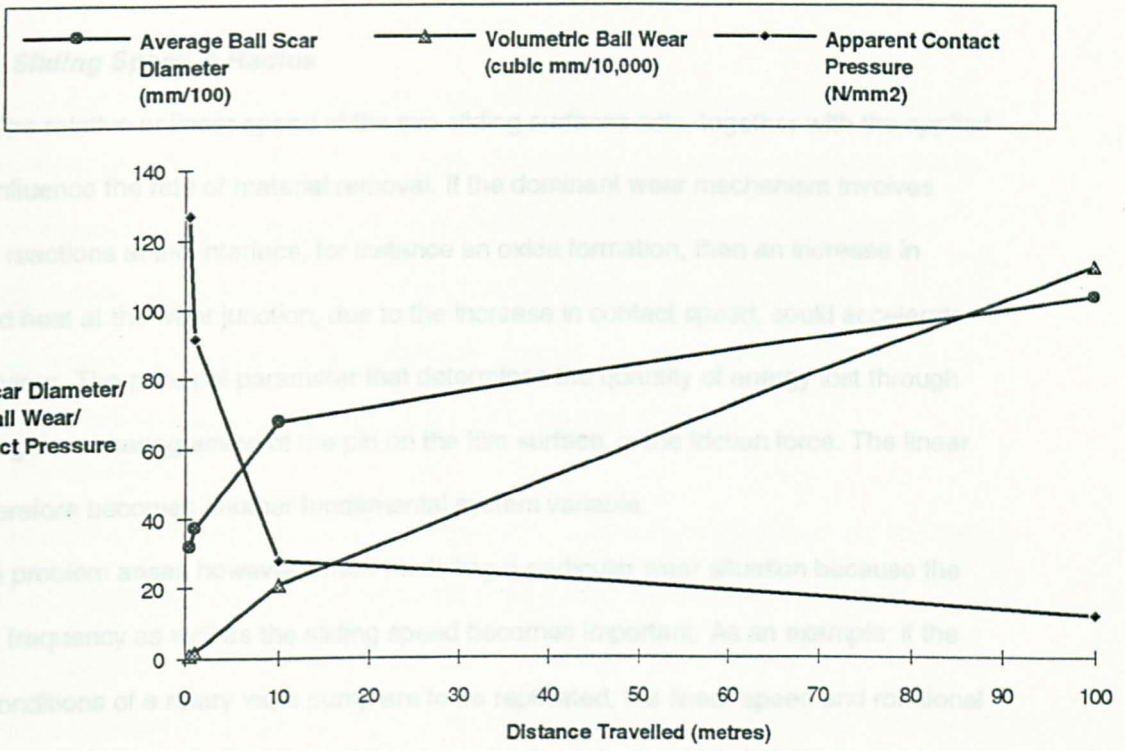


**Fig XXIX Typical Variation In Volumetric Wear and Contact Pressure With Sliding Distance For a SAE 52100 Pin Worn On DLC Coated Tool Steel**

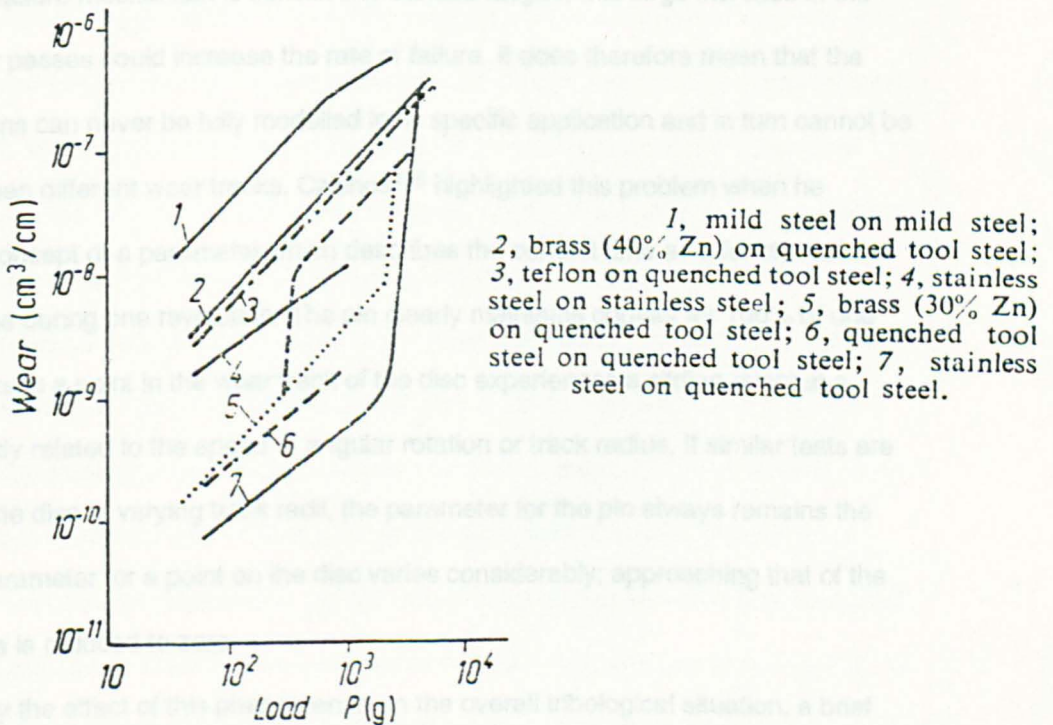


**Fig XXX Variation of Wear Rate With Load** <sup>226</sup>

### **c) Sliding Speed & Radius**

The relative or linear speed of the two sliding surfaces acts, together with the applied load, to influence the rate of material removal. If the dominant wear mechanism involves chemical reactions at the interface, for instance an oxide formation, then an increase in dissipated heat at the wear junction, due to the increase in contact speed, could accelerate this behaviour. The principal parameter that determines the quantity of energy lost through heat during the shearing action of the pin on the film surface, is the friction force. The linear speed therefore becomes another fundamental system variable.

A problem arises however, when modelling a particular wear situation because the rotational frequency as well as the sliding speed becomes important. As an example; if the contact conditions of a rotary vane pump are to be replicated, the linear speed and rotational frequency of the vane on the surface of the stator can be calculated. If modelling at a test scale is then performed, the linear contact speed can be maintained by applying a greater rotational speed at a smaller track radius. However, at these contact conditions the frequency or number of wear passes will be significantly higher for an equivalent test time or sliding distance. If the failure mechanism is sensitive to surface fatigue, this large increase in the number of wear passes could increase the rate of failure. It does therefore mean that the contact conditions can never be fully modelled for a specific application and in turn cannot be the same between different wear tracks. Czichos<sup>195</sup> highlighted this problem when he discussed the concept of a parameter which describes the contact time as a function of the total contact time during one revolution. The pin clearly maintains contact for 100% of one revolution, whereas a point in the wear track of the disc experiences a sliding event at a frequency directly related to the speed of angular rotation or track radius. If similar tests are performed on one disc at varying track radii, the parameter for the pin always remains the same but the parameter for a point on the disc varies considerably; approaching that of the pin as the radius is reduced to zero.

To study the effect of this phenomenon on the overall tribological situation, a brief experiment to measure the wear of SAE 52100 tool steel pins on titanium nitride coated discs, were performed under conditions of fixed sliding speed but varying track radii. Fig.XXXI

shows clearly that the pin and film wear increases with sliding distance as expected and as the test track radius extends, the wear rate tends to increase. This is a somewhat surprising result since it would be expected that the greater number of wear passes would lead to a higher level of wear. To overcome the problem, tests of different thin films were performed at similar radii, relative sliding speed and therefore frequency, so that the above affect could be ignored and a more accurate comparison of film properties be achieved.

**d) Pin Material**

The function of the pin is to maintain the applied pressure on the film during the test. As mentioned previously the pin undergoes wear itself during the test which causes a reduction in applied pressure. The pin therefore has the basic requirement of being hard and relatively wear resistant to maintain as near constant contact condition throughout the test as possible. The friction and wear characteristics are of course dependent upon which material is chosen for the pin and so VAMAS directed that a standard pin material of carbon-chrome tool steel should be used. This specification has since been found to result in greatly differing performances during a round robin<sup>199</sup> exercise based on the tribological behaviour of TiB<sub>2</sub>+BN and TiAlN coatings owing to the slightly different grades of the same material. An experiment was performed by wearing two grades of carbon-chrome tool steel material on a FAB source DLC film and it showed that whilst the M50 tool steel produced a typical well defined wear track, the SAE 52100 tool steel pin showed heavy transfer of the pin material to the disc (producing negative film wear)(Fig.XXXII). This behaviour is indicative of strong adhesive metal to metal contact and resulted in the rapid degradation of the surface finish, an accelerated removal of the pin material and a rapid rise in the friction coefficient to  $\mu \approx 0.5$ . EDX microanalysis showed a very similar spectrum for both of the carbon-chrome tool steel materials, although additional elements of sulphur and vanadium, together with traces of nickel, could be found in the composition of M50. It has been known for some time that small additions of alloying elements such as sulphur enhances the machineability of steels and Buckley demonstrated that as little as 0.45%S can markedly effect the wear performance of sliding pairs by the formation of iron sulphide at the interface<sup>199</sup>. EDX observations confirm the presence of a build up of sulphurous deposit at the contact regions of the M50 pin and

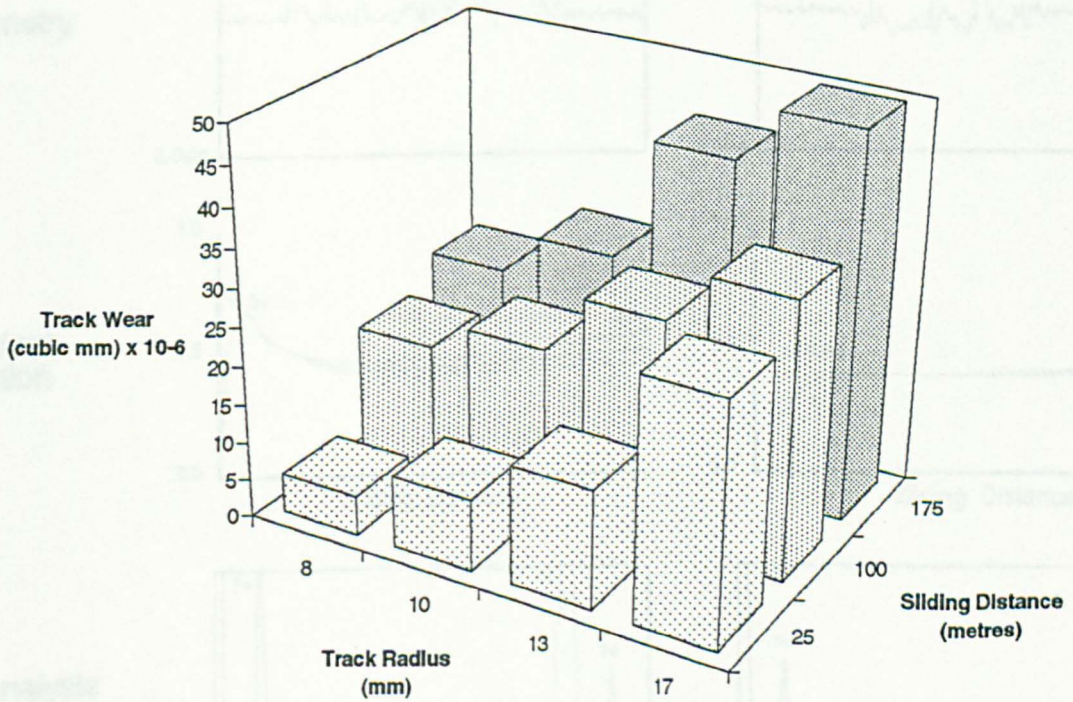
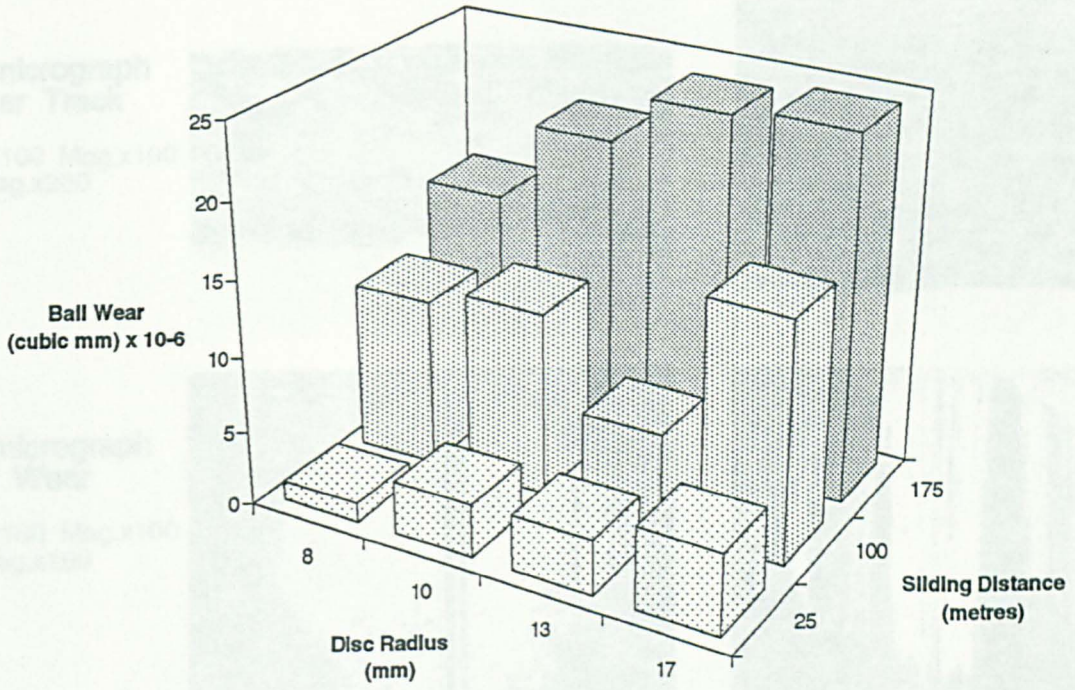
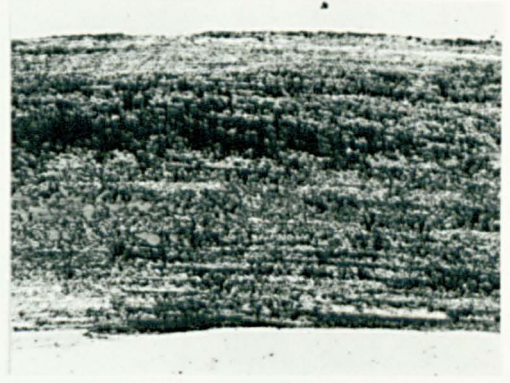


Fig XXXI Variation in Wear with Sliding Distance for Differing Track Radii

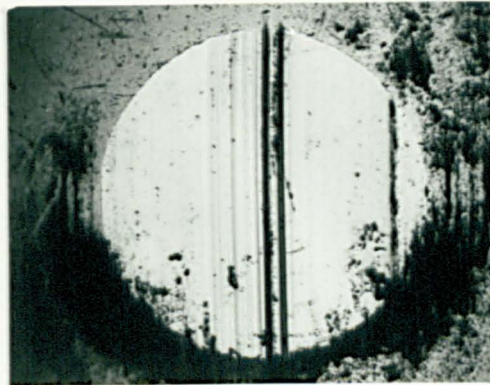
**Photomicrograph of Wear Track**

AISI 52100 Mag.x100  
M50 Mag.x200

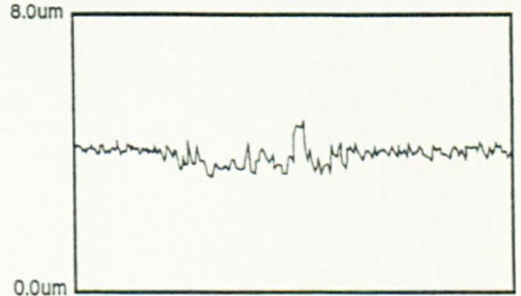
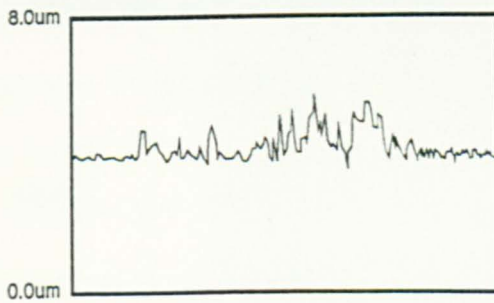


**Photomicrograph of Pin Wear**

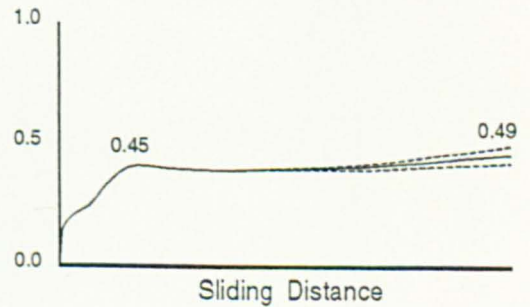
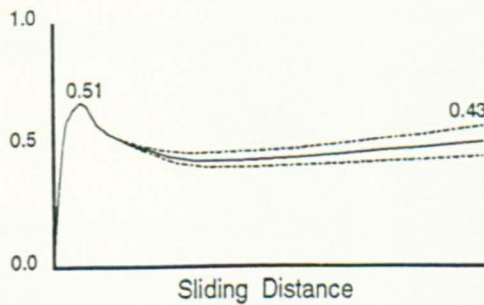
AISI 52100 Mag.x100  
M50 Mag.x100



**Profilometry**

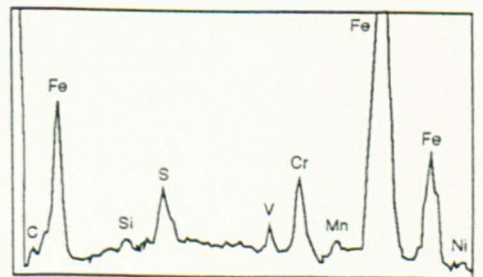
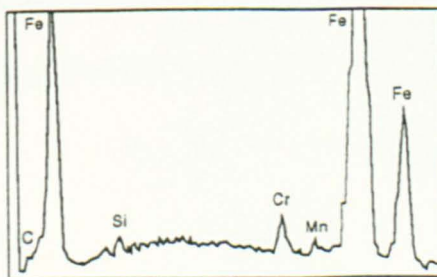


**Coefficient of Friction**



**EDX Microanalysis**

Beam Voltage - 7keV



wear track. The importance of the composition of the pin material has been made apparent and for this reason attention has been paid to maintain the same pin material (SAE 52100) throughout all the tribological tests to date.

**e) Tribological Methodology**

As mentioned previously, a set-up and operating procedure was adopted in accordance with that proposed by VAMAS and the UK Forum on Wear and Friction Testing. The subsequent measurement and interpretation of the resulting tribological performance and determination of the pin and disc wear volumes was performed in agreement with procedures outlined by the UKFWFT<sup>200</sup> and in full compliance with the German Standard for 'Model experiments on sliding friction in solids' (DIN 50 324)<sup>201</sup>.

Pin wear volumes were calculated by optically measuring the diameter of the wear scar in both the parallel and perpendicular directions to motion and assuming a near-flat wear profile, the volume could be calculated using the formula;

$$W_b = \frac{1}{3} \pi h^2 (3R - h) \quad (\text{mm}^3)$$

where:  $h = R - \sqrt{R^2 - \frac{d^2}{4}}$

R = radius of the pin

d = average pin scar diameter (L, l)

or from the approximate formula;

$$W_b = \frac{\pi d^4}{64R} \quad (\text{mm}^3)$$

This formula has been calculated to be correct to within 1% for pin wear diameters <0.3R. Again, in-line with German and proposed British Standards, the pin wear was expressed in terms of volumetric loss normalised with sliding distance and applied load. The pin wear coefficient can be calculated from the following formula;

$$K_b = \frac{W_b}{F_n \cdot s} \quad (\text{mm}^3/\text{Nm})$$

where:  $W_b$  = volumetric wear  
 $F_n$  = normal force  
 $s$  = sliding distance

The wear rate of the pin is a complex relationship, highly dependent upon lubricating factors, conformity between the surfaces, deformation, loading and environmental conditions. It reveals little about the wear resistant nature of the film since it is possible to have heavy counterface wear whether the film undergoes widespread or superficial wear. Indirect examination of the extent of film wear is therefore impossible to achieve from study of the counterface material alone. The degree of pin wear indicates fundamentally the level of Hertzian pressure to which the film/substrate combination is subjected.

Actual determination of the film wear, in contrast, is a far more elaborate and difficult procedure to perform accurately. Commonly, two methods (gravimetric and profilometry) are employed depending upon the quantity of material lost in the track profile during the wear process. Gravimetric techniques are more suited to high volume loss whereas profilometry is more useful for the volume losses associated with DLC thin films. For the more extreme wear resistant films, it becomes increasingly difficult to determine clearly the well defined track wear profile particularly when the films undergo modification by polishing wear which simply removes the highest surface asperities. In addition, the visual inspection of the wear track is made more difficult due to the transparent nature of these films. Despite these difficulties, the wear track volumetric loss was calculated using profilometry together with the following formula;

$$W_t = 2\pi r \cdot V_t \quad (\text{mm}^3)$$

where:  $r$  = track radius  
 $V_t$  = planimetric cross-sectional area of track

Based on this wear the wear track coefficient  $K_t$  could be estimated to be as follows;

$$K_t = \frac{W_t}{F_n \cdot s} \quad (\text{mm}^3/\text{Nm})$$

where:  $W_t$  = volumetric wear  
 $F_n$  = normal force  
 $s$  = sliding distance

As the aim of the wear tests was primarily to quantify the improved performance of the carbon based films over that of SAE 52100 pin run on uncoated ASP23 tool steel; several

wear tests were initially performed to establish the order of magnitude of both wear and friction for this uncoated metallic pairing. The results of these tests showed that the ball wear and film track width to be in the order of  $12-20 \times 10^{-6} \text{ mm}^3/\text{Nm}$  and  $64-87 \times 10^{-6} \text{ mm}^3/\text{Nm}$  respectively (Fig.XXXIII) with a range of friction values between  $\mu = 0.45-0.54$ . It was these tribological performances which were subsequently used as the 'standard' with which the carbon deposited coatings could be gauged.

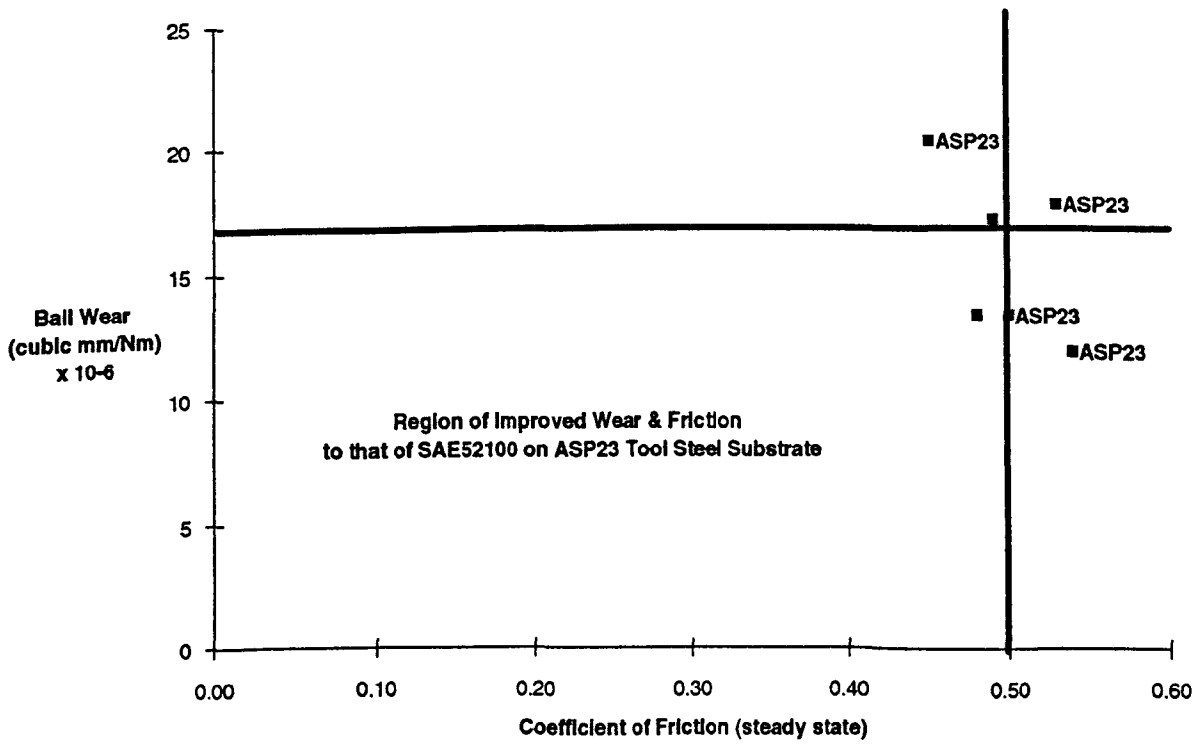
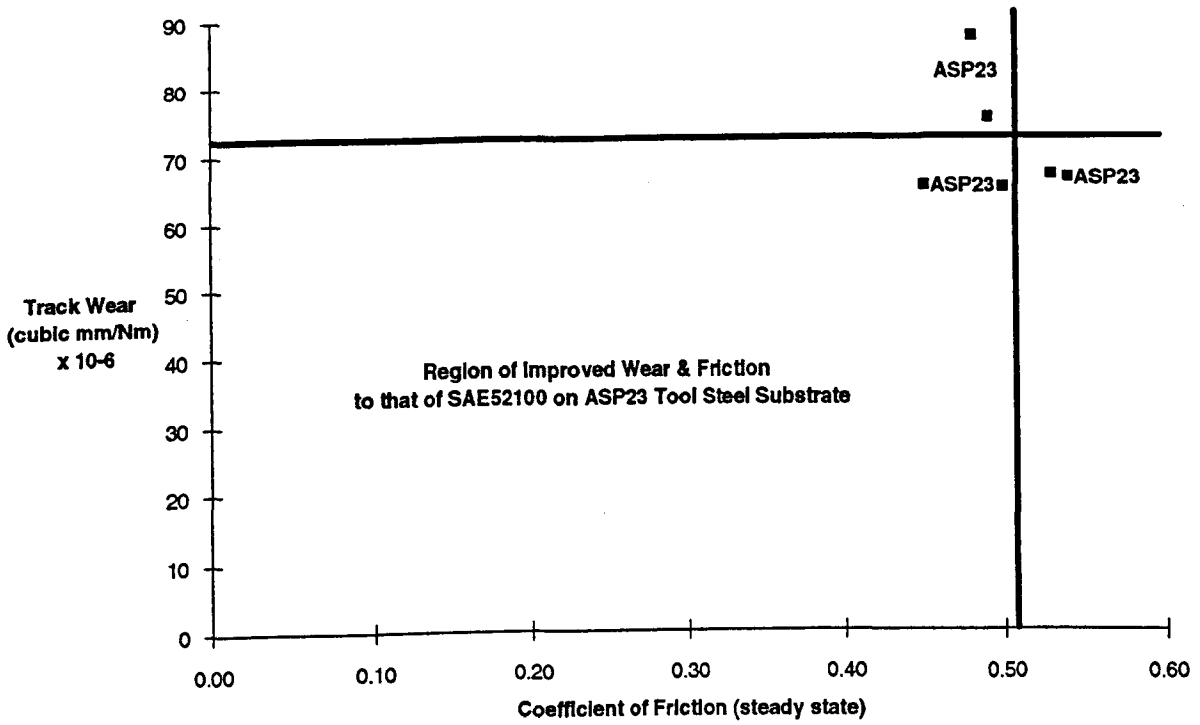


**Fig XXXIII The Wear of SAE 52100 Tool Steel Pin Material Against Uncoated ASP23**

## **4. Surface Analytical Studies**

### **a) Optical Microscopy**

Optical microscopy for topographic observation or detailed measurement was achieved using a Nikon Optiphot microscope. Observation of samples could be undertaken at magnifications of between x 10 to x 400 with an additional facility to record the images using a UFX-IIA photomicrographic attachment. A Nikon Filar Micrometer eyepiece was used to measure dimensions down to  $1\mu\text{m}$  with a vernier resolution of  $100\text{nm}$ . Optical microscopy was used during microindentation testing, film thickness measurement, wear scar examination, adhesion assessment, topographic and metallography studies. All these activities were performed routinely with further detailed work being fulfilled by the scanning electron microscope.

### **b) SEM/EDX**

Fine scale structural, topographic and dimensional measurements, beyond the scope of optical microscopy, were carried out using a scanning electron microscope (Fig.XXXIV) capable of providing photomicrographs up to magnifications of x 100,000 on suitable specimens. The process principally involves the generation of a primary beam of electrons from an emission source which are then accelerated in an electron column and focused with a maximum acceleration potential of between 5-30keV at the specimen. A scanning coil placed before the final lens causes the electron spot to raster in the form of a square. Various phenomenon occur at the surface of the sample including secondary electron emission which in this case is used to form the image. Some of the electrons are inelastically scattered by the K,L or N electron shells in the atom losing their energy in the form of X-rays and it is these which are detected in energy dispersive X-ray analysis (EDX). The energy lost is characteristic of the scattering atom and the intensity is used to establish the concentration of the element. EDX utilises a solid state detector to measure the X-ray radiation which is more sensitive to elements of higher atomic mass.

Structural examinations were undertaken with a Cambridge Stereoscan 200 scanning electron microscope and this provided confirmation of measurements made of microindentation hardness, profilometry and optical techniques. Qualitative chemical

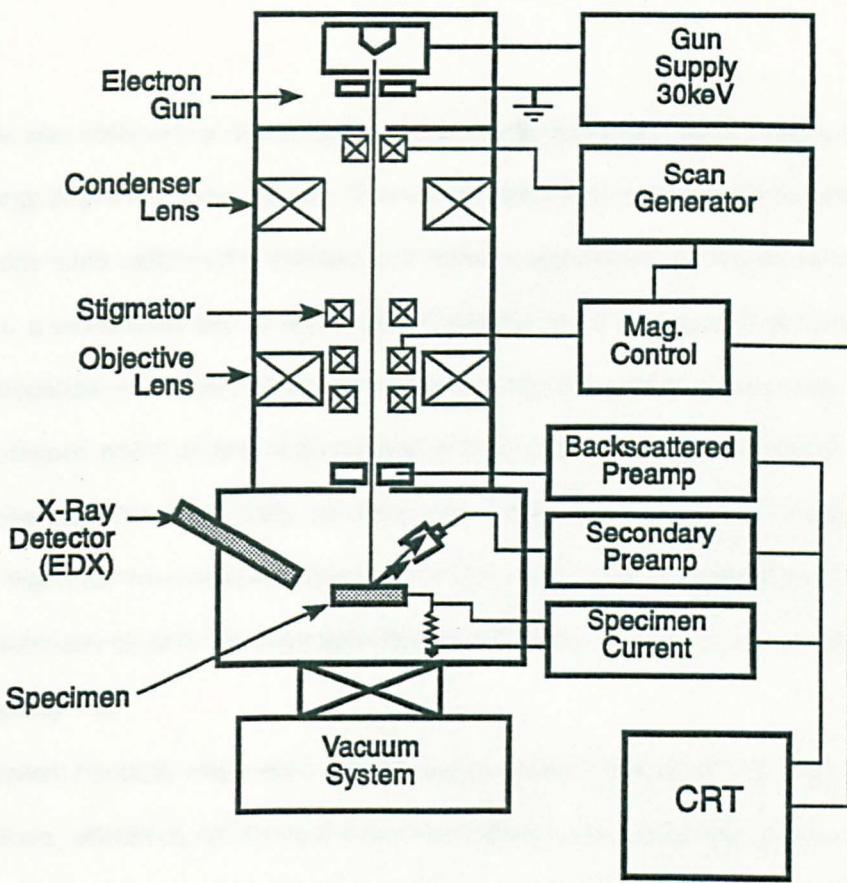


Fig XXXIV Schematic Layout of a Scanning Electron Microscope

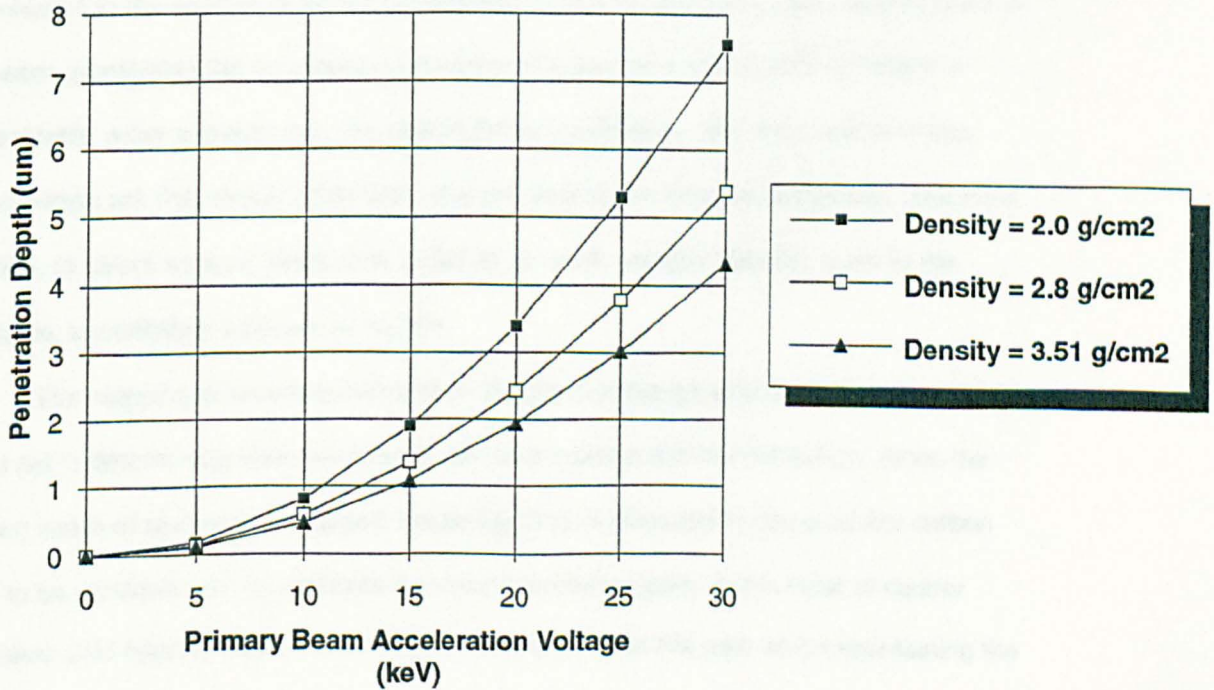


Fig XXXV Electron Beam Penetration versus Primary Beam Energy

microanalysis was obtained by detecting the characteristic X-ray emissions using a LINK QX2000 energy dispersive X-ray system. Semi-quantitative information could be obtained if X-ray emissions were calibrated to standards of known composition. For the detection of carbon layers, a windowless lithium drifted silicon detector Si(Li) was used. The sensitivity of this method depends on the mean free path of the arriving and emitted species and on any secondary collisions which causes radiation scatter in the vacuum. It is for the latter reason and the fact that contaminants readily condense onto the cryogenically cooled, windowless X-ray detector, that a minimum vacuum requirement of  $5 \times 10^{-5}$ Torr was maintained. This non-destructive technique gives a minimum detection limit of below 0.1% in the best conditions and more typically 1%.

A problem normally associated with thin layers is beam penetration through the film into the substrate, effectively rendering the film transparent to the detecting electron beam. Fig.XXXV shows the theoretical penetration depth for different acceleration voltages on the density of the material (diamond  $\rho=3.51\text{g/cm}^3$  and DLC  $\rho=2.0\text{-}2.8\text{g/cm}^3$ ). This penetration can be minimised by selecting a low beam acceleration voltage (7keV) for analysis of the films and increasing the apparent film thickness by orienting the electron beam to a grazing angle with respect to the sample. A further point to add is that the sampling zone parallel to the X-ray beam, penetrates the substance in the form of a pear shape (Fig.XXXVI), which is considerably wider at depth than the size of the focused beam. The implications of this phenomenon are that should cross-sectional analysis of thin films be performed, care must be taken to select an area sufficiently small so as not to sample material, such as the substrate, immediately adjacent to the film.

Dot mapping of selected elements in the pin or coating material allowed a further visual aid in determining material transfer, element location and concentration. Since the probing beam of electrons is charged, insulating films of diamond or diamond-like carbon need to be provided with an artificially provided conducting path. A thin layer of sputter deposited gold approximately 10nm thick is used to provide this path whilst maintaining the structural detail (Chap.III Sec.A(d)).

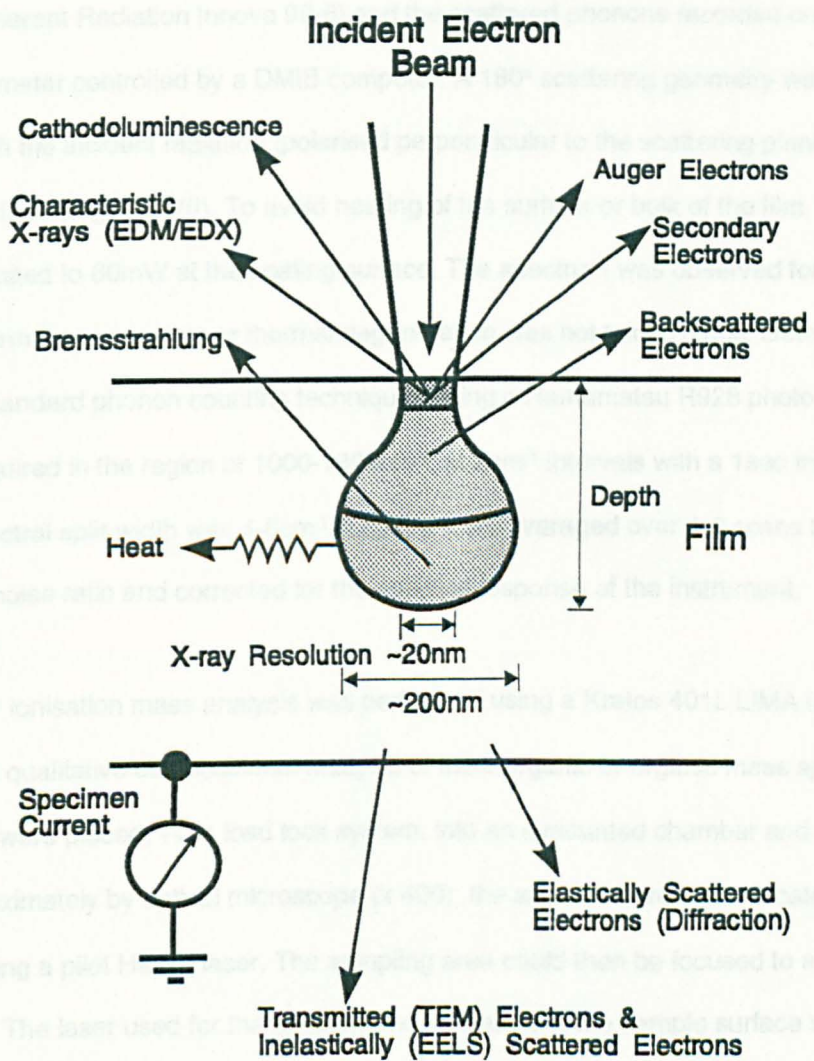


Fig XXXVI Energy Dispersive X-ray Sampling Zone

### **c) Raman**

Raman spectroscopy is a technique involving the inelastically scattered light from vibrational excitations within the sample. The excitation was achieved by a 488.0nm argon ion laser (Coherent Radiation Innova 90-6) and the scattered phonons recorded on a Spex 1403 spectrometer controlled by a DMIB computer. A 180° scattering geometry was employed with the incident radiation (polarised perpendicular to the scattering plane) normal to the film surface (Fig.XXXVII). To avoid heating of the surface or bulk of the film, the laser power was limited to 60mW at the coating surface. The spectrum was observed for several hours to confirm that annealing or thermal degeneration was not taking place. Detection was possible by standard phonon counting techniques using a Hamamatsu R928 photo multiplier. Data was acquired in the region of 1000-1800cm<sup>-1</sup>, at 2cm<sup>-1</sup> intervals with a 1sec integration time. The spectral split width was 4-5cm<sup>-1</sup>. Spectra were averaged over 4-6 scans to improve the signal to noise ratio and corrected for the spectral response of the instrument.

### **d) LIMA**

Laser ionisation mass analysis was performed using a Kratos 401L LIMA facility. It enables rapid qualitative compositional analysis of the inorganic or organic mass spectrum. The samples were placed, via a load lock system, into an evacuated chamber and once aligned approximately by optical microscope (x 400), the area of interest was located accurately using a pilot He:Ne laser. The sampling area could then be focused to a diameter of 1.5-2.0µm. The laser used for the ablation and ionisation of the sample surface was a Q-switched Quanta-Ray Nd:YAG laser (266nm, repetition rate - 1Hz) operating for a time of ~5ns. The energy delivered was in the range of 20-30mJ at a power output of ~10<sup>8</sup>Wcm<sup>-2</sup>. The resulting secondary ions were then redirected through, first an ion deflector and then reflected through a time of flight mass spectrometer towards an electron multiplier. Traces of ion intensity against time were then converted to an intensity against mass by a Hewlett-Packard 9000 series computer and the results printed on a 7550A graphics plotter. The LIMA technique has the ability to do composition analysis with depth profiling, the rate of profiling being determined by the laser energy and the material being sampled.

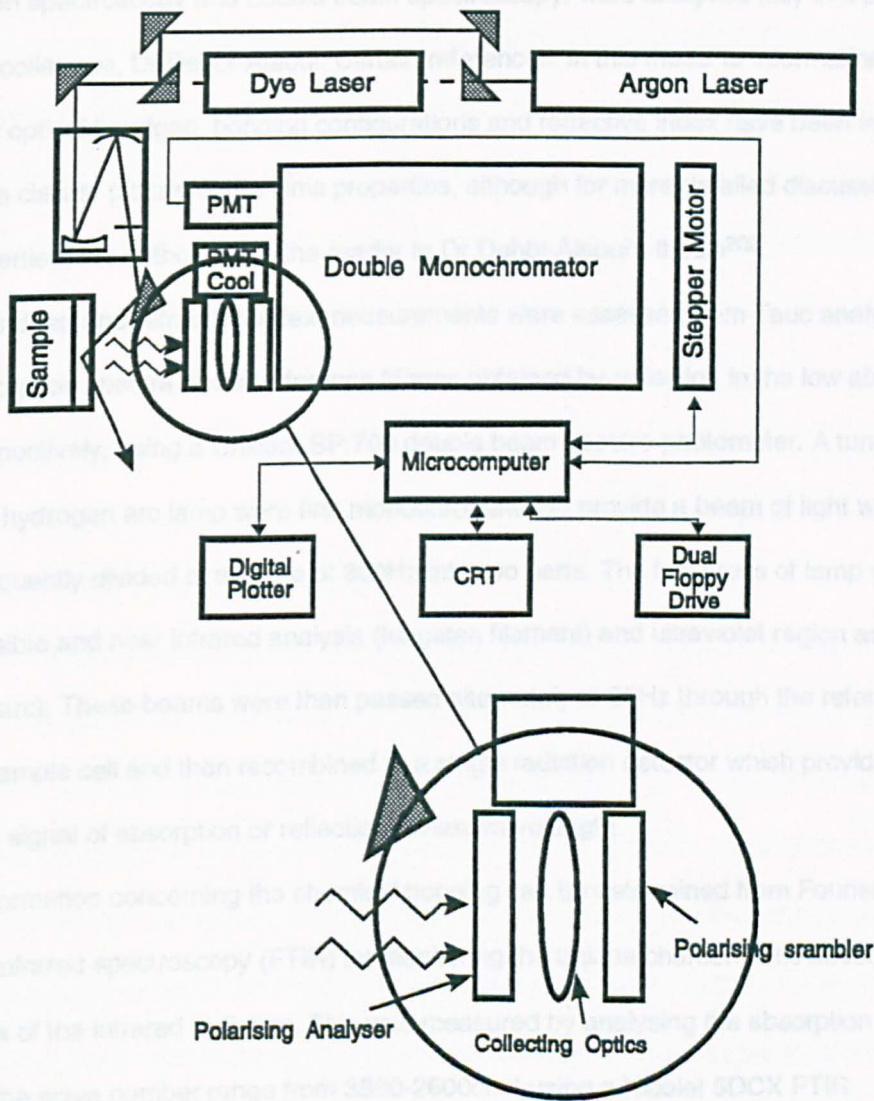


Fig XXXVII

Schematic Diagram of Raman Spectroscopy

### **e) Optical Spectroscopy/FTIR**

Optical evaluations of the amorphous diamond-like films, using single beam Fourier transmission spectroscopy and double beam spectroscopy, were analysed fully in a parallel study by a colleague, Dr. Dehbi-Alaoui. Certain references, in this thesis to information concerning optical bandgap, bonding configurations and refractive index have been included to provide a clearer picture of the films properties, although for more detailed discussions on these properties, the author refers the reader to Dr. Dehbi-Alaoui's thesis<sup>202</sup>.

Bandgap and refractive index measurements were assessed from Tauc analysed, visible absorption spectra and interference fringes obtained by reflection in the low absorption regime respectively, using a Unicam SP.700 double beam spectro-photometer. A tungsten filament or hydrogen arc lamp were first monochromated to provide a beam of light which was subsequently divided at the rate of 300Hz into two parts. The two types of lamp were used for visible and near infrared analysis (tungsten filament) and ultraviolet region analysis (hydrogen arc). These beams were then passed alternately at 25Hz through the reference cells and sample cell and then recombined at a single radiation detector which provided a continuous signal of absorption or reflection versus wavelength.

Information concerning the chemical bonding can be determined from Fourier transform Infrared spectroscopy (FTIR) by monitoring the unique characteristic absorption frequencies of the infrared radiation. This was measured by analysing the absorption band located in the wave number range from 3300-2600 $\text{cm}^{-1}$  using a Nicolet 5DCX FTIR spectrometer.

## **IV. RESULTS**

### **A. Initial Studies**

Since Aisenberg and Chabot deposited amorphous diamond-like coatings in 1971, such films have been produced by a great many different deposition methods including plasma assisted CVD, PVD and ion beam techniques from a variety of solid and gaseous precursors. There are, in turn, a great many derived system configurations within each generic deposition method so that there are perhaps, as many individual variants as there are research laboratories working in this field. Some of the early papers concentrated on the direct deposition of graphite in vacuo. The resulting films generally had poor structural properties since they tended to contain high levels of  $sp^2$  bonding. This result does not seem surprising since it is probable that, to a large degree, direct deposition of graphite without modification was occurring in most cases.

Plasma techniques however, utilise the ionisation of such evaporated species to improve the film properties, particularly adhesive strength and hardness, by imparting a directionality and energy to the evaporated flux. This is achieved by the application of a potential drop between the substrate and plasma so that the specimen surface becomes negatively biased with respect to the ionised species. The species are then accelerated towards the cathode or specimen holder with enough energy, depending upon the plasma conditions, to improve the interfacial mixing of the substrate surface with the initial atomic layers of coating to greatly enhance the adhesive properties. Furthermore, the residual energy of the particles upon impact is dissipated by either adatom mobility so that further structural reordering can take place or sputtering of the material.

At an early stage in this study, it was decided that a series of preliminary experiments would be performed to test the benefit of this ionisation mechanism. This was achieved by evaporating graphite directly onto a metallic substrate, secondly by evaporating and depositing graphite with the aid of an inert plasma and lastly by evaporating and depositing graphite in a hydrocarbon plasma<sup>203</sup>.

## 1. Preliminary Studies Into DC Evaporated PVD Films

### a) *Film Preparation & Experimental Details*

Carbon films were deposited in the experimental vacuum deposition system described in Chap.III Sec.A(a). The core of the arrangement consisted of a floating filament source providing a constant electron supply to an electron beam evaporation arrangement. A thermally insulating graphite crucible containing the evaporant was situated in the base of the chamber and made to attract the emitted electrons by the application of a positive DC voltage (0.75-4kV) through a 'focusing' ring placed just above the crucible. It has been suggested that at the high anodic potentials the ring served two functions. Firstly, to sustain a glow discharge of positive potential between the anodic ring and the chamber walls, thus turning the earthed filament source into a (relatively) biased electron emitter and directing a flux of high energy electrons towards the crucible. Its second purpose was to maintain a plasma within the ring itself, so as to ionise any subsequently evaporated species travelling from the crucible to the sample holder. Since the filament source, anodic ring and crucible were vertically aligned, the plasma could simultaneously ionise the evaporated species and be enhanced by the electron emission from the filament. Furthermore, the filament provided a mechanism for preheating the substrates to  $\sim 160^{\circ}\text{C}$  prior to deposition.

Following argon precleaning and filament preheating, identically prepared ASP23 tool steel and glass samples were subjected to the three deposition regimes;

- evaporate graphite at a pressure of less than  $5 \times 10^{-5}\text{Torr}$ , ring bias voltage of 4kV, 100mA and a maximum substrate temperature of  $350^{\circ}\text{C}$ .
- evaporate graphite in an inert argon plasma at a pressure of  $5 \times 10^{-5}\text{Torr}$ , ring bias voltage of 4kV, 100mA and a maximum substrate temperature of  $350^{\circ}\text{C}$ .
- evaporate graphite in a butane ( $\text{C}_4\text{H}_{10}$ ) plasma at a pressure of  $5 \times 10^{-2}\text{Torr}$ , ring bias voltage of 0.75kV, 300mA and a maximum substrate temperature of  $160^{\circ}\text{C}$ .

In such a way, carbon (C), amorphous ion assisted carbon (a-C) and amorphous hydrogenated ion assisted carbon (a-C:H) films could be produced. After deposition, the films were mechanically tested for microhardness, tribological properties and thermal stability.

Analysis of the plasma assisted coatings by analytical techniques including Raman, LIMA and

single beam FTIR were additionally carried out to reveal the extent to which the structure of the deposited film had been modified by the presence of ion assistance and/or the presence of hydrogen.

**b) Film Properties**

In both the cases involving plasma assisted deposition, amorphous films of well bonded hard carbon were deposited onto ASP23 tool steel and glass. The rate of deposition was highly dependent upon the substrate, with a rate of 1 $\mu$ m/hr for tool steel and 0.4 $\mu$ m/hr for glass. In the case of unmodified evaporated graphite, the film was particularly prone to spallation.

	DC Electron Evaporation	DC Argon Plasma + Electron Evaporation	DC Butane Plasma + Electron Evaporation
Microhardness H <sub>k</sub>	soft	2005 (15g)	4790 (25g)
Thermal Stability	<100°C	310°C	520°C
Durability To Sliding Wear	Immediate Failure 5N	Failure after 100m 5N	Failure after 100m 30N
Coefficient of Friction $\mu$	N/A	0.48	0.13
Structure	uneven deposition containing particulates	amorphous	dense amorphous, containing hydrogen

*Table VI Mechanical & Physical Properties of C, a-C & a-C:H DC PVD films*

It was found that the microhardness values of the plasma assisted coatings (Table VI) were considerably higher than those from evaporated graphite alone, reflected by a considerably improved resistance to sliding wear. Of the two plasma assisted coatings, the ultimate load sustainable before coating failure was witnessed could be increased from 5 to 30N and simultaneously the friction improved from  $\mu=0.48$  to 0.13, by the use of butane in the deposition process. However, the degree of ionisation between the two plasmas differed greatly. The inert argon plasma operating at pressure of  $5 \times 10^{-5}$ Torr, was noted to sustain a low intensity glow discharge indicating a low level of ionisation. In contrast, the butane plasma

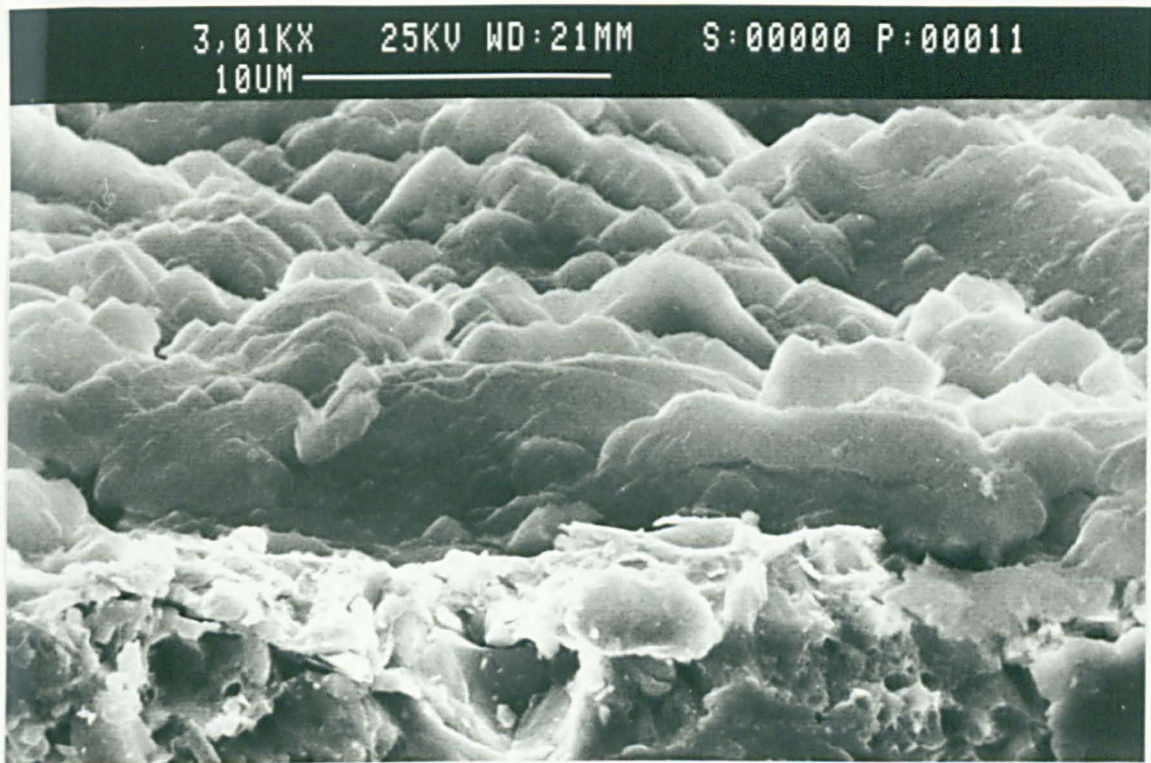
operated at  $5 \times 10^{-2}$  Torr exhibited an intense glow indicative of a much higher levels of ionisation. It was therefore concluded that the degree of ion bombardment was considerably greater for the a-C:H films than the a-C films, which goes some way to explaining the clear differences in material properties between these two plasma treated specimens.

SEM observation of the films showed both the plasma deposited a-C and a-C:H films to have a predominantly amorphous, dense, pinhole free morphology, attributable to the energetic bombardment during deposition. The presence of micro-particles, of up to  $1 \mu\text{m}$  in size, points to the method of tableting for the preparation of pellets of powdered graphite source material to be unsatisfactory. These morphologies were in stark contrast to the unevenly distributed film characteristics of the directly evaporated graphite which included large areas of randomly sized and distributed particulates, delamination and porosity (Fig.XXXVIII). The markedly improved morphologies using ion assistance seem to strengthen the importance of ion plating (even at a low level of ion energy activity) in the densification and structural reordering which subsequently improves the film's structural properties.

An important operating constraint in the use of hard carbon films for mechanical systems, is their high temperature instability. Results derived from observations of the coating's permanence when subjected to increased temperature showed clearly that once again the plasma assisted films maintained their mechanical and structural properties to a higher critical temperature than that of the evaporated graphite. Furthermore, the hydrogenated carbon films deposited at greater plasma intensities, displayed a slightly improved performance overall.

Micro-structural analysis, particularly transmission electron spectroscopy, by Fitzgerald & Henderson<sup>204</sup> and Tither et al<sup>205</sup> verify the predominantly amorphous nature of both sets of plasma assisted films. High resolution studies revealed the films to be not entirely amorphous however, with indications of nano-crystals randomly distributed throughout the samples. Diffraction patterns have also provided evidence of the presence of polycrystalline graphite (Fig.XXXIX), although the incidence of these crystalline components was reported to be nevertheless exceptionally low.

### Evaporated Graphite Deposition



### Plasma Assisted Graphite Deposition

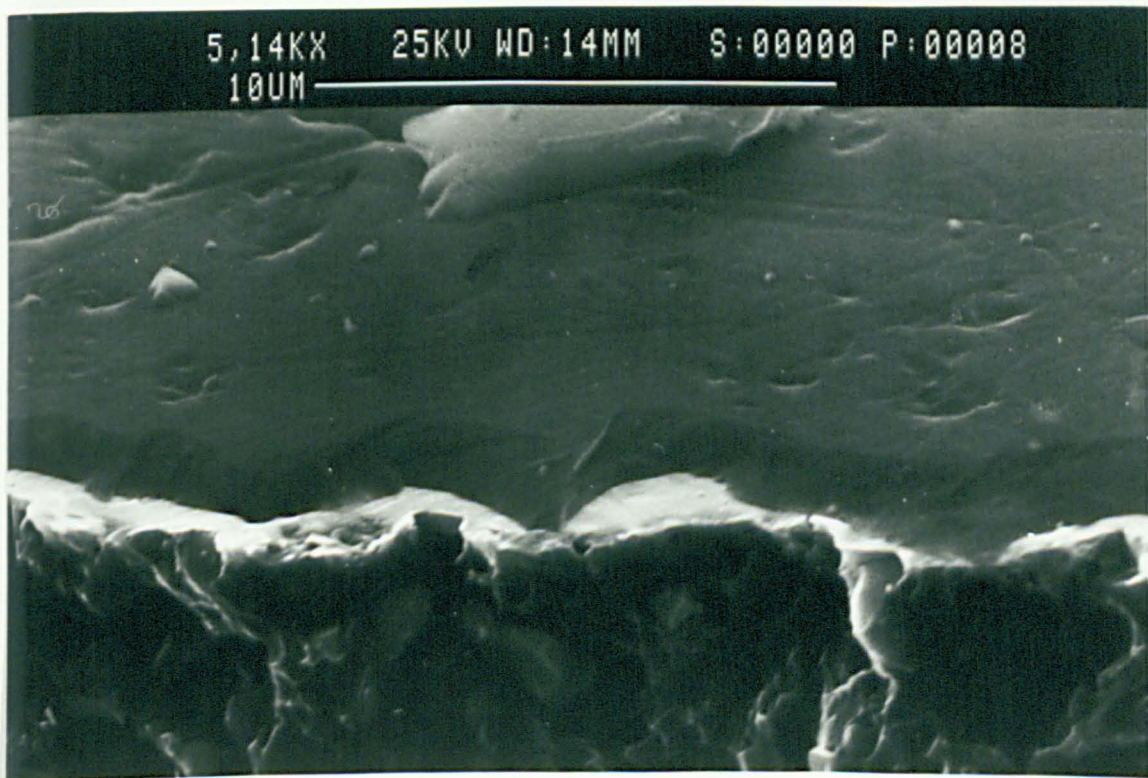
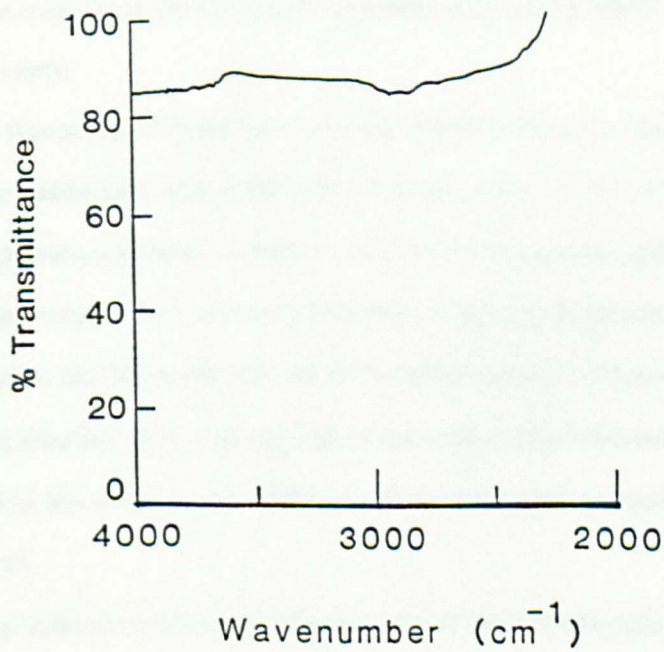
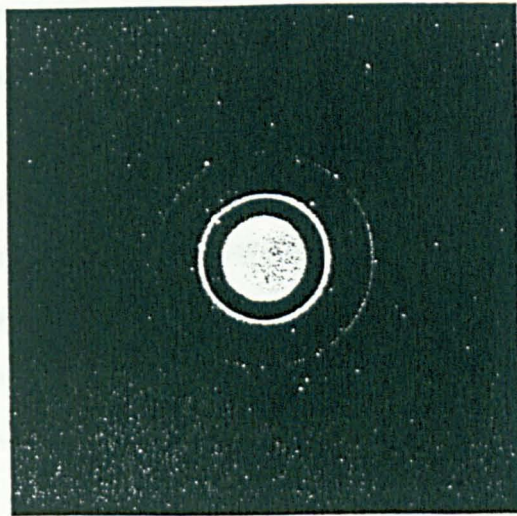


Fig XXXVIII

SEM Micrographs Showing The Difference Between Directly Evaporated Or Plasma Assisted Graphite Deposition



**Fig XXXIX** Electron Diffraction Pattern And Optical Transmission of a-C:H Plasma Assisted PVD Coating

Additional studies, using both XPS and Auger analysis, confirmed the detection of carbon with the characteristic bonding energies associated with that of graphite for both films. Secondary ion mass spectra (SIMS) of the butane plasma deposited samples showed C-C and C-H bonding arrangements with an overall estimated hydrogen concentration to be as high as  $45 \pm 15 \text{ at. \%}$ <sup>205</sup>. This figure includes both bonded and unbonded forms of hydrogen since the secondary ionisation process used to probe the sample surface is incapable of differentiating between the bonding arrangements prior to ionisation. It was therefore necessary to establish further, using FTIR, the degree of bonded hydrogen. Optical evaluations using single beam FTIR of the C-H and C-C absorption bands corroborate the presence of  $sp^3$  and  $sp^2$  C-H bonding in the butane plasma deposited films. In addition, detection of the undesirable  $sp^1$  C-H bonding and further confirmation of the presence of aromatic  $sp^2$  C-C attributable to the polycrystalline graphite rings, were also detected. The C-H band spectra in the region of  $2920 \text{ cm}^{-1}$  and  $sp^3$   $\text{CH}_2$  band spectra at  $2850 \text{ cm}^{-1}$  are weaker than those previously reported for a-C:H films of similar thickness<sup>206</sup> (Fig.XXXIX) and seem to indicate the existence of only small amounts of bonded hydrogen. The conclusion, therefore, is that the majority of the 45 at.% of hydrogen detected by SIMS is included in the film in an unbonded form.

Analysis of Raman spectra showed three significant features; a broad peak centred at  $1540 \text{ cm}^{-1}$ , with an associated broad shoulder at a lower wave number of  $1250\text{-}1300 \text{ cm}^{-1}$ . In addition a very weak feature situated at  $850 \text{ cm}^{-1}$  wave number was also detected, although its assignment remains unclear. The two main peaks are thought to be attributable to the G and D of crystalline graphite and highly disordered  $sp^2$  bonded carbon respectively (Fig.XL). It has been shown that the intensity ratio  $I(D)+I(G)$  is proportional to the reciprocal of the average crystal size. From this, the average size of the randomly distributed crystals was estimated to be in the order of  $50 \text{ \AA}$ .

Finally, laser ionisation mass analysis was unsuccessfully attempted on these films. The relatively weak  $^{12}\text{C}_3^+$ ,  $^{12}\text{C}_4^+$  ion signals were heavily disguised by the relatively strong signals for iron, chromium, aluminium, sodium and potassium emanating from the substrate. Selection of a reduced laser power improved the resolution between film and substrate very little.

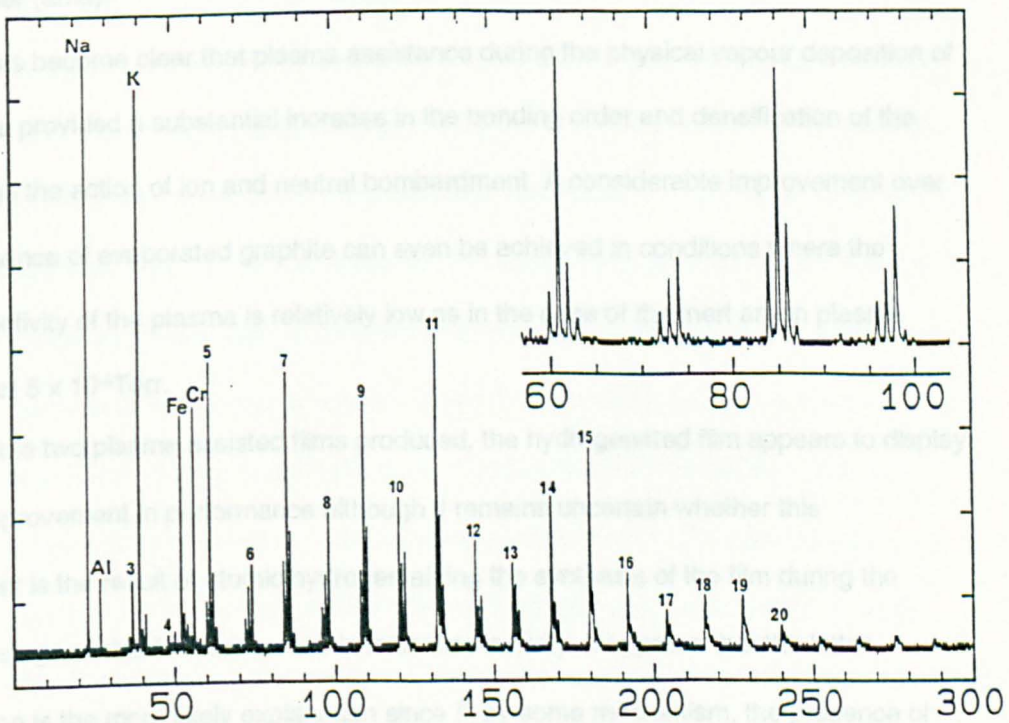
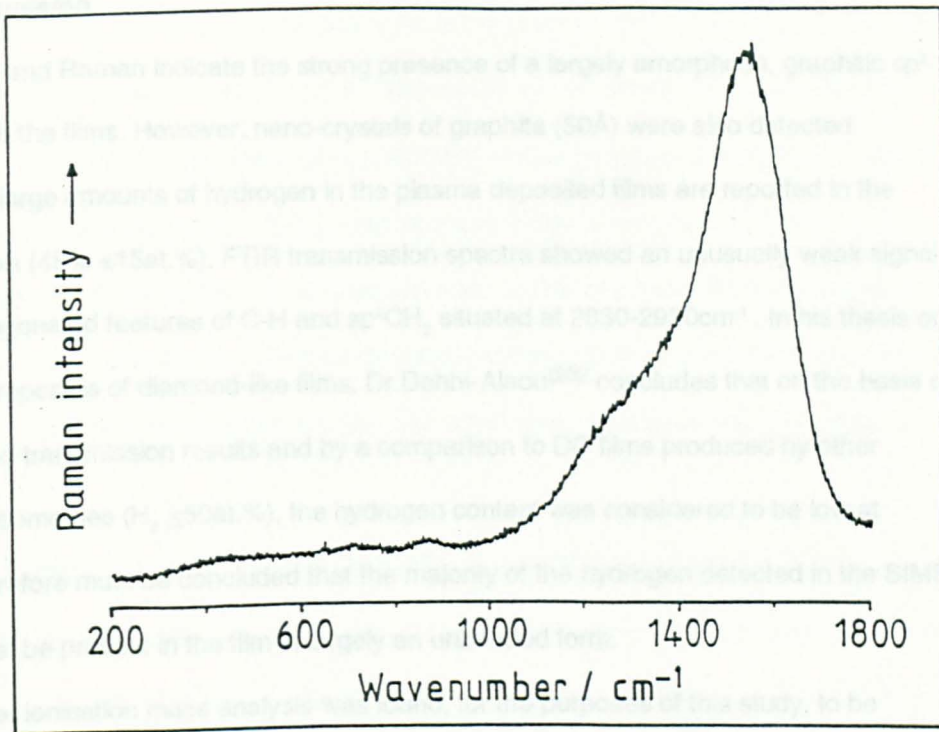


Fig XL Raman and LIMA Spectra of a DC Plasma Assisted PVD Coating

### **c) Discussion**

XPS and Raman indicate the strong presence of a largely amorphous, graphitic  $sp^2$  component in the films. However, nano-crystals of graphite (50Å) were also detected. Evidence of large amounts of hydrogen in the plasma deposited films are reported in the SIMS analysis ( $45\% \pm 15\text{at.}\%$ ). FTIR transmission spectra showed an unusually weak signal for the hydrogenated features of C-H and  $sp^3CH_2$  situated at  $2830-2920\text{cm}^{-1}$ . In his thesis on the optical properties of diamond-like films, Dr. Dehbi-Alaoui<sup>202</sup> concludes that on the basis of these infrared transmission results and by a comparison to DC films produced by other deposition geometries ( $H_2 \leq 50\text{at.}\%$ ), the hydrogen content was considered to be low at  $<10\%$ . It therefore must be concluded that the majority of the hydrogen detected in the SIMS analysis must be present in the film in largely an unbonded form.

Laser ionisation mass analysis was found, for the purposes of this study, to be effectively worthless for the examination of thin carbon films due both to the severity of the laser probing technique and the lack of sensitivity to elements other than those of high atomic mass number (amu).

It has become clear that plasma assistance during the physical vapour deposition of graphite has provided a substantial increase in the bonding order and densification of the films through the action of ion and neutral bombardment. A considerable improvement over the performance of evaporated graphite can even be achieved in conditions where the ionisation activity of the plasma is relatively low as in the case of the inert argon plasma deposition at  $5 \times 10^{-5}\text{Torr}$ .

Of the two plasma assisted films produced, the hydrogenated film appears to display a further improvement in performance although it remains uncertain whether this improvement is the result of atomic hydrogen aiding the synthesis of the film during the deposition stage or due to the increase in ionisation activity. It appears that the latter phenomenon is the more likely explanation since if, by some mechanism, the presence of hydrogen was benefiting the ordering and synthesis of the film, a greater amount of  $sp^3$  C-C bonded carbon would have been expected. As it was, the predominant structures detected were  $sp^2$  C-C with  $sp^2$  C-H and  $sp^3$  C-H present in smaller numbers. In this way the bonded

hydrogen in the films, which was estimated to be in the order of 10%, was probably included as the result of ion bombardment of partially disassociated C-H structures. Alternatively it could be argued that the large presence of unbonded atomic hydrogen (35 at.%) in the film is the result of its independent role in the growth process. What seems clear is that the individual roles of both the presence of hydrogen and the use of a more intense plasma, in this experiment are indiscernible, although the combined benefit during the deposition of graphite has been shown to improve the physical, tribological and structural properties considerably.

## **2. A Mechanical & Tribological Study of Doped Carbon Films**

Whilst the exact role of hydrogen during DC PVD deposition appears to be indistinct, it was subsequently learned from the literature that hydrogen could actively play a role in the nucleation and continued growth of  $sp^3$  bonded structures. This could only be achieved if atomic hydrogen were formed during ionisation. It would then either preferentially etch the graphite species relative to harder  $sp^3$  structures or terminate the carbon dangling bonds at the surface during growth. Before the implications of this mechanism were fully realised, it was thought from the emphasis of the scientific literature at the time that the route towards the production of harder denser and more tribological favourable films lay in the introduction of metallic impurities. This was further reinforced by reports by Dimigen at Philips that the inclusion of refractory metals such as tungsten and tantalum could improve the adhesion of hard carbon to metallic substrates by a factor of two<sup>166</sup>. In addition, increases in wear resistance by an order of magnitude and a corresponding reduction in the sensitivity to humidity changes have also been reported by doping with silicon<sup>94</sup>. The experimental emphasis was therefore temporarily shifted towards the study of the importance of such impurities rather than improvements in plasma properties, by performing similar doping experiments.

**a) Film Preparation & Experimental Details**

The surface preparation and cleaning of the ASP23 tool steel substrates was accomplished in a similar manner to the previous experiment. The deposition parameters remained unchanged, except for the addition of dopant material to graphite powder in the ratio of 50:50 being placed in the crucible for evaporation. Three different dopant compounds were chosen for this investigation; boron nitride, tungsten and titanium diboride/boron nitride. Once again the deposition took place in two plasma conditions;

- evaporated graphite in an inert argon plasma at a pressure of  $5 \times 10^{-5}$ Torr, ring bias voltage of 4kV, 100mA and a maximum substrate temperature of 350°C.
- evaporated graphite in a butane ( $C_4H_{10}$ ) plasma at a pressure of  $5 \times 10^{-2}$ Torr, ring bias voltage of 0.75kV, 300mA and a maximum substrate temperature of 160°C.

The resulting films were then tested for their mechanical properties; namely microhardness, sliding wear resistance and coefficient of friction under matching test conditions to those of the previous experiment

**b) Film Properties**

	DC Electron Evaporation	DC Butane Plasma Assisted Electron Evaporation
Graphite	2005 (15g)	4790 (25g)
Graphite + Boron Nitride	1760 (15g)	3460 (25g)
Graphite + Titanium Diboride + Boron Nitride	1370 (15g)	3750 (25g)
Graphite + Tungsten	1190 (15g)	3940 (25g)

*Table VII Average Microhardness Values of a-C and a-C:H Doped Films*

	DC Electron Evaporation	DC Butane Plasma Assisted Electron Evaporation
Graphite	310°C	520°C
Graphite + Boron Nitride	340°C	580°C
Graphite + Titanium Diboride + Boron Nitride	360°C	640°C
Graphite + Tungsten	400°C	720°C

*Table VIII Thermal Stability of a-C and a-C:H Doped Films (showing temperatures at which a visible deterioration occurred)*

### **c) Tribological Performance**

The wear results uncovered a large distinction between the performance of the hydrogenated a-C:H samples and those films synthesised into an inert argon plasma (a-C) (Fig.XLI). The wear of both the doped a-C films and their counterface material was comparable to that of the uncoated SAE 52100/ASP23 combination, indicating principally the early and complete failure of the carbon coating. The increased wear rate demonstrated by the pin was thought to be due to the consequential formation of large quantities of metal-containing wear debris from the particulate formations mentioned earlier, which continued to take part in the wear process as third bodies. This was assumed to be the reason why the rate of wear of the counterface material exceeded that of the 'standard' SAE 52100/ASP23 pairing.

It has been shown that a dramatic improvement in the wear resistance of the coatings by a factor of two could be achieved for hydrogenated deposition of the films (a-C:H) (Fig.XLII). Of all these films, those doped with boron nitride appeared to give the best results in terms of film wear reduction. This improvement in wear resistance has been achieved at the expense of a slightly higher coefficient of friction to  $\mu=0.16-0.20$  compared with undoped a-C:H films ( $\mu=0.13$ ). When one looks at the effect this wear resistance has on the rate of metal removal of the counterface, it can be clearly seen that it too has resulted in a substantial reduction in counterface wear. This reduction varied in extent, with boron nitride and titanium diboride/boron nitride doped films displaying the least deterioration of the pin. Thus for these samples the applied Hertzian contact was maintaining at a higher level throughout the test. In this light it can be generally concluded that of the doped combinations examined the boron nitride doped a-C:H films provided the greatest combined wear resistance to both the film and counterface materials for the lowest attainable frictional values.

### **d) Summary**

The most significant deduction to be drawn from the preceding experiments has been the marked improvement in overall performance of the hydrogenated plasma treated coatings, in terms of microhardness, thermal stability, adhesion and wear behaviour over

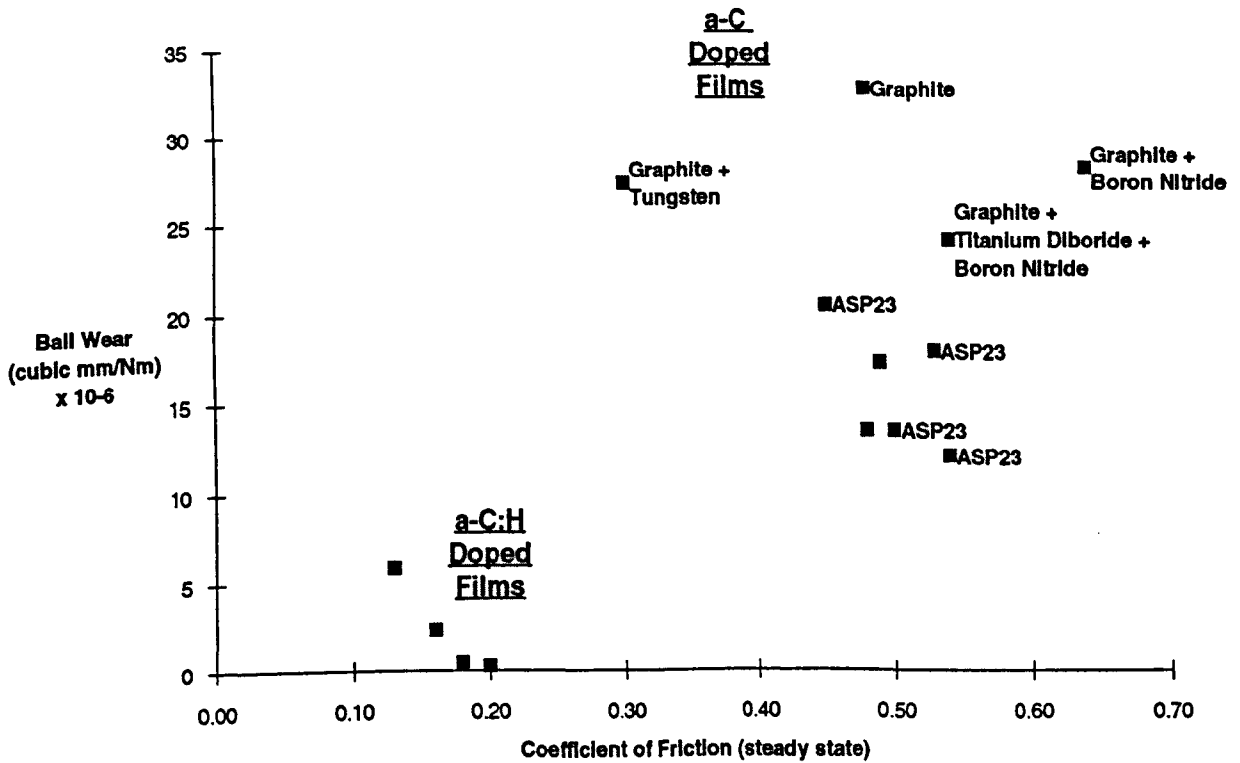
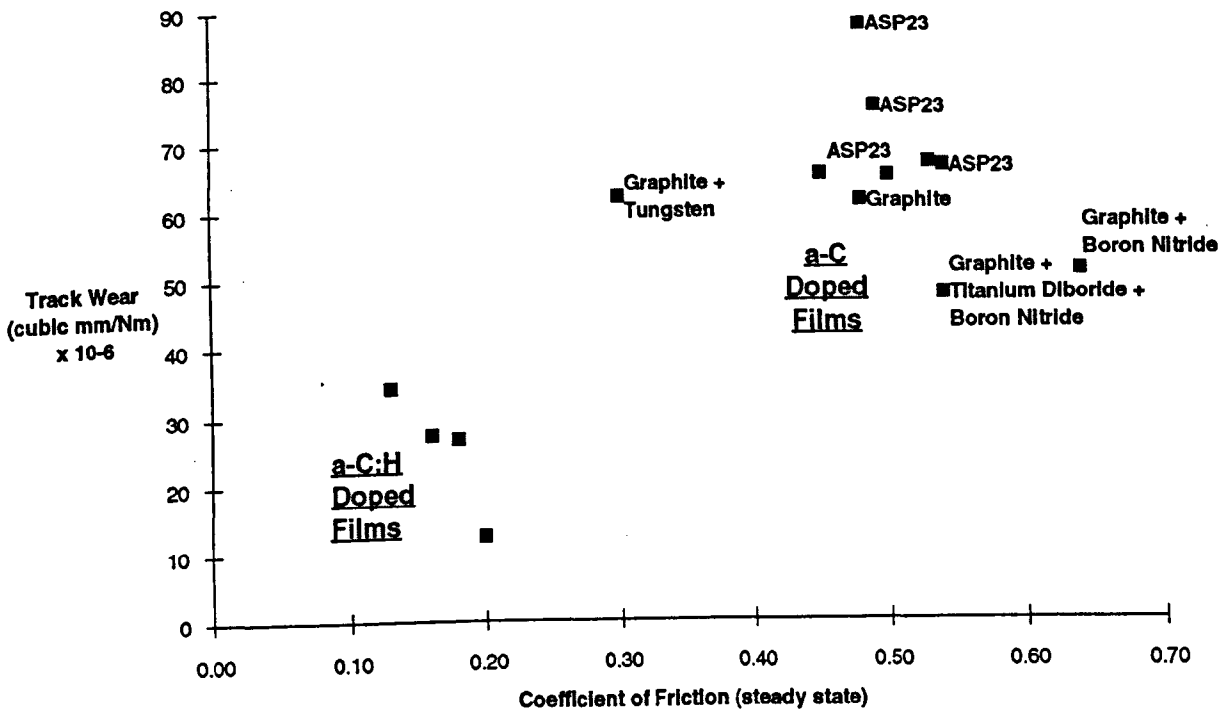
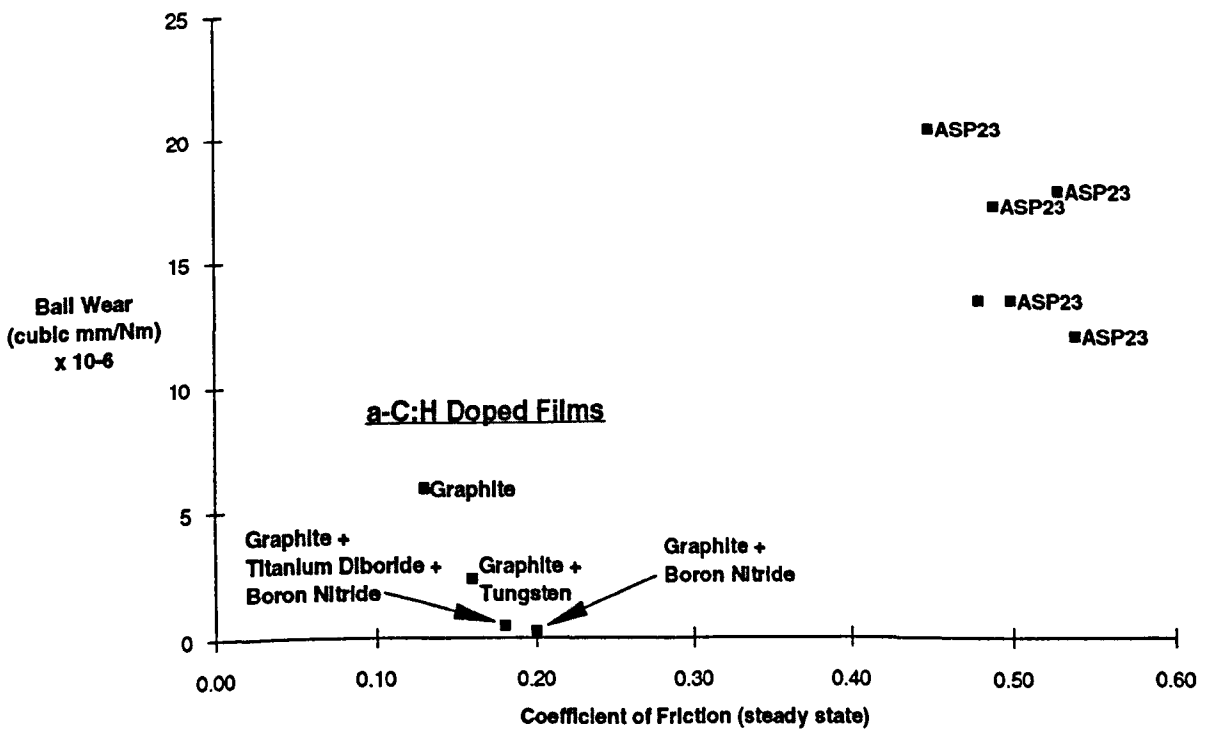
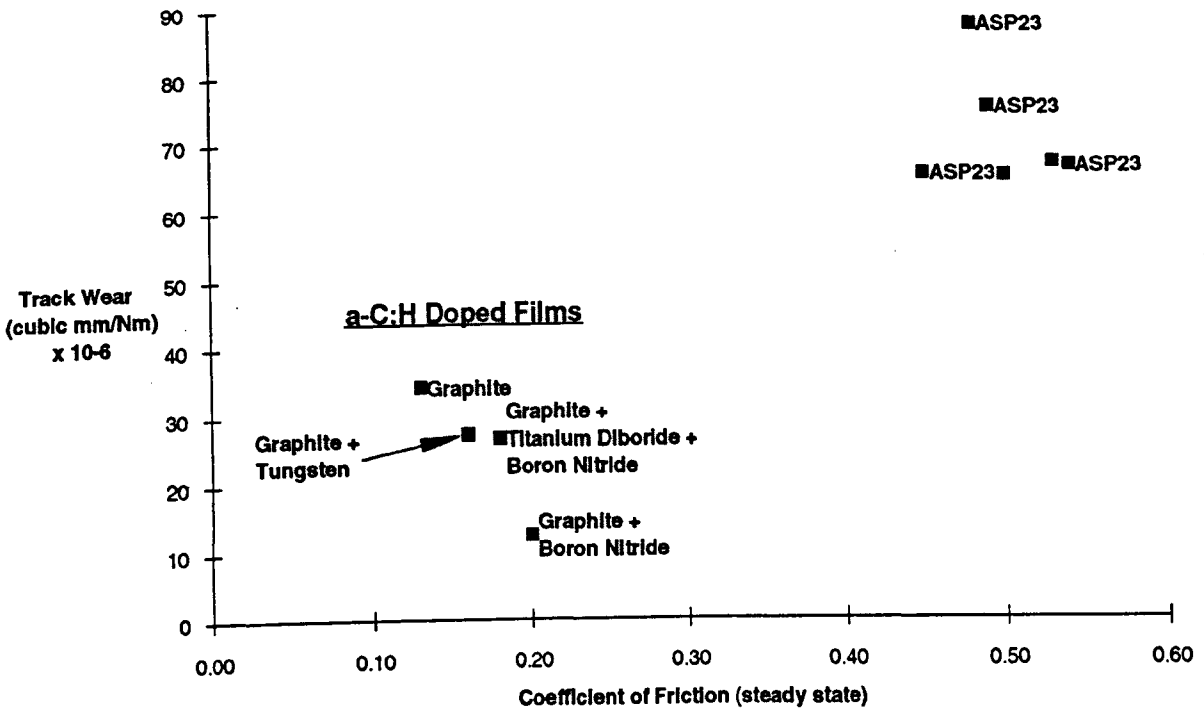


Fig XLI The Friction & Wear Performances Of Doped a-C And a-C:H Films versus Coefficient Of Friction



**Fig XLII The Friction & Wear Performances Of Doped a-C:H Films versus Coefficient Of Friction**

films deposited in a low intensity plasma conditions. The combined use of an intense plasma and the addition of a hydrocarbon precursor has been shown to have a significant affect on increasing the microhardness ( $H_k \approx 2000$  to  $4800 \text{ kg/mm}^2$ ,  $25 \text{ g}$ ) and their stability to thermal degradation ( $400^\circ$  to  $720^\circ \text{C}$ ). For these amorphous hydrogenated films (a-C:H) the most notable improvement in physical properties was a twofold decrease in the rate of film wear during dry sliding pin on disc tests under conditions of 10 Newton normal load and 100 metres sliding distance. A marked reduction in coefficient of friction from  $\mu=0.48$  to  $0.13$  was similarly achieved.

In contrast, doping with metallic components offers little improvement in tribological performance, with amorphous carbon films (a-C) showing levels of wear comparable to that of the metal/metal 'standard' pairing. At the same time hydrogenated films (a-C:H) showed an improved wear performance similar to the undoped hydrogenated sample although an increase in friction coefficient from  $\mu=0.13$  to  $\mu=0.18$  was also observed. It could be concluded that of the doped films, boron nitride inclusion offered the greatest film wear resistant under conditions of higher Hertzian contact pressure due to the lower levels of counterface pin wear. Whilst the doping of these films led to a slight general reduction in the microhardness value, the most significant benefit of the use of such films has been the considerably higher tolerance to temperature before visible degradation of the film can be observed.

## **B. Further Studies**

The encouraging tribological and mechanical performances of hydrogenated carbon films produced under DC plasma deposition, compared to those deposited by simple evaporation or low intensity plasma, indicated that further improvements in plasma processing could be the key to producing films with improved nucleation and structural properties. This could be achieved by further increasing the ionisation efficiency using thermionic emission enhancement to create more plasma activity whilst providing greater agitation and disassociation of the precursors by use of a higher frequency plasma. At the same time there is a need to understand and optimise the role of hydrogen in the plasma process and discover how the effect of residual amounts of hydrogen in the films effects their properties.

The slightly improved tribological results for metal-doped hydrogenated films over the undoped films produced in similar conditions, was considered to be further outweighed by the additional deposition costs of the precursors when the relatively cheap source gases such as hydrogen and butane could be utilised to similar effect. The presence of the metal dopants also creates a degree of cross-contamination which could only be controlled adequately by the mechanical cleaning of the stainless steel shrouds between every deposition involving a different dopant. This was particularly important because of the deposition arrangement used. In such an arrangement the chamber walls were held at earth potential, but cathodic in relation to the depositing species. Equal deposition, therefore, of the chamber walls and substrates would have occurred in these circumstances unless the evaporate possessed a strong directional flux towards the sample holder. Cross-sputtering of material from the chamber walls in subsequent experiments posed a serious problem therefore. Further still, metallic inclusions render the films conducting to a degree proportional to the molar content of the included metal<sup>166</sup>. For insulating wear resistant films such as those found on the surface of magnetic media storage discs or in applications where a high level of biocompatibility is required, these metallic doped coatings would be considered unsuitable.

As a consequence, future emphasis was shifted towards concentration of possible improvements in coating properties through plasma process enhancement and the controlled introduction of non-metallic impurities, such as hydrogen, as an alternative route to achieving the more desirable  $sp^3$  diamond-like structures.

## **1. Investigations into DC & 380kHz Radio Frequency EBPVD Films**

### **a) Film Preparation & Experimental Details**

Diamond-like carbon films were prepared for this part of the study by the hybrid thermionically assisted PVD technique (Chap.III Sec.A(b)). This method combines the evaporation of solid graphite from a differentially pumped electron gun (7kV, 200mA) into an 380 kHz RF or DC glow discharge at a pressure of 10mTorr. The plasma gases used to achieve amorphous carbon (a-C) or amorphous hydrogenated carbon (a-C:H) films were argon and butane respectively. The substrates were mounted on a specimen holder held at a fixed cathodic potential of between 0 to 1000V(DC) or 2500V(RF, DC offset). These produced maximum current densities of 0.9 & 13.7mA/cm<sup>2</sup> respectively. The substrates were suspended approximately 300mm above the graphite source and offset by 100mm. A filament made from a 380mm long, Ø0.5mm tungsten wire was positioned 150mm below the substrate. The coatings were tested for micro & nanohardness, adhesion strength, internal stress, conductivity, tribological performance and structurally analysed using a scanning electron microscope and Raman spectroscopy.

It should be noted that it was not possible to run an RF discharge with thermionic assistance since the increase in plasma activity, resulting from additional emission of electrons from the filament, created a very intense, unstable plasma. This quickly led to the breakdown of the insulation between the cathode and filament, resulting in excessive arcing and therefore represented the limit to which the plasma can be enhanced by electron emission.

### **b) Results - Adhesion & Deposition Rate**

The adhesive strengths of the carbon films were observed to be highly substrate sensitive (Table IX). All deposition runs using glass substrates produced adherent coatings with a deposition rate for a-C:H films produced in DC glow discharges of 4µm/hr cf. 0.2-0.8µm/hr for a-C films produced in argon DC glow discharges. The use of RF compared to DC plasmas created a situation where the growth rate for hydrogenated films decreased to 3µm/hr and non-hydrogenated films increased slightly to 1µm/hr. The deposition conditions on glass were in stark contrast to growth of DLC on ASP23 tool steel substrates where no net

Plasma	DC		RF		
Process	Argon + Graphite	Butane + Graphite	Argon + Graphite	Butane + Graphite	Butane + Graphite
<b>Glass &amp; Silicon</b>					<b>Tool Steel &amp; Mild Steel</b>
<b>Hardness</b>	Soft, Ductile	Soft, Brittle/Fragile	Hard 24.4GPa, Ductile,	Very Hard, 35.5GPa Elastic, E = 126.9GPa	Hard, 14.5GPa Elastic, E = 56.4GPa
<b>Adhesion</b>	Poor	Good	Poor	Good	Tool Steel - Poor
<b>Resistivity</b>	$10^{-2}$ - $10^4$ $\Omega$ cm	$10^0$ - $10^2$ $\Omega$ cm	$10^{-1}$ - $10^4$ $\Omega$ cm	$10^1$ - $10^4$ $\Omega$ cm	$10^5$ $\Omega$ cm
<b>Appearance</b>	Grey/Black	Yellow/Brown	Transparent	Semi-Transparent (Grey)	Brown/Black
<b>Deposition Rate</b>	0.2-0.8 $\mu$ m/hr	4 $\mu$ m/hr	1 $\mu$ m/hr	3 $\mu$ m/hr	1 $\mu$ m/hr
<b>Structure</b>	Dense,amorphous	Dense,amorphous	Dense,amorphous	Dense,amorphous	Dense,amorphous

**Table IX Summary Of Thermionically Assisted DC and Low Frequency Plasma Films**

film growth was achieved in any situation other than during RF butane plasma deposition.

For films deposited onto glass, it was noted that for both types of plasma condition (RF or DC), the adhesive strength of the films could be greatly improved using higher current densities (Fig.XLIII). Due to the higher current densities achievable in RF plasmas, the potential improvement in adhesive strength was therefore larger (note differences in scales). The most notable feature of the two sets of results is the substantial increase in critical load, required to cause failure between a-C:H and a-C films.

### **c) Internal Stress**

Residual stress measurements were performed on films created by the decomposition of butane in 1500V(DC offset) RF plasma with the evaporation of graphite. The results indicated that the compressive stress levels were lower in magnitude at room temperature, by approximately 60%, than those reported by Grill et al<sup>207</sup> for 13.56MHz RF deposited PACVD a-C:H films (Fig.XLIV). Some films were so sensitive to delamination as a result of this stress that complete loss of adhesion could be seen to occur within minutes of deposition when exposed to atmospheric conditions. Observations of both a-C and a-C:H films produced in DC and RF plasmas revealed stress, although at levels lower than those measured above. It seems likely that delamination was caused by the diffusion of moisture into the film/substrate interface<sup>208</sup> and some evidence to corroborate this comes from observations that the debonding behaviour seems to have been initiated at a discontinuity or sharp edge such as that provided by the periphery of the substrate.

The stresses could be annealed partially from the coating, in a manner similar to that reported by Dimigen at temperatures approaching 450°C<sup>166</sup>. This is in line with current observations by other authors who suggest that at around this temperature relaxation of the coating's structure is a result of unbonded hydrogen effusing from the coatings. Secondary annealing is also reported to occur at 650°C when sp<sup>3</sup> bonds begin to revert to more graphitic sp<sup>2</sup> structures<sup>209</sup>. Throughout this transitional temperature the films become progressively more optically absorbing and electrically conducting until at the higher temperature the properties resemble that of graphite. This two stage annealing process however, was not noted to occur in the above experiment since relaxation of the stress and changes in optical

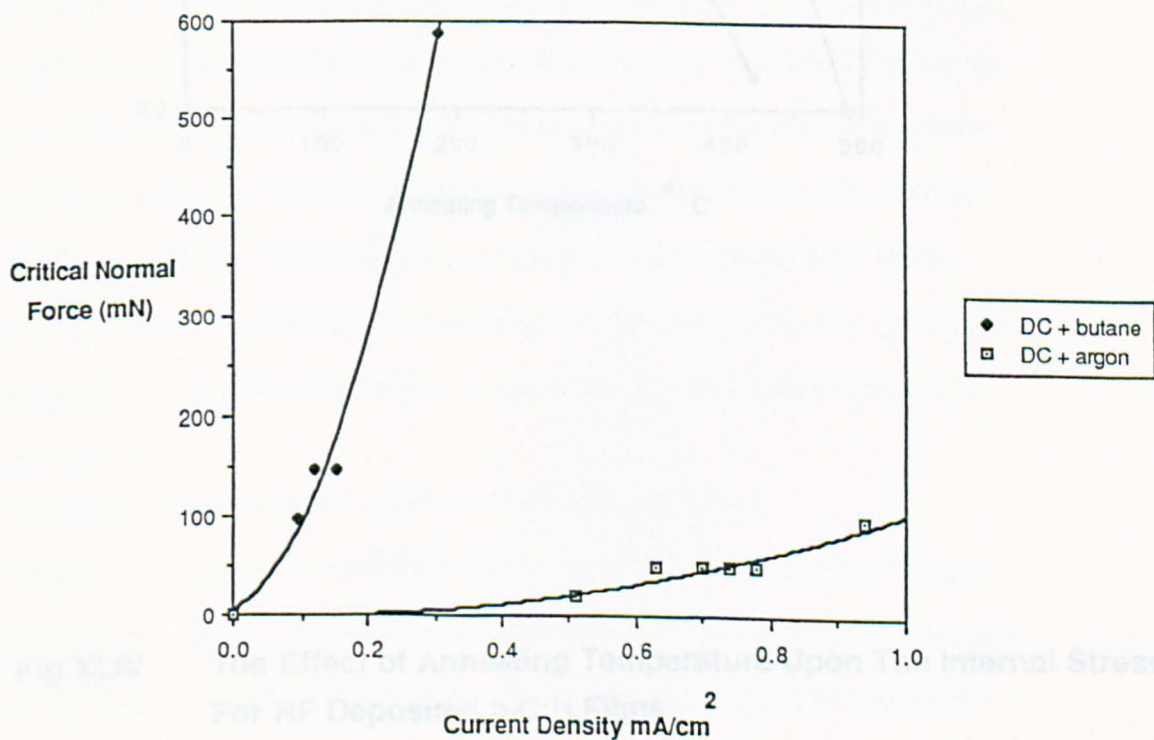
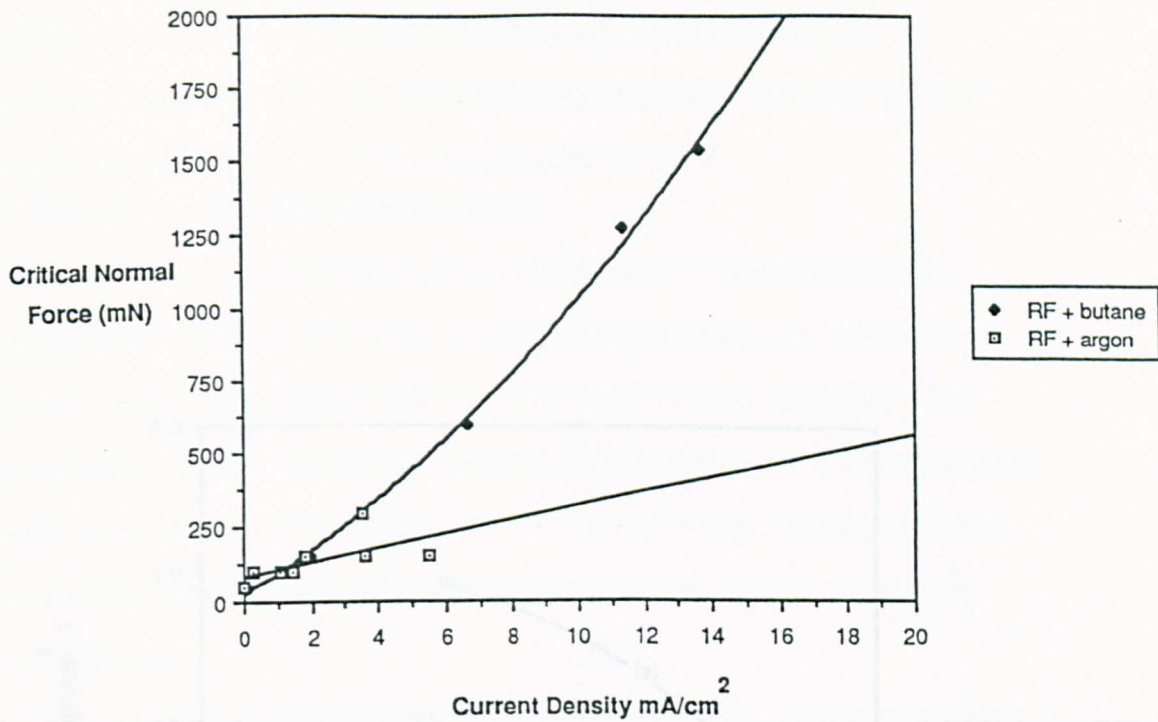


**Fig XLIII** The Adhesion Strength On Glass versus Current Density For a-C And a-C:H Films Produced in RF and DC Plasmas

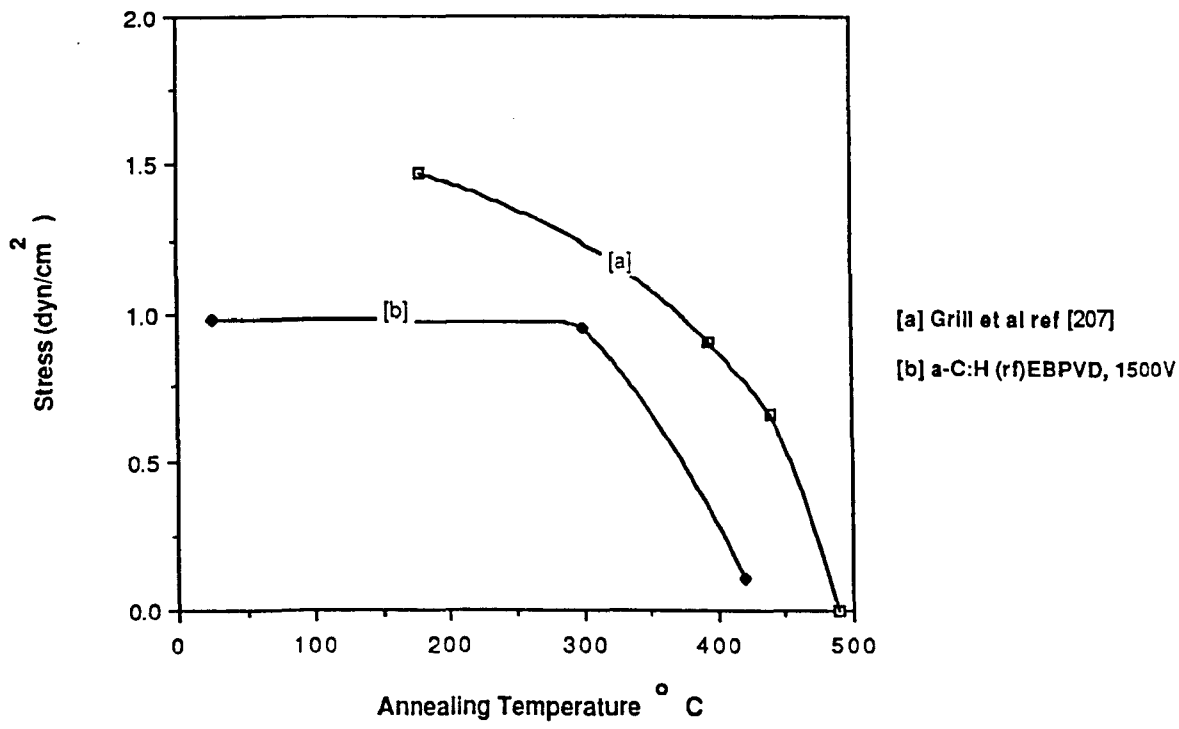


**Fig XLIV** The Effect of Annealing Temperature Upon The Internal Stress For RF Deposited a-C:H Films

characteristics were found to be coincident. Attempts were made to measure the microhardness of these annealed films between these transitional temperatures but were unsuccessful because the films became extremely brittle in nature.

#### **d) *Micro & Nanoindentation Measurements***

Microhardness measurements of DC plasma deposited films showed clearly a distinction between those nucleated in the presence of hydrogen and those which were not. In both cases the films were relatively soft,  $H_k \approx 700\text{-}1900\text{kg/mm}^2$  (15g), with only a slight tendency towards increased hardness with increase substrate potential. The distinction arises in the behaviour of the films when indented with a Knoop diamond; a-C films demonstrate a ductile deformation whereas the incorporating of hydrogen into a-C:H films causes brittle failure to be exhibited.

Radio frequency non-hydrogenated films demonstrated higher microhardness values,  $H_k \approx 2500\text{kg/mm}^2$  (15g), with ductile deformation similar to the DC non-hydrogenated films. However, the most significant increase in microhardness to  $H_k \approx 3600\text{kg/mm}^2$  (15g) occurred when films were deposited in a hydrogenated radio frequency plasma. It was noted this high apparent hardness was accompanied by high levels of elastic recovery of the film during the recovery of the indenter, making interpretation of these hardness values difficult. In order to resolve the elastic component from the plastic contribution, nanoindentation was performed on RF deposited a-C:H films. Measurements revealed that only a relatively small elastic constant,  $E = 56.4\text{GPa}$ , was present in the indentation of a-C:H films coated on a ASP23 tool steel substrate (Fig.XLV) with measurements on glass indicating the elastic constant to be greater ( $E = 126.9\text{GPa}$ ).

#### **e) *Analytical Characterisation: Electron Microscopy & Raman***

Structural examination using electron microscopy of film fracture sections revealed the compositions to be dense, amorphous and pinhole free in every case (Fig.XLVI). Analysis of the films by Raman spectroscopy showed no satisfactory spectra for DC coatings due to the intense fluorescence background which obscured any characteristic features (Fig.XLVIIa). Hydrogenated a-C:H radio frequency films again displayed different characteristics to the other films tested by displaying typical spectra for diamond-like carbon with unresolved D and

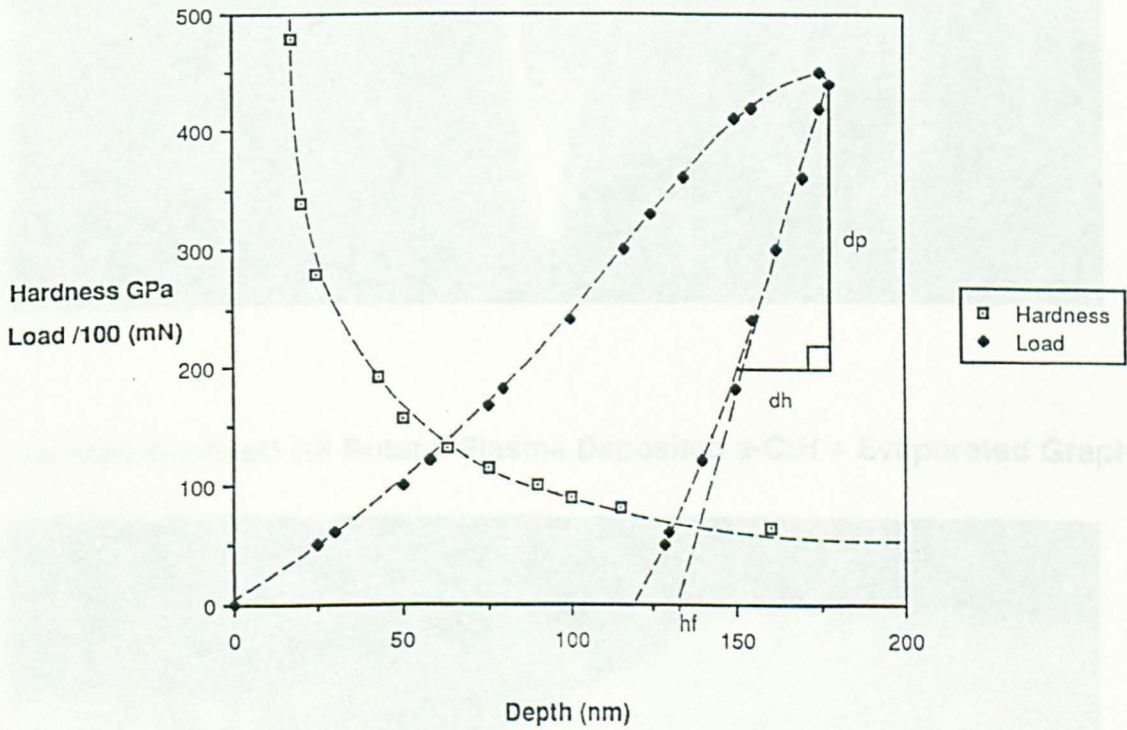
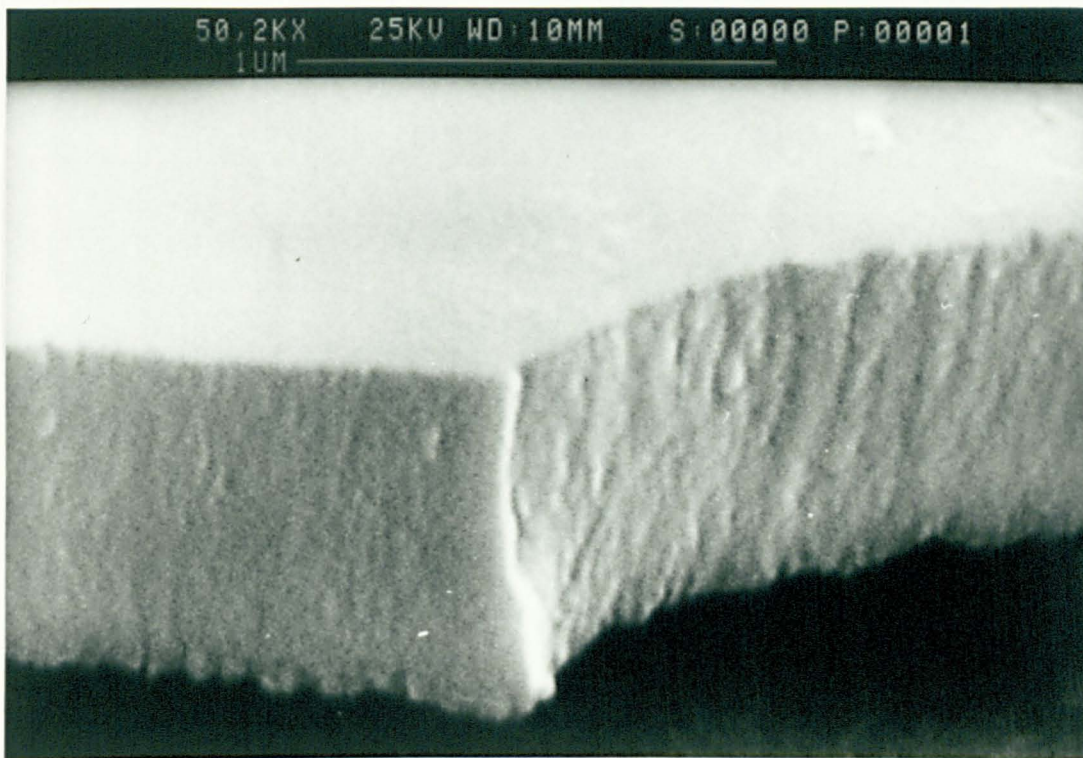


**Fig XLV** The Hardness and Load versus Nanoindentation Depth For RF Deposited a-C:H Films On ASP23 Tool Steel

(a) 1500V DC Butane Plasma Deposited a-C:H + Evaporated Graphite



(b) 1500V(DC offset) RF Butane Plasma Deposited a-C:H + Evaporated Graphite

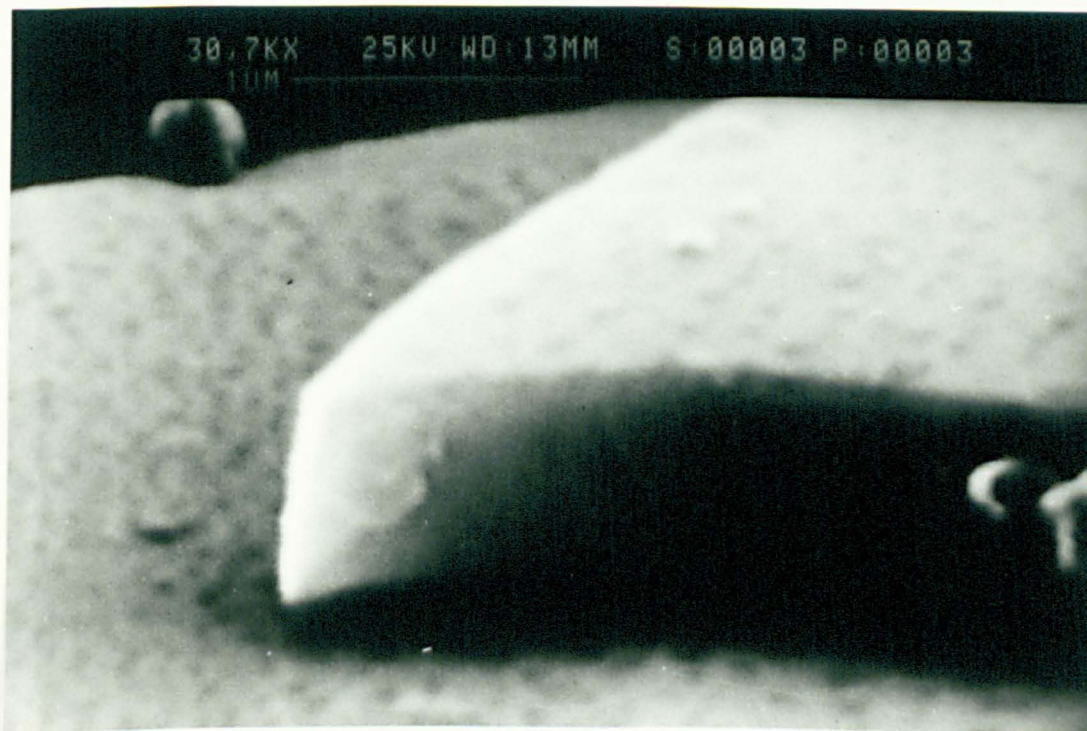
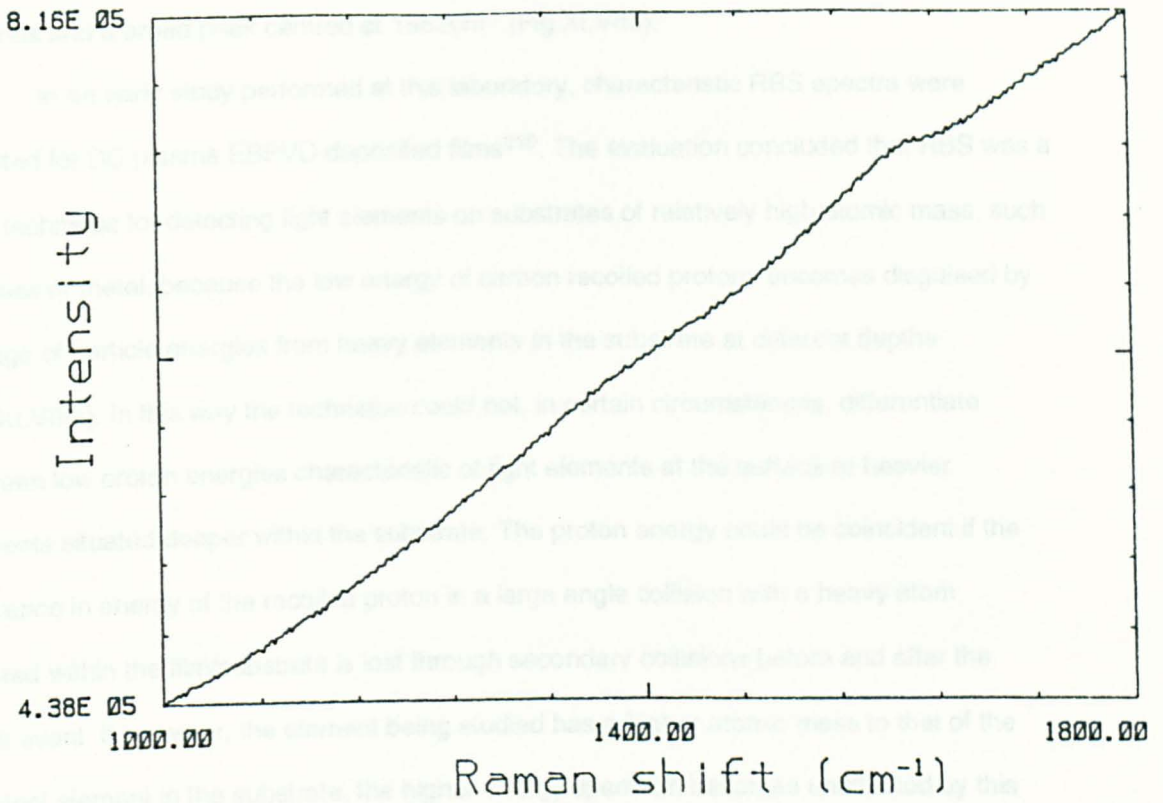


Fig XLVI Scanning Electron Photomicrographs of Fracture Cross Sections

(a) 800V DC Butane Plasma Deposited a-C:H



(b) 800V (DC offset) RF Butane Plasma Deposited a-C:H

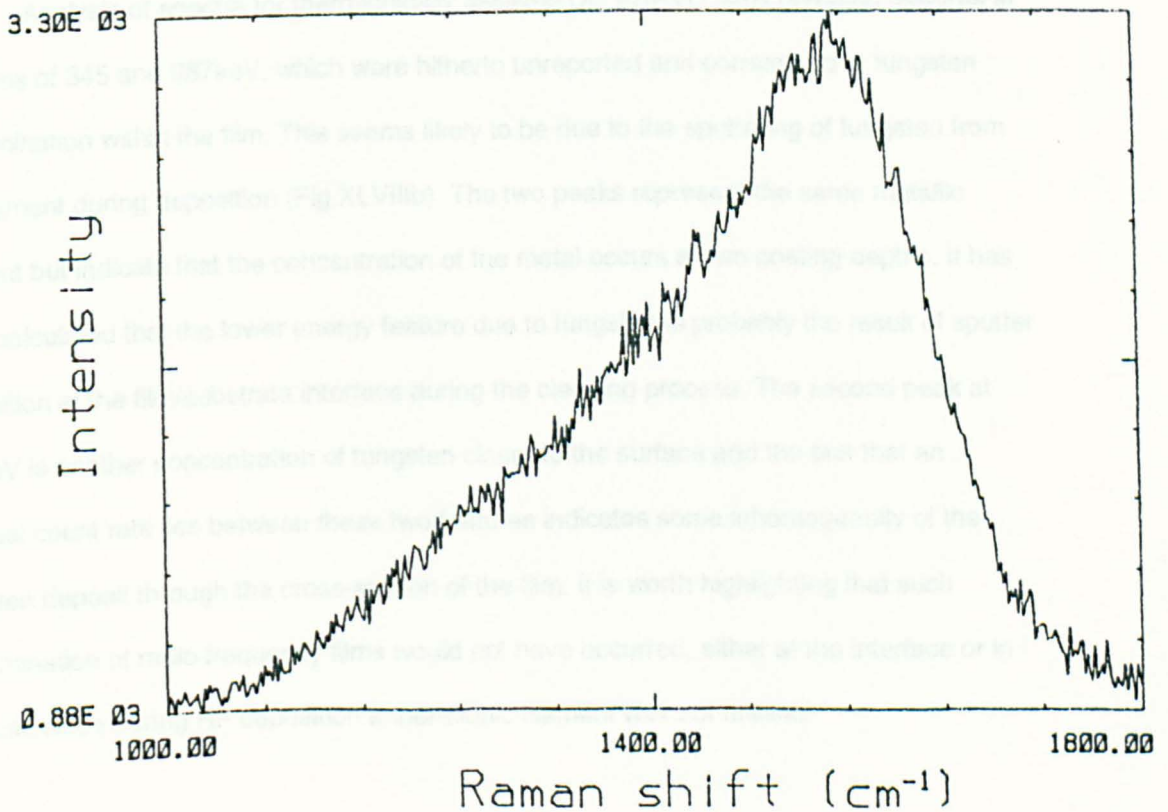


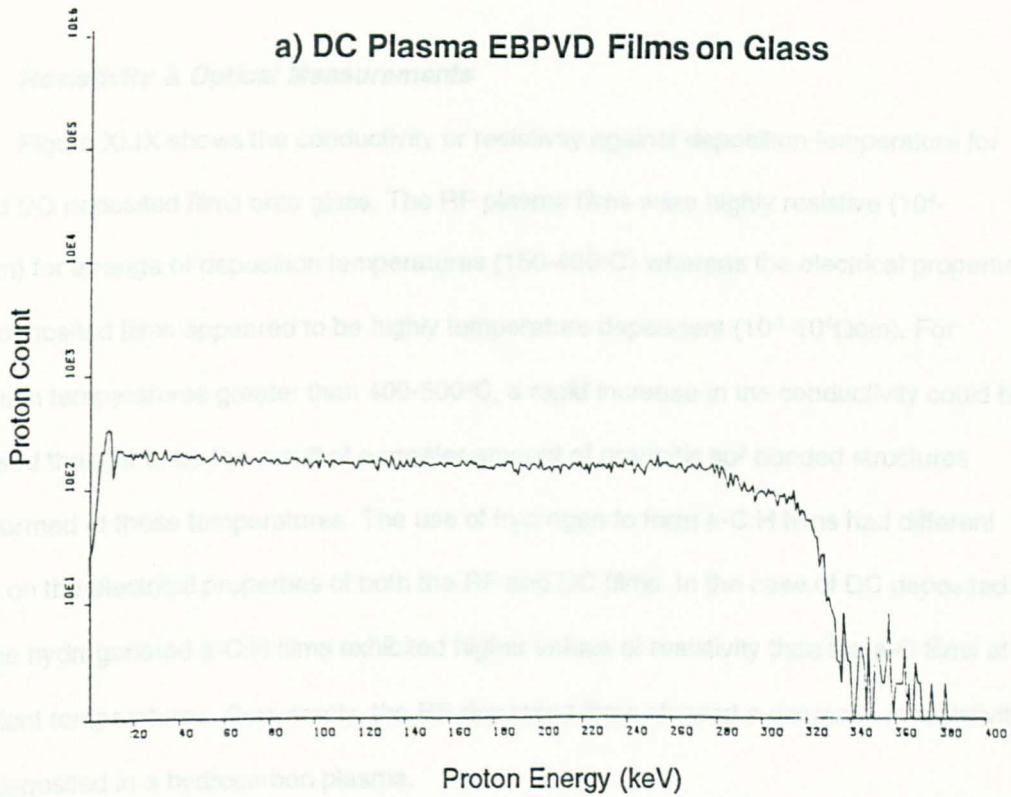
Fig XLVII Raman Spectra

G bands and a broad peak centred at  $1552\text{cm}^{-1}$  (Fig.XLVIIb).

In an early study performed at this laboratory, characteristic RBS spectra were reported for DC plasma EBPVD deposited films<sup>210</sup>. The evaluation concluded that RBS was a poor technique for detecting light elements on substrates of relatively high atomic mass, such as glass or metal, because the low energy of carbon recoiled protons becomes disguised by a range of particle energies from heavy elements in the substrate at different depths (Fig.XLVIIIa). In this way the technique could not, in certain circumstances, differentiate between low proton energies characteristic of light elements at the surface or heavier elements situated deeper within the substrate. The proton energy could be coincident if the difference in energy of the recoiled proton in a large angle collision with a heavy atom situated within the film/substrate is lost through secondary collisions before and after the recoil event. If however, the element being studied has a higher atomic mass to that of the heaviest element in the substrate, the higher energy spectrum becomes unaffected by this range of lower particle energies and it becomes easier to differentiate the signal for this element. It therefore provides a useful technique for detecting heavy atomic elements on a light matrix such as gold on glass.

Analysis of spectra for thermionically assisted DC EBPVD films revealed features at energies of 345 and 367keV, which were hitherto unreported and correspond to tungsten contamination within the film. This seems likely to be due to the sputtering of tungsten from the filament during deposition (Fig.XLVIIIb). The two peaks represent the same metallic element but indicate that the concentration of the metal occurs at two coating depths. It has been calculated that the lower energy feature due to tungsten is probably the result of sputter deposition at the film/substrate interface during the cleaning process. The second peak at 367keV is another concentration of tungsten closer to the surface and the fact that an unequal count rate lies between these two features indicates some inhomogeneity of the tungsten deposit through the cross-section of the film. It is worth highlighting that such contamination of radio frequency films would not have occurred, either at the interface or in the bulk, since during RF deposition a thermionic filament was not utilised.

### a) DC Plasma EBPVD Films on Glass



### b) Thermionically Assisted DC Plasma EBPVD Films on Glass

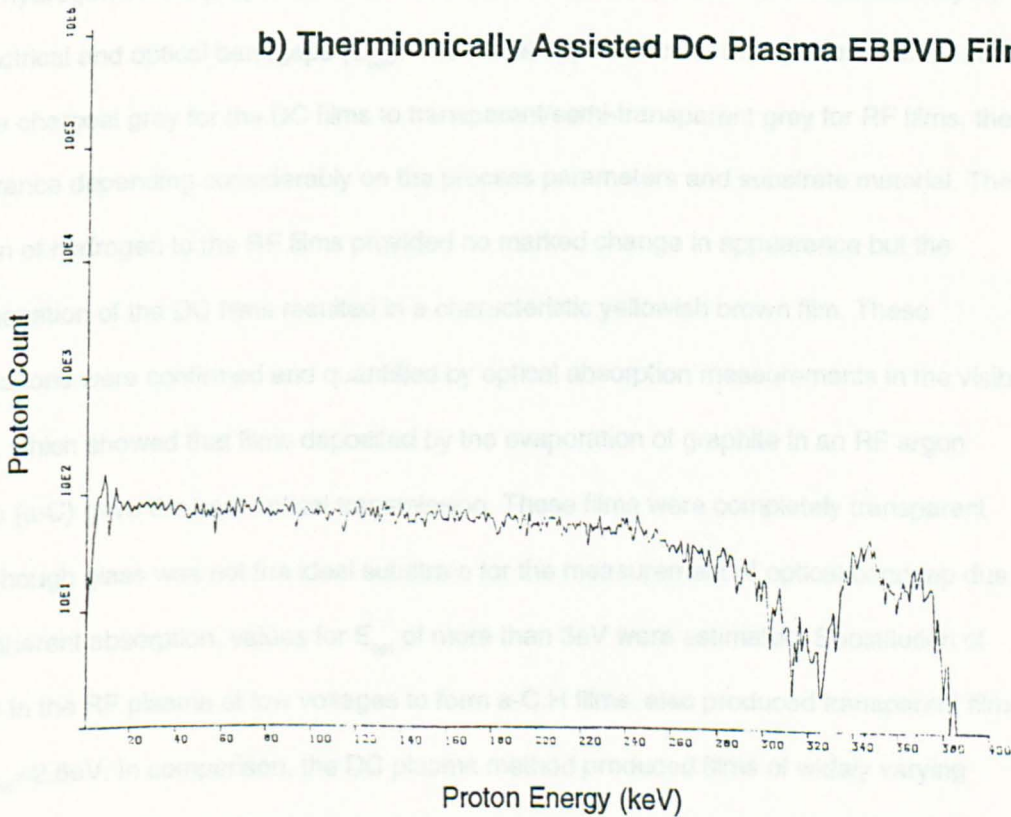
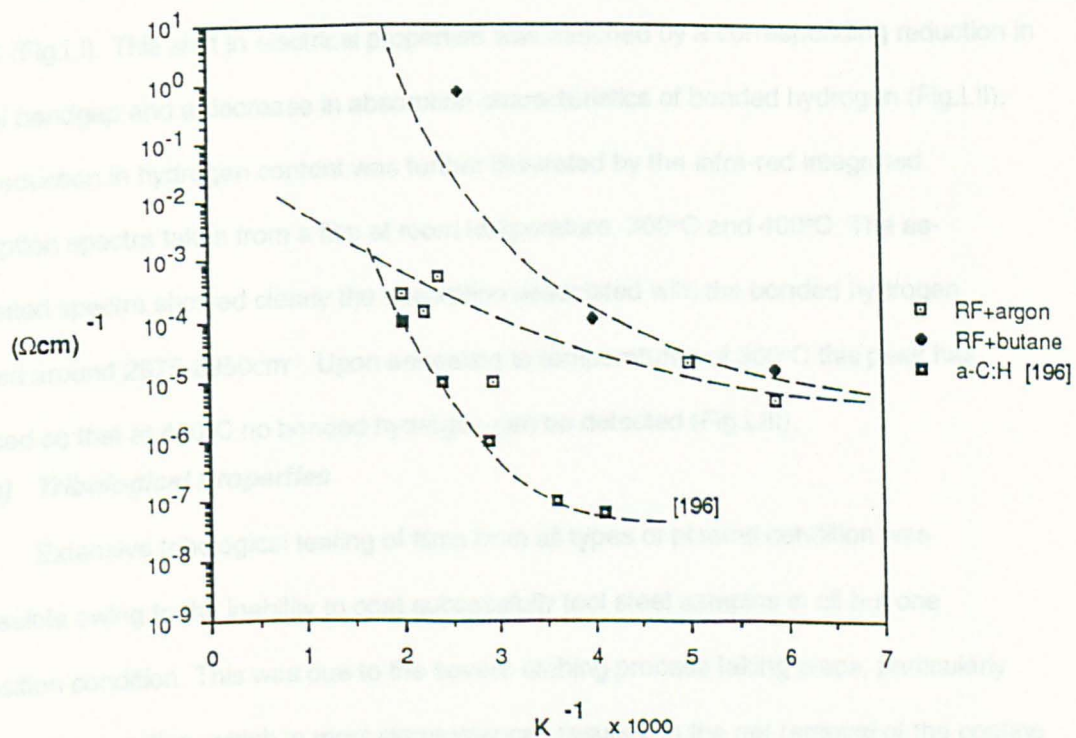
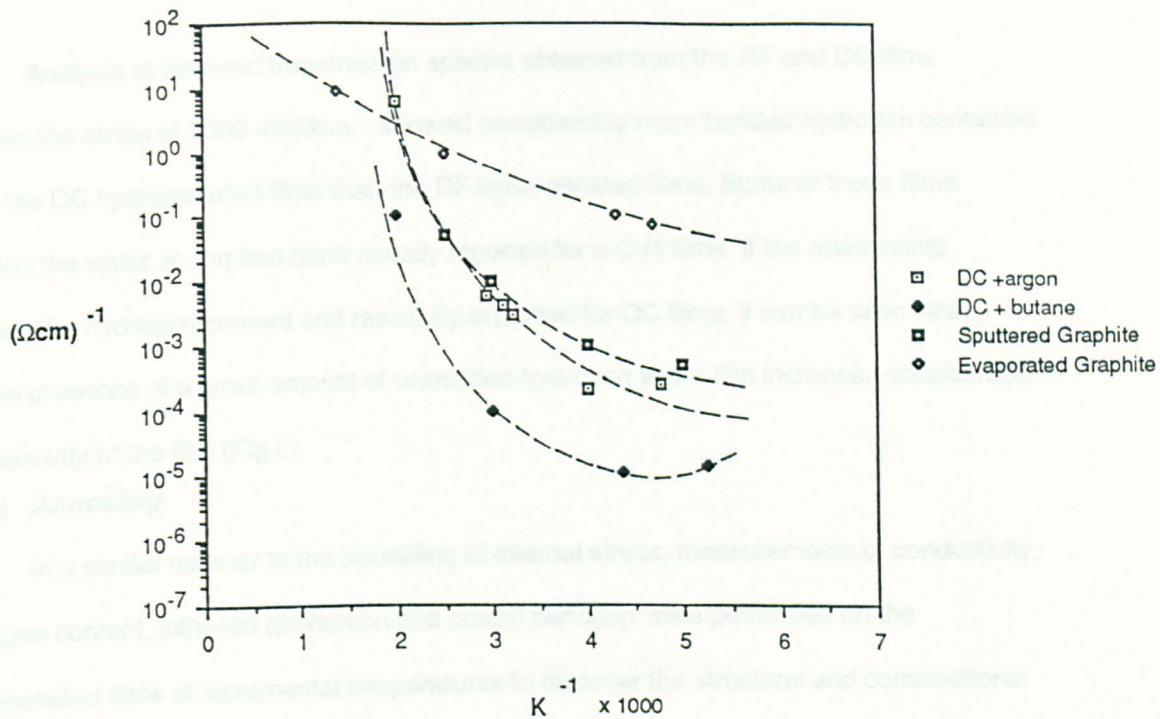


Fig XLVIII RBS Spectra

### **f) Resistivity & Optical Measurements**

Figure XLIX shows the conductivity or resistivity against deposition temperature for RF and DC deposited films onto glass. The RF plasma films were highly resistive ( $10^4$ - $10^5\Omega\text{cm}$ ) for a range of deposition temperatures (150-400°C) whereas the electrical properties of DC deposited films appeared to be highly temperature dependent ( $10^2$ - $10^4\Omega\text{cm}$ ). For deposition temperatures greater than 400-500°C, a rapid increase in the conductivity could be witnessed thought to be the result of a greater amount of graphitic  $\text{sp}^2$  bonded structures being formed at these temperatures. The use of hydrogen to form a-C:H films had different effects on the electrical properties of both the RF and DC films. In the case of DC deposited films the hydrogenated a-C:H films exhibited higher values of resistivity than the a-C films at equivalent temperatures. Conversely, the RF deposited films showed a decrease in resistivity when deposited in a hydrocarbon plasma.

Optical studies by Dr. Azzedine Dehbi-Alaoui<sup>211</sup> provided further indications of the role of hydrogen on the properties of the film, which are closely linked to the conductivity by the electrical and optical bandgaps ( $E_{\text{opt}}$ ). The visual appearance of the a-C films varied from opaque charcoal grey for the DC films to transparent/semi-transparent grey for RF films, the appearance depending considerably on the process parameters and substrate material. The addition of hydrogen to the RF films provided no marked change in appearance but the hydrogenation of the DC films resulted in a characteristic yellowish brown film. These observations were confirmed and quantified by optical absorption measurements in the visible region, which showed that films deposited by the evaporation of graphite in an RF argon plasma (a-C) gave the best optical transmission. These films were completely transparent and although glass was not the ideal substrate for the measurement of optical bandgap due to its inherent absorption, values for  $E_{\text{opt}}$  of more than 3eV were estimated. Substitution of butane in the RF plasma at low voltages to form a-C:H films, also produced transparent films with  $E_{\text{opt}}=2.6\text{eV}$ . In comparison, the DC plasma method produced films of widely varying optical properties ( $E_{\text{opt}}=0.46$ - $2.3\text{eV}$ ). Dr Dehbi-Alaoui reports that the optical bandgap decreases dramatically with increasing DC voltage, although no similar correlation was reported for RF films. In all cases the films were reported to have a refractive index of 2.0.



**Fig XLIX Conductivity versus Deposition Temperature For a-C And a-C:H Films Deposited On Glass In RF And DC Plasma**

Analysis of infra-red transmission spectra obtained from the RF and DC films between the range of 2000-4000 $\text{cm}^{-1}$ , showed considerably more bonded hydrogen contained within the DC hydrogenated films than the RF hydrogenated films. Some of these films revealed the water absorption band usually reported for a-C:H films. If the relationship between the hydrogen content and resistivity is plotted for DC films, it can be seen clearly that the presence of a small amount of unbonded hydrogen in the film increases considerably the resistivity of the film (Fig.L).

#### **g) Annealing**

In a similar manner to the annealing of internal stress, measurements of conductivity, hydrogen content, infra-red absorption and optical bandgap were performed on the hydrogenated films at incremental temperatures to discover the structural and compositional transformations taking place. Measurements for resistivity indicated clearly that the increase in conductivity of the film from  $\sim 10^4 \Omega\text{cm}$  to  $\sim 10^1 \Omega\text{cm}$ , initiates at a temperature band of 300-400°C (Fig.LI). This shift in electrical properties was matched by a corresponding reduction in optical bandgap and a decrease in absorption characteristics of bonded hydrogen (Fig.LII). This reduction in hydrogen content was further illustrated by the infra-red integrated absorption spectra taken from a film at room temperature, 300°C and 400°C. The as-deposited spectra showed clearly the absorption associated with the bonded hydrogen centred around 2875-2950 $\text{cm}^{-1}$ . Upon annealing to temperatures of 300°C this peak has reduced so that at 400°C no bonded hydrogen can be detected (Fig.LIII).

#### **h) Tribological Properties**

Extensive tribological testing of films from all types of plasma condition was impossible owing to the inability to coat successfully tool steel samples in all but one deposition condition. This was due to the severe etching process taking place, particularly during DC deposition, which in most circumstances resulted in the net removal of the coating material. Coatings of 1 $\mu\text{m}$  on ASP23 tool steel were achieved however, in conditions in which graphite was evaporated into a radio frequency butane plasma (a-C:H RF EBPVD).

Testing the RF a-C:H films exhibited a film wear of  $48 \times 10^{-6} \text{mm}^3/\text{Nm}$  which when compared to the 'standard' SAE 52100 pin on ASP23 disc material ( $K_b=64-87 \times 10^{-6} \text{mm}^3/\text{Nm}$ )

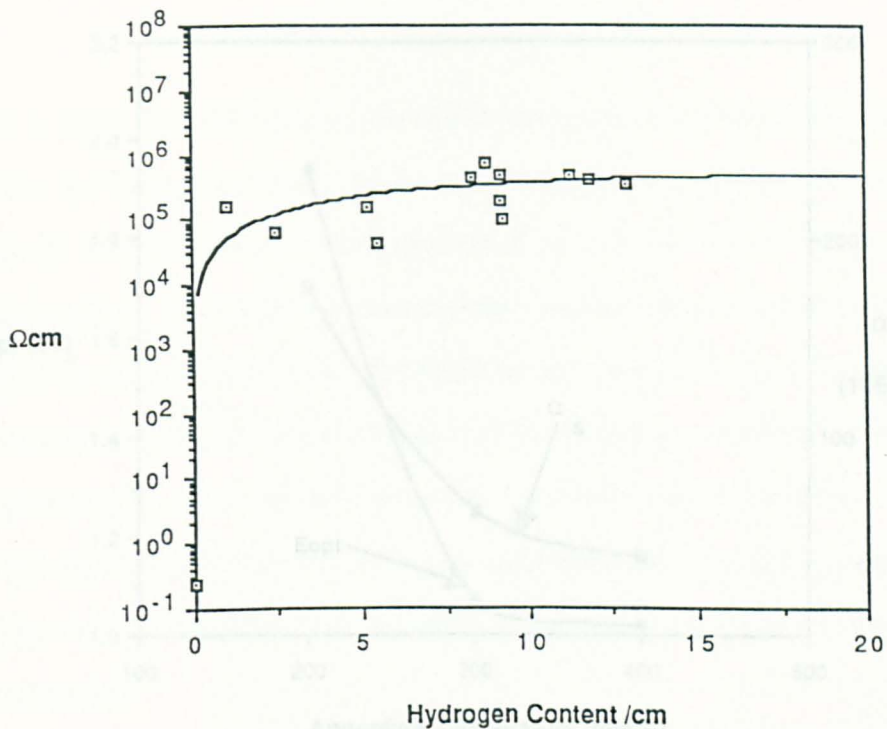


**Fig L Resistivity versus Hydrogen Content For a-C:H DC EBPVD Films On Glass**

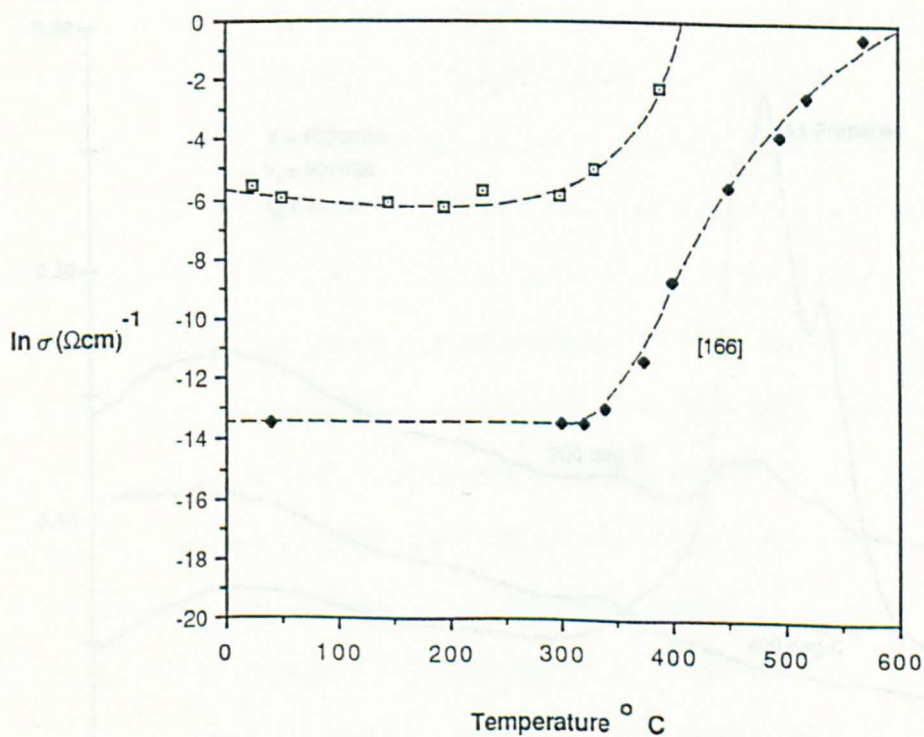


**Fig LI Conductivity versus Annealing Temperature For a-C:H EBPVD Films (500V)**

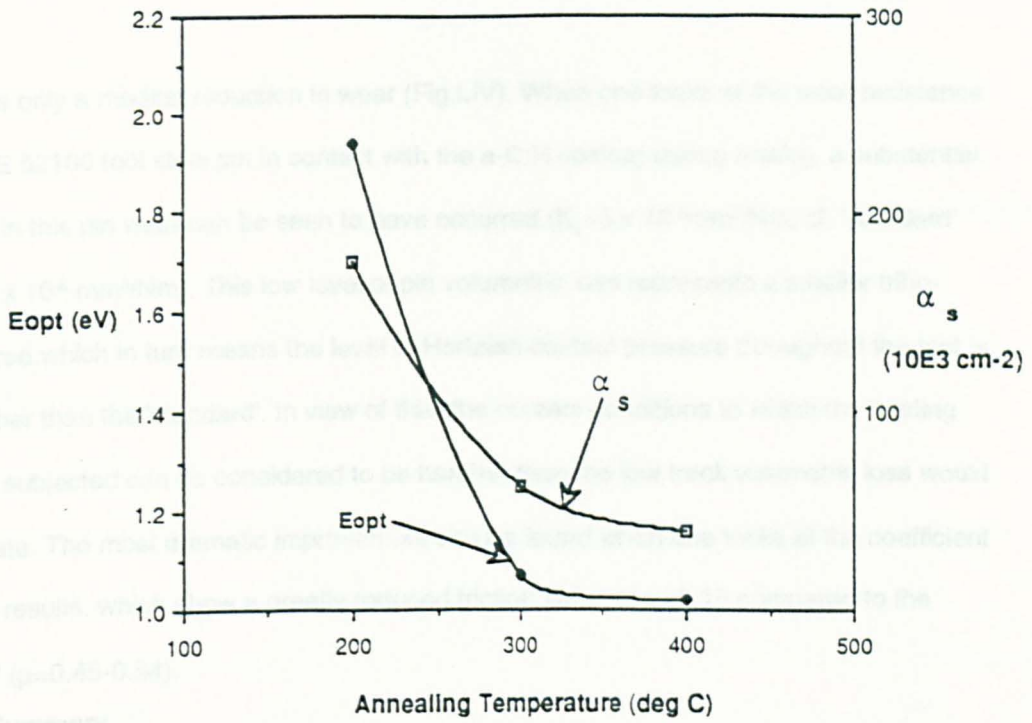


**Fig LII Optical Bandgap and Integrated C-H Absorption Characteristics versus Annealing Temperature for a-C:H EBPVD Films (500V)**

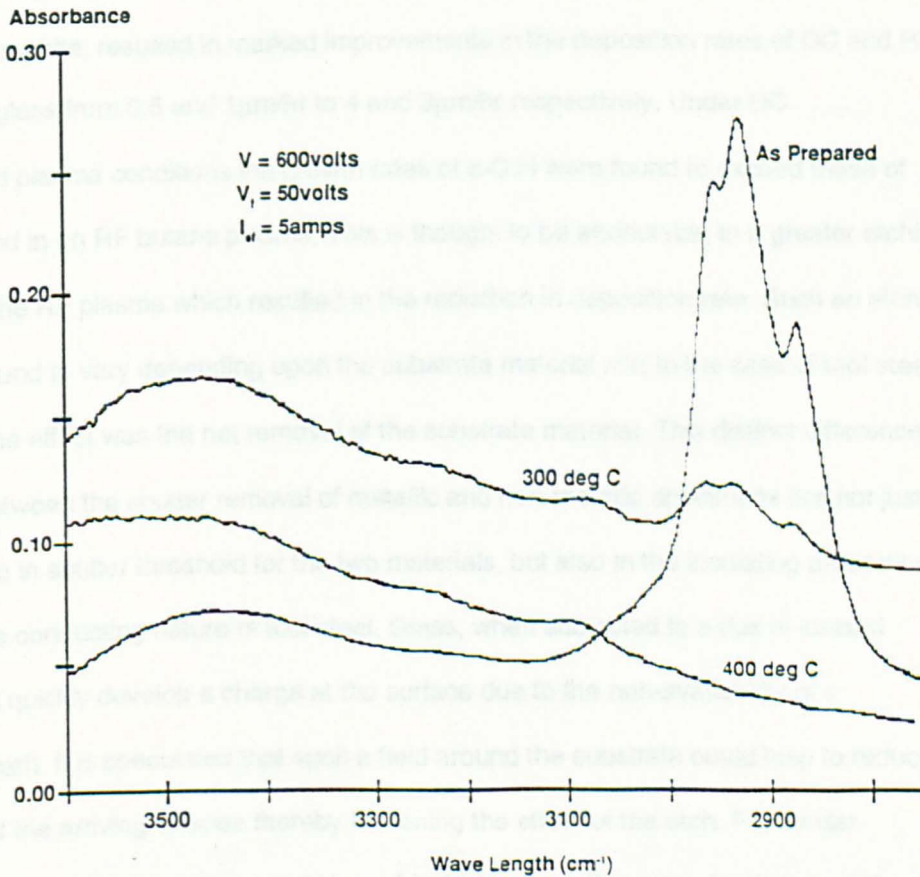


**Fig LIII Effect of Annealing on The Integrated C-H Absorption Bonding for a-C:H DC EBPVD Films (500V)**

represents only a modest reduction in wear (Fig.LIV). When one looks at the wear resistance of the SAE 52100 tool steel pin in contact with the a-C:H coating during testing, a substantial reduction in this pin wear can be seen to have occurred ( $K_b=5 \times 10^{-6} \text{mm}^3/\text{Nm}$ , cf. 'standard'  $K_b=12-20 \times 10^{-6} \text{mm}^3/\text{Nm}$ ). This low level of pin volumetric loss represents a smaller tribo-contact area which in turn means the level of Hertzian contact pressure throughout the test is much higher than the 'standard'. In view of this, the contact conditions to which the coating has been subjected can be considered to be harsher than the low track volumetric loss would first indicate. The most dramatic improvement can be found when one looks at the coefficient of friction results, which show a greatly reduced friction value of  $\mu=0.16$  compared to the 'standard' ( $\mu=0.45-0.54$ ).

***j) Summary***

The properties of both the RF and DC EBPVD films were found to be highly dependent upon the substrate material, current density and plasma gas used. The introduction of hydrogen, in the form of a butane precursor, to enhance the deposition of the evaporated graphite, resulted in marked improvements in the deposition rates of DC and RF a-C films on glass from 0.5 and  $1 \mu\text{m/hr}$  to 4 and  $3 \mu\text{m/hr}$  respectively. Under DC hydrogenated plasma conditions the growth rates of a-C:H were found to exceed those of films produced in an RF butane plasma. This is thought to be attributable to a greater etching influence of the RF plasma which resulted in the reduction in deposition rate. Such an etching affect was found to vary depending upon the substrate material and in the case of tool steel specimens the effect was the net removal of the substrate material. This distinct difference in behaviour between the sputter removal of metallic and non-metallic specimens lies not just in the difference in sputter threshold for the two materials, but also in the insulating properties of glass and the conducting nature of tool steel. Glass, when subjected to a flux of ionised particles, will quickly develop a charge at the surface due to the non-availability of a conducting path. It is speculated that such a field around the substrate could help to reduce the energy of the arriving species thereby lessening the effect of the etch. For similar conditions, the tool steel samples would be subjected to the full energy distribution of the arriving species. It is interesting to note that the only conditions under which a net deposit of

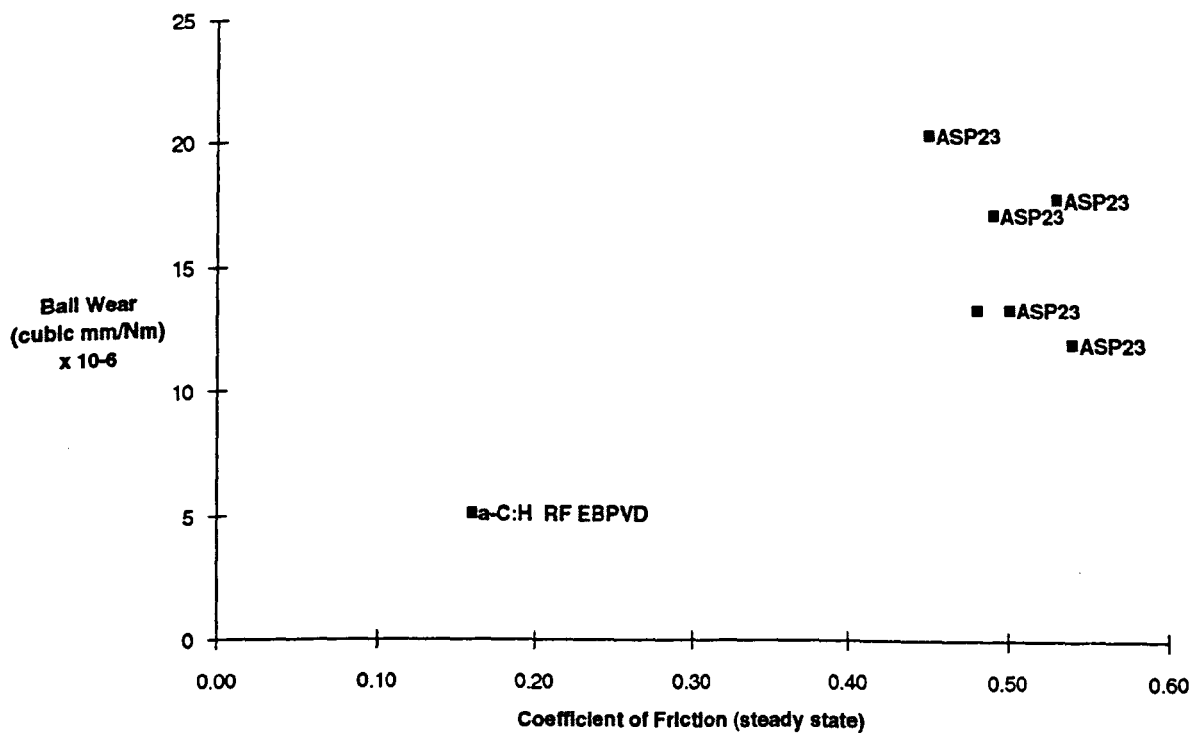
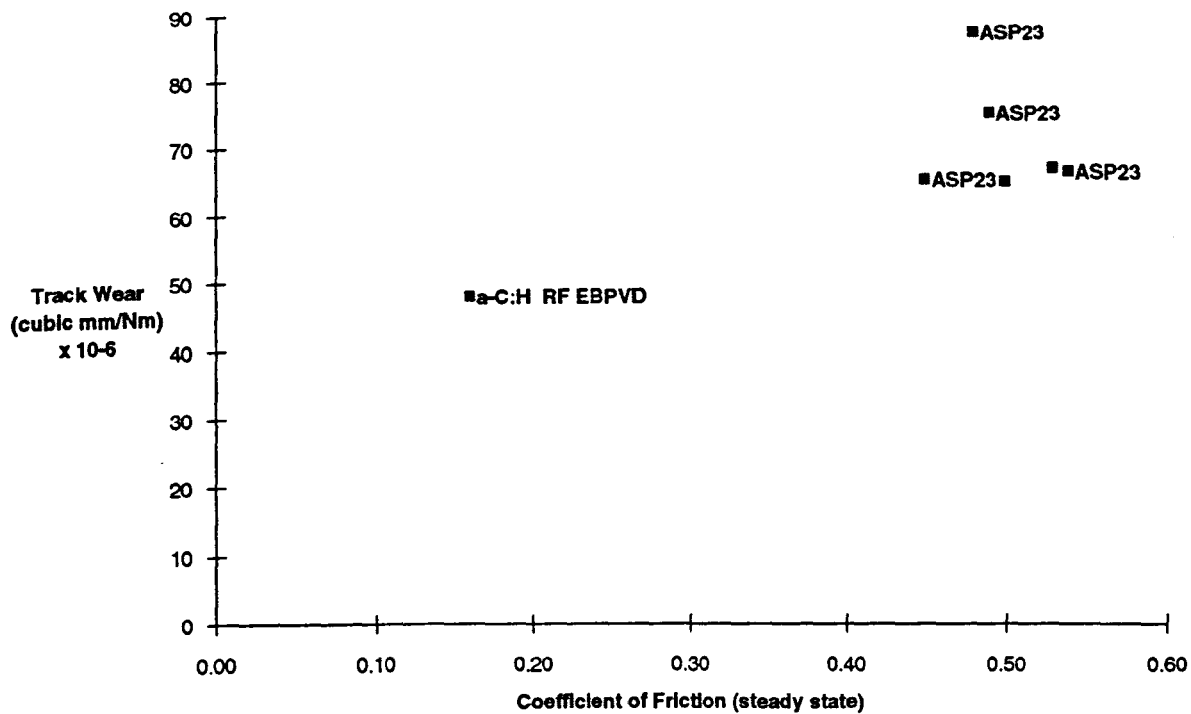


**Fig LIV The Friction & Wear Performance of a-C:H RF EBPVD Films versus Steady State Coefficient of Friction**

1.0 $\mu\text{m/hr}$  was achieved was on tool steel in an RF butane plasma at bias voltages less than 750V(DC offset). This provided the optimum growth conditions by a combination of low etching rate and maximum carbon flux (i.e. contributions from evaporated carbon and the disassociation of butane), hence a net deposit.

The adhesion of DLC to glass was found to be generally good, with a strong dependence on current density. A threefold increase in the critical load could be realised when using the radio frequency plasma techniques compared to the DC method, primarily because of the higher current densities achievable. The introduction of hydrogen was also noted to increase the adhesion in both deposition conditions.

All films were observed to contain internal stress which when measured was shown to be approximately 60% less than that of similar films previously reported. However, some films exhibited a rapid loss of adhesion, initiated at edges or discontinuities, within minutes of exposure to the atmosphere, leading to the conclusion that moisture absorption into the film/substrate interface was a probable cause for loss of adhesion.

Although examination by SEM showed all structures to be dense, amorphous and pin hole free, there was a considerable difference in their mechanical properties. DC a-C films were observed to be soft, giving values of typically 700-1900kg/mm<sup>2</sup> (15g), which were ductile in nature. RF films displayed consistently higher microhardness values of 2500kg/mm<sup>2</sup> (15g) for a-C films while an increase in microhardness to 3600kg/mm<sup>2</sup> (15g) was observed to occur with the addition of butane in the plasma. This increase, however, corresponds to a change in structural behaviour from a hard, ductile material to one which displayed large elastic recovery, making this increase in hardness possibly due to the relaxation of the indent rather than any increase in mechanical performance. Nanoindentation revealed a greater hardness of the films deposited onto glass, probably the result of better load support, as well as an increase in elastic modulus compared to tool steel.

Raman analyses of DC a-C:H films were found to be impossible due to intense fluorescence, however RF a-C:H films revealed the characteristic spectra for diamond-like carbon with unresolved D and G bands and a broad peak centred around 1552cm<sup>-1</sup>. Rutherford backscattering spectroscopy has been demonstrated to be a poor technique for

analysing light elements on a heavy matrix since the characteristic energies of recoiled protons from light elements at the surface and the energies of recoiled protons from heavy elements at depth, can coincide. Nevertheless, the technique exposed the presence of tungsten contamination at two main concentrations throughout the cross-section of the films produced as a result of the presence of a bias filament. The first is ascribed to the substrate/film interface and is presumed to have been deposited during the sputter-cleaning cycle. The second concentration is postulated to occur at the surface of the film because in certain circumstances the filament was left on after the evaporation of the graphite had ceased.

Optically, the films varied considerably (bandgap 0.46-2.3eV) from charcoal grey in appearance for DC a-C films, through to a yellowish brown colour characteristic of hydrogenated a-C:H films with a strong dependence on bias voltage and substrate temperature. Likewise the electrical properties of the films varied greatly from  $10^{-2}$ - $10^4 \Omega \text{cm}$  with a-C films displaying greater conductivity than a-C:H films. RF films displayed a smaller range of optical properties, from transparent ( $E_{\text{opt}} > 3\text{eV}$ ) for a-C through to semi transparent charcoal grey ( $E_{\text{opt}} 2.5\text{eV}$ ) for a-C:H films. In all case the films were reported to have a refractive index of 2.0. Analysis by infra-red spectroscopy revealed a higher amount of bonded hydrogen in the DC films to that of the RF plasma produced coatings, with the amount depending largely upon the deposition conditions. This therefore seems to confirm that there appears to be a strong dependence between the level of hydrogen in the film and the optical and electrical properties, where an increase in bonded hydrogen has the general effect of reducing the optical transmission and electrical resistivity.

The thermal stability of DLC films was tested by annealing the films up to temperatures of over 600°C. What was witnessed was a one stage annealing process at around a temperature of 400°C, whereupon the films rapidly became optical absorbing, electrically conducting and progressively relieved of internal stress, whilst simultaneously bonded and unbonded hydrogen is desorbed from the film.

The use of an RF plasma has been shown to produce films with superior frictional performances ( $\mu=0.16$ ) to that of the 'standard' SAE 52100 pin/ASP23 disc pairing, although

with a less startling improvement in film wear resistance. If however one notes the substantial reduction in wear of the counterface material then the Hertzian contact conditions for these films can be considered to be more arduous.

In summary, the influence of hydrogen on the optical and mechanical properties is significant in increasing the deposition rate, levels of elastic recovery and resistivity in DC films whilst decreasing the optical transmission and resistivity for RF films. Clearly, its influence is wide ranging and fundamental, although not entirely beneficial when one considers the poorer optical qualities. Other factors which have been shown to have a strong influence on the coating quality are variations in substrate deposition conditions, metallic (tungsten) contamination and thermal insensitivity, making the accurate assessment of the role of hydrogen more difficult to assess. Ultimately however, the improvements in terms of the combined structural and mechanical properties, as determined by the tribological assessment of the a-C:H produced by RF EBPVD appears to be relatively minor owing perhaps to the thin and poorly adherent nature of these films. This contrasts sharply with the previous assessment of DC evaporated PVD films reported during the initial studies, where hydrogenation of the hard carbon films produced a noticeable improvement in both the friction and wear properties.

## 2. Investigations Into Fast Atom Beam Films

The use of DC and RF plasma techniques during investigations, reported in the preceding section, highlighted several significant property advantages and disadvantages associated with these films. The most notable are good and controllable optical properties, high microhardness and elastic modulus, making these films good candidates for optical applications. In such applications, protection against erosive particles is also important and the high hardness and elastic modulus provide a combination of properties ideal for a light wear resistant, energy absorbing protective layer. The high resistivity also makes these materials attractive from the electrical and electronic point of view. However, it is the disappointing deposition results on tool steel and the high levels of degradation at relatively low temperatures which have been noted as particular areas for improvement. In the light of this, a further deposition method using a line of sight, beam process was investigated. This technique, known as Fast Atom Beam (FAB), differs from conventional ion source techniques in that it produces a highly directional beam of essentially neutral carbonaceous species (~98% neutral) due to a highly efficient charge exchange mechanism operating as the beam emerges from a graphite grid. Ionisation of the carrier gas within the source is enhanced by the saddle field effect, which induces the electrons emitted from a twin anode to travel in long spiralling paths within the source chamber, thereby increasing the probability of an ionisation event with a carrier gas molecule.

In an effort to improve the tribological performance of the these diamond-like coatings still further, experiments with intermediate layers of titanium nitride were also performed.

### **a) *Film Preparation & Experimental Details***

A more detailed description of the FAB B93 deposition equipment is given in Chap.III Sec.A(c). A neutral beam of hydrocarbon species emerges from a Ø25mm graphite aperture and is directed at samples placed normal to this beam at a distance of 300mm. Ultrasonic precleaning was supplemented by a hydrogen sputter etch using the source for 20 minutes (2kV, 0.1A). The source was then subsequently utilised for the deposition of diamond-like carbon, using one of the hydrocarbon source gases, by biasing the source anode between 1.0-2.5kV and 0.5-2.0A (typically 0.8-1.0kV, 1.0-1.5A). Source gases of butane, propane and

acetylene were investigated and these were fed into the core of the FAB source to achieve a chamber pressure of 10mTorr. During the length of a deposition experiment, which could last up to twenty four hours, the temperature of the samples achieved 35-50°C.

Two substrate combinations were used: ASP23 tool steel and cobalt-chrome, each coated with or without a TiN intermediate layer. This layer was deposited to a thickness of 3µm, for all samples, by the electron beam evaporation of titanium in a thermionically assisted DC nitrogen plasma; further details of this technique can be found in reference<sup>212</sup>. In addition, the surfaces of a number of ASP23 tool steel samples were prepared with a range of grit sizes from 0.06 to 260µm and DLC coated, so that the effect of a range of surfaces roughness on the friction behaviour during wear testing could be investigated.

The films were evaluated for their friction and wear properties under various conditions. Initially DLC films deposited onto titanium nitride coated tool steel and uncoated tool steel were tested under VAMAS pin on disc conditions; selected coatings were also assessed under varying humidity conditions (7-85%RH) and in the presence of different gaseous environments such as dry air, dry nitrogen and dry oxygen atmospheres. During such pin on disc tests, continuous recording of the frictional behaviour was performed whilst the atmospheric conditions within the testing environment were altered.

Structural examination of the films and wear sections were performed by Raman spectroscopy, nanoindentation and scanning electron microscopy. Qualitative and semi-quantitative chemical micro analysis was obtained by detecting the characteristic X-ray emissions through a windowless silicon detector using a LINK QX2000 energy dispersive X-ray system. To overcome the problem of beam penetration, which renders the film effectively transparent to the detecting electron beam at high energies, the samples were tilted away from the beam to increase the resolved film thickness and the energy reduced from 25 to 7 keV (Chap.III Sec.C4(b)). Dotmapping of the selected elements in the pin or film material allowed a visual determination of the levels and composition of the material transfer.

## **b) Results - Mechanical & Optical Properties**

The deposition rate of these films was found to be extremely low (typically 300nm/hr in the first hour) and highly dependent upon the axial position within the beam. The use of a carbon-rich gas such as acetylene, instead of propane, as the source gas had the effect of increasing the deposition by 1½ times with an imperceptible change in the optical and physical properties of the films. These deposition values can be regarded as the initial rates only, since during deposition, the graphite source anodes and walls gradually became coated with an insulating layer of carbon. This deposit, when analysed, showed a composition containing a high degree of sp<sup>3</sup> bonded carbon. The build-up of this deposit had the effect of reducing considerably the deposition with time, such that a 1µm film could take 6-8hrs to synthesise. Therefore, after every experiment, thorough cleaning of the interior of the source was necessary in order to be able to operate the source under optimum conditions at the start of each test.

Usually microhardnesses of FAB source films could be recorded to be as high as  $H_k=3000-4000\text{kg/mm}^2$  (25g) for films grown on glass, tool steel or cobalt-chrome, with little variation observed between substrates types. It was noted that when additional hydrogen (H<sub>2</sub>) was added to the hydrocarbon (C<sub>4</sub>H<sub>10</sub>) source gas, the films failed in a brittle fashion under the action of a micro-indenter in a similar way to that of hydrogenated DC and RF plasma deposited films studied earlier. Occasionally some films deposited would show a microhardness in excess of  $H_k=7000\text{kg/mm}^2$  (50g). Such films also displayed large amounts of elastic recovery which would result in the relaxation of the indent when the diamond indenter was unloaded. This behaviour may account for some of these anomalous values but it is thought that the development of the insulating layer of carbon within the source appears to play some role in this phenomenon. However a full understanding of this unpredictable nature of the source remains a point of study.

Adhesion to most substrates, including metallic specimens, was excellent although it was discovered that delamination was particularly sensitive to surface preparation and the cleaning process. If ultrasonic cleaning was disregarded or an inadequate hydrogen etch performed, localised debonding of the coating would be the result. In addition, the maximum

coating thickness of the film was limited to approximately  $3\mu\text{m}$  since large scale delamination would occur due to the presence of internal stresses at films greater than this thickness. These films have an  $\text{sp}^3:\text{sp}^2:\text{sp}^1$  ratio of 75:25:0 based upon infrared C-H bonding in the stretched region<sup>213</sup> and a lower level of bonded hydrogen in comparison to the hydrogenated 380kHz RF films grown in similar conditions to that of the previous section<sup>68</sup>. If additional hydrogen is introduced with the butane source gas the ratio of  $\text{sp}^3:\text{sp}^2:\text{sp}^1$  can be improved to 90:10:0 although with a corresponding increase in optical transmission and levels of stress.

Optically, FAB source films tended to cover a range of properties from semi-transparent, through all the interference colours to opaque grey/black depending upon the thickness of the film. Generally, the dark grey appearance indicated a thickness approaching  $1\mu\text{m}$  with an associated optical bandgap of 1eV. This optical transmission has been found to be heavily dependent upon the angle of incidence of the neutral beam to the surface of the specimen where orientations approaching grazing incidence gave films with an optical bandgap of 3.5-4.0eV and an  $\text{sp}^3:\text{sp}^2:\text{sp}^1$  ratio of 100:0:0<sup>213</sup>.

Under normal FAB source operation, the source anodes are biased to between 800-1000V with the current varying from 1.0-1.5A depending upon the conditions of the source and the chamber pressure. If films are deposited at higher voltages (2kV), the difference in adhesion is not at first apparent, however, after several months shelf testing at ambient conditions large scale debonding could be witnessed for all of the high energy deposited films. This behaviour is suggested to be the result of higher internal stresses within the films caused by the implantation of the structure by high energy species. Investigations into the hydrocarbon flow rate revealed a surprising lack of correlation with the levels of growth rate and microhardness. Thus the flux could be varied from 10-100sccm with the only apparent effect being to alter the voltage applied to the source anode. This is due to the fact that the flux and therefore the gas pressure in the chamber represent the impedance of the electrical system, any variation in this impedance is translated into a change in operating voltage. This change, although not great, could vary the voltage by 200 volts between the maximum and minimum range of flux.

### **c) Annealing**

The anomaly in microhardness results reported was thought to be largely attributable to the high level of elastic recovery, which in turn was thought to be the result of a high level of unbonded hydrogen, since the level of bonded hydrogen was known to be low. An annealing experiment was performed in an attempt to desorb this unbonded hydrogen from the film and measure the subsequent physical properties.

Approaching annealing temperatures of 350-400°C, the optical bandgap and bonded hydrogen levels decreased in a similar manner to those of the EBPVD films reported in the previous chapter. Microhardness testing of these films, after cooling to ambient temperatures, revealed no visible indentation up to loads of 25-50g. Further increases in load resulted in the brittle failure of the films.

### **d) Raman**

Analysis using Raman spectroscopy uncovered the typical spectra for hard a-C:H films exhibiting a dominance of  $sp^3$  fourfold co-ordinated carbon atoms (Fig.LV). In common with RF plasma EBPVD films, the main features detected were a broad peak centred around  $1515\text{cm}^{-1}$  and unresolved D ( $1350\text{cm}^{-1}$ ) and G ( $1600\text{cm}^{-1}$ ) peaks which signify the presence of graphitic micro-crystalline  $sp^2$  carbon.

In contrast to the plasma deposited films, a slight phase shift in the broad peak from  $1552\text{cm}^{-1}$  for RF EBPVD films to  $1515\text{cm}^{-1}$  for FAB source films was witnessed together with an additional decrease in the Raman scattering intensity. This phenomenon is connected to the reduced thickness of the films produced by the beam technique. Such a phase shift of main peak with thickness can be as great as  $70\text{cm}^{-1}$  as described by Ramsteiner et al<sup>30</sup>.

### **e) Tribological Properties - A Comparison**

Fast Atom Beam films deposited at room temperature onto hydrogen etched, bare metal substrates showed a considerable variation in tribological behaviour. For most of the films tested the friction and wear was excellent in comparison to the 'standard' SAE 52100 pin material against ASP23 tool steel substrate with no signs of cohesive failure after 100 metres sliding. The steady state coefficient of friction was recorded to be  $\mu=0.10-0.15$  and wear of the pin and film track between  $K_p=2-3 \times 10^{-6}\text{mm}^3/\text{Nm}$  and  $K_f=9-10 \times 10^{-6}\text{mm}^3/\text{Nm}$  respectively

(Fig.LVI). As explained previously, the mechanical properties were particularly sensitive to the conditions of the source and the axial position of the samples within the beam. Poor positioning produced a second category of films with consistently lower hardnesses and thicknesses. When subjected to the pin on disc test, the films displayed wear volumes almost comparable to the 'standard' pairing, due to a degree of cohesive failure, although their

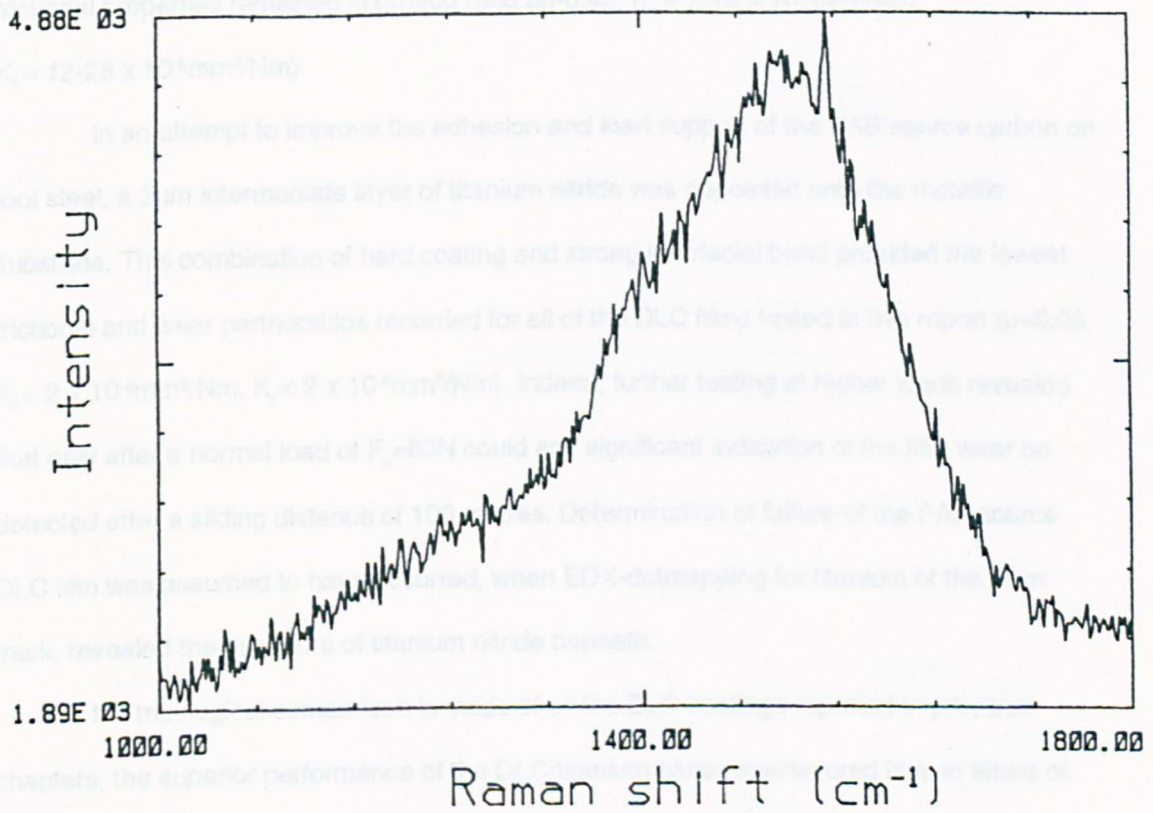


**Fig LV Typical Raman Spectra for a FAB Source Deposited DLC Film**

### g) The Effect of Surface Roughness

The surface finish is one of the many parameters which exclusively influences the tribological behaviour. To investigate this, tool steel samples were prepared with a range of grit sizes (0.05, 6, 15 & 260µm) and after coating with FAB source carbon, the resulting articles were initially analysed with a Talysurf profilometer for their surface roughness and

(Fig.LVI). As explained previously, the mechanical properties were particularly sensitive to the conditions of the source and the axial position of the samples within the beam. Poor positioning produced a second category of films with consistently lower hardnesses and thicknesses. When subjected to the pin on disc test, the films displayed wear volumes almost comparable to the 'standard' pairing, due to a degree of cohesive failure, although their frictional properties remained improved ( $\mu=0.36-0.42$ ,  $K_p = 7-15 \times 10^{-6}\text{mm}^3/\text{Nm}$ ,  $K_f = 12-28 \times 10^{-6}\text{mm}^3/\text{Nm}$ ).

In an attempt to improve the adhesion and load support of the FAB source carbon on tool steel, a  $3\mu\text{m}$  intermediate layer of titanium nitride was deposited onto the metallic substrate. This combination of hard coating and strong interfacial bond provided the lowest frictional and wear partnerships recorded for all of the DLC films tested in this report ( $\mu=0.05$ ,  $K_p = 2 \times 10^{-6}\text{mm}^3/\text{Nm}$ ,  $K_f < 2 \times 10^{-6}\text{mm}^3/\text{Nm}$ ). Indeed, further testing at higher loads revealed that only after a normal load of  $F_n=80\text{N}$  could any significant indication of the film wear be detected after a sliding distance of 100 metres. Determination of failure of the FAB source DLC film was assumed to have occurred, when EDX-dotmapping for titanium of the wear track, revealed the exposure of titanium nitride beneath.

If a tribological comparison is made of all the DLC coatings reported in previous chapters, the superior performance of the DLC/titanium nitride interlayered film, in terms of reduced friction, reduced film wear and low counterface material wear, can be seen more clearly (Fig.LVII). The reduction in wear of the film, as determined by the size of the wear track, is approximately two orders of magnitude lower when coated with the combination of diamond-like carbon and TiN compared to the uncoated specimen. The friction too was reduced remarkably by a order of magnitude over that of the uncoated substrate and three times less than the majority of the other DLC films.

#### **f) *The Effect of Surface Roughness***

The surface finish is one of the many parameters which markedly influences the tribological behaviour. To investigate this, tool steel samples were prepared with a range of grit sizes (0.06, 6, 15 &  $260\mu\text{m}$ ) and after coating with FAB source carbon, the resulting surfaces were initially analysed with a Talysurf profilometer for their surface roughness and

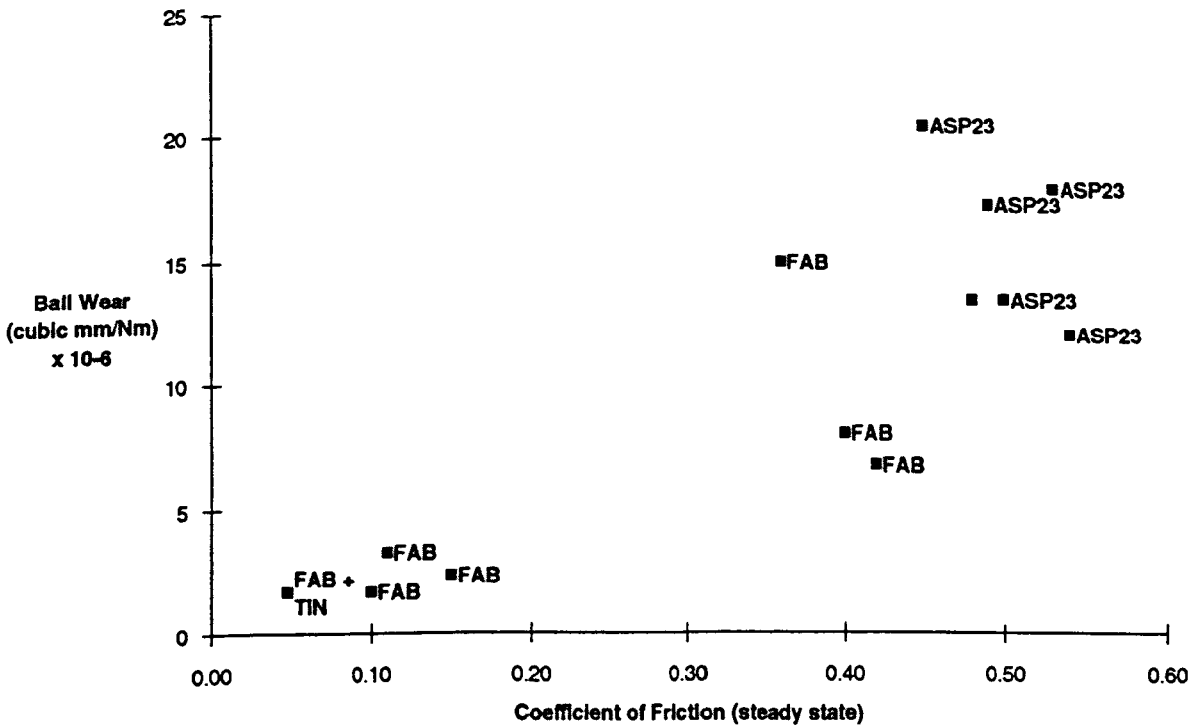
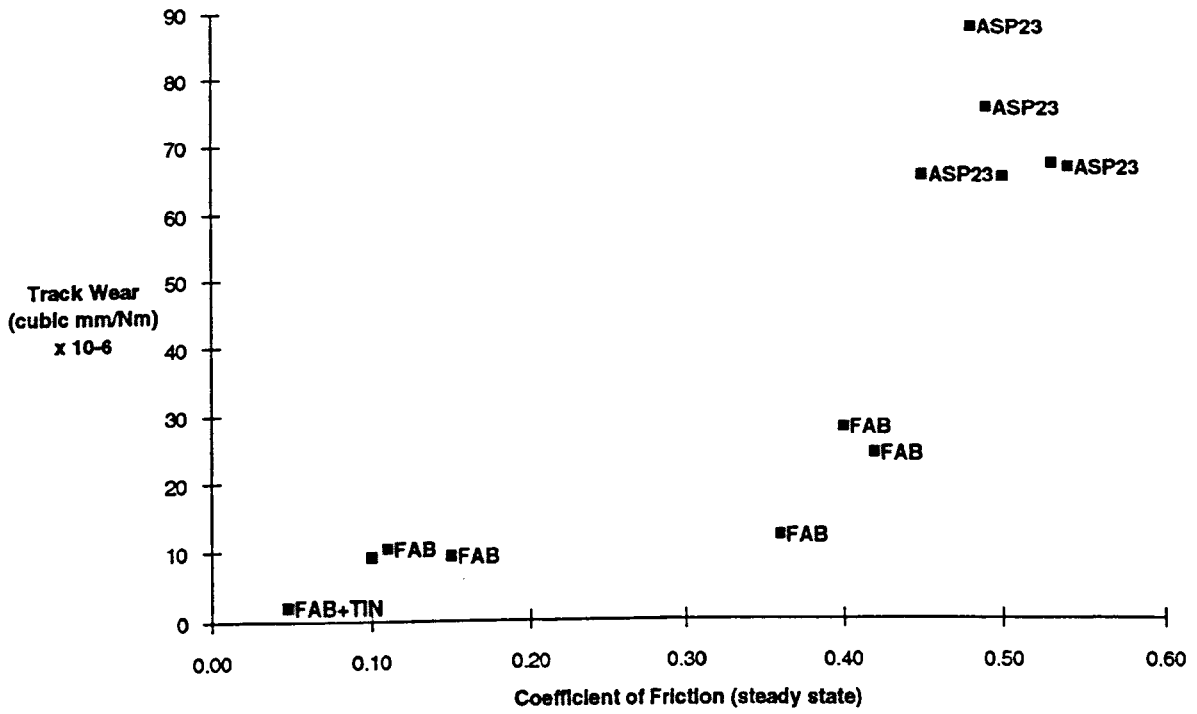


**Fig LVI The Friction & Wear Performances Of FAB Source Deposited Films versus Coefficient Of Friction**

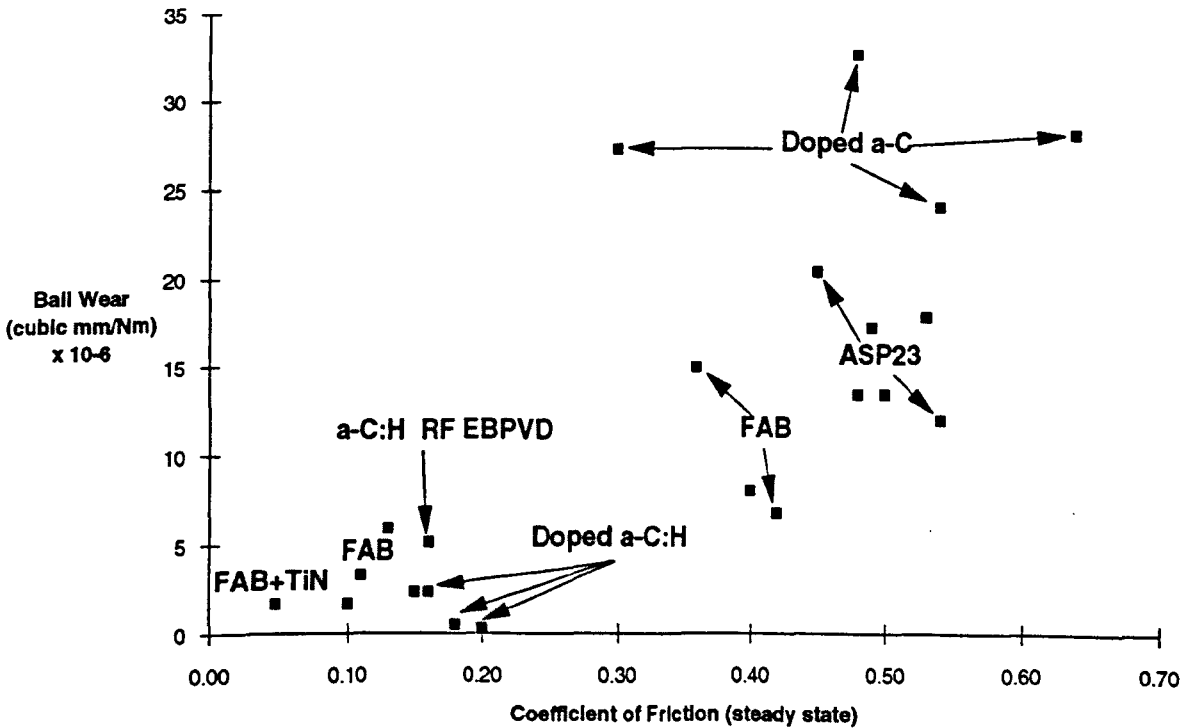
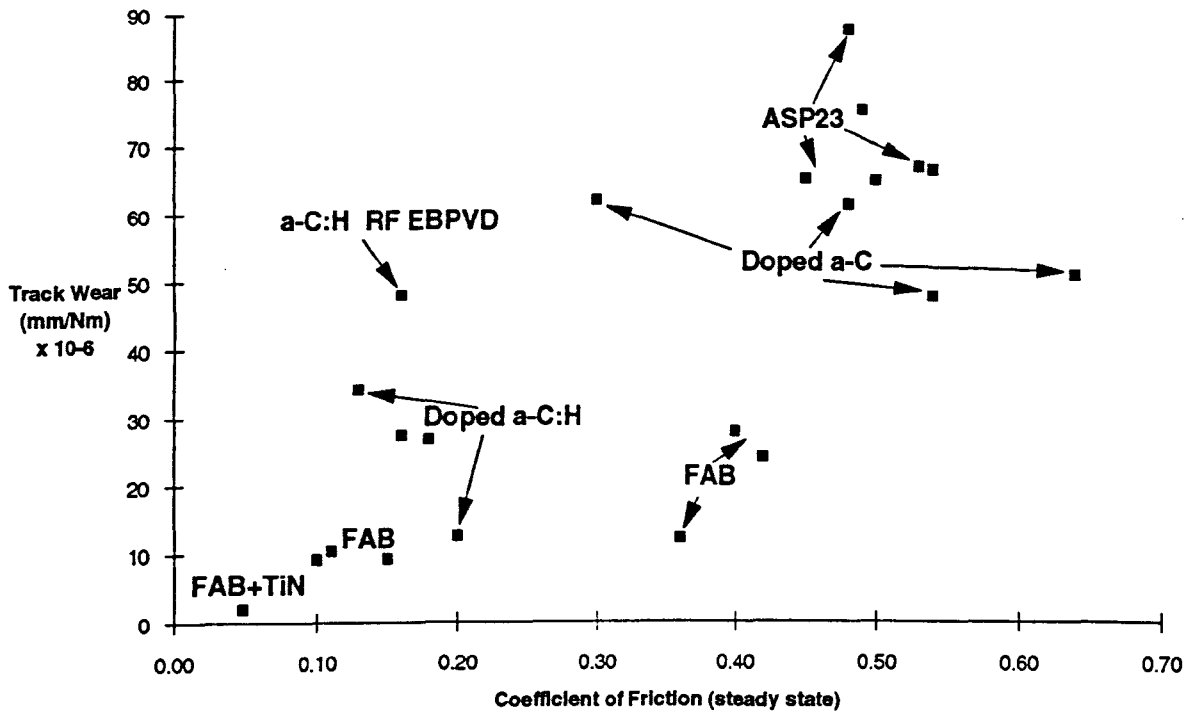


**Fig LVII A Tribological Comparison of the Film and Counterface Wear Of Doped, DC PVD, DC EBPBD, RF EBPVD and FAB Source DLC Films**

then evaluated for their frictional properties (Fig.LVIII). It was clear from the results, that as the surface finish of the disc becomes progressively smoother, this translated into a slight increase in the frictional force (Fig.LIX). Below  $R_a < 50\text{nm}$  this increase became more rapid, particularly for friction values taken at the initial stages of the test (sliding distance  $< 1\text{m}$ ). In fact, a good correlation between surface roughness and initial friction conditions has already been shown to exist<sup>214</sup>. This increase in friction value corresponds to a real increase in contact as a result of a marked improvement in conformity between the two materials, despite the same loading and test conditions. This behaviour is the result of the nature of the asperity contact. Intimate contact only occurs where the asperities of one surface touch the surface of the counterface. Since real surfaces are rough on an atomic level, the degree of contact can be very small depending upon the conditions of the surface finish and the degree of loading<sup>215</sup>. The frictional force required to slide one surface over another arises from the total resistance to shearing or sliding of these contact zones and therefore depends not only on the sum of the cross sectional asperity areas in contact but on shear properties of impurities (or coating) present between these surfaces. In this experiment the asperity height had been substantially reduced through polishing to give a surface roughness down to an  $R_a$  of  $< 10\text{nm}$ . This in turn greatly increases the contact area and results in the higher initial values of friction. This somewhat simple description of the contact conditions disregards the degree of deformation experienced by the film/substrate which will be considerable during the initial stages of the test. It therefore seems possible also that a large degree of ploughing deformation could have contributed to the higher measurements of initial friction. Such a deformation process would decrease with test duration as wear of the pin material gradually reduced the levels of contact pressure between the two surfaces.

After a sliding event, observations of the pin and track wear scars revealed a heavy adhesive contact condition between the SAE 52100 and ASP23 metallic surfaces indicating the early cohesive and adhesive failure of the DLC film. This heavy wear behaviour was the result of large deformations and failure of the film followed by strong adhesive bonding across the interface. The subsequent material transfer from one surface to another was the direct result of these interfacial bonds being stronger than the cohesive bonds in either of the two

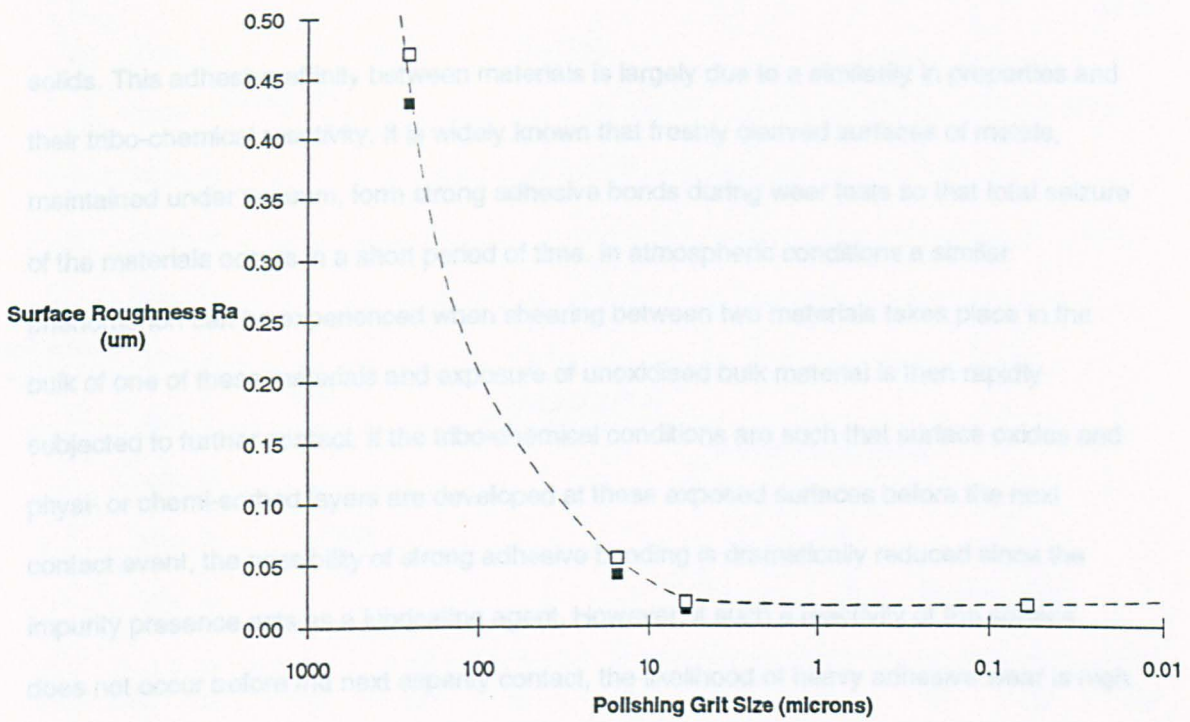


**Fig LVIII The Relationship Between Polishing Grit Size And The Surface Roughness**

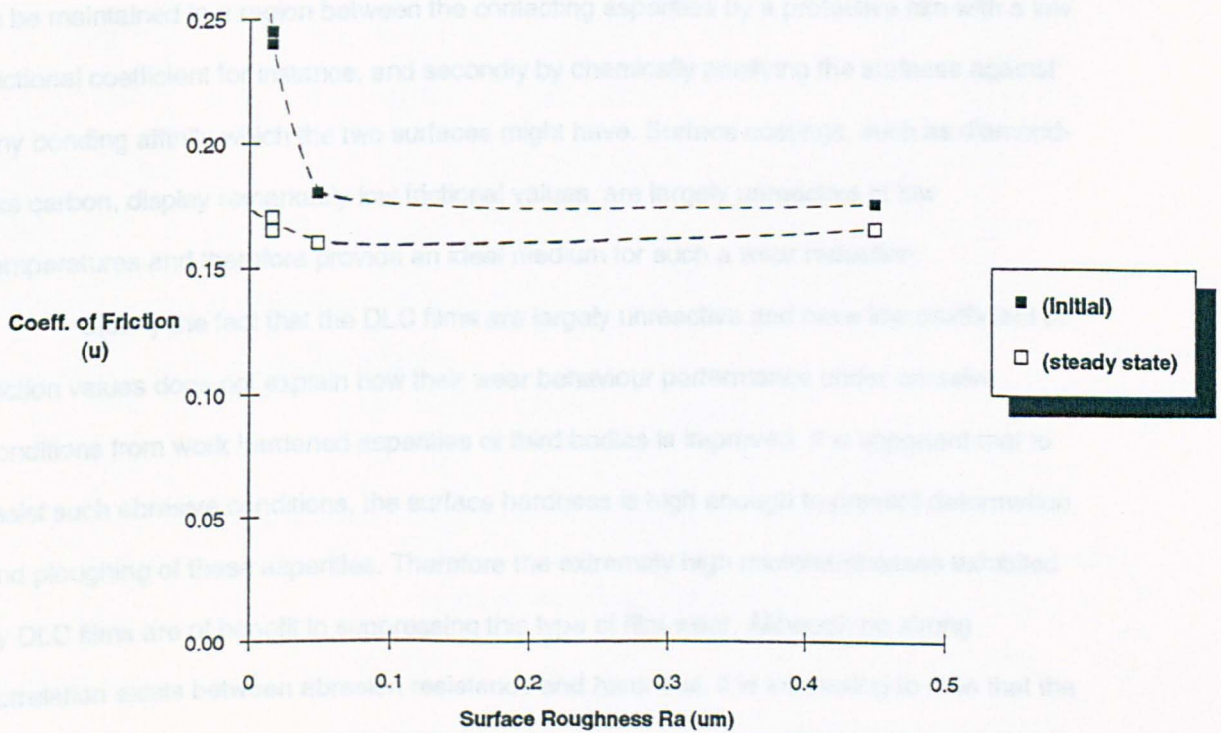


**Fig LIX The Relationship Between Surface Roughness And Coefficient Of Friction (Initial & Steady State)**

solids. This adhesive affinity between materials is largely due to a similarity in properties and their tribo-chemical reactivity. It is widely known that freshly cleaved surfaces of metals, maintained under vacuum, form strong adhesive bonds during wear tests so that total seizure of the materials occurs in a short period of time. In atmospheric conditions a similar phenomenon can be experienced when shearing between two materials takes place in the bulk of one of these materials and exposure of unoxidised bulk material is then rapidly subjected to further contact. If the tribo-chemical conditions are such that surface oxides and physi- or chemi-sorbed layers are developed at these exposed surfaces before the next contact event, the possibility of strong adhesive bonding is dramatically reduced since the impurity presence acts as a lubricating agent. However, if such a reactivity of the surface does not occur before the next asperity contact, the likelihood of heavy adhesive wear is high. The rate at which these layers are formed depends largely on the oxygen partial pressure, the chemical reactivity of the surfaces and the heat dissipated during the wear event. Therefore the chemical environment and reactivity of the surface becomes a significant factor in influencing the scale of adhesive wear taking place.

For an effective reduction of adhesive transfer wear, the weakest point of shear has to be maintained in a region between the contacting asperities by a protective film with a low frictional coefficient for instance, and secondly by chemically pacifying the surfaces against any bonding affinity which the two surfaces might have. Surface coatings, such as diamond-like carbon, display remarkably low frictional values, are largely unreactive at low temperatures and therefore provide an ideal medium for such a wear reduction.

Clearly the fact that the DLC films are largely unreactive and have low coefficient of friction values does not explain how their wear behaviour performance under abrasive conditions from work hardened asperities or third bodies is improved. It is important that to resist such abrasive conditions, the surface hardness is high enough to prevent deformation and ploughing of these asperities. Therefore the extremely high microhardnesses exhibited by DLC films are of benefit in suppressing this type of film wear. Although no strong correlation exists between abrasion resistance and hardness, it is interesting to note that the ranking order which occurs when plotting microhardness against friction and film wear is similar to their tribological performance (Fig.LX).

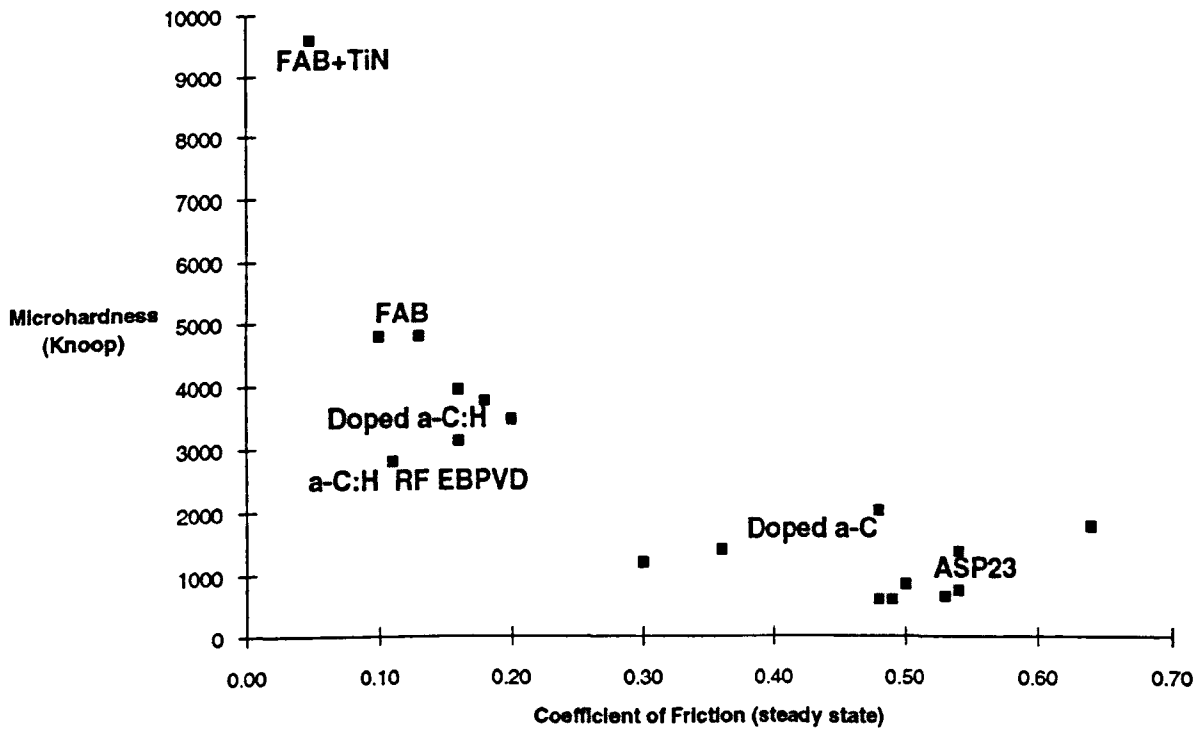
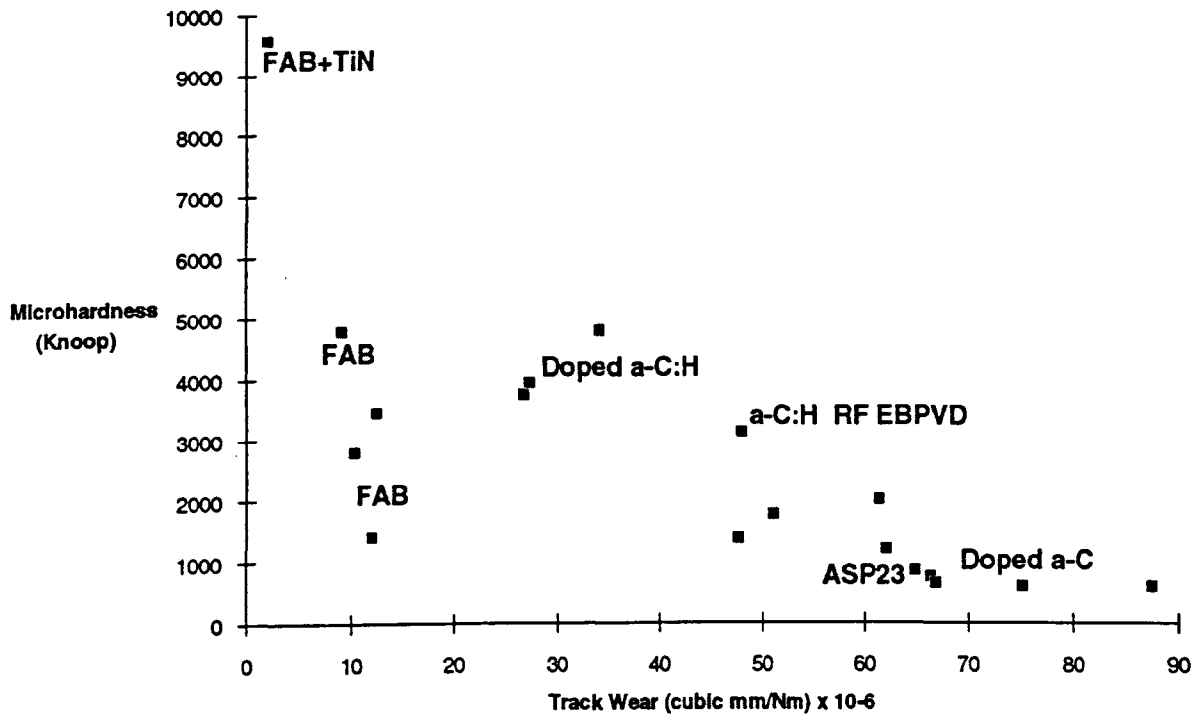


**Fig LX The Relationship Between Microhardness against Friction Coefficient And Track Wear**

### ***g) Humidity and Atmospheric Conditions***

Figure LXI illustrates the variation in friction with increasing humidity conditions in air (7-85%RH) for a FAB source film with a titanium nitride interlayer. It would seem that the overall change in frictional performance is minimal, although a trend towards a reduction with increasing humidity may be concluded. Other than weak chemi-sorption of water vapour at the coating surface and allowing for test variations with time, there appears to be little evidence of a tribo-chemically accelerated wear mechanism due to the presence of water vapour. Indeed EDX dotmapping for oxygen at the wear surface reveals little increase in oxide formation between high and low humidity conditions. Larger variations with humidity have been reported in the literature<sup>6,165</sup>, although these results were usually enhanced by long incubation periods at extremely high or low humidity conditions.

Nevertheless, evidence that some tribo-chemical activity is taking place is clearly shown in Fig LXII. During continuous frictional testing, the introduction of dry nitrogen gas into the test environment can be seen to reduce the resulting friction between the sliding pairs ( $\mu \approx 0.12$  -  $N_2$ , cf.  $\mu \approx 0.14$  - air). Once dry air was introduced back into the test environment, the conditions of friction revert back to their original value. However, when dry oxygen was introduced into the testing environment, a sharp increase in friction was observed to occur ( $\mu = 0.18$ ) which could be reduced partially by the reintroduction of dry nitrogen, although never fully recovering its original value. This had the effect of superimposing a gradual rising trend in the friction coefficient values during the cycling between oxygen and nitrogen atmospheres. Chemical analysis of the pin scar revealed the nature of this variation which is discussed in the following section.

### ***h) Chemical Effects at the Wear Interface.***

Analysis of the wear scars revealed two types of tribological behaviour amongst the carbon films. The first category was dominated by the soft, thin or poorly adhered carbon films which fail to prevent the early formation of steel on steel contact conditions, resulting in heavy adhesive type, material transfer and increased friction. EDX analysis revealed that material transfer was predominantly from the pin to the surface of the disc since only small traces of oxide were found on the pin scar. It is known that oxide formation will occur at the

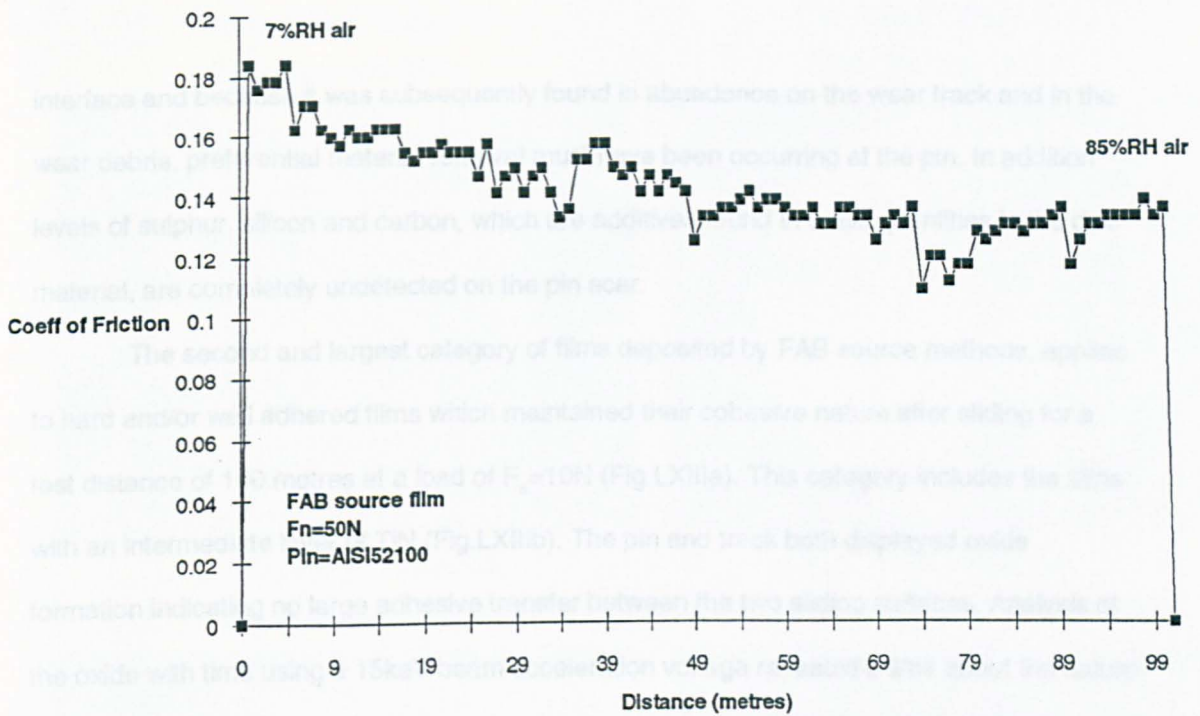


Fig LXI The Frictional Behaviour Of A FAB Source DLC With A Change In Humidity Conditions

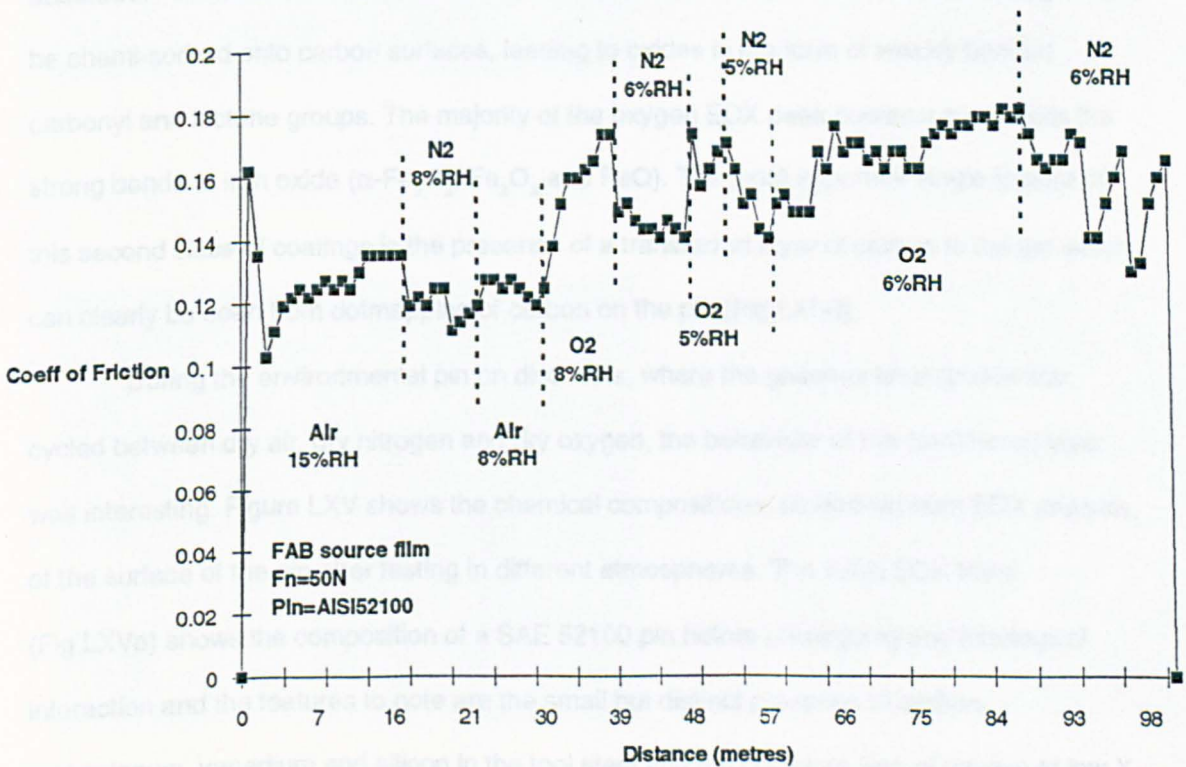
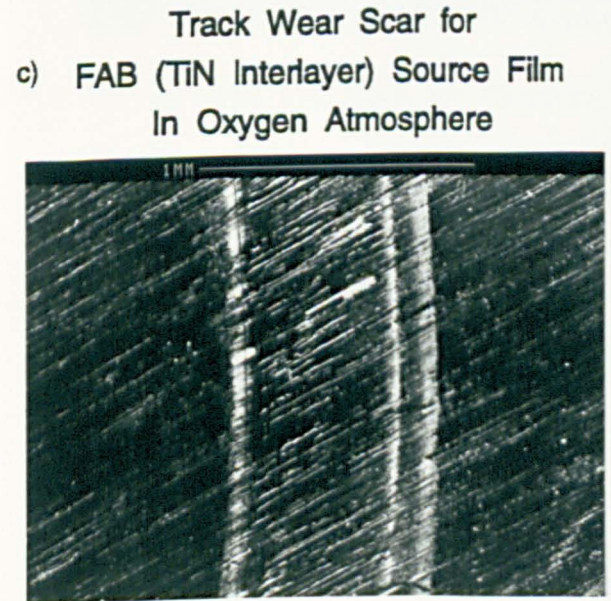
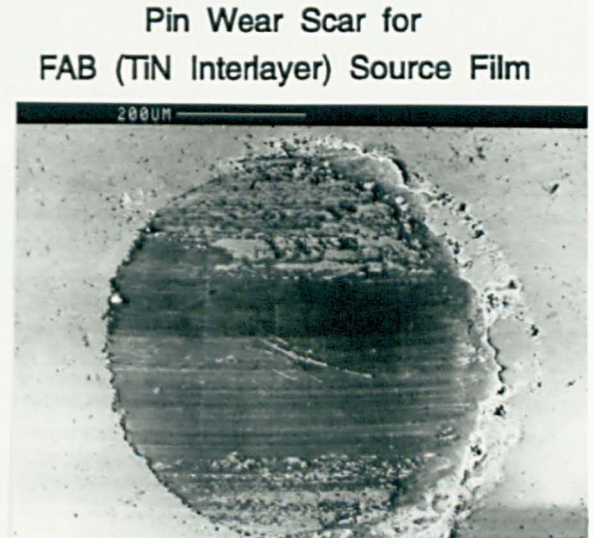
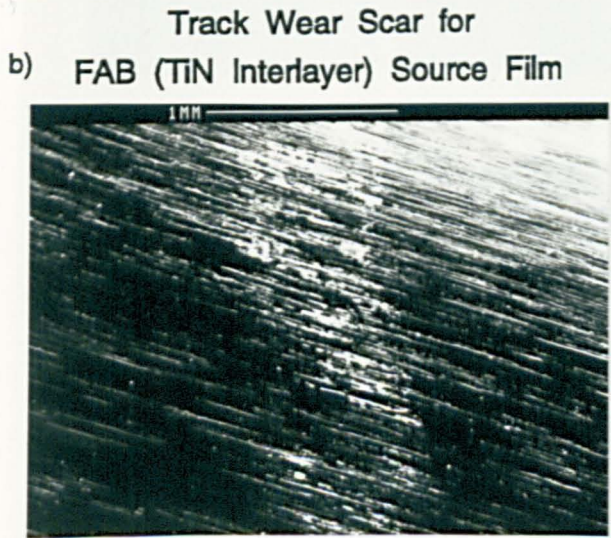
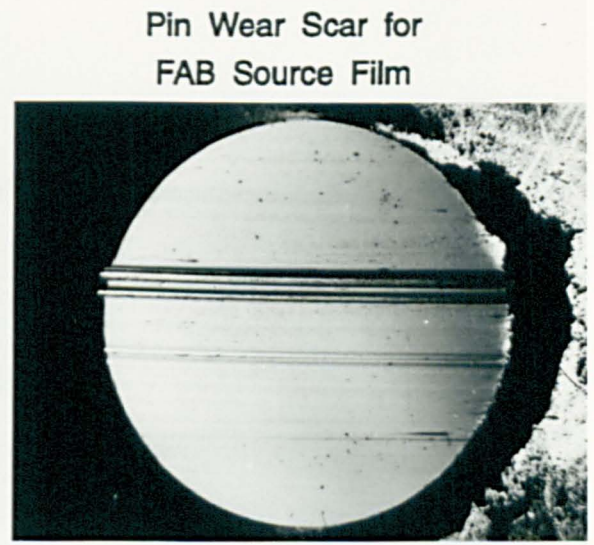


Fig LXII The Frictional Behaviour Of A FAB Source DLC Film With Changing Gaseous Environment (Dry Air, Dry Oxygen and Dry Nitrogen)

interface and because it was subsequently found in abundance on the wear track and in the wear debris, preferential material removal must have been occurring at the pin. In addition levels of sulphur, silicon and carbon, which are additives found in small quantities in the disc material, are completely undetected on the pin scar.

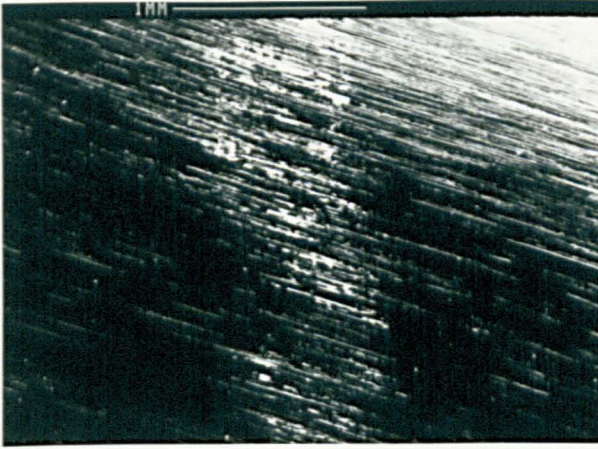
The second and largest category of films deposited by FAB source methods, applies to hard and/or well adhered films which maintained their cohesive nature after sliding for a test distance of 100 metres at a load of  $F_n=10\text{N}$  (Fig LXIIIa). This category includes the films with an intermediate layer of TiN (Fig.LXIIIb). The pin and track both displayed oxide formation indicating no large adhesive transfer between the two sliding surfaces. Analysis of the oxide with time using a 15keV beam acceleration voltage revealed a little about the nature of this oxide bonding. Over a period of twelve hours, the oxygen EDX peak FWHM value decreased slowly with time. This was thought to indicate the liberation of some weakly chemisorbed oxygen present either in the form of a lower oxide of iron or more probably through the emission of CO or CO<sub>2</sub> formed during the sliding event and subsequently weakly absorbed. This latter mechanism is discussed by Marchon et al<sup>172</sup> who state that oxygen can be chemisorbed onto carbon surfaces, leading to oxides in the form of weakly bonded carbonyl and lactone groups. The majority of the oxygen EDX peak however represents the strong bonds of iron oxide ( $\alpha\text{-Fe}_2\text{O}_3$ ,  $\text{Fe}_2\text{O}_3$  and FeO). The most important single feature of this second class of coatings is the presence of a transferred layer of carbon to the pin which can clearly be seen from dotmapping of carbon on the pin (Fig LXIVf).

During the environmental pin on disc tests, where the gaseous atmosphere was cycled between dry air, dry nitrogen and dry oxygen, the behaviour of this transferred layer was interesting. Figure LXV shows the chemical compositions, as derived from EDX analysis, of the surface of the pin after testing in different atmospheres. The initial EDX trace (Fig.LXVa) shows the composition of a SAE 52100 pin before undergoing any tribological interaction and the features to note are the small but distinct presence of carbon, molybdenum, vanadium and silicon in the tool steel and the complete lack of oxygen at low X-ray energies.

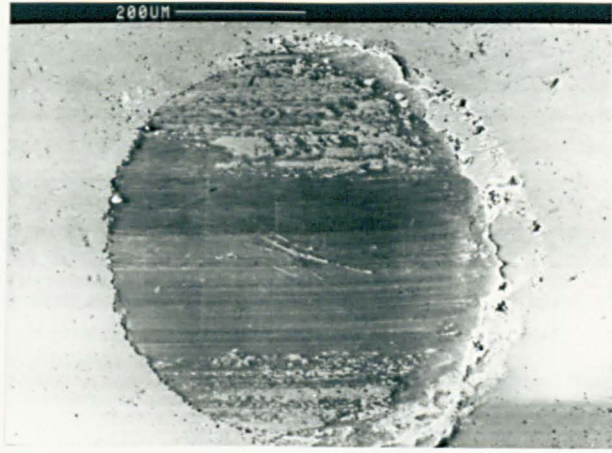


**Fig LXIII** The Effect Of A Intermediate Layer And Gaseous Environment On The Tribological Characteristics Of FAB Source Films

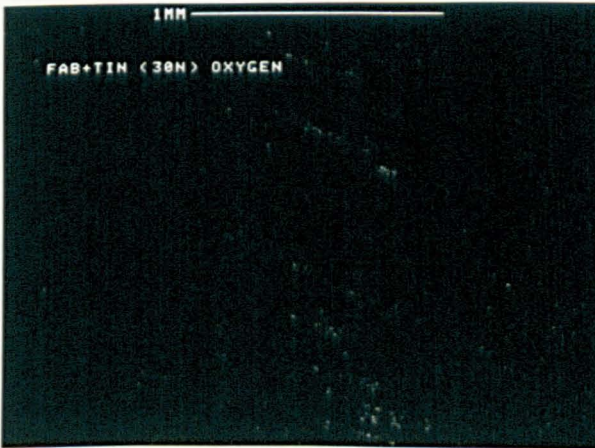
a) Track Wear Scar for  
FAB (TiN) Source Film



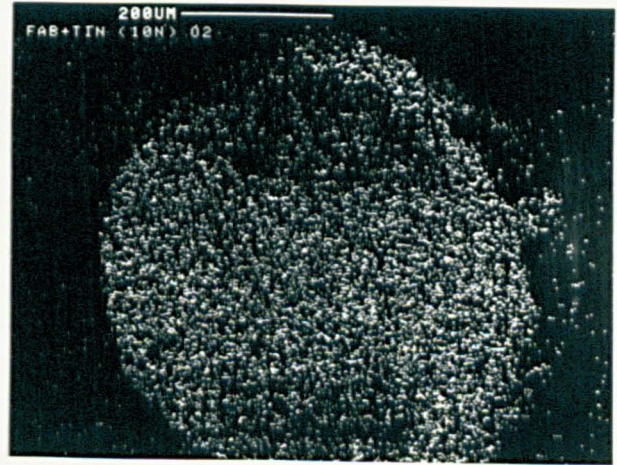
b) Pin Wear Scar for  
FAB (TiN) Source Film



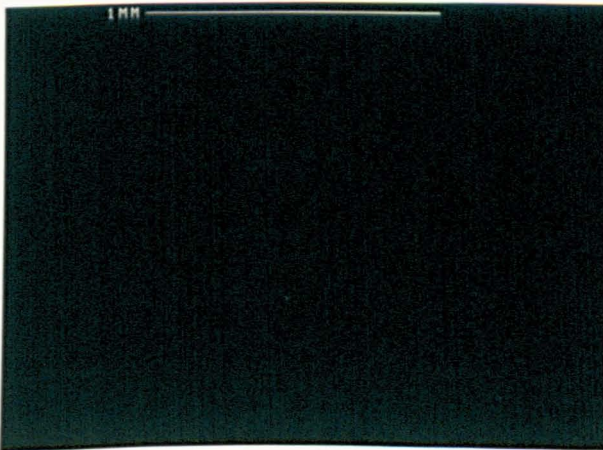
c) EDX Dot Map for Oxygen



d) EDX Dot Map For Oxygen



e) EDX Dot Map for Titanium



f) EDX Dot Map for Carbon

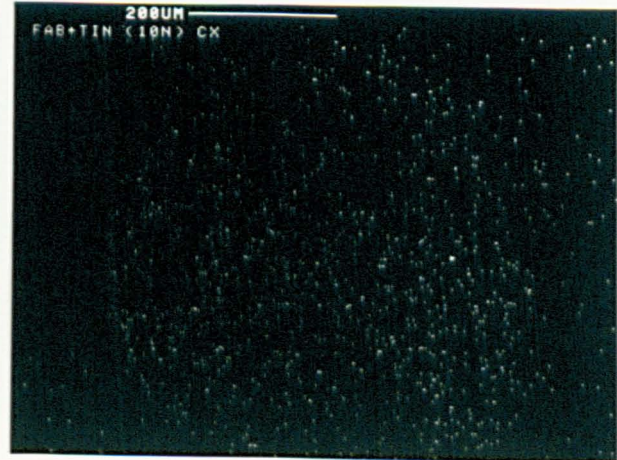
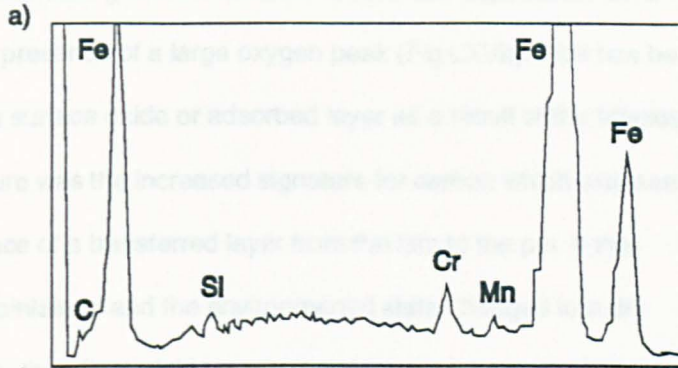


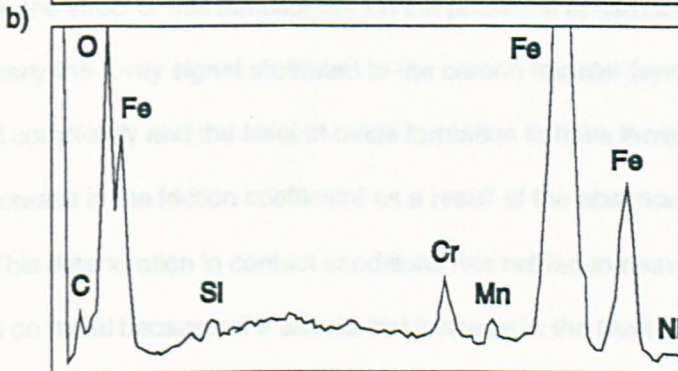
Fig LXIV Energy Dispersive X-ray Dotmapping Of A FAB Source  
DLC Film With A TiN Intermediate Layer

AISI 52100 Pin  
Bulk Analysis



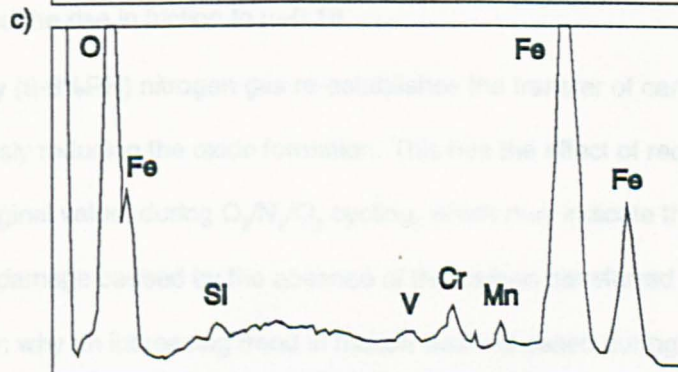
Live - 100s  
Real - 122s  
18% dead  
Preset - 100s  
7KeV  
FS = 2K  
177cts

Pin Scar Analysis  
after sliding on FAB(TiN)  
50%RH, 21deg C



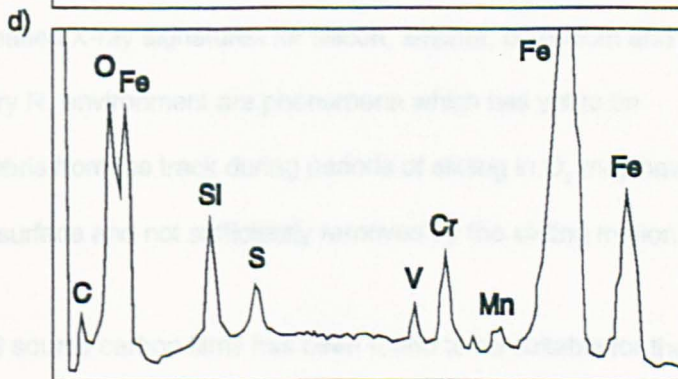
Live - 100s  
Real - 124s  
19% dead  
7KeV  
FS = 2K  
209cts

Pin Scar Analysis  
after sliding on FAB(TiN)  
in a 6-8%RH  
oxygen atmosphere



Live - 100s  
Real - 123s  
19% dead  
7KeV  
FS = 2K  
213cts

Pin Scar Analysis  
after sliding on FAB(TiN)  
in a 6-8%RH  
nitrogen atmosphere



Live - 100s  
Real - 141s  
29% dead  
7KeV  
FS = 2K  
196cts

Fig LXV Energy Dispersive X-ray Analysis Of The Pin Scar Surface Tested Under Different Atmospheric Conditions

Analysis of the scar after sliding with a FAB source DLC film deposited onto a TiN interlayer in dry air shows the presence of a large oxygen peak (Fig.LXVb). This has been attributed to the formation of a surface oxide or adsorbed layer as a result of the tribological interaction. An additional feature was the increased signature for carbon which was seen as further evidence of the presence of a transferred layer from the film to the pin. If the tribological conditions were maintained and the environmental state changed to a dry (6-8%RH) oxygen atmosphere, the effect of this atmosphere on the presence of carbon could be seen in Fig.LXVc. Quite clearly the X-ray signal attributed to the carbon transfer layer was observed to have disappeared completely and the level of oxide formation to have increased. This behaviour explains the increase in the friction coefficient as a result of the absence of the transferred carbon layer. This deterioration in contact conditions has not led to heavy adhesive wear typical of metal on metal because of a substantial increase in the level of surface oxide which has limited the rise in friction to  $\mu=0.18$ .

The introduction of dry (6-8%RH) nitrogen gas re-establishes the transfer of carbon (Fig.LXVd) whilst simultaneously reducing the oxide formation. This has the effect of reducing the friction coefficient to its original value, during  $O_2/N_2/O_2$  cycling, which may indicate the degree of permanent surface damage caused by the absence of the carbon transferred layer (Fig.LXIIIc). This would explain why an increasing trend in friction was witnessed during this atmospheric cycling. The increased X-ray signatures for silicon, sulphur, chromium and vanadium during sliding in a dry  $N_2$  environment are phenomena which has yet to be explained although transfer debris from the track during periods of sliding in  $O_2$  may have become embedded in the pin surface and not sufficiently removed by the sliding motion.

***i) Summary***

The deposition of FAB source carbon films has been found to be suitable for the synthesis of optically transmitting, hard layers, although the consistent production of these properties is highly dependent upon the position and angle of the substrate to the beam and the condition of the source. The introduction of additional hydrogen with the hydrocarbon source gas has been shown to improve the bonding arrangement and optical transmission but reduce the level of adhesion by increasing the internal stress and brittle behaviour of the

films. Structurally, the film displayed the characteristic Raman spectra for diamond-like films indicative of high levels of  $sp^3$  bonding.

Tribologically, the films exhibited excellent friction ( $\mu=0.10-0.11$ ) and wear resistant properties although the films prepared with inadequate surface preparation suffered from signs of early cohesive failure during the pin on disc test. FAB source films deposited onto intermediate layers of titanium nitride displayed a slightly improved friction value ( $\mu\approx 0.05$ ) with considerably improved resistance to film wear. The frictional behaviour was found to be largely insensitive to the humidity conditions although with the addition of a dry oxygen atmosphere, a rapid increase in wear and friction was noted to occur immediately. Analysis of the pin wear scar by EDX revealed the presence of a transferred layer of carbon which, under atmospheric or inert conditions, could maintain a region of low shear between the two surfaces and reduce the level of tribo-chemical contact. However, the introduction of oxygen removed this layer so that the metallic surface of the counterface was brought into direct contact with the DLC film and underwent accelerated wear.

### **C. The Presence of a Titanium Nitride Interlayer**

The improved wear performances of DLC films coated onto an intermediate layer of titanium nitride, under dry sliding conditions up to Hertzian contact pressure of 1.7GPa, were of particular interest. Volumetric wear rates and friction coefficients of the film surpassed any of the previously tested films ( $W_f < 2 \times 10^{-6} \text{mm}^3/\text{Nm}$ ,  $\mu=0.05$ ) and were shown to be insensitive to humidity changes. However the exact nature by which the TiN improved radically the tribological behaviour of the DLC films requires clarification. Initial thoughts were centred around either a process of increased load support provided by the TiN layer or an enhancement in the adhesion achieved by TiN's superior adhesive strength to steel. Initially it seemed that the most probable solution would be the load support theory since it appeared that the relatively soft underlying substrate material (ASP23) could not provide adequate support against deformation under high Hertzian pressures, without the assistance of an additional hard, thick interlayer. The objectives of the following work were then to establish the near surface structural properties of DLC films with or without the intermediate layer of TiN, using a commercially available nanoindenter to assess the contribution from this layer<sup>216</sup>.

#### ***a) Raman***

Fig.LXVI shows again the typical Raman spectra for a diamond-like carbon film with an intermediate layer of titanium nitride, displaying a high degree of  $sp^3$  bonded carbon. The presence of the titanium nitride layer appears to have modified the spectra very little from that of FAB source films deposited directly onto steel (Fig.LV), indicating that the improved behaviour could not possibly be due to marked change in the composition or structure. Again small shifts of  $\sim 13\text{cm}^{-1}$  (from  $1515\text{cm}^{-1}$  for FAB source film to  $1528\text{cm}^{-1}$  FAB source films on TiN) indicating a slight increase in thickness for films deposited onto TiN interlayers.

#### ***b) Nanoindentation***

It is commonly accepted that the depth at which the properties of a substrate begin to exert an influence on the properties of the coating depends on the ratio of the hardness of the film to that of the layer beneath<sup>217,218</sup>. For this reason it has become standard practice to limit the indentation depth to a maximum of 10% of the coating thickness. Conversely, by

varying the thickness of the DLC film and the penetration depth, the effect of the underlying layer and its mechanical properties on the measurement of the hardness and elastic modulus could be investigated.

New samples were prepared for this study using similar deposition conditions to the previous tribological investigation. A DC plasma PVD method was used to synthesize new

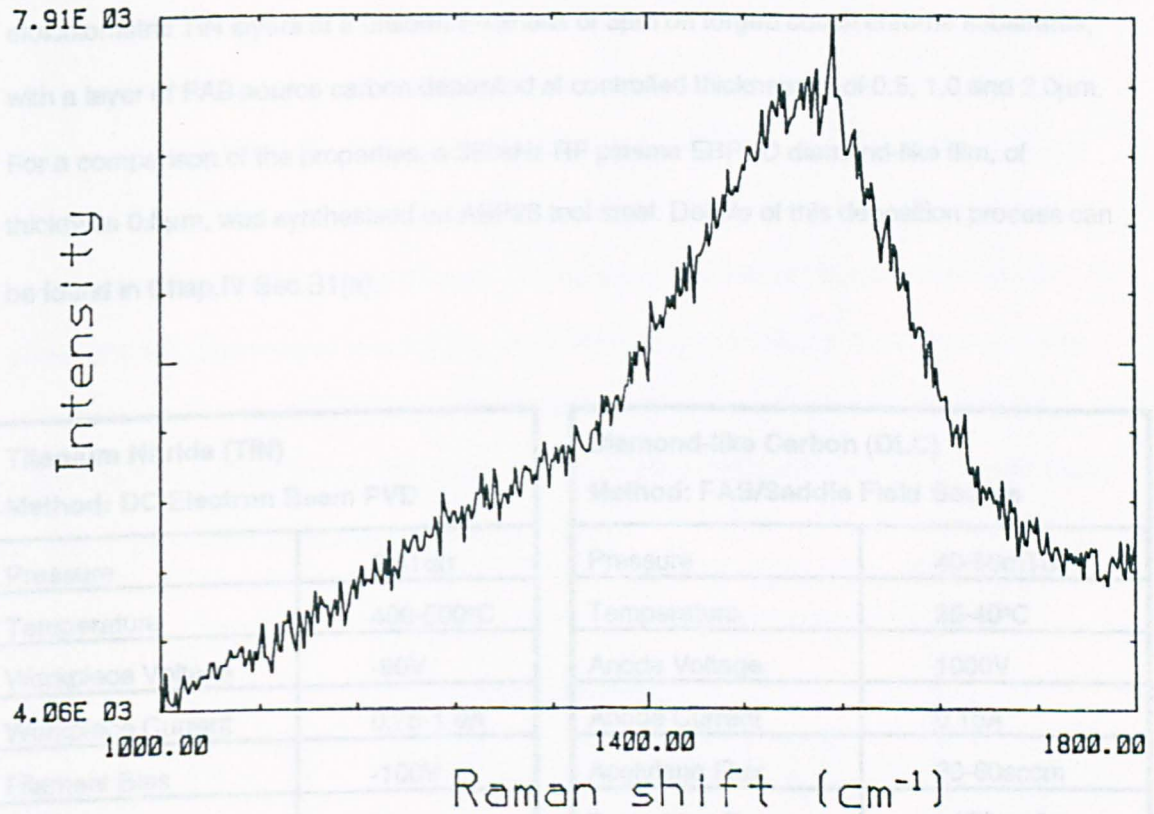


**Fig LXVI Raman Spectra for a FAB Source Film Deposited onto an Intermediate Layer of Titanium Nitride**

Surface Roughness	Ra (µm)
Co-Cr + Titanium Nitride	30.8
Co-Cr + Titanium Nitride	31.7
Co-Cr + TiN + DLC	35.0

**Table XI Surface Texture of Co-Cr + Chrome, FAB and TiN Specimens**

varying the thickness of the DLC film and the penetration depth, the effect of the underlying layer and its mechanical properties on the measurement of the hardness and elastic modulus could be investigated.

New samples were prepared for this study using similar deposition conditions to the previous tribological investigation. A DC plasma PVD method was used to synthesise near-stoichiometric TiN layers at a uniform thickness of 3 $\mu$ m on forged cobalt chrome substrates, with a layer of FAB source carbon deposited at controlled thicknesses of 0.5, 1.0 and 2.0 $\mu$ m. For a comparison of the properties, a 380kHz RF plasma EBPVD diamond-like film, of thickness 0.5 $\mu$ m, was synthesised on ASP23 tool steel. Details of this deposition process can be found in Chap.IV Sec.B1(a).

<b>Titanium Nitride (TiN)</b> Method: DC Electron Beam PVD		<b>Diamond-like Carbon (DLC)</b> Method: FAB/Saddle Field Source	
Pressure	5mTorr	Pressure	40-50mTorr
Temperature	400-500°C	Temperature	35-40°C
Workpiece Voltage	-90V	Anode Voltage	1000V
Workpiece Current	0.75-1.0A	Anode Current	0.15A
Filament Bias	-100V	Acetylene Flux	30-60sccm
Gun Voltage	7kV	Deposition Rate	<400 $\eta$ m/hr
Gun Current	300mA		
Deposition Rate	6 $\mu$ m/hr		

*Table X Deposition Details of FAB Source and TiN Intermediate Layers*

<b>Surface Roughness</b>	<b>Ra (<math>\eta</math>m)</b>
Cobalt-Chrome Substrate	20.8
Co-Cr + Titanium Nitride	34.7
Co-Cr + TiN + DLC	35.0

*Table XI Surface Texture of Cobalt-Chrome, FAB and TiN Specimens*

Nanoindentation was performed using a commercially available Nano Indentor II instrument to probe the properties of the uncoated cobalt-chrome substrate, the 3µm TiN layer and the three thicknesses of FAB source carbon. This indentation device utilises an electromagnetic coil to control the magnitude of the loads applied through the load train to a Berkovich type Ia diamond indenter and a capacitance gauge is used to measure the resultant penetration depth. A two dimensional array of indentation points were produced using an X-Y translatory stage upon which the specimens were supported during the experiment (Fig.LXVII). The instrument has been reported to possess a depth resolution of 0.2nm, a load resolution of 0.5µN and an X-Y positioning accuracy of 0.5µm<sup>219</sup>. During the test program indentation properties were determined at intervals of 25µm, for four linear arrays of five indents, using step loading to discrete maximum loads of 8, 21, 79 & 122mN consecutively. Due to previously reported problems with thermal and electronic drift, extremely high loading rates to maximum load<sup>220</sup> together with a dwell time at maximum load of 10sec. were adopted as the test protocol.

<b>Test Protocol</b>		
Loads:	8.0mN	(0.82g)
	21.0mN	(2.14g)
	79.0mN	(8.06g)
	122.0mN	(12.44g)
Loading rate:	1.85mN/sec	
Dwell Time:	10sec.	
Unloading from Max.:	16sec.	
Four arrays of five indents		
<b>Accuracy</b>		
Load Resolution:	0.5µN	
Depth Resolution:	0.2nm	
X-Y Positioning Accuracy:	0.5µm	

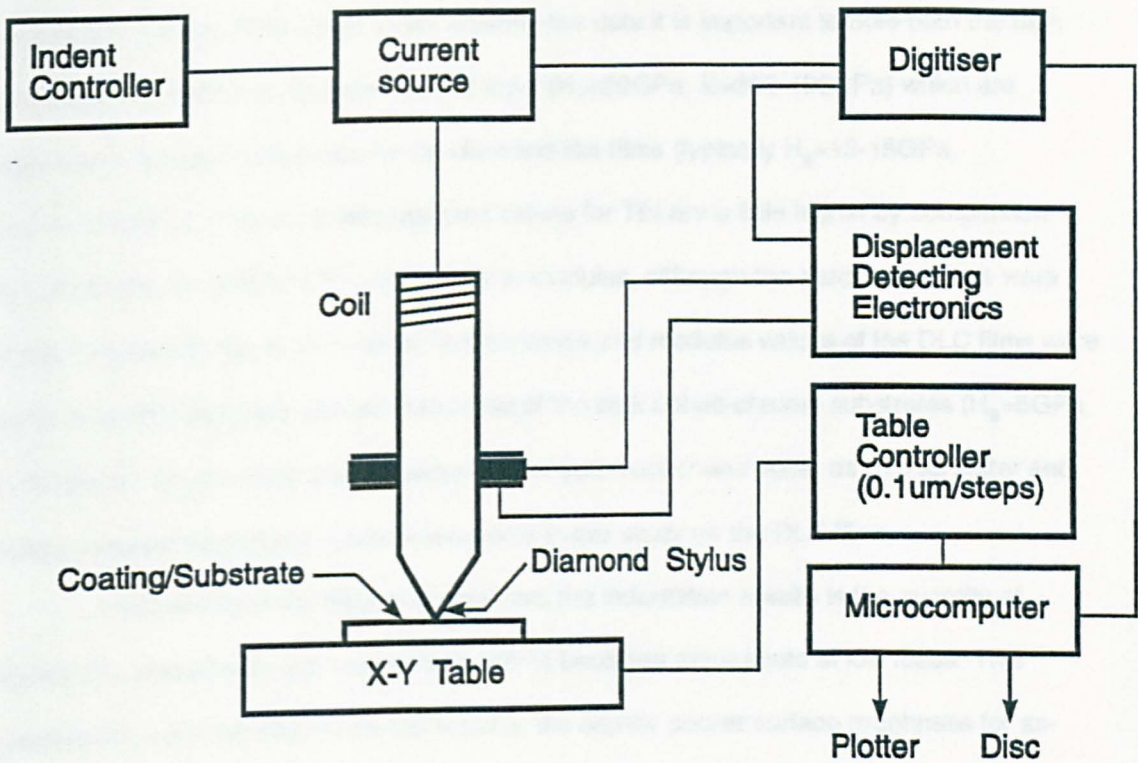


Fig LXVII A Schematic Representation Of The Nano Indentor II

### **c) Results**

The results of the nanoindentation experiment are presented in Table XII and graphically in Figs.LXVIII-LXXI. In considering the data it is important to note both the high hardness and elastic modulus of the TiN layer ( $H_B=20\text{GPa}$ ,  $E=300\text{-}400\text{GPa}$ ) which are significantly greater than those for the diamond-like films (typically  $H_B=13\text{-}15\text{GPa}$ ,  $E=200\text{-}250\text{GPa}$ ). The accepted published values for TiN are a little higher by comparison ( $H_B=22.5\text{GPa}$ ,  $E=590\text{GPa}$ )<sup>221</sup>, particularly in modulus, although the hardness values were within 12% of this figure. In contrast, the hardness and modulus values of the DLC films were found to be considerably greater than those of the bulk cobalt-chrome substrates ( $H_B=5\text{GPa}$ ,  $E=150\text{GPa}$ ). So one finds that consideration of both harder and stiffer as well as softer and more compliant underlying material are made in this study on the DLC films.

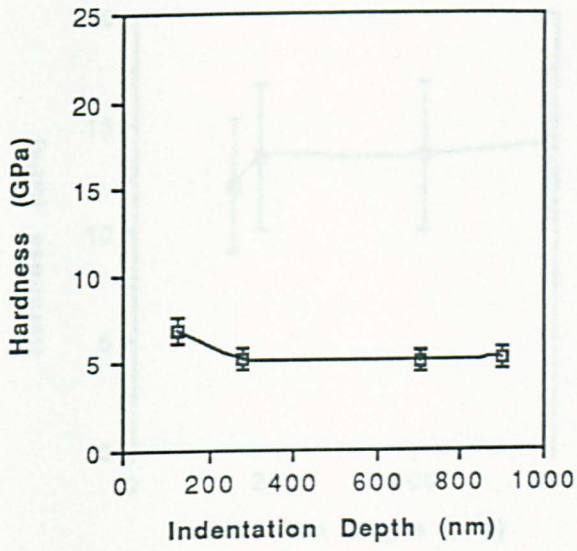
Another important feature to note from the indentation results is the quantity of scatter associated with each set of data, which becomes more acute at low loads. This phenomenon is suggested to be the result of the slightly poorer surface roughness for as-deposited DLC films (Table XI), contributing to the uncertain measurement of the elastic modulus and hardness. Typically, at the low indentation of 8mN, the resultant elastic plus plastic indentation depth was between 100 to 150nm. Previous research has emphasised limiting the surface texture of surfaces being tested in this way to  $R_a$  values of less than 20nm in order to reduce this amount of scatter<sup>222,223</sup>.

For higher indentation loads, the thinner of the DLC films begins to display a trend in hardness and modulus values which approaches that of the underlying material (i.e.TiN). For example, the 0.5µm DLC film exhibits a measured hardness of ~12GPa at 8mN load which increases to 14GPa for the highest load (122mN). This value remains significantly inferior to the measured TiN hardness value of 20GPa but significantly better than its hardness at low loads. A greater effect can be seen for the elastic modulus value. For the same DLC film (0.5µm), the modulus rises from 230GPa at shallow indentation depths of 130nm to 266GPa at depths of 590nm. At equivalent depths, the elastic modulus for TiN is approximately 280GPa and the value for the DLC represents 95% of this figure. Clearly, the elastic modulus of the TiN has a greater impact on the overlying DLC film than does its hardness.

Sample	Stepped Load (mN)	Nominal Indentation Depth ( $\eta$ m)	Hardness (GPa)	Variance	Elastic Modulus (GPa)	Variance
<b>Bare Co-Cr Substrate</b>	88.0	125	6.8	$\pm 0.8$	198	$\pm 15$
"	21.0	280	5.1	$\pm 0.06$	163	$\pm 5$
"	79.0	700	5.0	$\pm 0.09$	141	$\pm 3$
"	122.0	915	5.1	$\pm 0.05$	137	$\pm 5$
<b>Co-Cr + 3<math>\mu</math>mTiN</b>	88.0	103	19.7	$\pm 2.3$	447	$\pm 25$
"	21.0	155	18.4	$\pm 4.3$	340	$\pm 39$
"	79.0	350	20.0	$\pm 2.6$	302	$\pm 22$
"	122.0	450	20.0	$\pm 2.0$	294	$\pm 21$
<b>Co-Cr + 3.0<math>\mu</math>mTiN + 0.5<math>\mu</math>m DLC</b>	88.0	135	12.1	$\pm 0.9$	237	$\pm 9$
"	21.0	174	13.4	$\pm 1.7$	261	$\pm 24$
"	79.0	412	13.5	$\pm 1.1$	241	$\pm 13$
"	122.0	590	14.0	$\pm 3.6$	266	$\pm 43$
<b>Co-Cr + 3.0<math>\mu</math>mTiN + 1.0<math>\mu</math>m DLC</b>	88.0	150	10.7	$\pm 5.4$	172	$\pm 53$
"	21.0	197	14.8	$\pm 2.6$	203	$\pm 22$
"	79.0	440	13.4	$\pm 1.6$	187	$\pm 17$
"	122.0	555	14.8	$\pm 0.6$	188	$\pm 5$
<b>Co-Cr + 3.0<math>\mu</math>mTiN + 2.0<math>\mu</math>m DLC</b>	88.0	105	13.6	$\pm 3.4$	233	$\pm 36$
"	21.0	205	15.5	$\pm 2.3$	210	$\pm 24$
"	79.0	400	16.0	$\pm 2.0$	221	$\pm 20$
"	122.0	525	15.5	$\pm 1.9$	224	$\pm 20$
<b>ASP23 + 0.5<math>\mu</math>m DLC RF EBPVD</b>	88.0	118	12.7	$\pm 2.3$	168	$\pm 12$
"	21.0	206	12.7	$\pm 0.7$	175	$\pm 19$
"	79.0	525	8.5	$\pm 1.2$	204	$\pm 22$
"	122.0	684	8.9	$\pm 1.9$	200	$\pm 21$

**Table XII Penetration, Nanohardness, Elastic Modulus Results For Cobalt-Chrome, 3 $\mu$ m TiN Layer And 0.5,1.0 & 2.0 $\mu$ m Layers Of FAB Source DLC**

a) Forged Cobalt-Chrome Substrate



b) 3 $\mu$ m Thick Layer Of Titanium Nitride

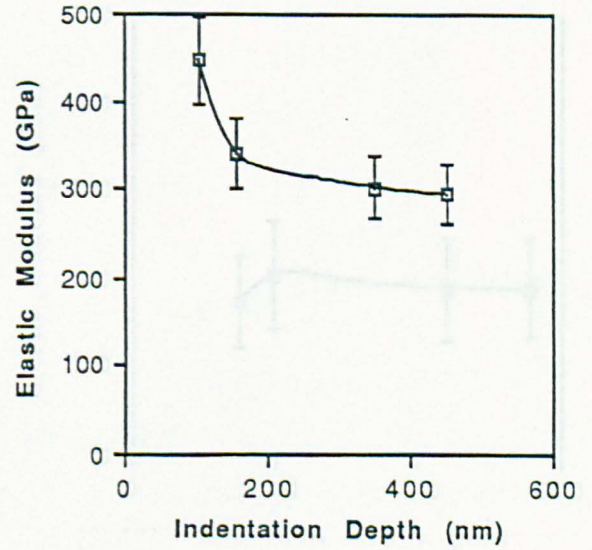
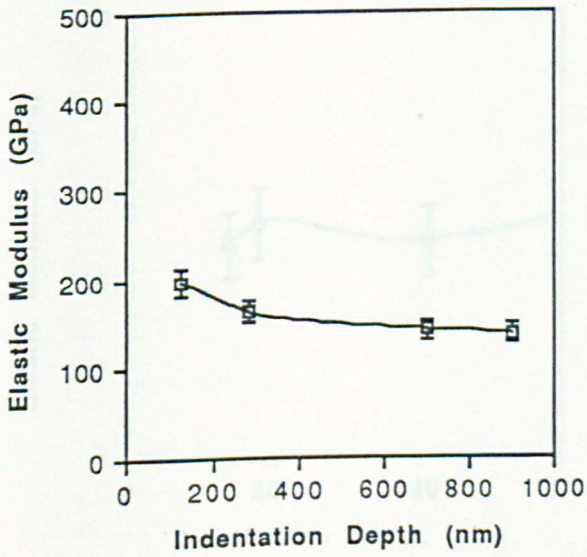
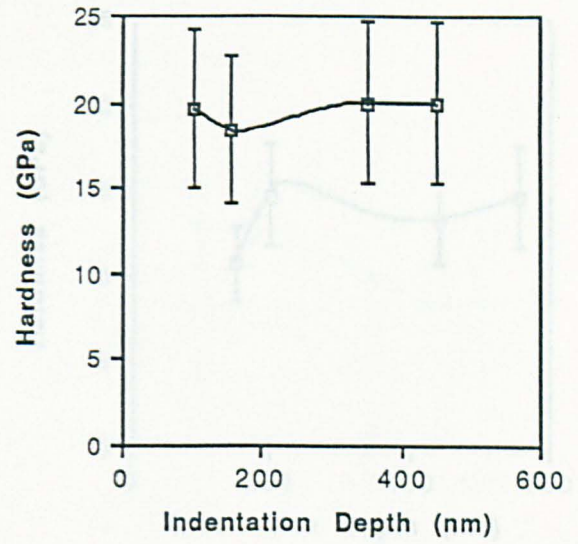


Fig LXVIII Nanohardness And Elastic Modulus versus Penetration Depth

a) 0.5 $\mu\text{m}$  DLC Film On 3 $\mu\text{m}$  Of Titanium Nitride      b) 1.0 $\mu\text{m}$  300kHz RF Plasma EDPVD  
 a) 0.5 $\mu\text{m}$  DLC Film On 3 $\mu\text{m}$  Of Titanium Nitride      b) 1.0 $\mu\text{m}$  DLC Film On 3 $\mu\text{m}$  Of Titanium Nitride

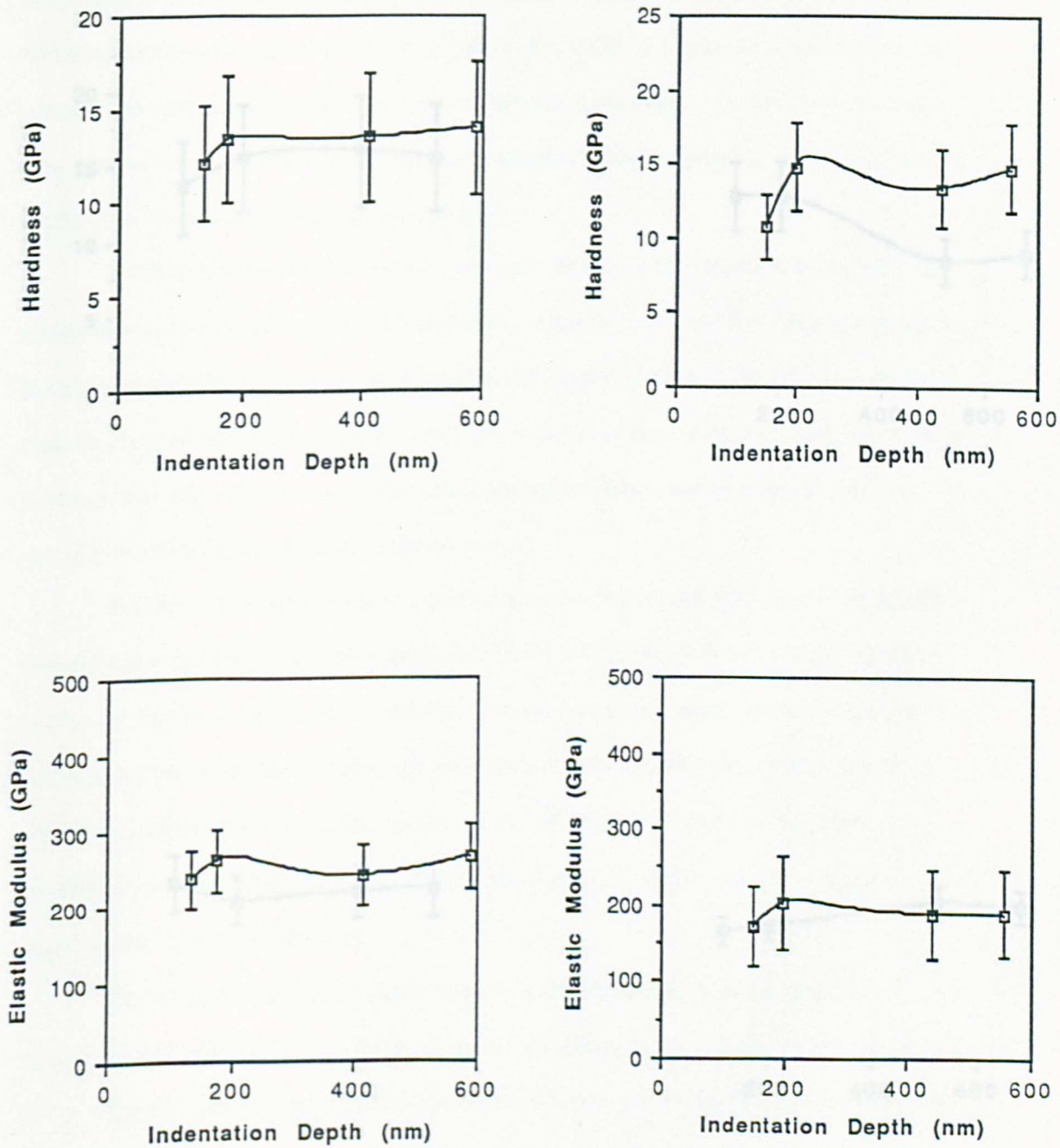
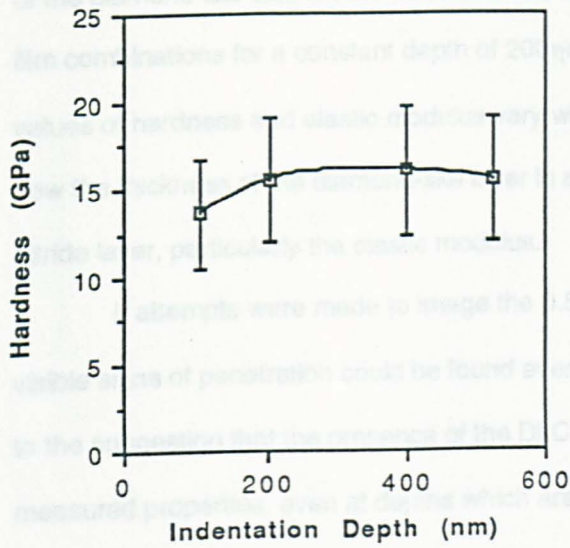


Fig LXIX Nanohardness And Elastic Modulus versus Penetration Depth

a) 2.0 $\mu\text{m}$  DLC Film On 3 $\mu\text{m}$  Of Titanium Nitride



b) 0.5 $\mu\text{m}$  380kHz RF Plasma EBPVD DLC Film On ASP23 Tool Steel

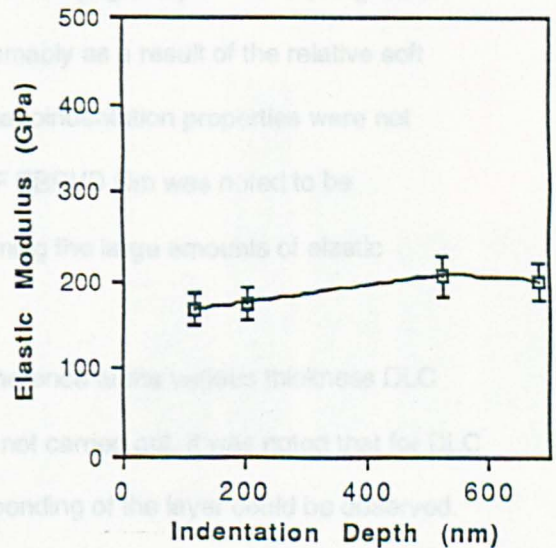
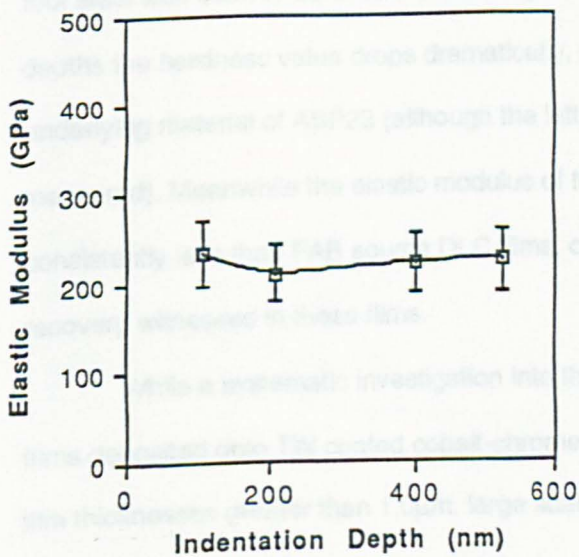
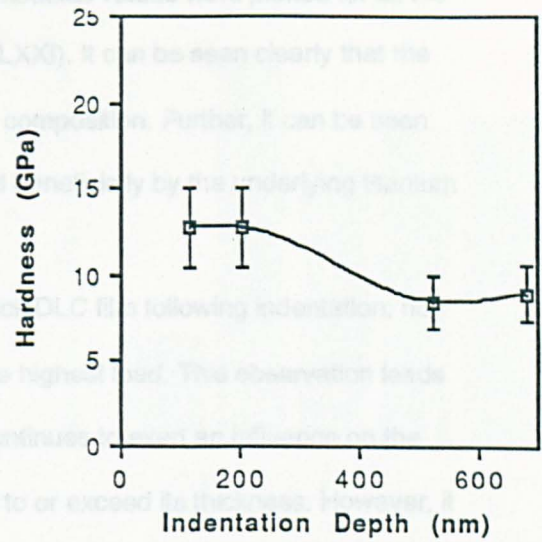


Fig LXX Nanohardness And Elastic Modulus versus Penetration Depth

In order to elucidate further the interaction of the underlying TiN film on the properties of the diamond-like carbon, the hardness and elastic modulus values were plotted for all the film combinations for a constant depth of 200nm (Fig.LXXI). It can be seen clearly that the values of hardness and elastic modulus vary with film composition. Further, it can be seen how the thickness of the diamond-like layer is affected beneficially by the underlying titanium nitride layer, particularly the elastic modulus.

If attempts were made to image the 0.5µm thick DLC film following indentation, no visible signs of penetration could be found even for the highest load. This observation leads to the suggestion that the presence of the DLC film continues to exert an influence on the measured properties, even at depths which are equal to or exceed its thickness. However, it is known that these films demonstrate extreme levels of elastic recovery which could be masking the true extent of the surface penetration.

For the shallowest indents, the hardness of the 380kHz RF EBPVD film on ASP23 tool steel was seen to be similar to the 0.5µm DLC on TiN (Fig.LXX). However, at greater depths the hardness value drops dramatically, presumably as a result of the relative soft underlying material of ASP23 (although the latter's nanoindentation properties were not measured). Meanwhile the elastic modulus of the RF EBPVD film was noted to be consistently less than FAB source DLC films, confirming the large amounts of elastic recovery witnessed in these films.

While a systematic investigation into the adherence of the various thickness DLC films deposited onto TiN coated cobalt-chrome was not carried out, it was noted that for DLC film thicknesses greater than 1.0µm, large scale debonding of the layer could be observed. Conversely, the 0.5µm DLC film showed essentially no tendency to detach spontaneously from the same substrate. It was assumed that this was the result of intrinsic residual stress as the film thickness increased until the adhesion or fracture strain of the DLC films was exceeded.

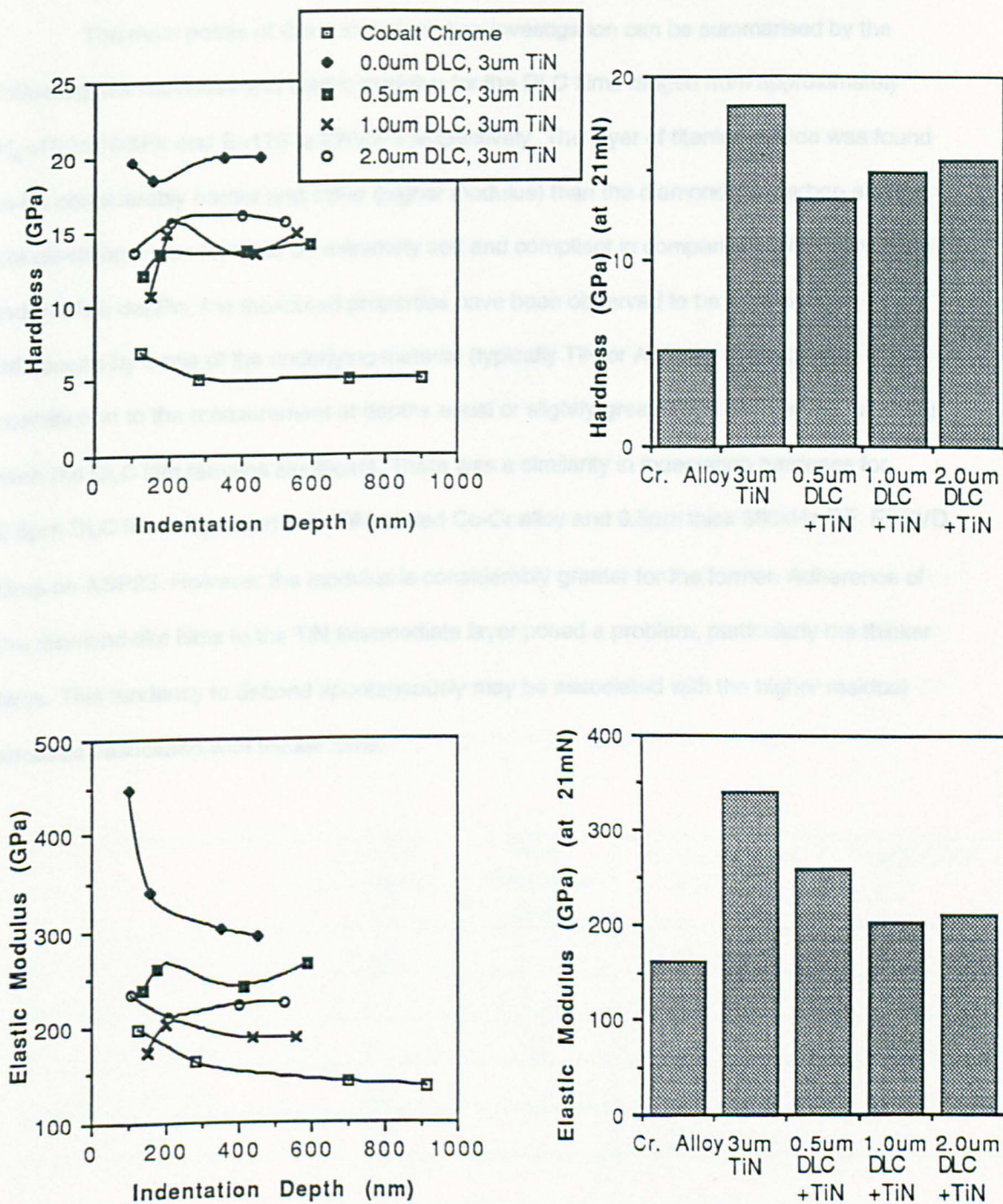


**Fig LXXI** Nanohardness And Elastic Modulus versus Penetration Depth For The Cobalt-Chrome Substrate, 3 $\mu$ m TiN Layer And 0.5, 1.0 & 2.0 $\mu$ m Layers Of FAB source DLC

#### ***d) Conclusions***

The main points of this nanoindentation investigation can be summarised by the following; the hardness and elastic modulus for the DLC films ranged from approximately  $H_b=10$  to  $15\text{GPa}$  and  $E=175$  to  $270\text{GPa}$  respectively. The layer of titanium nitride was found to be considerably harder and stiffer (higher modulus) than the diamond-like carbon and the cobalt-chrome was found to be extremely soft and compliant in comparison. With increasing indentation depths, the measured properties have been observed to be increasingly influenced by those of the underlying material (typically TiN or ASP23), although the contribution to the measurement at depths equal or slightly greater than the coating thickness from the DLC film remains significant. There was a similarity in indentation hardness for  $0.5\mu\text{m}$  DLC films deposited onto TiN coated Co-Cr alloy and  $0.5\mu\text{m}$  thick  $380\text{kHz}$  RF EBPVD films on ASP23. However the modulus is considerably greater for the former. Adherence of the diamond-like films to the TiN intermediate layer posed a problem, particularly the thicker films. This tendency to debond spontaneously may be associated with the higher residual stresses associated with thicker films.

## V. DISCUSSION & CONCLUSIONS

### a) *Recent Research*

The most recent activity has focused on reproducing films with an intermediate layer of titanium nitride and subjecting them to tribological wear tests to evaluate further the favourable deposition conditions. The films used were synthesised in the same conditions to those presented in Chapter IV, except in this particular study the thickness and surface finish were slightly different. A 0.7 $\mu\text{m}$  layer of FAB source DLC was coated onto a slightly thinner layer of titanium nitride than used in previous investigation (2.5 $\mu\text{m}$  cf. 3.0 $\mu\text{m}$ ). In addition, two thicknesses of FAB source DLC were deposited (thin - 0.2 $\mu\text{m}$ , thick - 1.4 $\mu\text{m}$ ) onto cobalt-chrome substrates and all of the films were tested by the pin on disc sliding wear test method. Microhardness indentation tests were carried out prior to the wear tests and revealed the layers to have the values given in the Table XIII. In the case of the FAB source DLC films varying amounts of elastic recovery were again witnessed and although the coating adhesion appeared to be good, films produced at thicknesses greater than 2 $\mu\text{m}$  showed areas of large scale debonding. Details of the sample arrangement and designations are given below:-

Sample	Surface Roughness ( $R_a$ )	Film Thickness ( $\mu\text{m}$ )	Microhardness ( $\text{Kg/mm}^2$ )	Designation
Cobalt-Chrome substrate	40-50	---	500 (25g)	---
Titanium Nitride Int. Layer	47	2.5	1300 (15g)	---
FAB source DLC film	51	0.2	1800 (25g)	Hu (thin)
FAB source DLC film	100	1.4	2500 (50g)	Hu (thick)
FAB source DLC/TiN	54	0.7	2000 (15g)	HuTiN

*Table XIII Surface Roughness, Thickness and Microhardness of FAB Source DLC and Titanium Nitride Intermediate Layers*

Details of the wear tests are given on the test protocol included in Appendix IV. However to summarise the results; the DLC carbon films deposited onto cobalt-chrome without the aid of an intermediate layer of TiN showed excellent wear resistance and friction ( $W_f = 3.9 \times 10^{-6} \text{mm}^3/\text{Nm}$ ,  $W_b = 0.3-0.8 \times 10^{-6} \text{mm}^3/\text{Nm}$ ,  $\mu = 0.15-0.17$ ). Indeed, for the two films tested (thin - 0.2 $\mu\text{m}$ , thick - 1.4 $\mu\text{m}$ ) the performance was superior to any FAB source DLC

films previously deposited directly onto metallic substrates. The thinner of the DLC films showed signs of localised failure of the film wear track after sliding a distance of 100metres at a 10N loading (Appendix IV, Fig.LXXIIa). The thicker films (1.4 $\mu$ m), although displaying a slight increase in wear, showed no signs of cohesive failure after the wear test (Appendix IV, Fig.LXXIIIa). Profilometry confirmed the volumetric wear rate of the thicker film was greater than that of the thinner film and this was highlighted by a maximum wear track depth of 0.3 $\mu$ m cf. 0.09 $\mu$ m for the 0.2 $\mu$ m thick DLC film. The coefficients of friction for both films were comparable, with a low steady state value of between  $\mu=0.15-0.17$ .

Samples	Wear		Friction	
	Pin (mm <sup>3</sup> /Nmx10 <sup>-6</sup> )	Film (mm <sup>3</sup> /Nmx10 <sup>-6</sup> )	initial	steady state
Hu (thin)	0.3	2.7	0.22	0.15
Hu (thick)	0.8	8.6	0.20	0.17
HuTiN	0.4	9.4	~0.3	~0.2-0.5

*Table XIV Wear & Friction Results of FAB Source and FAB Source Interlayered Films*

Tribological tests of the titanium nitride interlayered 0.7 $\mu$ m thick DLC film (Appendix.IV, Fig.LXXIVa) revealed this composite layer to have surprisingly poor wear properties in comparison to the other two coatings without the intermediate layer and in complete contrast to the performance of the previously TiN interlayered films. It was obvious from the photomicroscopy and profilometry results that complete failure of the film had occurred shortly after the start of the tests and appeared to be the result of adhesive failure at the film/interlayer interface. Efforts to vary the thickness of the TiN and the deposition conditions of the DLC failed to have any beneficial effect on this poor performance. The friction coefficient remained low for the duration of the test showing an initial value of  $\mu=0.3$ , leading to a considerably variable steady state value of between  $\mu=0.2-0.5$  during film failure. This tribological phenomenon was observed to occur for further multilayered films tested in the same way with none showing the low friction and extreme wear resistant properties of the previously tested TiN interlayered DLC films. After studying this TiN interlayered DLC film

more closely, it was concluded that the quality of the titanium nitride was different in both cases. For the tribological examination just reported, every effort was made to deposit layers of TiN with the characteristic golden appearance indicative of near stoichiometric composition. Films with compositions and appearances similar to this are used widely in commercial applications. However, closer examination of the original low friction, wear resistant film revealed the TiN composition to be far from stoichiometric, with an appearance resembling a rough, dull green/brown. This type of TiN is known to be the result from an abundance of nitrogen in the film and is caused by a relatively high nitrogen to titanium ratio in the plasma. This can be the result of a high N<sub>2</sub> gas flux or a low electron beam power and the resulting films are generally considered worthless in a commercial sense.

It was therefore concluded that the wear tests ought to be made comparable, in light of this discovery, by reproducing DLC coated samples with this second type of TiN so as to resemble more closely the film composition used in the initial experiment. A second set of films were produced with non-stoichiometric, nitrogen rich titanium nitride as the intermediate layer. The results of the tribological tests showed this new composite film to be as wear resistant as the original film, with little or no track wear as determined by profilometry (Appendix IV, Fig.LXXVa). However, the counterface pin material underwent relatively severe wear during the same test and some of this material was transferred from the pin to the wear track.

From visual examination of the sample, it appeared that the surface was dull and rough in appearance, leading to the conclusion that this surface roughness was the cause of the high level of pin wear. However, after studying the texture of the film with profilometry it became apparent that the roughness average was superior to any of the other films tested ( $R_a=30\eta\text{m}$  cf.  $50\eta\text{m}$ ), and that the appearance was due to the DLC layer optically transmitting the dark layer of titanium nitride beneath.

A small region (~1mm wide) of TiN, masked during the deposition of DLC was exposed to the same sliding wear regime as the rest of the DLC/TiN coating. After the test, photomicroscopy of this region revealed an extremely heavy transfer of counterface material in this region in comparison to the worn track coated with DLC (Appendix IV, Fig.LXXVb).

This behaviour was indicative of a comparatively heavy adhesive contact between the SAE 52100 material worn on titanium nitride and serves to highlight the improvement in this contact condition when coated with a hard layer of carbon.

The causes behind such a radically different tribological behaviour, were thought to be fundamentally the result of the greater adhesive strength between FAB source DLC and non-stoichiometric TiN than FAB source DLC to stoichiometric TiN used previously. This was deemed the probable cause since the contribution to the load support, as a result of the hard intermediate layer beneath, was clearly similar in both cases. Besides, nanoindentation tests performed indicated little evidence to the support the idea that the DLC was significantly structurally enhanced by the presence of a layer of TiN beneath its surface. This lack of effect may be characteristic of the fact that TiN itself was unable to resist sufficiently the deformation of the relative soft substrate. It was noted previously that adhesion of the DLC films to metal substrates and TiN films was poor when deposited in layers thicker than 2-3 $\mu$ m due, it was thought, to the high levels of intrinsic stress in the film overcoming the adhesive strength at this thickness. Although the levels of stress were not ascertained for FAB source DLC films, it seems more likely that a large contribution to the problem lay in poor adhesion rather than high stress since these films contained low amounts of bonded hydrogen and in most cases could be lifted off the substrate by the light application of a coin. These observations was further backed up by the apparent failure mode of the DLC/TiN(stoichiometric) films during sliding wear tests which appears to be caused by the delamination of the film from the substrate at the interface, leaving a stepped wear track profile (Appendix IV, Fig. LXXIVa) rather than cohesive failure or gradual wearing of the surface.

The structure of nitrogen rich TiN was suspected to be highly columnar in nature which led to one of the two possible theories behind the mechanism of enhancement adhesion as a result of this intermediate layer. Clearly, adhesion can be improved by various processes including mechanical keying, chemical bonding and restructuring, diffusion or atomic/electrostatic attraction. The latter two possibilities can be ruled out because of the low temperature of deposition involved in both deposition processes and the electrically

conducting nature of most of the composite film. It therefore leaves two possibilities to be considered. Mechanical keying of the DLC into the undulations and pores present on the TiN surface seems to be probable especially when one considers that the compositional difference between the two TiN films was thought to lead to a corresponding change in the film structure into a columnar habit. Such a structure would provide many sites for penetration and interlacing of the deposited DLC film into the fissures between the columnar growths. This theory assumes that the surface to be coated would be either relatively rough, due to polishing defects of columnar film growth, or have sufficient defects on the surface which could be accessed by the depositing film. The evidence suggests the contrary; that is the surface of the TiN before deposition with DLC is extremely smooth ( $R_a=30\text{nm}$ ) and pin hole free reducing the probability that mechanical keying could have been the significant factor in the increase in adhesion between the two surfaces.

There remains the possibility that some chemical interaction between the surfaces may have occurred. Certainly, with carbon being the dominant specie in the DLC film and titanium and nitrogen the principle components of the TiN, the range of possibilities for chemical interaction are limited. The most likely formation therefore is a TiC sublayer being formed at the interface between the titanium nitride and DLC layers. Such a strong link would explain the increase in adhesion strength and ultimately the superior tribological performance. During scratch testing, the critical load of  $F_c \sim 50\text{N}$  can be measured for TiN films on steel substrates, demonstrating the high level of adhesive strength probably as a result of a combination of implantation and diffusion processes. DLC films typically have a critical load to failure in the region of  $F_c=1.5\text{-}3.0\text{N}$  (Chap.IV Sec.B1(b)) which is clearly far inferior to that of the TiN. This large discrepancy between the level of energy needed to debond the layers indicates that, during shearing or deformation processes, the most likely point of failure of the composite layer is liable to be at the DLC/TiN interface rather than the TiN/substrate region. Any improvements in the adhesion strength at this interface by the formation of a TiC sublayer would certainly be of benefit.

To test this theory in practice, micro-adhesion tests (using a nanoindenter) on this composite layer would have to be performed to confirm this improved adhesive strength over DLC films deposited onto bare metal substrates and to assess more closely the region and modes of failure. Such tests have not been carried out to this point in time but remain the next point of study. To corroborate this the work on the existence of a sublayer of TiC, the use of analytical techniques such as GDOS (Glow Discharge Optical Spectroscopy) could be used for assessing the composition of the films. If sampling is performed in conjunction with ion milling techniques, compositional depth profiles could be obtained which could determine whether there is a graded transition layer or a clearly defined junction between the DLC/TiN and TiN/substrate interfaces and its composition. This would help to indicate the type of interface, whether it be a relative thick diffusion layer, a well defined mechanically keyed interface or a graded TiC bonded sublayer.

#### ***b) Review of Tribology***

Attempts at doping carbon films were initially the result of encouraging tribological results reported in the literature for films doped with ruthenium, tantalum and tungsten. Research showed that both the levels of doping, the type of metal used and the environmental conditions under which they were tested were highly critical parameters but an increase in film wear resistance and an insensitivity to tribological changes with humidity conditions could be achieved. Therefore duplicate experiments were performed using dopants such as tungsten, titanium diboride and boron nitride, the results of which revealed a less startling improvement in wear resistance and in most cases a deterioration in the friction coefficient over those films which were undoped by the same technique. It appeared that numerous particulates deposited during the evaporation of the graphite and the dopant material, created a rough surface texture which greatly increased the rate and variability of the counterface wear. This made it difficult to interpret the film wear more accurately since clearly all the films had undergone sliding under different Hertzian contact conditions throughout the test. Hydrogenation of the plasma during film growth proved the key to achieving much improved wear and friction performances over inert plasma or evaporated graphite deposition with the difference in doping or undoped films being slight. With only a

moderate effect on the wear resistance and with the corresponding decrease in friction coefficient, it was concluded that the benefit of doping carbon films compared to using hydrogen in the deposition stage, was minimal. Furthermore the additional deposition costs and problems associated with cross contamination of the dopants between depositions made this approach to achieving consistent hard and wear resistant layers of carbon at sufficient rates impractical. It appeared that the only clear advantage of using metallic dopants in any of the films was to improve the temperature at which thermal degradation of the film occurred.

Despite these disappointing indications from the metallic dopants, doping with silicon continues to be reported in the scientific literature in connection with wear resistance of DLC films. Improvements to sliding wear by an order of magnitude and a simultaneous reduction in sensitivity to humidity changes have also been cited<sup>94</sup>. In recent tests on commercially available coatings, varying degrees of silicon contamination have been recorded by EDX techniques although it remains uncertain whether its presence is intentional or unintentional (e.g. due to back streaming of diffusion pump vapours). It must be assumed that the effect of silicon impurities must differ considerably to that of metallic elements because of the large discrepancy in performance. This could be due to the relatively large difference in the molecular size between silicon and metals like tungsten which allows the silicon to be incorporated within the a-C:H lattice without causing undue structural mismatch. Or it may be that chemically the silicon can be bonded more readily within the carbon film and with stronger bonds; although evidence of the extent and type of bonding occurring during doping is lacking.

What was demonstrated more fully by these doping experiments was the improvement in film properties and deposition performance as a result of the use of a hydrocarbon precursor in the plasma instead of an inert gas such as argon. It had been established by the evaporation of graphite into an inert plasma that ionisation of this species had improved the structural properties over that of unmodified evaporated graphite. However, tribological tests had shown that the performance of these films were only marginally better than that for SAE 52100 tool steel sliding on ASP23. Careful examination of the wear mechanisms uncovered no obvious explanation although it is assumed that the relatively

large amounts of wear debris had acted as third bodies which accelerated the rate of wear of the film. The relatively poor microhardness results also indicated that the ability of these films to resist this abrasive wear were somewhat limited. The use of a hydrocarbon precursor during the deposition stage to form a-C:H films improved the tribological behaviour considerably, with the wear resistance improving by a factor of two.

There was therefore strong evidence to suggest that the presence of hydrogen at the synthesis stage could greatly improve the physical properties of the film and that although in most cases the amount of hydrogen in the film remained low, it helped to contribute to a low frictional value. A similar observation has been made by Dimigen et al<sup>137</sup>, who studied hydrogenated amorphous carbon films up to annealing temperatures of 550°C and observed a rise in friction as a result of the loss of hydrogen.

Tribological testing of thermionically assisted DC EBPVD and low frequency 380kHz RF films was problematic due to the lack of deposition on tool steel in any conditions other than butane RF plasma EBPVD. These films were found to have only moderate tribological properties both in film wear resistance and frictional performance. Alternatively FAB source films deposited under 'normal' conditions produced films of high hardness although a variation was often detected. This behaviour has not been satisfactorily solved since the variation appears to concern the inhomogeneous coating of the graphite source with DLC rather than any intrinsic parameter, compounded by a variable apparent hardness due to an increase in elasticity of the film. This variability in properties resulted in two categories of films; those which were relatively soft and failed prematurely during pin on disc testing to give a volumetric wear only slightly improved over that of the 'standard', although the friction continued to remain low. The second category of FAB source films displayed extremely high hardness values and exhibited a wear resistance superior to any of the other films not enhanced by an interlayer. Studies showed that this was due to a reduction in abrasive damage, subjected to the film by the pin material, whilst protecting the underlying metallic substrate from achieving heavy adhesive contact with the counterface even when the majority of the film had been removed. EDX analysis using dotmapping techniques revealed the existence of a transferred layer of carbon on the surface of the pin so that ultimately, the

shear zone resided in an area between two layers of carbon at the interface. During environmental controlled wear testing, it became obvious that the different behaviour between tests performed in an inert dry nitrogen atmosphere and that performed in a dry oxidising atmosphere, was attributable to the performance of this transferred carbon layer. Inert atmospheres appeared to maintain and even encourage the formation of this layer, thus achieving similar wear and friction performances to samples tested under ambient conditions. Whenever oxygen was admitted into the test chamber, the complete loss of this transferred carbon layer was witnessed, leading to a rapid deterioration in friction coefficient. The exact mechanism by which the carbon was lost is unclear although it is known that under the high flash temperatures and varying local humidity conditions caused by the micro-contact conditions, the oxygen can react with the carbon to ultimately form products of reaction such as CO and CO<sub>2</sub>. In such a way, the thin transferred layer of carbon could be removed from the counterface and shearing between the surfaces became more severe.

**c) *Pin on disc***

Many points have been highlighted during this study concerning areas of improvement in test preparation, operation and interpretation of results. The most fundamental problem associated with wear testing using the pin on disc arrangement is that as the pin undergoes wear during the test, the contact area increases and the Hertzian pressure drops. Since the cross section of the pin is non-uniform and the volumetric wear rate of the pin has been shown to be approximately constant, then the area of the wear scar increases at an exponential rate for the first few metres of sliding. Therefore the Hertzian pressure decreases rapidly at the beginning of the test. Results have shown that this drop in pressure can be greater than 50% within the first 10 metres sliding distance for SAE 52100 pin material on FAB source DLC films under VAMAS conditions. This behaviour implies two things; firstly prolonged sliding distances create a situation increasingly less representative of the original condition and are therefore unnecessary, and secondly the factors affecting the rate of counterface wear such as surface roughness, contact load and material deformation become increasingly important if variability in this situation is to be minimised.

The obvious proposal would be to introduce a harder counterface material such as  $\text{Al}_2\text{O}_3$  to reduce the rate of wear and thereby maintain the Hertzian contact conditions for longer. However such a material would be expensive especially for routine testing and in addition, apart from the contact pressure requirement there is also a material requirement. Simulation of real applications under test environments requires matching conditions which often demands metallic counterfaces. A pin material with a constant cross section has been attempted before although the problems associated with alignment are often critical in ensuring even contact pressure. It seems therefore inevitable that no ideal material or geometry exists for the use as a counterface for hard coatings, such as diamond-like carbon, since all materials will wear to a degree and that more importantly, the criteria is often the choice of pin material.

Experiments have shown that large differences in the mode of sliding can occur for materials of the same nominal composition. In the case of M50 and SAE 52100 pins tested against ASP23 tool steel disc material, the M50 produced a typical well defined wear track profile normally associated with pin on disc testing. However, SAE 52100 material resulted in very heavy adhesive shearing of the surfaces so that the disc material achieved a net transfer of material from the pin leading to what could be described as negative wear. VAMAS specifications call for a pin material made of carbon-chrome although clearly from this experimental demonstration, a more exacting composition and grade needs to be specified.

Another problem connected to the configuration of the test machine is the problem of achieving near representative conditions between tracks of differing radii on the same sample. It is clear that in order to maintain constant linear speed between different tracks the rotational speed must be increased as the track radii reduces. This however, increases the parameter of rotational frequency or number of wear passes, which in some wear situations could be more important than the sliding distance. For a material which would be sensitive to such a fatigue related parameter as rotational frequency, one would expect an increase in volumetric wear to result as the track radii decreased. However for the experiments performed in this study on titanium nitride at different track radii the opposite effect was noticed i.e. a reduction in wear with reduced track radii. When one considers that the

volumetric wear is calculated from the circumferential distance multiplied by the wear profile cross section as determined by profilometry. Then two tracks of differing radii should have the same volumetric wear for similar sliding conditions so that the increase in wear track cross sectional area for the smaller track must equal the loss in volume due to the shortening of the circumference. However, in practice the increase in cross sectional area is within the error of profilometry measurement itself and therefore the volumetric wear is dominated by the circumferential measurement. In the light of this, it is not surprising that such a sensitive effect as fatigue accelerated wear is not discerned by such a technique involving different track radii. Indeed, the results showed that the track volumetric wear had a strong correlation with sliding distance and increased track radius. For the above reasons, experiments performed during this study, only one common track radius was used to judge and compare data between samples.

Interpretation of pin on disc results relies heavily upon accurate measurement of the wear volumes and friction force involved. Measurement of the pin and track volume more specifically, uses techniques which require a degree of subjectivity and assumption. For instance, the pin wear volume can be calculated reasonably accurately by optical measurement of the wear scar diameter and assuming that the scar is flat. In practice the wear scar is not flat but the variation from this is so small that the error is estimated to be only  $\pm 7\%$  vol. The volume of the wear track moreover, requires the accurate measurement of both the cross sectional wear volume using profilometry and the optical measurement of the track radius. For more wear resistant combinations the wear volume of the track became indistinguishable from the surface topography so that accurate measurement and determination of the cross section is impossible. At the beginning of this study such low volumetric wear presented no problems since most of the carbon coatings produced at the time exhibited wear which was readily measurable by profilometry. But the wear resistance of films, particularly FAB source deposited films and those deposited with a titanium nitride interlayer, made measurement difficult. The obvious solution to this problem would be to increase the load or sliding distance until distinguishable wear was determined on the test specimen but there lies a problem in accurate comparison of wear data between these

different conditions. However, for reasons outlined on the discussion of Hertzian pressure, an increase in the sliding distance would be inappropriate whilst an increase in load by the same amount would not necessarily increase the volume by the same factor. Higher loads involve more heat dissipation at the wear junction and for any conditions where a threshold in energy is required to initiate some form of endothermic tribo-chemically reaction, could lead to an increase in the wear mechanism. For this reason, although the data is presented in units of  $\text{mm}^3/\text{Nm}$ , this does not mean that it can be directly compared to volumetric wear rates performed at different loads or sliding distance.

#### ***d) Process Control***

Many processes have been addressed in this study and their variety assists in demonstrating the many different coating variants which can be produced. However, from a mechanical and tribological properties point of view, the most impressive films have been the Fast Atom Beam and the low frequency 380kHz RF EBPVD films, which have shown considerable improvements over the initial attempts to directly deposit graphite. There has been a general trend towards improved mechanical and structural properties, which can be broadly attributed to two phenomenon. Firstly the introduction of plasma assistance to provide a controlled mechanism for disassociation and acceleration of the arriving species and secondly the use of hydrogen as one of the mediums by which the synthesis of the films can be controlled. Another factor which greatly influences the nucleation and growth and which is not one of the deposition parameters, is the choice of substrate and its preparation. Indeed the growth characteristics of radio frequency EBPVD DLC films on a glass substrate showed a rate of synthesis markedly different to that on metal, although the film properties remain apparently similar. Failure to provide adequate or thorough substrate preparation often affected considerably the stress and adhesion between coatings produced from the same deposition method, in the same conditions.

If one considers again the range of films produced; from evaporated graphite through to DC plasma evaporation, thermionically assisted DC EBPVD, low frequency RF EBPVD and Fast Atom Beam and simultaneously consider the range of material properties detailed in the experimental section, it becomes clear that firstly the introduction and then the refinement

of plasma processing techniques has gradually led to superior films. The process of ion assistance has been shown initially to alter significantly the densification and structure of the films over that of simple evaporation. Techniques utilising ionisation enhancement methods such as thermionic assistance or higher frequency plasmas to increase the ionisation efficiency during deposition, have provided further improvements by increasing the number of ionised species with better defined ranges of energies. This improvement in processing technique has generally led to a corresponding improved bonding configuration, higher deposition rates, better processing control and the inclusion of less impurities such as argon and hydrogen. The FAB source ionised species were generated at a graphite anode where the use of the saddle field phenomenon allows greater control over the emitted electrons. This increases the time of flight of the electrons within the source and increases the probability of ionisation thereby improving the efficiency. Levels of ion activity were so high that unless low rates of hydrocarbon flux were used (<100sccm), the excessive energy of the species would cause arcing at the beam aperture. In the case of low frequency RF plasma deposited films, ionisation intensities were achieved at such a level that attempts to enhance the plasma with electron emission from a biased filament caused rapid breakdown of the plasma into arcing. The use of 13.56MHz or 2.45GHz microwave devices for producing more active plasmas would continue to increase this level of ionisation and disassociation of the precursors facilitating the use of lower bias voltages, although the use of such techniques is limited to non-conducting substrates and matching networks are required.

From a commercial or scaling-up point of view, the deposition methods vary considerably, with each method suffering from various physical or performance limitations. The FAB source technique, while producing films of good quality at very stable operating conditions, has extremely low deposition rates, is limited to 'in line of sight' coverage (and therefore to substrates of simple geometry) and has a deposition coverage which reduces considerably as the point of deposition moves further from the central axis of the beam. The two crucially important advantages in using such a technique however, lie in its ability to coat in relative poor vacuum conditions and because of its low deposition temperature (30-50°C) allows coating of plastics and polymers to be performed without structural damage or

distortion.

Plasma techniques such as radio frequency 380kHz EBPVD, provide extensive and even coverage over objects of difficult geometry although the uniform coating of deep re-entrant holes remains a problem. Plasma techniques generally enable higher rates of deposition, provide greater adhesion due to a mixture of interfacial diffusion and implantation, although in turn they require higher deposition temperatures and lower vacuum conditions.

The lower ionisation efficiency and poor disassociation of even the thermionically enhanced DC deposited films produced largely soft, sometimes polymeric films with high impurity content. Without the aid of thermionic assistance it is doubted whether films other than soft graphitic type films could be produced without recourse to doping the film with metallic species.

#### ***e) The Role of Hydrogen***

The presence of hydrogen has been seen to affect the films performance in three ways. Firstly during the processing stage where the presence of hydrogen has been demonstrated to be beneficial in achieving structures containing a high degree of  $sp^3$  bonded carbon. Current theory also suggests that the atomic hydrogen in high percentages leads to either passivation of the surface from graphitic growth or actively etches the graphite  $sp^2$  structures as they form. Either way, it is supposed that the hydrogen suppresses the growth of graphite in relation to the more desirable and stronger  $sp^3$  bonded diamond-like structures.

A second way in which the hydrogen can influence the mechanical and optical properties of the film is if, after the deposition stage, hydrogen remains captive in the film in a bonded form. Such a level of bonded hydrogen as detected by FTIR, can vary from a few percent to  $\leq 50$ at.%, with decreasing hardness, resistivity, optical bandgap and density resulting from the higher levels of inclusion.

Finally, some of the hydrogen will also be included in the films in an unbonded, molecular form by being encapsulated in voids. This unbonded form can be detected by knowing the bonded contribution and the total level of hydrogen present as determined by a technique such as SIMS. The unbonded contribution is usually low although even at these levels it is thought that it gives rise to residual stresses in the film.

If one takes a closer look at the coatings produced in this study with regard to the role of hydrogen, the introduction of butane plasma during the deposition of hybrid DC films resulted in higher hardness, good adhesion, higher thermal stability and better tribological performances. This was thought to be achieved primarily by the application of hydrogen in the glow discharge process and its low levels of inclusion in the film in a bonded form (~10%). SIMS analysis recorded levels of total hydrogen content to be 45 at.% of which the majority appears to be incorporated in an unbonded form. Such a high level of hydrogen in this form suggests a large amount of defects, pores or voids which would be necessary to accommodate this volume although doubts about the accuracy of the initial measurement remain.

Thermionically assisted DC EBPVD films displayed a high dependence on the presence of hydrogen in the plasma on the synthesis of the films, with a five fold increase in the deposition rate on glass as the result. In the main, the bonded hydrogen, which is indicated to be high according to optical studies performed by Dr. Dehbi-Alaoui, generally had a detrimental effect on both the optical transmission and electrical resistivity properties. If this is contrasted with the relatively low levels of bonded hydrogen encountered when studying the 380kHz RF synthesised coatings, the variation in the properties of these films was noted to be correspondingly more consistent and superior. In common with the DC films, the deposition rate was considerably improved from 1 $\mu$ m/hr to 3 $\mu$ m/hr for deposition on glass and this is attributed to the constructive role of hydrogen during the deposition stage. However, for both techniques deposition with or without a butane plasma failed to produce any coating on metallic substrates with the exception being hydrogenated RF films on tool steel. This phenomenon was essentially due to the high rate of sputter etching over that of the deposition rate, revealing a net removal of the substrate surface. In the case of the butane RF plasma deposition, the increase in carbon flux from the hydrocarbon seems to have been sufficient to enable the synthesis rate to exceed the etching effect, resulting in the films growing at 1 $\mu$ m/hr. Measurements of stress in hydrogenated RF films revealed the levels to be reasonably low compared to films reported under similar conditions by Grill<sup>176</sup>. Raman

spectra exposed the characteristic trace for diamond-like carbon with a high proportion of  $sp^3$  bonding and the high resistivity measurements confirmed the beneficial effects of a reduced presence of bonded hydrogen in the film.

Fast Atom Beam films deposited under normal conditions were found to have a level of bonded hydrogen in proportion to the amount of hydrocarbon precursor added. However, the level of bonded hydrogen remained low when compared to DC films in general (~10%). The use of different types of hydrogen precursors was noted to have remarkably little effect on the physical properties although it was noted that a marginally increased deposition rate could also be achieved. Under these conditions  $sp^3:sp^2:sp^1$  ratios were analysed to be 75:25:0 with an increase to 90:10:0 possible if additional hydrogen was added to the hydrocarbon precursor. Interestingly enough recent work by Dr. Dehbi-Alaoui showed that for samples placed at orientations approaching grazing incidence with the beam,  $sp^3:sp^2:sp^1$  ratios of 100:0:0 could be approached with an extremely high optical transmission (3.5-4.0eV). This unusual observation implies that a reduction in the velocity of the species normal to the film surface could improve the films structural properties markedly. In addition, it implies that the energies used for the deposition of DLC may be too high and thus be causing implantation of the film at such an energy that localised modification or permanent damage is occurring during the deposition of films under 'normal' conditions.

The levels of unbonded hydrogen were not determined for FAB source films but its existence is highlighted by signs of film stress and large amounts of elastic recovery experienced with films of this type. During annealing of all the films, a change in the physical properties was suspected to be firstly caused by the liberation of bonded and unbonded hydrogen and then thermal damage to the  $sp^3$  bonding at a higher temperature. In all the experiments performed, the distinction between the two events could not be determined since they appeared to occur at the same time. Approaching 400-500°C the films began to show signs of optical and electrical change together with a large reduction in the levels of stress. It is suspected that to this point annealing provides a useful method for driving off the included hydrogen, although as a result microscopic evidence of blistering and pitting of the film surface was sometimes observed to occur. If microindentation hardness analysis is

undertaken at this point, the film is shown to be extremely hard and brittle. Further heating above 500°C is thought to physically restructure the film since it displayed friability and debonded rapidly from the substrate although direct evidence of this reordering is unavailable. Although no in-situ wear tests were performed whilst annealing, Dimigen et al<sup>137</sup> reported that up to temperatures of 500°C a simultaneous increase in steady state coefficient of friction from  $\mu=0.02-0.68$  was witnessed. This was reported to imply the significance of hydrogen in the film for improving the tribological performance. In common with this work, above the temperature of 550-600°C total loss of the film from the substrate was also reported.

The buckling and generation of wrinkles in the film seem to be largely the result of high stress at the interface caused by the accommodation of unbonded hydrogen. There are though some contributory factors such as film thickness, high energy deposition conditions and the quality of the pretreatment procedure which can also have a significance on the magnitude of the stress and/or the adhesion of the film. Another parameter influencing this phenomenon is either the type of environment or the pressure differential experienced by the film after deposition when it is brought back to atmosphere. It was noted that as soon as some of the more highly stressed films were released from the vacuum atmosphere, areas of debonding were witnessed to form spontaneously. In certain, extreme cases within minutes, total spallation of the film could be seen to have happened. It may be that trapped hydrogen in pores under the film surface remains under vacuum after air admit and causes the film to contract. This would appear to be possible but unlikely since it would lead to a tensile stress which would resist buckling. What looks more likely is an accumulation of internal stress either by thermal mismatch or from the intrinsic nature of the film, to a level just less than that needed to overcome the adhesion strength. On exposure to air, moisture permeates into the film/substrate interface causing a reduction in adhesion below that needed to overcome the stress and buckling of the film occurs. It is therefore more a degradation of the adhesion strength than an increase in stress. This observation is corroborated by correlation between this behaviour and the presence of high humidity<sup>224</sup>. Furthermore, the initial point at which this loss of adhesion was noted to occur was at some discontinuity such as that provided by the sample edge or a defect in the film where infiltration of moisture would most likely occur.

### **f) Test Methodologies**

Throughout all of the experimental aspects of this report, the test methods were critically appraised for their accuracy, reliability and suitability in analysing thin layers of hard carbon. Due to the often extreme properties of this type of material certain techniques were found to be unsuitable and others to be suitable only in specific circumstances or after certain precautionary measures had been taken.

Knoop microhardness indentation techniques were shown to be useful for determining approximately the hardness values and the degree of elastic recovery encountered in thin films, although Vickers indentations were found to be entirely inappropriate since the depth to load ratio was too high. The high levels of hardness and the small depths of indentation required to avoid any substrate deformation effects produced a situation where accurate measurement of hardness was continually problematic. The necessary use of low indentation loads to achieve the shallow indents resulted in considerable indentation-load effects which effectively exaggerated the hardness at lower loads. In addition, the levels of elastic recovery witnessed in some of the films could greatly inflate some of these values. Optical measurements of the indentation diagonals using the Leitz Miniload eyepiece was found to be entirely unsuited for measuring diagonals less than  $15\mu\text{m}$ , however the use of a Nikon Optiphot x400 microscope with a Filar micrometer eyepiece proved to give more exacting results. It is felt by the author that while Knoop microindentation techniques provide a convenient method for assessing the approximate hardness, the special demands of DLC films require a technique with a sensitivity an order of magnitude greater. Nanoindentation has been found to be suitable for this purpose for many reasons; it can operate with indentations below  $100\text{nm}$  down to a depth resolution of  $0.2\text{nm}$ , can resolve the elastic and plastic contributions for each indent and has been found to be capable of studying the effective hardness through the film's depth profile, due to the underlying material.

Tests for adhesion using a diamond stylus scratch tester were found to be, in most instances, too crude for the testing of thin DLC films. It was therefore disregarded for all but the most adherent coatings and a method utilising the Leitz Miniload was adopted. This

method involved the use of the microindenter loading system to load a diamond stylus in a range from 10-500g, with the scratch being produced by manually traversing the X-Y table. As with both techniques the interpretation of the exact point of adhesive failure was found to involve a degree of subjective judgement.

Of the analytical techniques available, the most useful for probing the bonding and compositional make up of the films were found to be FTIR and EDX respectively. The later technique however, required certain measures to overcome charging of the insulating DLC surface by including a sputtered layer of gold at the surface and reducing the angle of incidence of the beam so that the apparent thickness of the film increased. Techniques such as LIMA and RBS were found to be wholly inappropriate for testing DLC films since primarily these techniques were more suited to the detection of heavy elements on lighter matrices. The van der Pauw technique for measuring resistivity has proved to be a reliable way of determining the conductivity, the characteristics of which were found to mirror closely the optical properties. Extreme caution was necessary when operating this technique since photo-voltaic effects from excessive light during testing or electrochemical reaction between the sample terminals and the film were possible causes of extraneous voltages and with careful experimental preparation these were kept to a minimum.

## VI. RECOMMENDATIONS FOR FUTURE WORK

### A. Fundamental Studies

- The problems associated with FAB source deposition have been detailed in the discussion section and principally the two most fundamental limitations are; the poor coverage due to the narrow beam width and the deposition of an insulating layer within the source which reduces the deposition rate and produces anomalous results. Development therefore of a wider and more uniform beam pattern needs to be addressed since currently a maximum coverage, at a distance of 300mm from the source, is area of only  $\varnothing 50-60$ mm. This requires a redesign of the grid aperture and source anodes to provide maximum beam width without loss of deposition rate. The problem associated with the formation of an insulating layer on all the surfaces exposed within the source restricts, with time, the emission of electrons from the anode surfaces, leading to a gradual reduction in ionisation and therefore deposition rate. The nature of this build up is not well understood nor is its relationship with the anomalously high hardness values. Such an effect is clearly worth studying, together with methods such as hydrogen etching cycles to reduce the build up, since diamond-like films produced by this source have an obvious potential for producing wear resistant films, all be it on samples 'in line of sight'.
- Study of the transferred layer of carbon between the film and the counterface material is an important area of future research particularly the loadings and atmospheric conditions under which it is formed and maintained. This research has shown that heavily oxidising atmospheres discourage the formation of this layer, although its performance in other environmental conditions such as vacuum and high humidity would also be of interest.
- The use of thin layers of titanium nitride as an intermediate layer continues to be an area of interest particularly the work related to uncovering the mechanism for the improved tribological results. It is strongly suspected that improved adhesion to nitrogen rich titanium nitride provides these optimum conditions, although micro-scratch adhesion tests using a nanoindenter would be useful to test this assumption. In addition, an analytical method for the detection of the chemical composition or bonding arrangements, used in conjunction with a depth profiling technique, would provide a useful means to study the

nature of the interfacial regions in terms of whether it has a graded or well defined junction and what, if any, chemical interactions are occurring. It is suspected that a sublayer or interfacial zone of TiC is being formed thus enhancing the previously poor adhesion between the DLC and the TiN. Techniques such as GDOS or ESCA would be beneficial for determining the character of these interfacial regions and this is seen as the key to furthering the understanding of the beneficial effects of incorporating TiN as one of the layers for supporting a DLC film.

- Indications using enhanced triode arrangements and radio frequency plasmas show that efficient ionisation of the depositing species is essential for dense and mechanical superior films. Future work on 13.56MHz radio frequency or 2.45GHz microwave techniques would be of interest to determine if further improvements in the structural properties of the film can be achieved. High bandgap, 100% sp<sup>3</sup> bonded films were formed by FAB source methods at low grazing incidence indicating energy of the arriving species can be effectively reduced and still produce optical and structural desirable films. Study of RF and microwave deposition may be able to similarly deposit at low energies by virtue of the high level of ionisation and disassociation and the production of a more clearly defined band of energy species.
- Recent testing of commercially available DLC coatings has uncovered the incorporation of silicon in various quantities which appears to have been added intentionally. Some reports in the scientific literature relate how the use of silicon aids markedly the tribological properties of DLC films. Future work using silicon doping and its effect on the film properties is therefore thought to be necessary in this respect although further plans to dope with metallic elements have been deemed unnecessary.

## **B. Analytical Characterisation and Test Development**

- Whilst pin on disc has been shown to be a suitable method for assessing the abrasive and adhesive resistance in dry sliding contact, diamond-like thin films have posed many problems associated with measurement of such low values of wear and friction. The inherent problem of variable Hertzian contact pressure presents the problem of

introducing a harder more wear resistant counterface material such as  $Al_2O_3$  or the continued use of a metallic pin. If the latter is adopted, despite the variable contact conditions, research has shown that a tighter specification of the grade and composition of the pin material is necessary to eradicate a potentially large discrepancy in interlaboratory results. Clearly, further work needs to be performed to establish a standard wear condition using similar materials and parameters which is more exacting than the current VAMAS guidelines. Likewise, guidelines on the evaluations of the wear data, criteria for failure and standardisation of the measurement techniques would also be extremely useful. Such guidelines may suggest testing films until failure and presenting the sliding distance or number of wear passes as the indication of the level of wear, although the criteria of film failure in these circumstances needs to be defined. Finally, as with microhardness measurements, situations of volumetric wear loss should be accompanied by the testing conditions involved, particularly Hertzian contact levels, relative speed, counterface material, humidity and temperature since meaningful interpretation of results without this information is difficult. Furthermore, tribological studies ought to make available wear data performed on standard reference materials so as to provide a more complete picture of the durability characteristics of the film/substrate combination.

- Microhardness evaluation has been shown to be almost inappropriate for the evaluation of DLC films independent of elastic recovery, substrate load support and load-indentation size effects. It is recommended that future work on microhardness measurement is restricted to a comparative technique only with nanoindentation being adopted as the means for probing the hardness, elastic, plastic, adhesive and frictional properties on a nanometer level.

## REFERENCES

- 1 'Effect of Humidity on Friction at Magnetic Head/Hard-Disk Interfaces'  
R.Timsit & G.Stratford, Vol.5, STLE SP-25, p.17-23, 1988
- 2 'Comprehensive Inorganic Chemistry'  
A.Holliday, G.Hughes & S.Walker, Vol.1, No.13, Carbon, p.1182
- 3 'A New Allotropic Form Of Carbon From The Ries Crater'  
A.Gorest & G.Donnay, Science Vol.161, p.363-364, July 1968
- 4 D.Fedoseev, B.Derjaguin & I.Varasavskaja  
Surf.Coatings Technol, 38 (1989) No.1-2, p.12
- 5 'On Crystalline Structure Of Carbyne'  
V.Kasatochkin et al, Carbon, Vol.11, pp.70-72, 1973
- 6 'Amorphous Carbon'  
J.Robertson, Advances In Physics, Vol.35, No.4, p.317-374, 1986
- 7 S.Berg & L-P.Andersson  
Thin Solid Films, Vol.58, (1979), p.117-120
- 8 J.Woolam, B.De, Chen, J.Pouch & S.Alterovitz,  
MRS, EA-19, p.27-32, 1983
- 9 TechMonitoring™ Service Profile Of Diamond Thin Films (DTF)  
SRI International, 4 Addiscombe Rd, Croydon, 1991
- 10 'Diamond Thin Films - New Opportunities'  
IRD Inc. Connecticut, USA, 1991
- 11 'Diamond Thin Films - The Threshold Of Commercialisation'  
IRD Inc. Report #733, Connecticut, USA, April 1991
- 12 R.Rustrum  
Nature, Vol.325, Jan 1987
- 13 P.Bachmann & R.Messier  
Chemical & Engineering News, Vol.67, No.20, May 1989
- 14 J.Prins  
Appl.Phys.Lett. 950(15), 1982
- 15 K.Okano  
Diamond Depositions: Sci. & Technol. Vol.1, No.4, p.5, Feb 1991
- 16 R.Messier & W.Yarborough  
Physics Today, S.65, Jan 1989
- 17 R.DeVries  
Ann.Rev.Mater.Sci. Vol.17, No.161, 1989

- 18 J.Russell  
Diamond Depositions: Sci. & Technol. Vol.2, No.4, p.11, July 1991
- 19 J.Russell  
Diamond Depositions: Sci. & Technol. Vol.2, No.5, p.12, August 1991
- 20 D.Mir  
Thin Solid Films, Vol.144, (1986), p.201-209
- 21 M.Moran  
Diamond Depositions: Sci. & Technol. Vol.2, No.1, p.5, March 1991
- 22 A.Harker  
Diamond Depositions: Sci. & Technol. Vol.2, No.5, p.10, Aug 1991
- 23 B.Dischler & G.Brandt  
Industrial Diamond Review, Vol.3, No.85, p.131
- 24 E.Dunlop, J.Haupt, K.Schmidt & W.Gissler  
presented at Diamond Films '91, Nice, France
- 25 J.Russell  
Diamond Depositions: Sci. & Technol. Vol.2, No.1, p.6, March 1991
- 26 R.Chang & T.Ong  
Appl.Phys.Lett. Jan 28th 1991
- 27 R.Messier, A.Badzian, T.Badzian, K.Spear, P.Bachmann & R.Roy  
Thin Solid Films, Vol.153, (1987), p.1-9
- 28 S.Solin & A.Ramdas,  
Phys.Rev.B, Vol.1, No.4, (1970) p.1687-1698
- 29 W.Yarborough & R.Messier,  
Science, Vol.247, p.688-696, Feb 1990
- 30 M.Ramsteiner, J.Wagner, Ch.Wild & P.Koidl,  
J.Appl.Phys. 62(2), July 1987
- 31 D.Knight & W.White,  
J.Mater.Res. Vol.4(2), Mar/Apr 1989
- 32 I.Newton  
Opticks (London) 1704
- 33 G.Averani & C.Targioni  
Litterati Ital. Vol.8, 221, p.1711
- 34 A-L.Lavoisier  
Memoire Academia des Sciences, 1772
- 35 S.Tennant  
Phil.Trans.R.Soc. Vol.97, p.267, 1797

- 36 'Diamonds'  
G.Davies, Adam Hilger Ltd, Bristol. 1984
- 37 'A History Of Synthetic Diamond And Carbon Film Production'  
M.Simpson, Univ.Carbon Films & Mats.Grp. Sept.1987
- 38 H.Moissan  
The Electric Furnace (transl.) AT de Monilpied (London, E.Arnold)
- 39 J.Hershey  
Trans.Kansas Acad.Sci. Vol.40 213, 1940
- 40 F.Simon  
Handbuch der Physik, Vol.10, 350, 1926
- 41 F.Rossini & R.Jessop  
J.Res., NBS Vol.21, 491, 1938
- 42 O.Liepunsky  
Usp.Khim. Vol.8, 1519, 1939
- 43 P.Bridgeman  
J.Chem.Phys. Vol.15, 92, 1947
- 44 F.Bundy, H.Hall, H.Strong & R.Wentorf  
Nature, 176(1955), p.51-54
- 45 S.Bolton  
Z Electrochem, Vol. 17, No.971, 1911
- 46 B.Derjaguin, B.Spitsyn, A.Aleksenko, A.Gorodetsky, A.Zahharov & R.Nazarova  
Dokl. Akad. Nauk. SSSR 213 (1973)
- 47 W.Eversole  
United States Patent Office No. 3,030,187, 17 April 1962
- 48 W.Eversole  
United States Patent Office No. 3,030,188, 17 April 1962
- 49 H.Schmellenmeier  
Z.Phys.Chem.Leipzig, 205(1955-56), p.349-350
- 50 T.Anthony  
Vacuum Vol.41, No.4-6, p.1356-1359, 1990
- 51 M.Frenklach & K.Spear  
J.Mater.Res. Vol.3(1), Jan/Feb 1988
- 52 L.Schäfer & C.-P.Klages  
Surf.Coat.Technol. 47(1991), p.13-21
- 53 S.Harris & L.Martin  
J.Mater.Res. Vol.5(11), Nov 1990

- 54 C.Chu, M.D'Evelyn, R.Hauge & J.Margrave  
J.Mater.Res. Vol.5(11), Nov 1990
- 55 S.Matsumoto, Y.Sato, M.Kamo & Setaka  
Jap.J.Appl.Phys, Vol.21, No.4, April 1982 p.L183-L185
- 56 S.Masumoto, Y.Sato, M.Tsutsumi & N.Setaka  
J.Mats.Sci. Vol.17 (1982) p.3106-3112
- 57 S.Matsumoto  
J.Mats.Sci.Letts. Vol.4, (1985) p.600-602
- 58 M.Kamo, Y.Sato, S.Matsumoto & N.Setaka  
J.Crys.Growth, Vol.62 (1983) p.642-644
- 59 D.Thompson  
Mats.Sci.Forum, Vol.52&53, (1989), P.515-542
- 60 P.Joffreau, R.Bichler, R.Haubner & B.Lux  
Hard Mat.Prod., London, April 11-13, 1988
- 61 A.Sawabe & T.Inuzuka  
Appl.Phys.Lett. 46(2), Jan 1985, p.146-147
- 62 S.Matsumoto & Y.Matsui  
J.Mats.Sci. Vol.18, (1983) P.1785-1793
- 63 F.Jansen, M.Machonkin & D.Kuhman  
J.Vac.Sci.Technol. Vol.A8(5), p.3785-3790, 1990
- 64 D.Belton & S.Schmieg  
General Motors Research Laboratories, Warren, Michigan, 48090
- 65 S.Sharma, R.Hyer, C.Dark, M.Green & T.Black  
J.Mater.Res. p. 71-75, April 1989
- 66 D.Whitmell & R.Williamson  
Thin Solid Films, Vol.35, (1976), p.255-261
- 67 Y.Catherine & P.Couderc  
Thin Solid Films, Vol.144, (1986), p.265-280
- 68 A.Dehibi-Alaoui, A.James & A.Matthews  
Surf.Coat.Technol. 43/44 (1990), p.88
- 69 A.Bubbenzer, B.Dischler, G.Brandt & P.Koidl  
J.Appl.Phys. 1983, Vol. 54, p.4590
- 70 S.Ojha, H.Norstrom & D.McCulluch  
Thin Solid Films, Vol.60, (1979), p.213-225
- 71 P.Koidl, Ch.Wild, B.Dischler, J.Wagner & M.Ramsteiner  
Mats.Sci.Forum, Vols.52&53 (1983), p.41-70

- 72 Ch.Wild, J.Wagner & P.Koidl  
J.Vac.Sci.Technol. 1987, Vol.A5(4), p.2227-2230
- 73 R.Memming, H.J.Tolle, & P.E.Wierenga  
Thin Solid Films, Vol.143, (1986) p.31-41
- 74 S.Yugo & T.Muto  
Vacuum, Vol.41, No.4-6, p.1364-1367, 1990
- 75 T.Taguchi, M.Morikawa, Y.Hiratsuka & K.Toyoda  
MRS, June 1979, Vol.17. p.123-129.
- 76 B.Singh, O.Mesker, A.Levine & Y.Arie  
Appl.Phys.Lett. 52(20), May 1988, p.1658-1660
- 77 Y.Shing & F.Pool  
Vacuum, Vol.41, No.4-6, p.1368-1370, 1990
- 78 Y.Hirose  
proc. 1st Int.Conf. New Diamond Sci. & Technol., 1-09, p.38-39, 1988
- 79 Y.Matsui, A.Yuuchi, M.Sahara & Y.Hirose  
Jap.J.Appl.Phys. Vol.28, No.9, Sept 1989, p.1718-1724
- 80 M.Kawarada, K.Kuihara, K.Sasaki, A.Teshima & N.Koshino  
proc. 1st Int.Conf. New Diamond Sci. & Technol. 1-11, 1988
- 81 N.Agarwal & A.Haubold  
Thin Solid Films, Vol.40, (1977), p.299-308
- 82 S.Aisenberg & R.Chabot  
J.Appl.Phys. 1971, Vol. 42, No.7 p.2953-2959
- 83 E.Spencer, P.Schmidt, D.Joy & F.Sansalone  
Appl.Phys.Lett. 29(2), July 1976, p.118-121
- 84 C.Weissmantel, E.Ackermann, K.Bewilogua, G.Hecht, H.Kupfer & B.Rau  
J.Vac.Sci.Technol. 1986, Vol.A4(6), p.2892-2899
- 85 P.Martin, S.Filipcuk, R.Neterfield, J.Field, D.Whitnall & D.McKenzie  
J.Mats.Sci.Letts, Vol.7,(1988) P.410-412
- 86 J.Koshinen  
Fin.Soc.Sci & Letts. Physico-Mathematicae 81/1987, Dissertationes No.10
- 87 J.Franks  
J.Vac.Sci.Technol. 1989, Vol.A7(3), p.2307-2310
- 88 D.Kerwin, I.Spain, R.Robinson, B.Daubin, M.Dubus & J.Fontenille  
Thin Solid Films, Vol.148, (1987), p.311-321
- 89 W.Sainty, P.Martin, R.Netterfield, D.McKenzie, D.Cockayne & D.Dwarte  
J.Appl.Phys. 1988, Vol. 64(8), p.3980-3987

- 90 F.Jansen, M.Mackonkin, S.Kaplan & S.Hark  
J.Vac.Sci.Technol. 1985, Vol.A3(3), p.605-609
- 91 M.Kitabatake & W.Kiyotaka  
J.Vac.Sci.Technol. 1988, Vol.A6(3), p.1793-1797
- 92 S.Kasi, H.Kang & J.Rabalais  
J.Vac.Sci.Technol. 1988, Vol.A6(3), p.1788-1792
- 93 M.Allouard & J.Pavin  
Surf. & Coatings Technol, 47 (1991) p.433-444
- 94 J.Owens  
MSc Thesis, Lancaster University, 1991
- 95 N.Savides  
J.Appl.Phys. 1984, Vol. 55(12), p.4232-4239
- 96 J.Koskinen, A.Antila & J-P.Hirvonen  
Surf. & Coatings Technol, 47 (1991) p.180-187
- 97 I.Aksenov & V.Strel'nitskij  
Surf. & Coatings Technol, 47 (1991) p.98-105
- 98 A.Richter, H-J.Scheibe, W.Pompe, K-W.Brzezinka & I.Muhling  
J.Non-Cryt.Solids, Vol.88, (1986) p.131-144
- 99 S.Fujimori & K.Nagai  
Jap.J.Appl.Phys. Vol.20, No.3, 1981 p.L194-L196
- 100 A.Sokolowska, K.Zdunek, H.Grigoiew & Z.Romanowski  
J.Mats.Sci. Vol.21 (1986) p.763-767
- 101 L-P.Andersson  
Thin Solid Films, Vol.86, (1981), p.193-200
- 102 J.Knight, T.Page & H.Chandler  
proc. of Int.Conf.Metal.Coatings & Thin Films '91
- 103 S.Yugo & T.Kimura  
proc. 1st Int.Conf. New Diamond Sci. & Technol., p.130-131, 1988
- 104 R.Ramesham, T.Roppel & C.Ellis  
Adv.Coat. & Surf.Technol. Vol.4, No.1, Jan 1991
- 105 J.Valdes, J.Michel, J.Mucha, L.Seibles & H.Huggins  
presented at the American Electrochemical Society Meeting, May 1991
- 106 P.Kimura  
Diamond Depositions: Sci. & Technol. Vol.2, No.5, p.14, Aug 1991
- 107 J.Margraves  
Diamond Depositions: Sci & Technol. Vol.2, No.4, p.11, July 1991

- 108 Japanese News Briefs, Hitachi Ltd.  
Diamond Depositions: Sci. & Technol. Vol.2, No.4, p.15, 1991
- 109 Y.Muranaka, H.Yamahita & H.Miyadera  
J.Vac.Technol. Vol.9, No.1, 1991
- 110 K.Snail & C.Vold  
proc. of the Electrochemical Society meeting, Washington, May 1991
- 111 R.Rudder, M.Buck & H.Seki  
proc. of the MRS, Vol.162, p.97, 1989
- 112 R.Rudder  
Elect.Letts.Vol.24,1220,1989
- 113 E.Pfender, Q.Han, T.Or, Z.Lu & J.Heberlein  
proc. of the 2nd Euro.Conf.on Diamond, Diamond-like & Rel.Coatings, 3.4, 1991
- 114 G.Janssen, W.van Enkevort, W.Vollenberg & L.Gilling  
proc. of the 2nd Euro.Conf.on Diamond, Diamond-like & Rel.Coatings, 11.4, 1991
- 115 K.Ravi & A.Joshi  
Appl.Phys.Lett. Jan 21st, 1991
- 116 K.Churian  
Surf.Coatings Technol, 47 (1991) p.127-143
- 117 J.Prins  
US Patent No.4,997,636, 1991
- 118 J.Narayan  
Science, p.416-419, April 1991
- 119 J.Narayan  
proc.of the 2nd Euro.Conf.on Diamond, Diamond-like & Related Coatings, 11.4, 1991
- 120 S.Lee  
proc, of the Electrochemical Society, May 1991
- 121 T.Anthony, W.Banholzer, J.Fleischer, L.Wei, P.Kuo, R.Thomas & R.Pryor  
Physics Review B, Vol.42, No.2, (1990) p.1104-1111
- 122 D.Brenner, J.A.Harrison, C.White & R.Colton  
proc. of the ICMC&TF, E4(6), April 24th, 1991
- 123 W.Krätschmer, L.Lamb, K.Fostiropoulos & D.Huffman  
Nature Vol.347, Aug 1990, p.354-358
- 124 Y.Guo, N.Karasawa & W.Goddard III  
Nature Vol.351, 6th June 1991, p.466
- 125 J.Baggott  
New Scientist, 6th July 1991

- 126 'Combustion Synthesis of Buckminsterfullerene', J.McKinnon, W.Bell & R.Barkley  
submitted to Combustion & Flame, March 1991
- 127 J.Howard, J.McKinnon, Y.Makarovsky, A.Lafleur & M.Johnson  
Nature, Vol.352, p.139-141, 11th July 1991
- 128 L.Pang, A.Vassallo & M.Wilson (CSIRO)  
Scientific Correspondance in Nature Aug 8th, 1991
- 129 R.Haddon, A.Hebard, M.Rosseinsky, D.Murphy, S.Duclos, K.Lyons, B.Miller, et al  
Nature Vol.350, p.320-322, 28th March 1991
- 130 P.Stephens, L.Mihaly, P.Lee, R.Whetton, S-M.Huang, R.Kaner, F.Deiderich &  
K.Holczer, Nature Vol.351, p.632-634, 20th June 1991
- 131 E.Geake  
New Scientist, p.21, 27th July 1991
- 132 D.Whitehouse  
Tribology Int., 1974 p.249-259
- 133 'Principles and Applications of Tribology'  
D.F.Moore, Pergamon Press, Oxford, 1975, p.388
- 134 'Tribology'  
H.Czichos, Elsevier, Amsterdam, 1978, p.400
- 135 K. Holmberg  
Technical Research Centre of Finland, Pub. 16, 1984, p.81
- 136 'Friction and Lubrication of Solids. Part I'  
P.Bowden & D.Tabor, Claredon Press, Oxford, 1950, p. 374
- 137 'Surface Effects In Adhesion, Friction, Wear & Lubrication'  
D.Buckley, Tribology Series 5, p.318, 1981
- 138 P.Suh  
Tribophysics, Prentice Hall, Englewood Cliffs, New Jersey, USA, 1986, p.489
- 139 'Friction and Lubrication of Solids. Part II'  
P.Bowden & D.Tabor, Claredon Press, Oxford, 1964
- 140 'Friction and Wear of Materials'  
E.Rabinowicz, John Wiley & Sons, New York, 1965
- 141 I.Kragelsky  
J.Basic Eng., Trans ASME, 1965, p.785-790
- 142 D.Rigney & P.Hirth  
Wear, 53 (1979), 2, p.345-370
- 143 P.Green  
Proc.R.Soc., 228a, 1955, p.191

- 144 M.Edwards & J.Halling  
J.Mech.Eng.Sci., 10, 1968, 2, p.101-110
- 145 D.Landheer & H.Zaat  
Wear, 27 (1974), p.129-145
- 146 P.Heilmann & D.Rigney  
Wear, 72 (1981), p.185-217
- 147 D.Tabor  
J.Lub.Tech., Trans.ASME, 103, 1981, p.169-179
- 148 P.Suh & H.Sin  
Wear, 69 (1981), p.91-114
- 149 'Friction & Wear Transitions of Materials - Break-through, Run-in, Wear-in'  
P.Blau, Noyes Publications, Park Ridge, New Jersey, USA, 1989, p476
- 150 S.Franklin  
Philips CFT Technology, CTR 545.91.0043, 1991, p24
- 151 E.Rabinowicz  
Wear, 100 (1984), p.533-541
- 152 'Friction & Wear Transitions of Materials - Break-through, Run-in, Wear-in'  
P.Blau, Noyes Publications, Park Ridge, New Jersey, USA, 1989, p476
- 153 'Friction and Wear of Materials'  
E.Rabinowicz, John Wiley & Sons, New York, 1965
- 154 T.Eyre  
Tribology Int., 1976, p.203-212
- 155 D.Tabor  
J.Lub.Tech., Trans.ASME, 1977, p.387-395
- 156 'On The Wear Mechanisms & The Wear Equations'  
S.Jahanmir, The MIT Press, London, 1980, p.455-467.
- 157 J.Archard  
J.Appl.Phys., 24(1953), p.981-988
- 158 M.Kruschov  
Wear, 28 (1974), p.69-88
- 159 K-H Zum Gahr  
5th Int. Congress on Tribology, Vol.2, Helsinki, 1989, p.34-39
- 160 'Tribology'  
H.Czichos, Elsevier, Amsterdam, 1978, p.400
- 161 T.Quinn  
Tribology Int. 16, 1983, 6, p.305-315

- 162 J.Sullivan  
Inst.Mech.Eng., C144/87, 1987, p.293-301
- 163 T.Quinn & W.Winer  
Wear, 102 (1985), p.67-80
- 164 K.Tanaka  
Wear, 100 (1984) p.243-262
- 165 K.Enke  
Thin Solid Films, Vol.80, (1981), p.227-234
- 166 H.Dimigen, H.Hübsch & R.Memming  
Appl.Phys.Lett. 50(16), 1987, p.1056-1058
- 167 K.Enke, H.Dimigen & H.Hübsch  
Appl.Phys.Lett. 36(4), Feb 1980, p.291-292
- 168 R.Savage & D.Schaefer  
J.App.Phys. Vol.27, No.2, 1956, p.136-138
- 169 R.Savage  
J.Appl.Phys, Vol.19, No.1, 1948, p.1-10
- 170 'Friction of Diamond, Graphite and Carbon'  
F.Bowden & J.Young, March 1951
- 171 J.Judge & D.Speliotis  
IEEE Trans. Mags. Vol.MAG-23, No.5, Sept 1987, p.3402-3404
- 172 B.Marchon, N.Heiman & M.Khan  
IEEE TRans. Mags. Vol.26, No.1, Jan 1990, p.168-170
- 173 T.Doan & N.Macintosh  
STLE Vol.5, SP-25, p.6, 1988
- 174 P.Blau, C.Yust, L.Heatherly & R.Clausing  
Tribology Series 17, Elsevier, Paper XVIII(i), p.399-407, 1990
- 175 J.Franks  
Vacuum, Vol.34, p.259, 1987
- 176 L.J.van der Pauw  
Philips Res. Repts. Vol.13, p.1-9, Feb.1958
- 177 P.M.Hemenger  
Rev. Sci. Instrum., Vol.44, No.6, June 1973
- 178 'Handbook of Thin Film Technology',  
L.I.Maissel & R.Glang, McGraw Hill, 1970, pp.12-23
- 179 M.E.Thomas, M.P.Hartnett & J.G.McKay  
J.Vac Sci.Technol. Vol. A(6), No. 4, July/Aug 1988

- 180 M.Louie & R.Christy  
Thin Solid Films, Vol.154, (1987), p.291-299
- 181 B.Jonsson & S.Hogmark  
Thin Solid Films, Vol.114,(1984), p.257-269
- 182 C.Brookes & P.Green  
Nature, 246(1973), p.119-122
- 183 F.Knoop, C.Peters & W.Emerson  
J.Res.Nat.Bar.Std. 23, 1939, p.31-61
- 184 H.K.Pulker  
'Coatings On Glass', Elsevier, Amsterdam, 1984, p.353
- 185 H.M.Pollock, D.Maugis & M.Barquins  
STP 889, American Society for Testing and Materials, 1986.
- 186 M.Kruschov & E.Berkovich  
Industrial Diamond Review, 11(1951), p.42-44
- 187 J.Ross, H.Pollock, J.Pivin & J.Takadoun,  
Thin Solid Films, 148 (1987) 171.
- 188 'Test Methods for Measurement of the Properties of Thin Films & Coatings'  
A.Matthews & P.Holiday, Report for the Nat.Phys.Lab., Teddington, 1991
- 189 J.Valli, U.Makela & A.Matthews  
Surface Engineering, 2, 49, 1986
- 190 D.Kerwin, I.Spain, R.Robinson, B.Daudin, M.Dubus & J.Fontenille  
Thin Solid Films, Vol.148, (1987), p.311
- 191 P.Steinmann, Y.Tardy & H.Hintermann  
Thin Solid Films, Vol.154, (1987), p.333-349
- 192 A.P.Mercer & I.M.Hutchings,  
Dept.of Metallurgy & Mats.Sci. University of Cambridge, United Kingdom
- 193 H.Ronkainen, S.Varjus, K.Homberg, K.S.Fancey, A.Matthews, B.Matthes &  
E.Broszeit, Elsevier Trib. Series 17, 1990, p.453-463
- 194 M.G.Gee & E.A.Almond,  
Mat.Sci.& Tech. Vol.4, p.655-663, July 1988
- 195 'International Multilaboratory Wear Tests: VAMAS 2nd Round Robin',  
H.Czichos, S.Becker & J.Lexow, Fed.Inst. Mats R & D, D-1000 Berlin 45
- 196 B.Marchon, S.Vierk, N.Heiman, R.Fischer & M.R.Khan,  
STLE SP-26 p.71-80, 1989
- 197 H.Heinzelmann, E.Meyer, L.Scandella, P.Grutter, Th.Jung, H.Hug, H.-R.Hidber,  
H.-J.Guntherodt & C.Schmidt, Wear, 135 (1989) p.109-117

- 198 F.E.Kennedy,  
Wear, 100(1984)p.453-476
- 199 'Surface Effects In Adhesion, Friction, Wear & Lubrication'  
D.Buckley, Tribology Series 5, p.238-239, 1981.
- 200 'Guidelines For Unlubricated Pin on Disc Wear Tests'  
M.Gee, UK Forum on Wear & Friction Testing, National Physical Laboratory, UK
- 201 'Measuring Friction & Wear, Model Experiments On Sliding Friction In Solids'  
German Standard DIN 50 324
- 202 A.Dehibi-Alaoui  
PhD Thesis, University of Hull, in preparation
- 203 A.Matthews, D.Tither & P.Holiday  
Proc. EUROTRIB '89, Helsinki, Finland. June 1989
- 204 A.Fitzgerald & A.Henderson  
'Mircobeam Analysis Studies Of a-C:H Films' , Trans.Tech.Pub. 1989
- 205 D.Tither, A.Dehibi-Alaoui, P.Holiday, A.Matthews, A.Fitzgerald, A.Henderson et al  
Carbon, Vol.28, No.5, pp.641-655, 1990
- 206 J.Zelez  
RCA Review, Vol.43, p.665, 1982
- 207 A.Grill, V.Patel & B.Meyerson  
NATO ASI on Diamond & Diamond-like Films & Coatings, Italy, Aug. 1990
- 208 H.Tsai & D.B.Bogy  
J.Vac.Sci.Technol. A5(6), Nov/Dec 1987
- 209 J.C.Angus,  
Thin Solid Films, 118, (1984), p.311-320
- 210 'Ionisation Assisted Deposition of Carbon'  
M.Drew, Fourth Year Dissertation, Dept. of EDM, Hull University, 1987
- 211 A.Dehibi-Alaoui, P.Holiday & A.Matthews  
Surf.Coatings Technol, 47 (1991) p.327-335
- 212 A.Leyland  
PhD thesis, University of Hull, 1991
- 213 A.Dehibi-Alaoui, A.Matthews & J.Franks  
Surf.Coat.Technol. 47, (1991), p.722-729
- 214 T.Q.Doan & N.Macintosh,  
Trib.& Mechs.of Mag.Storage Sys.Vol.V, STLE SP-25, pp.17, 1988.
- 215 D.A.Rigney, L.H.Chen, M.G.S.Naylor and A.R.Rosenfield,  
Wear, 100(1984)p.195-219

- 216 J.Pethica, R.Hutchings & W.Oliver  
Philos.Mag. A,48 (1983), p.595
- 217 J.Ross, H.Pollock, J.Pavin & J.Takadom  
Thin Solid Films, 148, (1987), p.171
- 218 C.Felman, F.Orday & J.Bernstien  
J.Vac.Sci.Technol. A, 8 (1990), p.117
- 219 M.Doerner & W.Nix  
J.Mater.Res. 1, (1986), p.601
- 220 G.Was, S.Mantl & W.Oliver  
J.Mater.Res. 6, (1991), p.1200
- 221 H.Holleck  
J.Vac.Sci.Technol. A, 4 (1986), p.2661
- 222 C.Beetz, C.Cooper & T.Perry  
J.Mater.Res. 5, (1990), p.2555
- 223 C.Cooper & C.Beetz  
Surf.Coat.Technol., 47 (1991), p.375
- 224 H.Tsai  
Mats.Sci.Forum Vols.52&53 (1989), p.71-102
- 225 F.Bundy  
Science, Vol.137, 1962, p.1057
- 226 'Tribology of Thin Layers'  
I.Ilicu, Tribology Series 4, Elsevier, 1980

## **APPENDIX I**

### **Nominal Steel & Metal Alloy Compositions (wt%)**

**Nominal Steel & Metal Alloy Compositions (wt%)**

<b>Material</b>	<b>C</b>	<b>Si</b>	<b>Mn</b>	<b>P/S</b>	<b>Cr</b>	<b>Co</b>	<b>Mo</b>	<b>V</b>	<b>Ni</b>
SAE52100	0.98/1.10	0.15/0.30	0.25/0.45	0.025	1.30/1.60	-	-	-	-
ASP23	1.25	0.75	0.15	0.05	3.5	0.4	6	2.5	0.15
M50	0.45/0.55	n/a	0.6/1.0	0.05	-	-	-	-	-
Cobalt-Chrome	0.3	1	1	-	27-30	35	5-7	-	-
304	0.06	0.2/1.0	0.5/2.0	0.04	17.5/19	-	-	-	8/11

## **APPENDIX II**

### **Hydrocarbon and Organic Precursors**

## Hydrocarbon and Organic Precursors

$\text{CH}_3\text{OH}$	methanol (methyl alcohol)
$\text{C}_3\text{H}_8$	propane
$\text{C}_4\text{H}_{10}$	butane
$\text{C}_6\text{H}_6$	benzene
$\text{C}_2\text{H}_5\text{OH}$	ethanol (ethyl alcohol)
$(\text{CH}_3)_2\text{CHOH}$	isopropyl alcohol
$(\text{CH}_3)_3\text{COH}$	2-methyl-2-propanol
$\text{CH}_3\text{COCH}_3$	acetone
$[(\text{CH}_3)_2\text{CH}]_2\text{O}$	isopropyl ether
$\text{CH}_3\text{COOCH}_3$	methyl acetate
$\text{C}_2\text{H}_5\text{OC}_2\text{H}_5$	diethyl ether
$(\text{CH}_3)_3\text{N}$	trimethylamine
$\text{CH}_4$	methane
$\text{C}_2\text{H}_2$	acetylene
$\text{CH}_3\text{CHO}$	acetaldehyde
$\text{C}_6\text{H}_5\text{-CH}_3$	toluene

## **APPENDIX III**

### **Applications & Products**

## **Applications & Products**

### **Cutting Tools**

- Twist Drills
- Cutting Tools & Inserts
- Oil Drilling Tools
- Circuit Board Drills
- Slitter Blades
- Surgical Scalpels and reduced penetration force needles
- Industrial Knives
- End Mills

### **Wear Parts**

- Jet/Nozzle Wear Coatings
- Ball/Roller Bearing Surfaces
- Wire Transport Guides
- Extrusion and Drawing Dies
- Abrasive Unlubricated Pump Seal Coatings
- Medical Implants
- Computer Disc Surface Coatings
- Chemically Inert Coatings
- TAB Bonding Tools

### **Heat Sinks & Electronic Substrates**

- Microwave Power Devices
- Heat Sinks
- Thermode (TAB) Tips
- High Thermal Conductivity PC Boards
- Laser Diode Heat Sinks
- Target Heat Sinks
- Passivation Coatings

### **Optical Devices**

- Mirror Coatings
- SEM Thin Windows
- IR Domes
- Lithography Masking
- Laser/Accelerator Windows
- X-ray Windows
- UV light emitting diodes & lasers
- Scratch Proof Plastic Lenses

### **Electronic Devices**

- Radiation Resistant Circuits
- High Voltage Switching
- Insulator/Silicon IC Combinations
- 1000°C+ IC Systems
- High Power Transistors
- High Power Microwave Devices
- Radiation-hardened semiconductor devices
- High temperature electronics
- Substrates for high-density high-speed integrated circuits

### **Application**

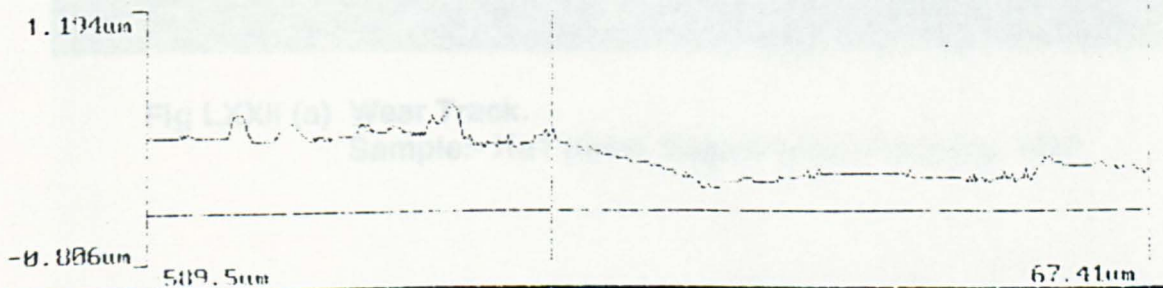
- High Frequency Audio Speaker Diaphragms
- Implants

## **APPENDIX IV**

### **Examples of Protocol Data Sheets**

<b>Sample Designation: Hu1 (thin)</b>		
<b>Institute/Laboratory: RCSE, Hull University</b>		
<b>Tested By: Peter Holiday</b>		
<b>Date: 11/3/91</b>		
<b>Dimensions: Ø40mm x 2.5mm disc</b>		
<b>Composition/Grade: cobalt-chrome</b>		
<b>Micro Hardness</b>	Hk = 800 Kg/mm <sup>2</sup> , 25 g	<b>Notes:</b>
<b>Surface Roughness</b>	Ra = 0.050 µm	
<b>Coating Intermediate Layer</b>		
<b>Composition:</b>	<b>None</b>	<b>Notes:</b>
<b>Thickness:</b>	t = µm	
<b>Micro Hardness</b>	Hv = Kg/mm <sup>2</sup> , g	
<b>Surface Roughness</b>	Ra = µm	
<b>Surface Layer</b>		
<b>Composition:</b>	<b>DLC Carbon</b>	<b>Notes: FAB source</b>
<b>Thickness:</b>	t = 0.17 µm	thin
<b>Micro Hardness:</b>	Hk = 1779 Kg/mm <sup>2</sup> , 25 g	impossible to ident with 10 or 15g - elastic recovery
<b>Surface Roughness</b>	Ra = 0.0513 µm	
<b>Pin on Disc</b>		
<b>Sample Cleaning: Ultrasonic in freon, acetone wipe</b>		
<b>Testing Temperature:</b>	T = 21 ± 1 °C	<b>Notes:</b>
<b>Relative Humidity</b>	RH = 50 ± 2.5 %	
<b>Normal Force</b>	F = 10.0 N	
<b>Sliding Velocity</b>	v = 0.1 m/s	
<b>Track Diameter</b>	Ø = 16.0 mm	
<b>Rotational Speed</b>	n = 119 rpm	
<b>Test Duration</b>	t = 16.7 min	
<b>Sliding Distance</b>	s = 100.0 m	

<b>Results</b>		
<b>Coefficient of Friction</b>		
Initial	$\mu = 0.22$	Notes: high initial $\mu \rightarrow$ low steady state $\mu$ which is typical
Steady state	$\mu = 0.15$	
<b>Wear</b>		
Pin	$\varnothing = 0.42 \text{ mm}$	$V = 0.3 \times 10^{-6} \text{ mm}^3/\text{Nm}$
Disc	$w = \sim 320 \text{ }\mu\text{m}$	$V = 2.7 \times 10^{-6} \text{ mm}^3/\text{Nm}$
Sliding Distance to Failure: $>100.0 \text{ m}$		
Debris: <b>no debris</b>		
Wear Surface Profilometry:		



Clear Region	Move Marker	Data Selection	Set X: -326.0um
		INCLUDE EXCLUDE OFF	Datum Z: 0.211um
Analyse Region	Options	Form Options	Save Data
			Return to Previous

Localised failures on an otherwise polished track  
 Maximum depth of track  $0.09\mu\text{m}$  (cf.  $0.17\mu\text{m}$  - thickness of film)  
 Note:- thin transfer layer on pin indicated by interference fringes

<b>Scratch Testing</b>			
Ambient Temperature:	T =	$\pm$	$^{\circ}\text{C}$
Relative Humidity	RH =	$\pm$	%
Maximum Load	F =		N
Loading Rate			N/s
Scratching Speed	v =		mm/s
<b>Results</b>			
Critical Load	trace	Lc =	N
	acoustic	Lc =	N

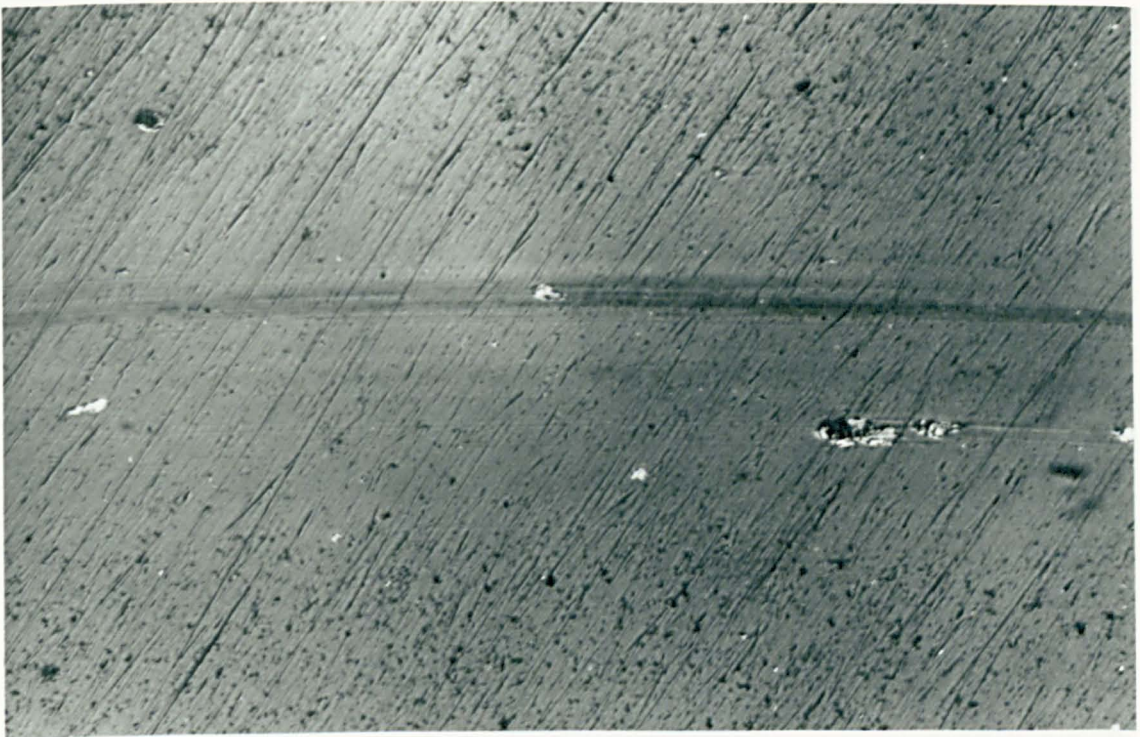


**Fig LXXII (a) Wear Track.**  
**Sample:- Hu1 (thin). Magnification (approx. x80)**

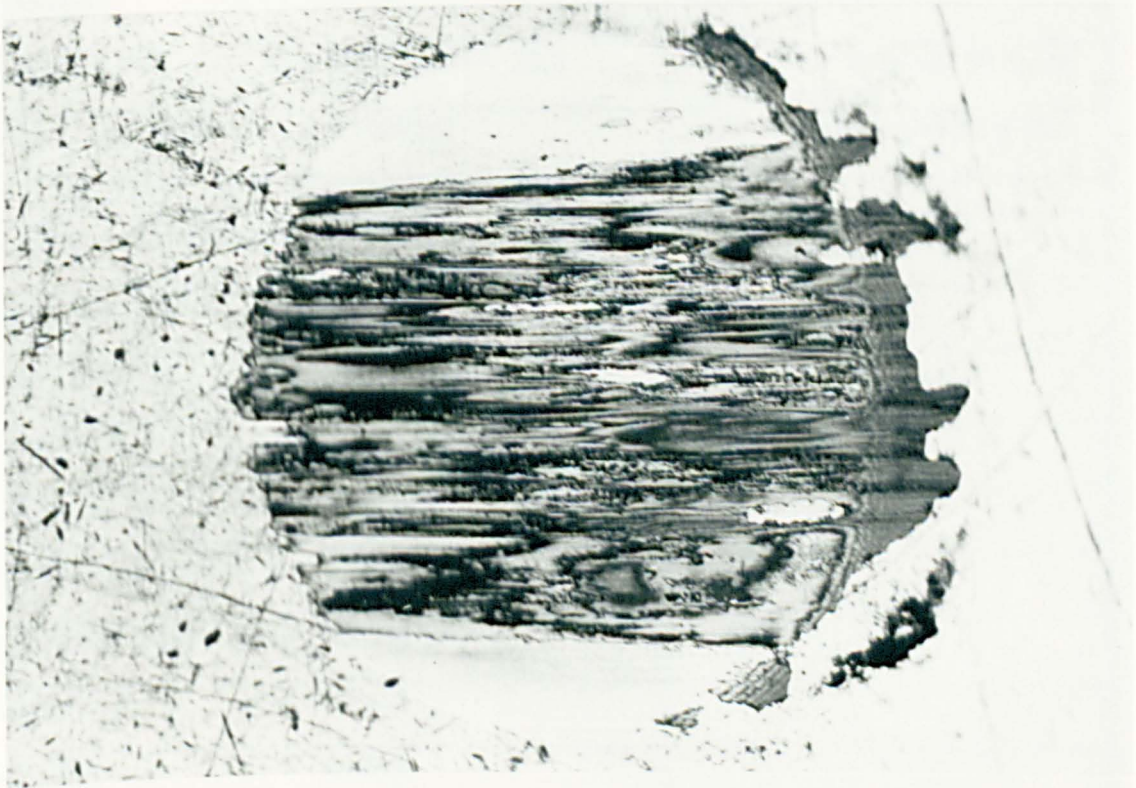
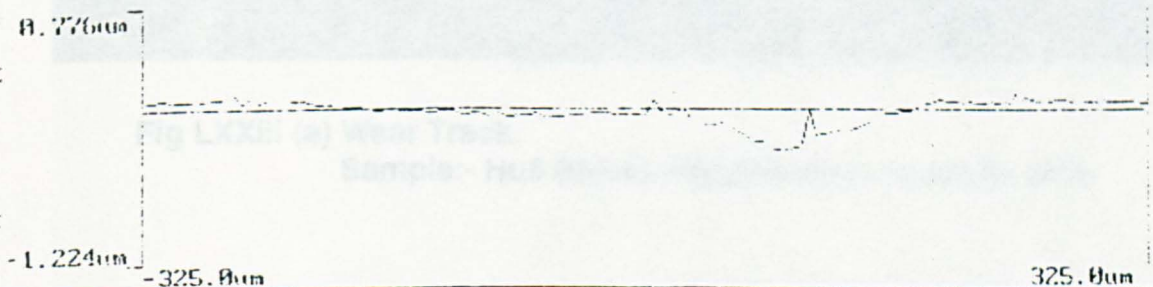


**Fig LXXII (b) Pin Wear.**  
**Sample:- Hu1 (thin). Magnification (approx. x80)**

<b>Sample Designation: Hu6 (thick)</b>		
Institute/Laboratory: <b>RCSE, Hull University</b>		
Tested By: <b>Peter Holiday</b>		
Date: <b>11/3/91</b>		
Dimensions: <b>Ø40mm x 2.5mm disc</b>		
Composition/Grade: <b>cobalt-chrome</b>		
Micro Hardness	Hk = 800 Kg/mm <sup>2</sup> , 25 g	Notes:
Surface Roughness	Ra = 0.050 µm	
<b>Coating</b>		
<b>Intermediate Layer</b>		
Composition:	<b>None</b>	Notes:
Thickness:	t = µm	
Micro Hardness	Hv = Kg/mm <sup>2</sup> , g	
Surface Roughness	Ra = µm	
<b>Surface Layer</b>		
Composition:	<b>DLC Carbon</b>	Notes: <b>FAB source</b>
Thickness:	t = 1.44 µm	thicker than Hu1
Micro Hardness:	Hk = 2500 Kg/mm <sup>2</sup> , 25 g	impossible to ident with 10 or 15g - elastic recovery
Surface Roughness	Ra = 0.1000 µm	higher surface roughness to Hu1
<b>Pin on Disc</b>		
Sample Cleaning: <b>Ultrasonic in freon, acetone wipe</b>		
Testing Temperature:	T = 21 ± 1 °C	Notes:
Relative Humidity	RH = 50 ± 2.5 %	
Normal Force	F = 10.0 N	
Sliding Velocity	v = 0.1 m/s	
Track Diameter	Ø = 16.0 mm	
Rotational Speed	n = 119 rpm	
Test Duration	t = 16.7 min	
Sliding Distance	s = 100.0 m	

Results		
Coefficient of Friction		
Initial	$\mu = 0.20$	Notes: high initial $\mu \rightarrow$ low steady state $\mu$ which is typical
Steady state	$\mu = 0.17$	
Wear		
Pin	$\varnothing = 0.53 \text{ mm}$	$V = 0.8 \times 10^{-6} \text{ mm}^3/\text{Nm}$
Disc	$w = 190 \mu\text{m}$	$V = 8.6 \times 10^{-6} \text{ mm}^3/\text{Nm}$
Sliding Distance to Failure: $>100.0 \text{ m}$		
Debris: <b>no debris</b>		
Wear Surface Profilometry:		



Clear Region	Move Marker	Data Selection INCLUDE EXCLUDE	Set X: 185.5um Datum Z: 0.822um
Analyse Region	Options	Form Options	Save Data
			Return to Previous

Maximum track depth  $0.3\mu\text{m}$  (cf.  $1.44\mu\text{m}$ )

Note:- severe wear due to surface roughness - no transfer layer

Scratch Testing			
Ambient Temperature:	T =	$\pm$ °C	Notes:
Relative Humidity	RH =	$\pm$ %	
Maximum Load	F =	N	
Loading Rate		N/s	
Scratching Speed	v =	mm/s	
Results			
Critical Load	trace	Lc =	N
	acoustic	Lc =	N

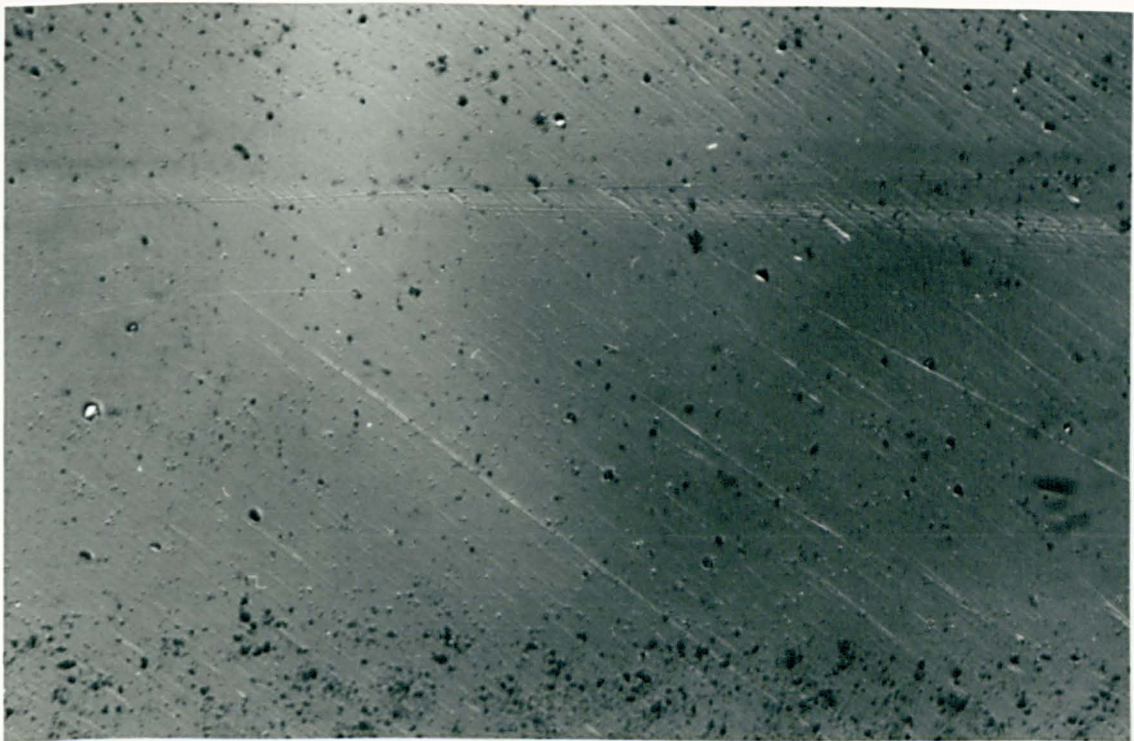


**Fig LXXIII (a) Wear Track.**  
Sample:- Hu6 (thick). Magnification (approx. x80)

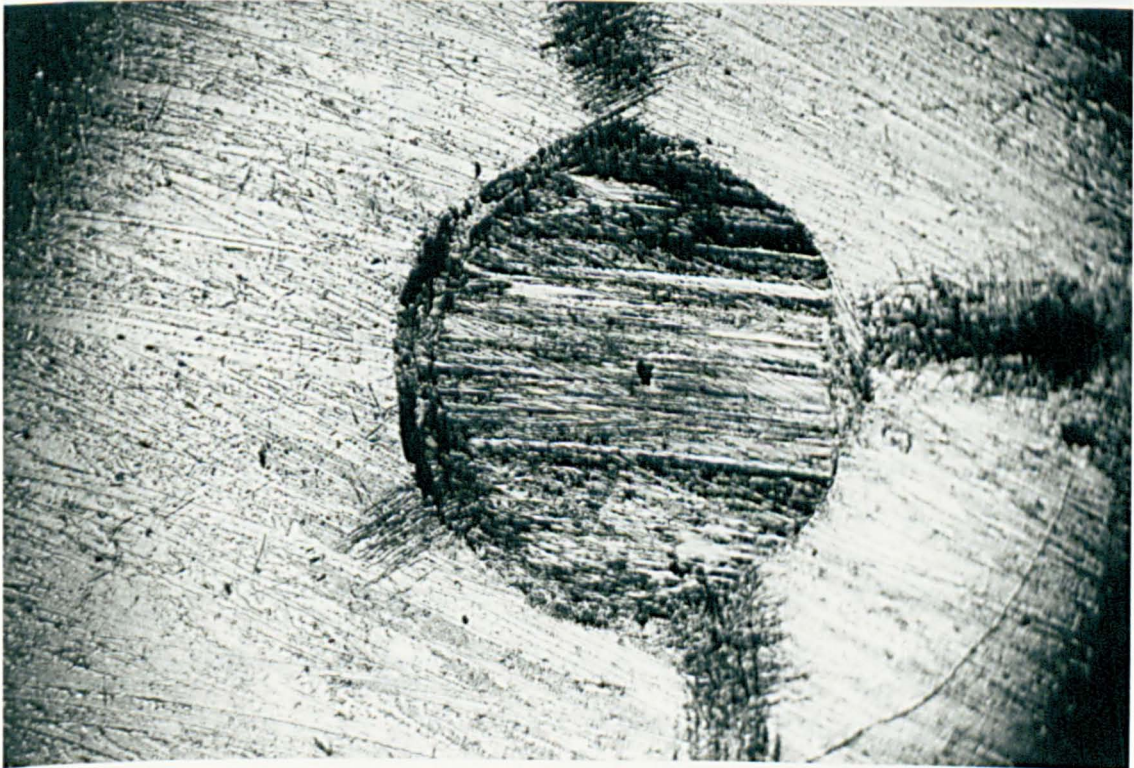
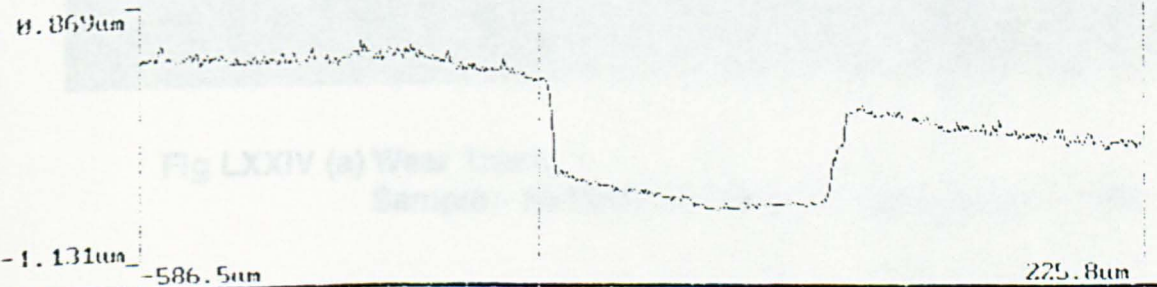


**Fig LXXIII (b) Pin Wear.**  
Sample:- Hu6 (thick). Magnification (approx. x80)

<b>Sample Designation: HuTiN/DLC</b>		
Institute/Laboratory: RCSE, Hull University		
Tested By: Peter Holiday		
Date: 11/3/91		
Dimensions: Ø40mm x 2.5mm disc		
Composition/Grade: cobalt-chrome		
Micro Hardness	Hk = 800 Kg/mm <sup>2</sup> , 25 g	Notes:
Surface Roughness	Ra = 0.050 µm	
<b>Coating Intermediate Layer</b>		
Composition:	Titanium Nitride	Notes: DC EBPVD
Thickness:	t = 2.5 µm	
Micro Hardness	Hv = 1300 Kg/mm <sup>2</sup> , 15 g	Note: only Vickers hardness data available
Surface Roughness	Ra = 0.047 µm	
<b>Surface Layer</b>		
Composition:	DLC Carbon	Notes: FAB source
Thickness:	t = 0.70 µm	
Micro Hardness:	Hk = 2000 Kg/mm <sup>2</sup> , 15 g	
Surface Roughness	Ra = 0.0540 µm	
<b>Pin on Disc</b>		
Sample Cleaning: Ultrasonic in freon, acetone wipe		
Testing Temperature:	T = 21 ± 1 °C	Notes:
Relative Humidity	RH = 50 ± 2.5 %	
Normal Force	F = 10.0 N	
Sliding Velocity	v = 0.1 m/s	
Track Diameter	Ø = 16.0 mm	
Rotational Speed	n = 119 rpm	
Test Duration	t = 16.7 min	
Sliding Distance	s = 100.0 m	

<b>Results</b>		
<b>Coefficient of Friction</b>		
Initial	$\mu = -0.30$	Notes: high friction due to excessive wear
Steady state	$\mu = -0.50$	
<b>Wear</b>		
Pin	$\varnothing = 0.44 \text{ mm}$	$V = 0.4 \times 10^{-6} \text{ mm}^3/\text{Nm}$
Disc	$w = 265 \mu\text{m}$	$V = 9.4 \times 10^{-6} \text{ mm}^3/\text{Nm}$
Sliding Distance to Failure: <1.0 m		
Debris: <b>no debris</b>		
Wear Surface Profilometry:		



Clear Region	Move Marker ← →	Data Selection INCLUDE EXCLUDE OFF	Set X: -265.2um Datum Z: 0.244um
Analyse Region	Options	Form Options	Save Data
			Return to Previous

Total failure of the film - maximum depth of wear track 0.7μm (cf. 0.7μm - thickness of film)

<b>Scratch Testing</b>			
Ambient Temperature:	T =	± °C	Notes:
Relative Humidity	RH =	± %	
Maximum Load	F =	N	
Loading Rate		N/s	
Scratching Speed	v =	mm/s	
<b>Results</b>			
Critical Load	trace	Lc =	N
	acoustic	Lc =	N

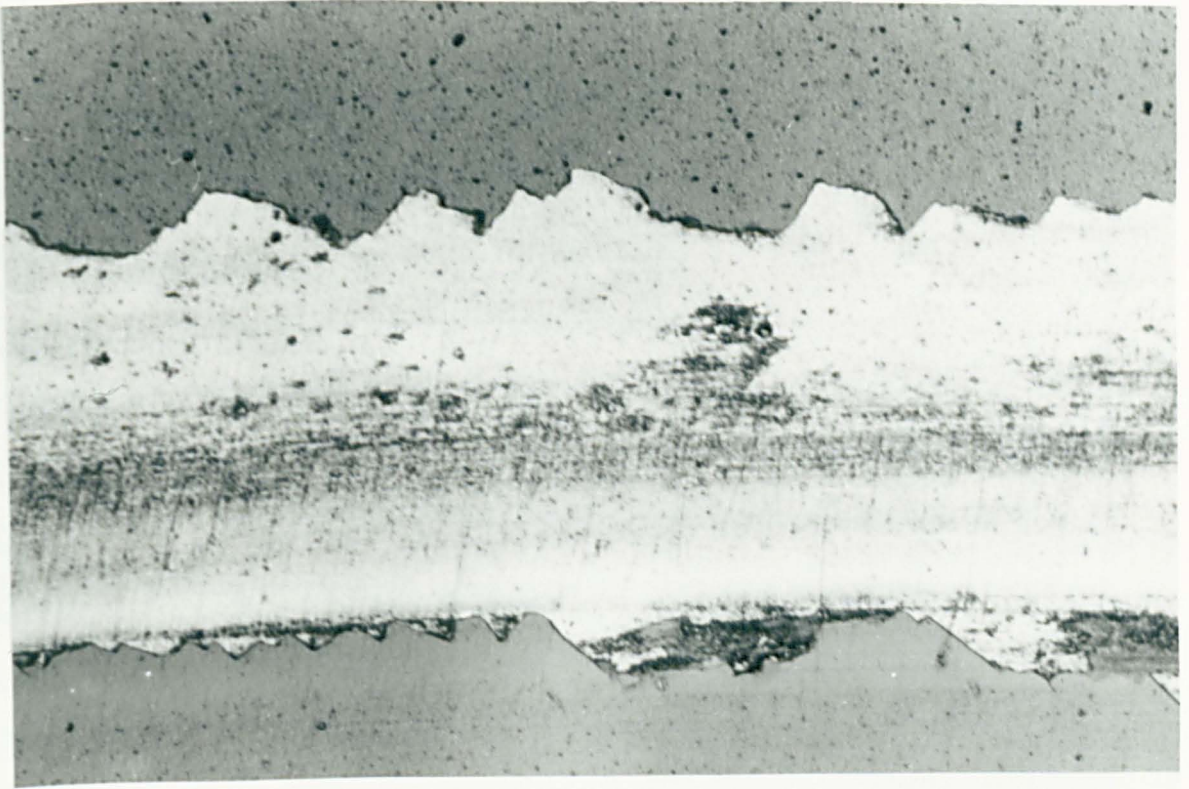


**Fig LXXIV (a) Wear Track.**  
**Sample:- HuTiN/DLC. Magnification (approx. x80)**

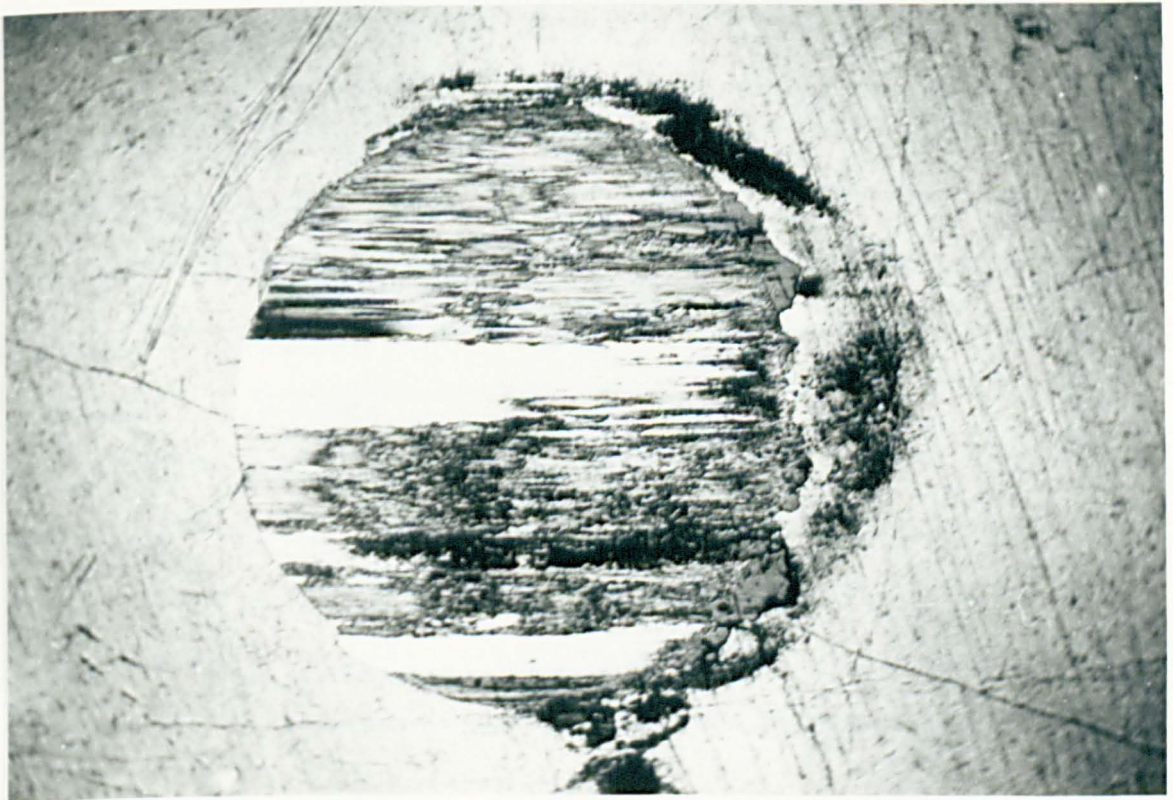


**Fig LXXIV (b) Pin Wear.**  
**Sample:- HuTiN/DLC . Magnification (approx. x80)**

<b>Sample Designation: HuTiN/DLC (nitrogen rich)</b>		
Institute/Laboratory: <b>RCSE, Hull University</b>		
Tested By: <b>Peter Holiday</b>		
Date: <b>11/3/91</b>		
Dimensions: <b>Ø40mm x 2.5mm disc</b>		
Composition/Grade: <b>tool steel</b>		
Micro Hardness	H <sub>k</sub> = Kg/mm <sup>2</sup> , g	Notes:
Surface Roughness	R <sub>a</sub> = µm	
<b>Coating Intermediate Layer</b>		
Composition:	<b>Titanium Nitride</b>	Notes: <b>DC EBPVD</b>
Thickness:	t = µm	
Micro Hardness	H <sub>v</sub> = Kg/mm <sup>2</sup> , g	Note:
Surface Roughness	R <sub>a</sub> = 0.050 µm	
<b>Surface Layer</b>		
Composition:	<b>DLC Carbon</b>	Notes: <b>FAB source</b>
Thickness:	t = ~0.70 µm	
Micro Hardness:	H <sub>k</sub> = Kg/mm <sup>2</sup> , g	
Surface Roughness	R <sub>a</sub> = µm	
<b>Pin on Disc</b>		
Sample Cleaning: <b>Ultrasonic in freon, acetone wipe</b>		
Testing Temperature:	T = 21 ± 1 °C	Notes:
Relative Humidity	RH = 50 ± 2.5 %	
Normal Force	F = 10.0 N	
Sliding Velocity	v = 0.1 m/s	
Track Diameter	Ø = 16.0 mm	
Rotational Speed	n = 119 rpm	
Test Duration	t = 16.7 min	
Sliding Distance	s = 100.0 m	

### Results

#### Coefficient of Friction

Initial	$\mu = 0.20$	Notes:
Steady state	$\mu = 0.20$	

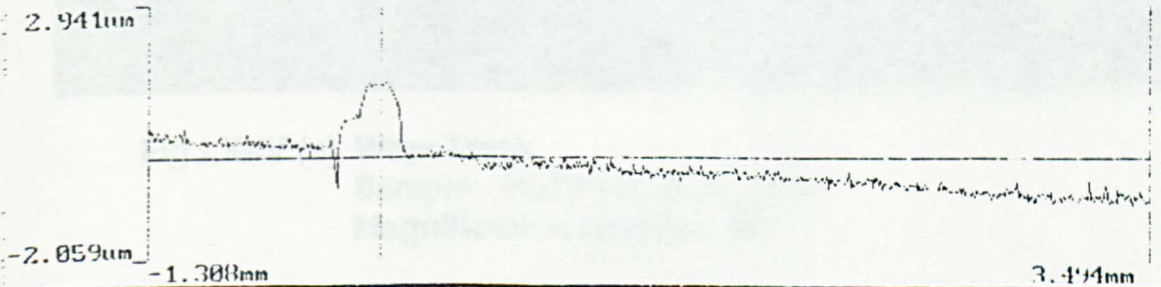
#### Wear

Pin	$\varnothing =$ mm	V =	mm <sup>3</sup> /Nm
Disc	w = 754 $\mu$ m	V =	mm <sup>3</sup> /Nm

Sliding Distance to Failure: >100.0 m

Debris: **no debris**

#### Wear Surface Profilometry:



Clear Region	Move Marker ← →	Data Selection INCLUDE EXCLUDE OFF	Set X: -197.1µm Datum Z: 1.315µm
Analyse Region	Options	Form Options	Save Data
			Return to Previous

#### Scratch Testing

Ambient Temperature:	T = ± °C	Notes:
Relative Humidity	RH = ± %	
Maximum Load	F = N	
Loading Rate	N/s	
Scratching Speed	v = mm/s	

#### Results

Critical Load	trace	Lc =	N
	acoustic	Lc =	N

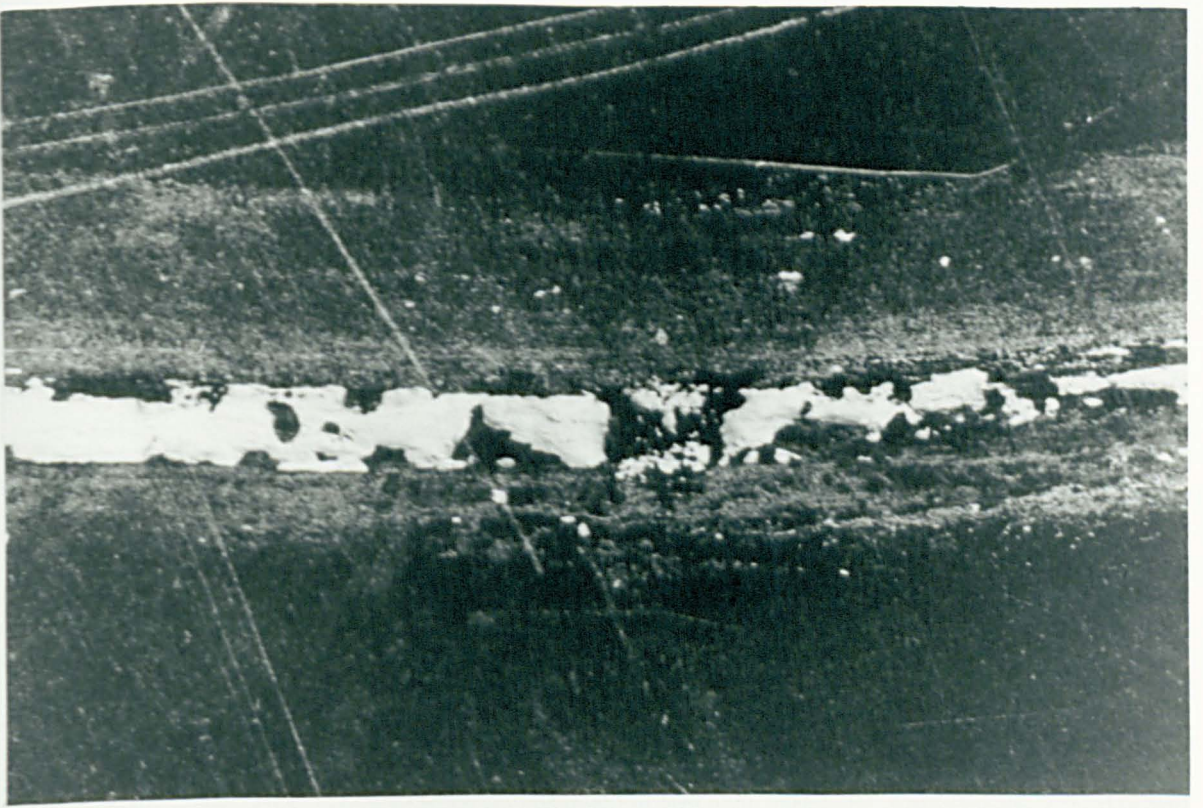


**Fig LXXV (a) Wear Track.**  
**Sample:- HuTiN/DLC (N<sub>2</sub> Rich)**  
**Magnification (approx. x80)**

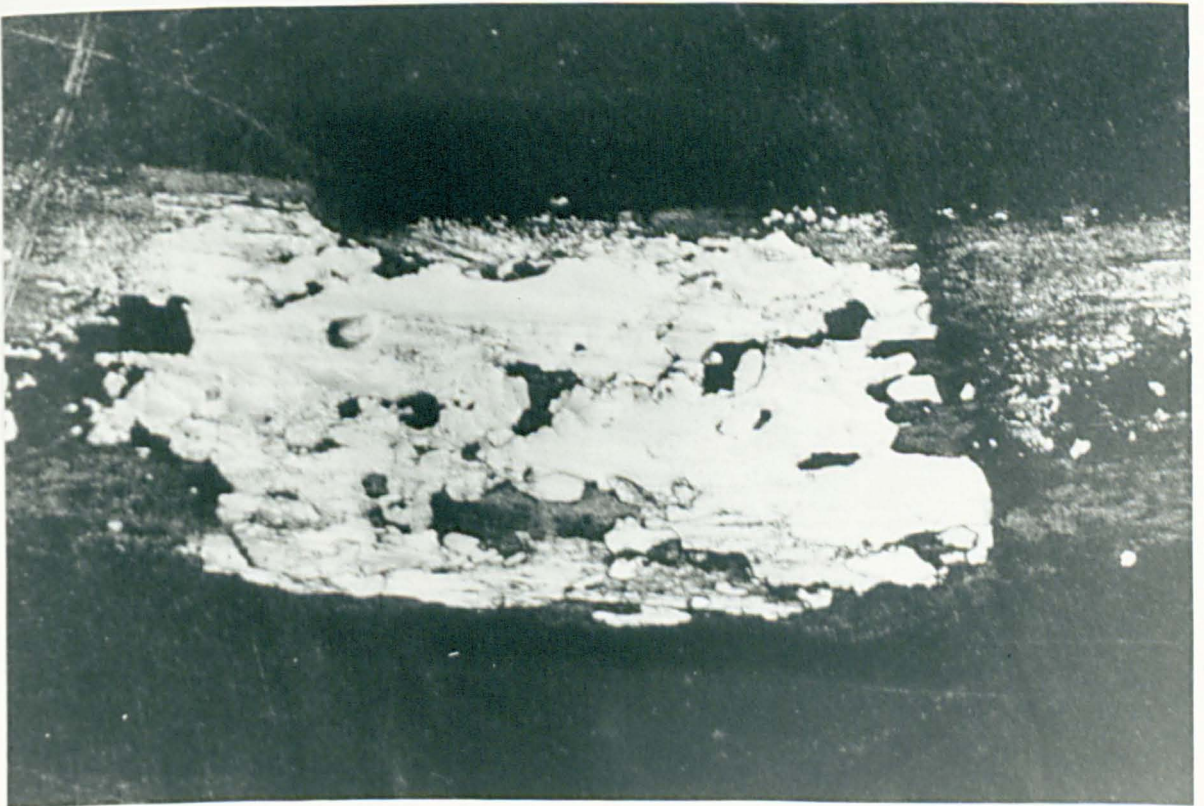


**Fig LXXV (b) Wear Track (enlarged).**  
**Sample:- HuTiN/DLC (N<sub>2</sub> Rich)**  
**Magnification (approx. x240)**